Comprehensive Theory of Heat Transfer in Heterogeneous Materials

by

Gregory W. Vogl

Masters Thesis submitted to the Faculty of the
Virginia Polytechnic Institute and State University
in partial fulfillment of the requirement for the degree of

Master of Science
in
Engineering Mechanics

Mark S. Cramer, Chair
L. Glenn Kraige
Surot Thangjitham

January 6, 2003
Blacksburg, Virginia

Keywords: Heat Transfer, Heterogeneous Materials

Comprehensive Theory of Heat Transfer in Heterogeneous Materials

by

Gregory W. Vogl

Abstract

For over forty years, researchers have attempted to refine the Fourier heat equation to model heat transfer in engineering materials. The equation cannot accurately predict temperatures in some applications, such as during transients in microscale ($< 10^{-12}$ s) situations. However, even in situations where the time duration is relatively large, the Fourier heat equation might fail to predict observed non-Fourier behavior. Therefore, non-Fourier models must be created for certain engineering applications, in which accurate temperature modeling is necessary for design purposes.

In this thesis, we use the Fourier heat equation to create a general non-Fourier, but diffusive, equation that governs the matrix temperature in a composite material. The composite is composed of a matrix with embedded particles. We let the composite materials be governed by Fourier's law and let the heat transfer between the matrix and particles be governed by contact conductance. After we make certain assumptions, we derive a general integro-differential equation governing the matrix temperature. We then non-dimensionalize the general equation and show that our model reduces to that used by other researchers under a special limit of a non-dimensional parameter.

We formulate an initial-boundary-value problem in order to study the behavior of the general matrix temperature equation. We show that the thermalization time governs the transition of the general equation from its small-time limit to its large-time limit, which are both Fourier heat equations. We also conclude that our general model cannot accurately describe temperature changes in an experimental sand composite.

In loving memory of my grandpa, Frank Vogl

Acknowledgements

How do I acknowledge those who try to give me more than I ever need or want? I will try. Thanks, Mom and Dad. Thanks for all the love, hope, and faith that brought me here and enabled me to work and finish this thesis.

Grant Vogl, my brother, I owe you many thanks for helping me create the plots in this work. I would not have such nice figures without the time and expertise that you gave freely.

I cannot forget to acknowledge the man that made this thesis possible. Dr. Mark S. Cramer, thanks for your time, patience, understanding, and genius. I have truly enjoyed working with you. The partial funding was also a blessing.

To my other committee members, Drs. L. Glenn Kraige and Surot Thangjitham, I thank you both for your time, flexibility, and honest comments.

Dr. James R. Leith at the University of New Mexico, thanks for pointing me in the right direction to get needed data.

To all family and friends that kept me smiling and laughing these past years… thank you.

To all those that I have forgotten but should have acknowledged, please accept my apology and sincere gratitude.

Table of Contents

APPENDICES

List of Figures and Tables

FIGURE TITLE

TABLE TITLE

Chapter 1
Introduction

1.1 Fourier Heat Equation

The most widely used equation governing heat propagation in isotropic media is Fourier's law of heat conduction,

$$\mathbf{q} = -k\nabla T\,, \tag{1.1.1}$$

where $\mathbf{q}$ is the local heat flux across a surface, k is the local thermal conductivity of the media, and ∇T is the local gradient of temperature T in the media. The energy equation for a rigid material with no volumetric energy supply is

$$\rho c\,\partial_t T = \nabla\cdot\mathbf{q}\,, \tag{1.1.2}$$

where ρ is the material density, c is the specific heat capacity, ∂_t is the partial differential operator with respect to time t, and $\nabla\cdot\mathbf{q}$ is the divergence of the heat flux $\mathbf{q}$. When Fourier's law (1.1.1) is substituted into the energy equation (1.1.2) for a homogeneous material with constant material properties, we obtain Fourier's heat equation

$$\partial_t T = \alpha\nabla^2 T\,, \tag{1.1.3}$$

where

$$\alpha = \frac{k}{\rho c} \tag{1.1.4}$$

is the thermal diffusivity of the material and ∇^2 is the spatial Laplacian operator.

Even though Fourier's heat equation (1.1.3) is an excellent model for many heat transfer problems, the model is not physically realistic. Equation (1.1.3) is a parabolic equation. As a result, any temperature disturbance will propagate at an infinite speed through the media [1]. Thus, use of (1.1.1) results in thermal waves traveling at an infinite speed, which is physically unrealizable [2].

Because Fourier's law does not predict finite wave speeds, the law does not accurately approximate the heat transfer in certain cases. The assumption of instantaneous energy transmission fails during a short duration of an initial transient, or when the thermal propagation speed is not high, such as in low temperature cases [1]. In other words, Fourier's law breaks down at temperatures near absolute zero or when the observation time is extremely small during a transient. For these cases, the fact that thermal disturbances travel with finite speeds of propagation must invalidate Fourier's law (1.1.1). Thus, the wave nature of thermal transport becomes dominant, rendering Fourier's law to be invalid as an approximation for these cases [3].

From an engineering standpoint, it may be essential to model the heat transfer for the cases where Fourier's law fails. For example, Fourier's law does not accurately predict the transient temperature during *microscale* ($< 10^{-12}$ s) laser heating of thin metal films ($\leq 10^{-6}$ m) [4]. Therefore, *non-Fourier* behaviors may be significant for such microscale applications as pulsed-laser processing of metal and semiconductors, thin-film applications, and even laser surgery [5]. In fact, laser and microwave heating with extremely short durations or very high frequencies have been used for numerous purposes like surface melting of metal and sintering of ceramics [6]. Also, Fourier's law may fail to approximate transient temperatures for *macroscale* situations, where time scales are relatively large compared to those for microscale conditions [4]. Because non-Fourier behavior exists in engineering applications, Fourier's law should be modified for such applications.

1.2 Hyperbolic Heat Equation

Non-Fourier heat conduction models have been proposed to replace models based on Fourier's law. Specifically, non-Fourier models have been designed to predict *second sound* in solids, which is the finite wave speed of heat propagation [7]. One non-Fourier model is based on the modified flux law,

$$\mathbf{q} + \tau \partial_t \mathbf{q} = -k \nabla T , \tag{1.2.1}$$

where τ is called the *relaxation time* [1]. The heat flux vector now has a memory that keeps track of the time-history of the temperature gradient [8]. Equation (1.2.1) was first proposed independently by researchers Cattaneo [9] and Vernotte [10].

When (1.2.1) is combined with the energy equation (1.1.2), we obtain the *hyperbolic heat equation*,

$$\partial_t T + \tau \partial_t^2 T = \alpha \nabla^2 T \,. \tag{1.2.2}$$

Equation (1.2.2) is known as a hyperbolic heat equation (or a telegraph equation) because of the additional term that modifies the parabolic Fourier heat equation (1.1.3) [6]. The hyperbolic heat equation has two double-derivative terms in (1.2.2), which are called the *wave terms*. Unlike Fourier's law (1.1.1), the modified heat flux (1.2.1) predicts a finite speed of heat propagation because of the relaxation time τ associated with heat transfer [7]. In fact, it can be shown that the speed C of heat propagation is

$$C = \sqrt{\alpha/\tau} \,. \tag{1.2.3}$$

As τ decreases, the thermal wave speed C increases. Discontinuities of temperature and temperature gradient at the wavefront and thermal shocks around a moving point source are results of the finite speed C of propagation [6]. Typical wave speeds in metals are on the order of 10^5 m/s [11].

The hyperbolic model (1.2.2) of heat transfer has been used to model heat transfer in the cases where Fourier's heat equation fails to predict accurate temperatures. For instance, researchers like Glass et al. [3] have investigated the discontinuity of temperature gradient at the thermal wavefront. Others like Yang [1] have applied the hyperbolic heat model to thermal shocks around a fast-moving heat source, and some have even applied the hyperbolic heat equation to study heat transfer near a rapidly propagating crack tip. Various solutions of the hyperbolic model for finite mediums under different initial and boundary conditions can also be found in literature. Most solutions were attained for a pulse heat flux or a sudden temperature change [6]. Tang and Araki [6] have even solved (1.2.2) in a finite medium with a periodic surface heat flux, finding that the wave part reflects off the boundaries while dissipating until the response becomes periodic.

While the hyperbolic model was created to deal with the problems associated with the Fourier model, the hyperbolic heat equation (1.2.2) is still in question for multiple reasons. First, it is not based on the details of energy transport in the material, such as the interaction of electrons and phonons (vibrations of the metal lattice) [7]. Second, material properties may not be able to be regarded as constant. The relaxation time τ is generally temperature-dependent [8]

and the thermal conductivity α depends on processing parameters, such as the laser pulse duration and intensity, during short-pulse laser heating [7]. These facts provide impetus for deriving an equation that is grounded more on a physical basis than the hyperbolic heat equation (1.2.2).

1.3 Dual-Phase-Lag Equation

The modified heat flux (1.2.1) is sometimes derived from the lag equation

$$\mathbf{q}(\mathbf{r}, t+\tau) = -k\nabla T(\mathbf{r}, t), \tag{1.3.1}$$

which holds at a given spatial position **r** and time *t* for sufficiently small τ [8]. Physically, (1.3.1) means that the heat flux lags behind the temperature gradient. In an attempt to derive a more robust model, researchers have proposed that

$$\mathbf{q}(\mathbf{r}, t+\tau_q) = -k\nabla T(\mathbf{r}, t+\tau_T), \tag{1.3.2}$$

where τ_q and τ_T are two separate time lags [11]. Antaki [4] used a linearized and truncated form of (1.3.2),

$$\mathbf{q} + \tau_q \partial_t \mathbf{q} = -k\nabla T - \tau_T k \partial_t \nabla T, \tag{1.3.3}$$

and combined it with the energy equation (1.1.2) to obtain

$$\frac{1}{\alpha}\partial_t T + \frac{\tau_q}{\alpha}\partial_t{}^2 T = \nabla^2 T + \tau_T \partial_t \nabla^2 T. \tag{1.3.4}$$

Equation (1.3.4) is called the *dual-phase-lag* (DPL) equation because it was based on a heat flux depending on two time lags [11]. The two times τ_q and τ_T account for the non-zero times required by both the heat flux and temperature gradient to gradually respond to thermal disturbances, such as an imposed heat flux. The DPL equation reduces to the non-Fourier Cattaneo-Vernotte model (1.2.2) by setting $\tau_T = 0$ and reduces to Fourier's heat equation (1.1.3) by setting $\tau_q = \tau_T = 0$ [4].

Compared to the hyperbolic heat equation (1.2.2), the DPL model (1.3.4) has an additional *mixed-derivative* term. Now, as with the hyperbolic model, the time lag associated with heat flux causes wavelike behavior. However, the new time lag τ_T creates a mixed-

derivative term that smoothes the sharp wavefronts caused by τ_q through conduction, resulting in non-Fourier diffusion-like conduction [4]. The mixed-derivative term causes strong attenuation of the sharp wavefront, causing the large heat-affected zone to resemble that due to diffusion [13]. Therefore, the mixed-derivative term destroys the wave structure by rendering the equation to be parabolic, meaning that temperature disturbances will propagate at an infinite speed in the media, as with Fourier's heat equation (1.1.3) [14]. Furthermore, unlike Fourier's heat equation, the temperature in the hyperbolic and dual-phase-lag models is sensitive to temperature rate. However, because of the stronger dissipation from the mixed derivative term, the degree of possible temperature over-shooting in the dual-phase-lag model caused by initial temperature rates is not as large as that for the hyperbolic model [13]. Thus, even though the dual-phase-lag equation (1.3.4) is physically unrealizable because of its parabolic nature, it still may be a better approximation than the hyperbolic model (1.1.4) for engineering purposes because of the physically realistic dissipation caused by the mixed-derivative term.

1.4 Examples of Dual-Phase-Lag Equation

Instead of using the energy equation (1.1.2) and heat flux law (1.3.3), researchers have derived DPL equations from first principles. One type of dual-phase-lag equation was derived for metals on a microscopic basis by numerous researchers, e.g., Qiu and Tien [12] and Tzou et al. [13]. The DPL model accounts for the interaction of electrons at temperature T_e and the metal lattice at temperature T_l through *two* coupled energy equations,

$$C_e \partial_t T_e = K \nabla^2 T_e - G(T_e - T_l) \tag{1.4.1}$$

and

$$C_l \partial_t T_l = G(T_e - T_l), \tag{1.4.2}$$

where K is the thermal conductivity of the electron gas, G is the electron-phonon coupling factor, and C_e and C_l are the heat capacities of the electron gas and the metal lattice, respectively [13]. As seen in (1.4.1), *diffusion* governs heat transfer in the electron gas and heat is transferred to the metal lattice in a *lumped-capacity* sense through the coupling factor G. In other words, the rate of energy increase in the metal lattice is proportional to the temperature difference between the

metal lattice and the electrons, according to (1.4.2). By eliminating the electron gas temperature T_e from equations (1.4.1) and (1.4.2) for constant thermal properties, one can show that

$$\frac{1}{\alpha_T}\partial_t T_l + \frac{1}{C_T^{\,2}}\partial_t^{\,2} T_l = \nabla^2 T_l + \frac{\alpha_e}{C_T^{\,2}}\partial_t \nabla^2 T_l, \tag{1.4.3}$$

where

$$\alpha_T = \frac{K}{C_e + C_l} \tag{1.4.4}$$

is the *equivalent* thermal diffusivity,

$$C_T = \sqrt{\frac{KG}{C_e C_l}} \tag{1.4.5}$$

is the thermal wave speed, and α_e is the thermal diffusivity of the electron gas. Indeed, the governing equation (1.4.3) for the metal lattice temperature T_l is a type of dual-phase-lag equation (1.3.4). Equation (1.4.3) is also known as a *two-step* model, because it was created from combining two coupled equations that model the first step (diffusion in the gas) and the second step (heat transfer to the metal lattice) of energy transfer in the material.

The DPL model (1.4.3) was developed for metals that are homogeneous from a macroscopic perspective. The model may not apply to *non-homogeneous* materials, like sand with an irregular grain structure or processed meats [2]. In fact, non-Fourier heat transfer in these materials has seldom been investigated. However, Mitra et al. [15] produced evidence that suggests the existence of non-Fourier, specifically hyperbolic, heat conduction behavior in processed meats. Typical thermal wave speeds were stated to be on the order of 0.1 mm/s for the processed meats used by Mitra et al. and for the sand investigated by Kaminski [16]. These results are suspect, which led Herwig and Beckert [2] to experimentally investigate the supposedly non-Fourier behavior for processed meats and sand. They found only Fourier-like conduction behavior and were unable to reproduce the results of Mitra et al. and Kaminski.

A theoretical investigation of heat transfer in non-homogeneous materials may be useful in challenging or supporting experimental results. One non-homogeneous material that has been investigated theoretically is a matrix embedded with small particles that are not necessarily microscopic. Vick and Scott [17] used a two-step model to approximate the matrix temperature T_m for the composite. In fact, the assumptions used by Vick and Scott for their non-

homogeneous composite are analogous to those used by Tzou et al. [13] to derive the DPL model (1.4.3) for metals. The matrix material is like the electrons and the particles are analogous to the metal lattice. In other words, the matrix material is assumed to be *diffusive* (like the electrons) while heat transfers from the matrix to the particles in a *lumped-capacity* sense (like the heat transfer from the electrons to the metal lattice). It should be noted that the lumped-capacity approximation means that effective properties of the particle can be used because the temperature change is assumed to be approximately uniform within any particle. With these assumptions, Vick and Scott obtained

$$\frac{1}{\alpha_{eff}}\partial_t T_m + \frac{\tau_{eff}}{\alpha_{eff}}\partial_t{}^2 T_m = \nabla^2 T_m + \tau_{eff}\frac{\alpha_m}{\alpha_{eff}}\partial_t \nabla^2 T_m , \tag{1.4.6}$$

where α_{eff} is the effective thermal diffusivity, α_m is the thermal diffusivity of the matrix, and τ_{eff} is the effective relaxation time [17]. Like (1.4.3) that governs the metal lattice temperature in an electron-lattice system, (1.4.6) is a type of dual-phase-lag equation (1.3.4).

1.5 Goal of Thesis

We desire to approximate the matrix temperature in a composite material similar to that used by Vick and Scott [17]. However, we will take a more general approach and will *not* assume that heat transfers to the particles in a lumped-capacity sense. Instead, a general integro-differential equation will be produced in this thesis that approximates the matrix temperature while accounting for the detailed transfer of heat *within* the particles. It will also be shown that our general equation will reduce to that derived by Vick and Scott.

Our general heat equation will be solved for a semi-infinite case in order to learn about the physics of heat transfer in the composite. Specifically, we desire to determine if thermal waves are visible in the non-homogeneous material, how the matrix temperature behaves for both relatively small and large times, and how the physical parameters affect this behavior.

Lastly, we will attempt to verify our general integro-differential equation by using it to determine if it can predict experimental values collected from an experiment with sand.

Chapter 2

Problem Formulation

2.1 Introduction

In this chapter, we formulate the problem studied in this thesis. We choose to study heat transfer in a matrix that has embedded particles. First, we will define the composite material for which heat transfer will be studied by describing its geometry and material properties. Then, a general element of the composite is described and assumptions are made regarding the element. Finally, heat transfer constitutive equations for our composite are given.

2.2 Geometry and Material Properties of Composite

We choose to study the heat transfer in a composite medium composed of a solid matrix with embedded solid particles. The matrix has a uniform thermal conductivity k_m, density ρ_m, and specific heat c_m. Every particle will be taken to be spherical with radius R, surface area $a_p = 4\pi R^2$, and volume $v_p = \frac{4}{3}\pi R^3$, and has uniform thermal conductivity k_p, density ρ_p, and specific heat c_p. Figure 2.1 depicts a cross section of three embedded particles surrounded by matrix material. All particles, including those in Figure 2.1, are randomly distributed throughout the composite and the average number of particles per unit total composite volume is taken to be n_p. In addition, the distance d between the centers of neighboring particles is assumed to have a small coefficient of variation.

As indicated in Figure 2.1, a surface of contact conductance μ will be taken to separate each particle from the matrix. The contact conductance μ is assumed to be a non-negative real number and relates to the heat transfer between the matrix and the particles. If μ is zero, then no heat is conducted between the matrix and the particles. On the other hand, if μ is infinite, then "perfect contact" between the particles and the matrix exists, which means that heat is transferred

between the particles and matrix as if the contact layers did not exist. Physically, contact conductance is typically due to the presence of a thin layer of air, vapor, or solid insulating matter between two materials.

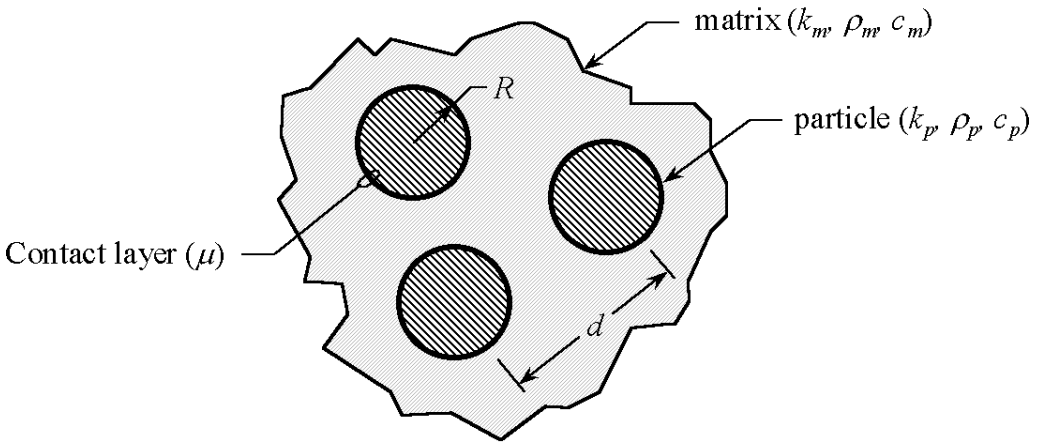

Figure 2.1: Cross Section of Particles Embedded in Matrix

2.3 Temperature and Energy in Composite

We will denote the local particle and matrix temperatures as T_p and T_m, respectively. Initially, the particles and the matrix may have different temperatures, but for all practical purposes, both the particle and matrix temperature will be uniform throughout the composite. For instance, radiation heating could be used to heat all aluminum particles to a higher temperature than a glass matrix. Consequently, we will take the initial particle temperature be uniform at T_p^0 and the initial matrix temperature to be uniform at T_m^0, i.e.,

$$T_p = T_p^0 \text{ and } T_m = T_m^0 \text{ at } t = 0\,, \tag{2.3.1}$$

at every respective particle and matrix material point.

We also let the local particle and matrix specific energies be e_p and e_m, respectively, where

$$c_i = \frac{de_i}{dT_i} \tag{2.3.2}$$

for i being p or m.

2.4 General Element of Composite

We want to derive an approximate equation that describes the matrix temperature T_m by using the model of our composite described in the previous sections of this chapter. The first step is to create a general element and the second step is to make certain assumptions concerning the element.

Figure 2.2 depicts a general element of the composite medium. Fully dashed circles denote particles embedded wholly in the matrix. Typical partial particles, which are produced during the creation of the element, are partially embedded in the general element of the figure. The two types of surfaces that bound the matrix are also seen in Figure 2.2. The first surface, S_e, is the exposed surface that bounds the matrix volume, represented by the gray surface in the figure. The second surface, S_c, is the collection of contact surfaces separating the particles from the matrix, represented by the dashed hidden lines in Figure 2.2. Furthermore, the total elemental volume is V_T and the volume occupied by the particles and the matrix in the element are V_p and V_m, respectively. Thus,

$$V_T = V_p + V_m . \tag{2.4.1}$$

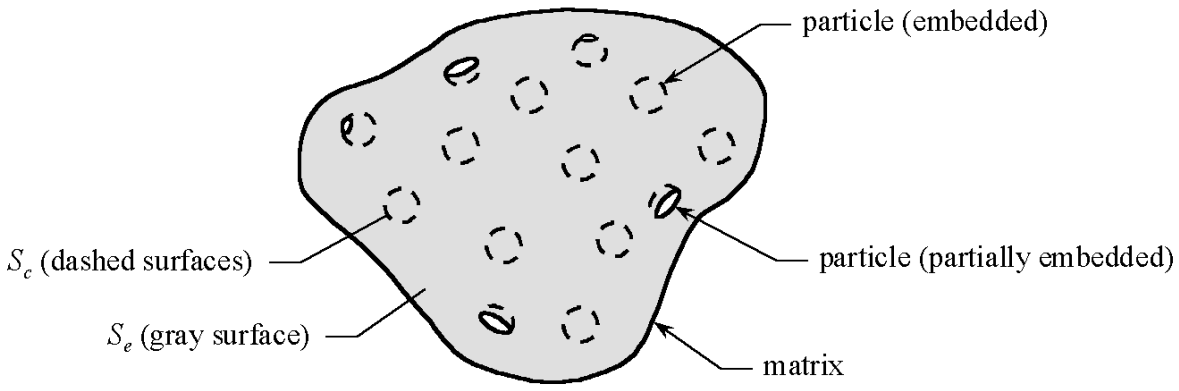

Figure 2.2: General Element of Composite Medium

2.5 Assumptions for General Element

Certain assumptions will now be made concerning the element of Figure 2.2. First of all, the element is assumed to be large enough to encompass a sufficient number of particles such that we can express the number of particles within the element to be $n_p V_T$. We can then multiply the number of particles by the volume of a particle v_p to find that

$$V_p = (n_p V_T) v_p . \tag{2.5.1}$$

Substitution of (2.5.1) into (2.4.1) yields

$$V_m = (1 - n_p v_p) V_T , \tag{2.5.2}$$

where $n_p v_p$ is the particle-to-composite volume ratio. We restrict the volume ratio to be small relative to one, i.e., $n_p v_p << 1$, such that a majority of the composite is matrix material. Second, the particles are assumed to be small enough such that each particle has a uniform matrix temperature T_m on the outer surface of each contact layer. Last of all, we assume that the matrix temperature T_m in the element of Figure 2.2 is nearly uniform on a scale compared to the particle diameter. However, on a much larger scale, the matrix temperature is generally not uniform. These conditions will ensure that the local matrix temperatures in the element are not significantly altered by the presence of the particles.

Our assumptions can be used to determine certain properties of the particle and matrix temperatures. Each particle is initially uniform in temperature and is assumed to have a uniform boundary temperature. In addition, because there is no preferred direction in the energy and Fourier equations, it follows from symmetry arguments that T_p is *only* a function of radius r for each particle. In other words, we will assume that

$$T_p = T_p(r) . \tag{2.5.3}$$

Second, because the matrix temperature T_m is assumed to be fairly uniform in the element of Figure 2.2, it is implied that approximately the *same* uniform matrix temperature T_m surrounds each particle in the element. In other words, matrix material points on the surface S_c are assumed to have the same matrix temperature.

2.6 Heat Transfer Constitutive Equations

Like the geometry and material properties of our composite, the heat transfer in our composite also needs to be modeled. We assume that Fourier's law of heat conduction applies within the particles and the matrix. According to (1.1.1), the heat flux **q** is then

$$\mathbf{q} = -k_i \nabla T_i , \tag{2.6.1}$$

where ∇ is the spatial gradient operator, and i is p or m, depending upon whether the location where **q** is being evaluated at is in a particle or the matrix, respectively.

To model the heat transfer between the particles and the matrix through the contact conductance layers, we use the concept of contact conductance μ. The standard model for contact conductance takes the normal component q_μ of the heat flux across a contact surface to be proportional to the difference of temperatures on both sides of the contact surface. Because of (2.5.3) and our assumption that each particle is surrounded by the same uniform matrix temperature T_m, the heat flux q_μ into each particle is radially-directed with a magnitude of

$$q_\mu = \mu(T_m - T_p(R)) . \tag{2.6.2}$$

According to (2.6.2), when "perfect contact" occurs, i.e. when μ becomes infinite, the temperature difference across a contact layer is zero. The zero temperature difference validates our previous statement that the contact layers can be regarded as non-existent for infinite contact conductance. It is also worthwhile to note that (2.6.2) is really an approximation of Fourier's law (2.6.1) for sufficiently thin films.

For visualization purposes, the heat fluxes defined in (2.6.1) and (2.6.2) are illustrated in Figure 2.3 for part of a particulate cross section. One can see that the heat flux is radially directed inside the spherical particle. The heat flux is radially directed throughout the particle because of Fourier's law (2.6.1) and the spherical symmetry of temperature in each particle, according to (2.5.3). As seen in Figure 2.3, the heat flux vector $\mathbf{q}_\mu$ at the surface of the sphere is

$$\mathbf{q}_\mu = q_\mu \mathbf{n} = \mu(T_m - T_p(R))\mathbf{n} , \tag{2.6.3}$$

where **n** is the outward unit normal to the matrix at the contact surface. Furthermore, one can see in Figure 2.3 that the direction of the heat flux in the matrix is general. Even though we assumed that the matrix temperature is nearly uniform in the vicinity of a particle, we do not know how the matrix temperature actually varies around a particle. Consequently, the general gradient of

the matrix temperature is unknown near a particle. This explains why the direction of the heat flux in the matrix is unknown and why a general direction is seen for the matrix heat flux in Figure 2.3.

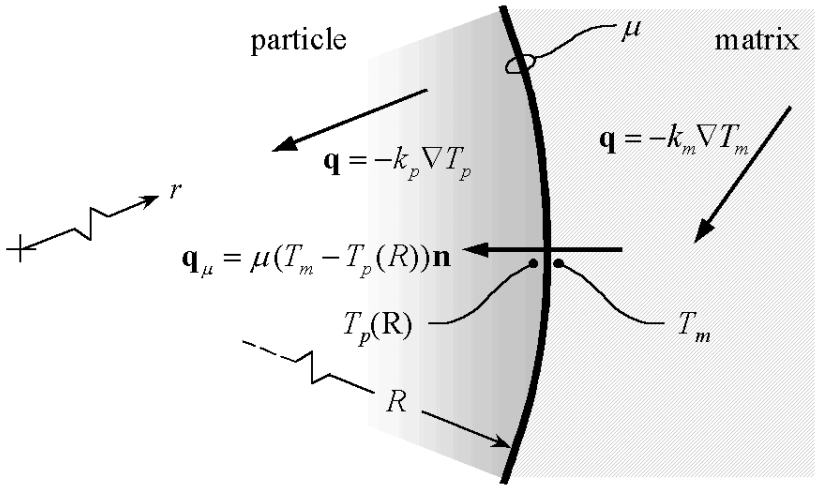

Figure 2.3: Visualization of Heat Transfer Constitutive Equations

We are now ready to derive an approximation of the matrix temperature T_m based on the problem formulation described in this chapter.

Chapter 3

Generation of General Matrix Temperature Equation – Part I

3.1 Introduction

The problem formulation from Chapter 2 will now be used to derive the equation governing matrix temperature T_m. We will first derive the general energy equation for the matrix. Then, we use the assumptions stated in Chapter 2 to reduce the general energy equation to a form that involves the temperature difference across the contact conductance layers. This form of the energy equation will be used in the next chapter to create the final form of the general energy equation, which involves only the matrix temperature.

3.2 Creation of General Energy Equation for Matrix

The energy equation for the matrix material of the element seen in Figure 2.2 is

$$\frac{d}{dt}\int_{V_m} \rho_m e_m \, dV + \int_{S_e+S_c} \mathbf{q}\cdot\mathbf{n}\, dS = 0, \tag{3.2.1}$$

where **n** is the outward unit normal to the surfaces bounding the matrix volume V_m. In words, (3.2.1) is interpreted as stating that the time rate of change of the total energy of the matrix is equal to the flux of energy conducted into the matrix volume.

Since there is no material deformation, the limits on the volume integral in (3.2.1) are constant. Thus, we may write (3.2.1) as

$$\int_{V_m} \rho_m \partial_t e_m \, dV + \int_{S_e+S_c} \mathbf{q}\cdot\mathbf{n}\, dS = 0. \tag{3.2.2}$$

We use the chain-rule for differentiation and substitute (2.3.2) into (3.2.2) to obtain

$$\int_{V_m} \rho_m c_m \partial_t T_m \, dV + \int_{S_e} \mathbf{q}\cdot\mathbf{n}\, dS + \int_{S_c} \mathbf{q}\cdot\mathbf{n}\, dS = 0. \tag{3.2.3}$$

The second integral in (3.2.2) was separated into its two component surface integrals for (3.2.3) because we need to apply the constitutive equations (2.6.1) and (2.6.2) separately to the first and second surface integrals, respectively.

3.3 Approximation of General Energy Equation

We will approximate the second surface integral in (3.2.3) first. Because the heat flux q_μ into each particle is the same for each particle in the element, we can let

$$Q = a_p \, q_\mu \,, \tag{3.3.1}$$

where Q is the heat energy per time entering any particle in the element, a_p is the surface area of the sphere, and q_μ is the heat flux into the particles of the element of Figure 2.2 and is defined in (2.6.2). If we multiply Q by the number of particles in the element, $n_p V_T$, we find that the total energy rate out of the matrix through the contact conductance surfaces S_c is

$$\int_{S_c} \mathbf{q} \cdot \mathbf{n} \, dS = (n_p V_T) Q \,. \tag{3.3.2}$$

We then substitute (3.3.2) into (3.2.3) to find that

$$\int_{V_m} \rho_m \, c_m \partial_t T_m \, dV + \int_{S_e} \mathbf{q} \cdot \mathbf{n} \, dS + (n_p V_T) Q = 0 \,. \tag{3.3.3}$$

We now approximate the remaining surface integral in (3.3.3). First, a rectangular element is created in a x-y-z Cartesian coordinate system with dimensions $\Delta x \times \Delta y \times \Delta z$, as seen in Figure 3.1. The surface integral of (3.3.3) is then

$$\int_{S_e} \mathbf{q} \cdot \mathbf{n} \, dS = \underset{\substack{\text{front}\\ \text{face}}}{\int} q_x dS - \underset{\substack{\text{back}\\ \text{face}}}{\int} q_x dS + \underset{\substack{\text{right}\\ \text{face}}}{\int} q_y dS - \underset{\substack{\text{left}\\ \text{face}}}{\int} q_y dS + \underset{\substack{\text{top}\\ \text{face}}}{\int} q_z dS - \underset{\substack{\text{bottom}\\ \text{face}}}{\int} q_z dS \,, \tag{3.3.4}$$

where the faces are the external surfaces bounding the matrix, and $\mathbf{q} = q_x \mathbf{i} + q_y \mathbf{j} + q_z \mathbf{k}$ for $\mathbf{i}$, $\mathbf{j}$, and $\mathbf{k}$ being the unit vectors associated with the x, y, and z coordinates, respectively.

The integrals in (3.3.4) now need to be approximated. The particles significantly affect the *integrands* in (3.3.4) because the particles affect the local heat transfer in the matrix. Consequently, approximating the integrands with the influence of the particles taken into account is difficult and, in fact, beyond the scope of this paper. Instead of making a local assumption about the *integrands* and then integrating those expressions, we will make a global assumption

about how the particles affect the *integrals*. We assume that the particles do not influence the integrals of (3.3.4) significantly, such that we regard the integrands as being determined by Fourier's law (2.6.1) for the matrix, as if the particles do not affect the heat transfer through the external surfaces bounding the matrix. This means that we approximate (3.3.4) as

$$\int_{S_e} \mathbf{q}\cdot\mathbf{n}\,dS = \left((Aq_x)\Big|_{\substack{front\\face}} - (Aq_x)\Big|_{\substack{back\\face}}\right) + \left((Aq_y)\Big|_{\substack{right\\face}} - (Aq_y)\Big|_{\substack{left\\face}}\right) + \left((Aq_z)\Big|_{\substack{top\\face}} - (Aq_z)\Big|_{\substack{bottom\\face}}\right), \quad (3.3.5)$$

where every A in (3.3.5) is the area of its respective face, and all of the heat fluxes in (3.3.5) are determined by (2.6.1) for the matrix.

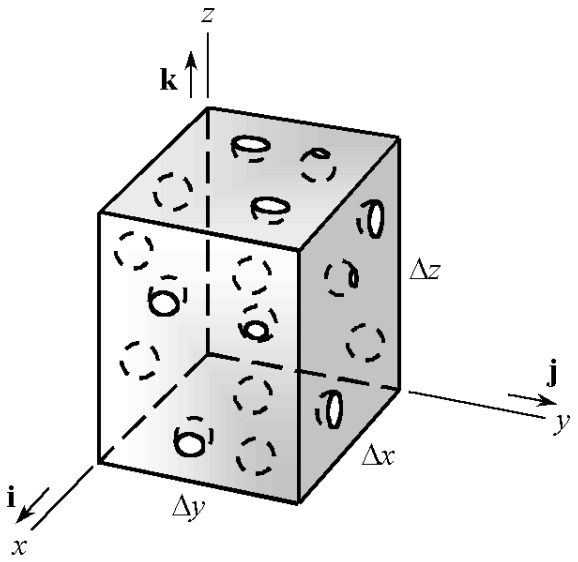

Figure 3.1: Typical Rectangular Element of Composite

Before we continue approximating (3.3.5), we desire to justify our assumption that we can ignore the influence of the particles on the integrals in (3.3.4). Now, the particles cause variations in **q** at the external surfaces bounding the matrix of the element of Figure 3.1. However, when we assume that the particles do not affect the integrals of (3.3.4) significantly, we are really assuming that the *sum* of the variations in **q** at the surfaces bounding the matrix is negligible. This assumption seems reasonable from a physical standpoint. We remind ourselves that the multitude of particles randomly dispersed around all surfaces of the element of Figure 3.1 all have roughly the same heat flux q_μ. Therefore, it seems reasonable to assume that the contribution to any integral in (3.3.4) from the particles *inside* the element and near the bounding

surface S_e is significantly reduced by the contribution due to the particles *outside* the element and near S_e. Therefore, we are somewhat justified in ignoring the influence of the particles on the integrals in (3.3.4).

We now continue to approximate (3.3.5) even further. In Appendix A, we show that, when a plane intersects our composite, the area of intersection between the plane and the matrix is a fraction $(1-n_p v_p)$ of the area of intersection between the plane and the composite (matrix and particles). Equation (A.2.5) is used to determine the matrix areas in (3.3.5), by comparing Figure 3.1 to Figure A.1 and by using the dimensions Δx, Δy, and Δz of Figure 3.1. According to (A.2.5), (3.3.5) is approximated as

$$\begin{aligned}\int_{S_e} \mathbf{q}\cdot\mathbf{n}\,dS = {} & (1-n_p v_p)\Delta y\Delta z\left(q_x\Big|_{\substack{front\\face}} - q_x\Big|_{\substack{back\\face}}\right) + (1-n_p v_p)\Delta x\Delta z\left(q_y\Big|_{\substack{right\\face}} - q_y\Big|_{\substack{left\\face}}\right) \\ & + (1-n_p v_p)\Delta x\Delta y\left(q_z\Big|_{\substack{top\\face}} - q_z\Big|_{\substack{bottom\\face}}\right)\end{aligned}. \tag{3.3.6}$$

We rearrange (3.3.6) to obtain

$$\int_{S_e} \mathbf{q}\cdot\mathbf{n}\,dS = (1-n_p v_p)\Delta x\Delta y\Delta z\left\{\frac{q_x\Big|_{\substack{front\\face}} - q_x\Big|_{\substack{back\\face}}}{\Delta x} + \frac{q_y\Big|_{\substack{right\\face}} - q_y\Big|_{\substack{left\\face}}}{\Delta y} + \frac{q_z\Big|_{\substack{top\\face}} - q_z\Big|_{\substack{bottom\\face}}}{\Delta z}\right\}. \tag{3.3.7}$$

Because $V_T = \Delta x\Delta y\Delta z$ for Figure 3.1, the volume relation in (2.5.2) can be used to show that

$$\int_{S_e} \mathbf{q}\cdot\mathbf{n}\,dS = V_m\left\{\frac{q_x\Big|_{\substack{front\\face}} - q_x\Big|_{\substack{back\\face}}}{\Delta x} + \frac{q_y\Big|_{\substack{right\\face}} - q_y\Big|_{\substack{left\\face}}}{\Delta y} + \frac{q_z\Big|_{\substack{top\\face}} - q_z\Big|_{\substack{bottom\\face}}}{\Delta z}\right\}. \tag{3.3.8}$$

In the limit of Δx, Δy, and $\Delta z \to 0$, (3.3.8) becomes

$$\int_{S_e} \mathbf{q}\cdot\mathbf{n}\,dS = V_m\left\{\frac{\partial q_x}{\partial x} + \frac{\partial q_y}{\partial y} + \frac{\partial q_z}{\partial z}\right\}, \tag{3.3.9}$$

which is recognized to be

$$\int_{S_e} \mathbf{q}\cdot\mathbf{n}\,dS = V_m \nabla\cdot\mathbf{q}, \tag{3.3.10}$$

where $\mathbf{q}$ is determined from (2.6.1) for the matrix.

When we substitute (3.3.1) and (3.3.10) into (3.3.3), we find that the energy equation for the matrix is approximately

$$\int_{V_m} \rho_m c_m \partial_t T_m \, dV + V_m \nabla \cdot \mathbf{q} + (n_p a_p V_T) q_\mu = 0 . \tag{3.3.11}$$

Then, substitution of (2.5.2) into (3.3.11) yields

$$\int_{V_m} \rho_m c_m \partial_t T_m \, dV + V_m \nabla \cdot \mathbf{q} + \frac{n_p a_p}{1 - n_p v_p} V_m \, q_\mu = 0 . \tag{3.3.12}$$

After division by V_m and taking the limit as $V_m \to 0$, the previous equation becomes

$$\rho_m c_m \partial_t T_m + \nabla \cdot \mathbf{q} + \frac{n_p a_p}{1 - n_p v_p} q_\mu = 0 . \tag{3.3.13}$$

For spherical particles, we also know that the surface area and volume are related by

$$a_p = \frac{3 v_p}{R} . \tag{3.3.14}$$

Substitution of (3.3.14) into (3.3.13) yields

$$\rho_m c_m \partial_t T_m + \nabla \cdot \mathbf{q} + \frac{3}{R} \frac{n_p v_p}{1 - n_p v_p} q_\mu = 0 . \tag{3.3.15}$$

We now simplify (3.3.15) by making use of our constitutive heat transfer equations, (2.6.1) and (2.6.2). Equation (2.6.1) for the matrix is first substituted into (3.3.15) to give

$$\partial_t T_m - \alpha_m \nabla^2 T_m + \frac{3}{R} \frac{1}{\rho_m c_m} \frac{n_p v_p}{1 - n_p v_p} q_\mu = 0 , \tag{3.3.16}$$

where

$$\alpha_m = \frac{k_m}{\rho_m c_m} \tag{3.3.17}$$

and is recognized as the matrix thermal diffusivity. Then, we find that

$$\partial_t T_m - \alpha_m \nabla^2 T_m + \frac{3}{R} \frac{\mu}{\rho_m c_m} \frac{n_p v_p}{1 - n_p v_p} (T_m - T_p(R)) = 0 , \tag{3.3.18}$$

when (2.6.2) is substituted into (3.3.16).

Equation (3.3.18) is the heat equation for the composite medium. We note that it contains the particle temperature $T_p(R)$ at the contact surfaces; thus, (3.3.18) constitutes one equation for the two variables T_m and $T_p(R)$ at space **x** and time *t*. In the next chapter, we will substitute an expression for $T_p(R)$ into (3.3.18) to obtain a heat equation for the composite that involves *only* the matrix temperature as the dependent variable.

Chapter 4

Generation of General Matrix Temperature Equation – Part II

4.1 Introduction

The generation of the general matrix temperature equation begun in Chapter 3 is finished in this chapter. In this chapter, we use our general energy equation (3.3.18) to generate the general integro-differential equation that governs non-dimensional matrix temperature, out of which two non-dimensional parameters are produced. The physical significances of these parameters are described and then limits on the two parameters and set based on physical values. After two time scales are found based on physical processes, the time scales are used to non-dimensionalize the general integro-differential equation. Finally, we produce a general differential equation that governs the matrix temperature.

4.2 Derivation of General Integro-Differential Equation for Matrix Temperature

We now begin to use (3.3.18) to generate the general integro-differential equation that governs matrix temperature. We start by partially non-dimensionalizing our general energy equation (3.3.18) with respect to temperature by defining

$$\theta_m = \frac{T_m - T_m^0}{T_{ref}} \text{ and } \theta_p = \frac{T_p - T_p^0}{T_{ref}}, \tag{4.2.1}$$

where T_{ref} is a given reference temperature and θ_m and θ_p are the non-dimensional matrix and particle temperatures, respectively. Equation (3.3.18) now becomes

$$\partial_t \theta_m - \alpha_m \nabla^2 \theta_m + \frac{3}{R} \frac{\mu}{\rho_m c_m} \frac{n_p v_p}{1 - n_p v_p} (\theta_m - \theta_p(R) - \Delta\theta_0) = 0, \tag{4.2.2}$$

where

$$\Delta\theta_0 = \frac{T_p^0 - T_m^0}{T_{ref}}, \tag{4.2.3}$$

and the initial condition (2.3.1) becomes

$$\theta_p = \theta_m = 0 \text{ at } t = 0 \tag{4.2.4}$$

for all material points.

Thus far, our general equation (4.2.2) contains *both* $\theta_p(R)$ and θ_m, but we desire to have a general equation that contains *only* the non-dimensional matrix temperature θ_m. Consequently, we need to find how $\theta_p(R)$ depends on θ_m, or more specifically, the time history of θ_m. This step is completed in Appendix C by using the Laplace transform. In order to use the results from Appendix C, we need to transform the general equation (4.2.2) by using the Laplace transform. The Laplace transform of a function is defined in Appendix B. Using properties (B.2.1) and (B.2.3) of the Laplace transform along with the formulas (B.3.1) and (B.3.4), we take the Laplace transform of (4.2.2) to find that

$$s\overline{\theta}_m - \theta_m\big|_{t=0} - \alpha_m \nabla^2 \overline{\theta}_m + \frac{3}{R}\frac{\mu}{\rho_m c_m}\frac{n_p v_p}{1 - n_p v_p}(\overline{\theta}_m - \overline{\theta}_p(R) - \overline{\Delta\theta_0}) = 0, \tag{4.2.5}$$

where an overbar denotes the Laplace transform of the function, s is the independent variable for the Laplace domain, and $\theta_m\big|_{t=0}$ is the initial value of the matrix temperature θ_m. Because θ_m is initially zero, according to the initial condition (4.2.4), we find that (4.2.5) is

$$s\overline{\theta}_m - \alpha_m \nabla^2 \overline{\theta}_m + \frac{3}{R}\frac{\mu}{\rho_m c_m}\frac{n_p v_p}{1 - n_p v_p}(\overline{\theta}_m - \overline{\theta}_p(R) - \overline{\Delta\theta_0}) = 0. \tag{4.2.6}$$

In Appendix C, we have determined the relationship between $\overline{\theta}_p(R)$ and $\overline{\theta}_m$. When we substitute the relation (C.2.12) from Appendix C into (4.2.6), we find after some rearrangement that

$$\begin{aligned} &s\overline{\theta}_m - \alpha_m\nabla^2\overline{\theta}_m + \frac{k_p}{\mu}\left(m\coth mR - \frac{1}{R}\right)(s\overline{\theta}_m - \alpha_m\nabla^2\overline{\theta}_m) \\ &+ \frac{3}{R}\frac{k_p}{\rho_m c_m}\frac{n_p v_p}{1 - n_p v_p}\left(m\coth mR - \frac{1}{R}\right)(\overline{\theta}_m - \overline{\Delta\theta_0}) = 0 \end{aligned}, \tag{4.2.7}$$

where

$$m = \sqrt{s/\alpha_p}. \tag{4.2.8}$$

We recognize (4.2.7) as the Laplace transform of the general non-dimensional matrix temperature equation. As desired, $\bar{\theta}_m$ is the only Laplace-transformed dependent variable in the equation. We can now invert the equation to find the general equation governing θ_m. Using the inverses (D.3.12) and (D.4.8) in Appendix D, we invert (4.2.7) to find that, after considerable rearrangement,

$$\begin{aligned}&\Phi_2\left(\partial_t\theta_m-\alpha_m\nabla^2\theta_m+\frac{6\Phi_1}{\tau_p}\int_0^t\Psi(t-\tau)\partial_t\theta_m d\tau\right)+2\int_0^t\Psi(t-\tau)\partial_t(\partial_t\theta_m-\alpha_m\nabla^2\theta_m)d\tau\\&+2\left(\partial_t\theta_m\big|_{t=0}-\frac{3\Phi_1\Phi_2}{\tau_p}\Delta\theta_0\right)\Psi(t)=0\end{aligned}\quad,\qquad(4.2.9)$$

where

$$\Phi_1=\frac{\rho_p\,c_p}{\rho_m\,c_m}\frac{n_p v_p}{1-n_p v_p}\qquad(4.2.10)$$

and

$$\Phi_2=\mu R/k_p\qquad(4.2.11)$$

are two non-dimensional parameters,

$$\tau_p=R^2/\alpha_p\qquad(4.2.12)$$

is the time scale associated with the particles,

$$\alpha_p=k_p/\rho_p c_p\qquad(4.2.13)$$

is the thermal diffusivity of the particulate material, and

$$\Psi(\eta)=\sum_{n=1}^{\infty}e^{-n^2\pi^2\eta/\tau_p}\,,\qquad(4.2.14)$$

which is related to the theta function of the third kind [18].

Equation (4.2.9) is the general integro-differential equation for matrix temperature, but it contains the unknown initial value $\partial_t\theta_m\big|_{t=0}$ of the function $\partial_t\theta_m$. In order to determine $\partial_t\theta_m\big|_{t=0}$, we start by manipulating the general equation (4.2.2). With some rearrangement, the general equation (4.2.2) can be shown to be

$$\partial_t\theta_m-\alpha_m\nabla^2\theta_m+\frac{3\Phi_1\Phi_2}{\tau_p}(\theta_m-\theta_p(R)-\Delta\theta_0)=0\qquad(4.2.15)$$

through use of the definitions of τ_p, Φ_1, and Φ_2. Next, we take the limit of (4.2.15) as time approaches zero. The Laplacian term $\nabla^2\theta_m$, matrix temperature θ_m, and particle surface temperature $\theta_p(R)$ are all zero at zero time, according to the initial condition (4.2.4). Because those three terms vanish as time approaches zero, we find that

$$\partial_t\theta_m - \frac{3\Phi_1\Phi_2}{\tau_p}\Delta\theta_0 = 0 \text{ at } t = 0. \tag{4.2.16}$$

In other words,

$$\partial_t\theta_m\big|_{t=0} = \frac{3\Phi_1\Phi_2}{\tau_p}\Delta\theta_0. \tag{4.2.17}$$

Thus, because $\Delta\theta_0$ is known, the initial rate of matrix temperature is determined according to (4.2.17). According to the definition of $\Delta\theta_0$ in (4.2.3), if the particles have a higher initial temperature than the matrix, then $\Delta\theta_0$ is positive. Consequently, the initial matrix temperature rate $\partial_t\theta_m\big|_{t=0}$ is *positive* when the particles are initially hotter than the matrix. Because the particles would transfer heat to the matrix in such a situation, it makes sense that the matrix would initially increase in temperature.

Substitution of the initial temperature rate (4.2.17) into (4.2.9) yields our general equation governing matrix temperature,

$$\Phi_2\left(\partial_t\theta_m - \alpha_m\nabla^2\theta_m + \frac{6\Phi_1}{\tau_p}\int_0^t \Psi(t-\tau)\partial_t\theta_m d\tau\right) + 2\int_0^t \Psi(t-\tau)\,\partial_t(\partial_t\theta_m - \alpha_m\nabla^2\theta_m)d\tau = 0. \tag{4.2.18}$$

Equation (4.2.18) is the general integro-differential equation for matrix temperature that will be used for analysis in this thesis. The equation was derived by using the problem formulation in Chapter 2, which includes the initial condition (2.3.1) that the uniform matrix and particles temperatures may differ. Consequently, the general matrix temperature equation (4.2.18) is similar to Fourier's heat equation (1.1.3) in the respect that they both only require initial matrix and particle temperatures but *not* any other initial conditions for solvability. Indeed, because (4.2.18) is based on Fourier's law (1.1.1) for heat flux within the matrix and particles, it makes sense that (4.2.18) only requires zero-order initial information.

4.3 Physical Significance of Non-Dimensional Parameters

Two non-dimensional parameters, Φ_1 and Φ_2, exist in our general integro-differential equation (4.2.18) that governs the matrix temperature in our composite. We will now determine the physical significance of both parameters.

The physical meaning of Φ_1 can be determined by manipulating its definition in (4.2.10). Multiplication and division of Φ_1 by a general composite volume V_T yields

$$\Phi_1 = \frac{\rho_p c_p n_p v_p V_T}{\rho_m c_m (1 - n_p v_p) V_T}. \tag{4.3.1}$$

According to the definitions (2.5.1) and (2.5.2) of V_p and V_m, respectively, we find that

$$\Phi_1 = \frac{\rho_p c_p V_p}{\rho_m c_m V_m}, \tag{4.3.2}$$

where V_p and V_m are the respective total particle and matrix volumes. Because mass is equal to the product of density and volume, (4.3.2) is

$$\Phi_1 = \frac{m_p c_p}{m_m c_m}, \tag{4.3.3}$$

where m_p and m_m are the total particle and matrix masses in the composite, respectively. Equation (4.3.3) means that the parameter Φ_1 is the ratio of the total thermal capacity of the particles to that of the matrix. That is, Φ_1 is a ratio of the energies required to heat up the particles and the matrix the same degree in a general composite volume. As Φ_1 increases, the particles are able to store more energy relative to the matrix.

As with Φ_1, the significance of Φ_2 can be determined by manipulating its definition. The non-dimensional parameter Φ_2 is

$$\Phi_2 = \frac{\mu R}{k_p} = \frac{\mu}{k_p / R} = \frac{\text{surface conductance}}{\text{internal conductance of solid across length } R} = \frac{\text{internal resistance of solid across length } R}{\text{surface resistance}}, \tag{4.3.4}$$

according to its definition in (4.2.11). Consequently, the parameter Φ_2 is a type of Biot number [20]. It basically represents a ratio of surface conductance to the internal conductance of the spherical particles. In other words, Φ_2 is a ratio of the internal resistance to the surface resistance of heat transfer for a particle. When $\Phi_2 << 1$, the internal resistance is much smaller than the

surface resistance, which means that the temperatures in the particle are able to become uniform much faster than the surface temperature of the particle can equilibrate with the temperature of the external matrix. On the other hand, when $\Phi_2 >> 1$, the surface conductance is much larger than the internal conductance, which means that the surface temperature of the particle is able to equilibrate with the external matrix much faster than the temperatures in the particle become uniform.

4.4 Ranges for Non-Dimensional Parameters

Now that we have described the physical significances of the non-dimensional parameters in the general equation (4.2.18) for matrix temperature, we will now discuss the typical physical ranges for Φ_1 and Φ_2.

We can create limits for Φ_1 based on physical reasoning. First, typical ranges exist for the ratio of $\rho_p c_p$ to $\rho_m c_m$, which is the ratio of the thermal capacities, seen in the definition of Φ_1 in (4.2.10). In Table 4.1, we have recorded densities (ρ), specific heats (c), and thermal capacities (the product of ρ and c) obtained from Reference 19 for a selection of particle and matrix materials. Because the particle and matrix materials are solids, the ratios of $\rho_p c_p$ to $\rho_m c_m$ range from about 0.30 to 3.5. As a specific example, the ratio of $\rho_p c_p$ to $\rho_m c_m$ is about 3.47 for a particle made of platinum and a matrix composed of lead. Second, there is a restriction on the particle-to-matrix volume ratio $n_p v_p / (1 - n_p v_p)$ that is seen in the expression for Φ_1. Because $n_p v_p << 1$, the particle-to-matrix volume ratio is also small relative to one. After taking into account the restrictions on the two ratios, $\rho_p c_p / \rho_m c_m$ and $n_p v_p / (1 - n_p v_p)$, that constitute Φ_1, we set Φ_1 to be of $O(1)$ at most, where $O(1)$ denotes that a term neither vanishes nor becomes unbounded as a given parameter vanishes, with the understanding that Φ_1 cannot be very large compared to one.

We now need to set the range for Φ_2, the other non-dimensional parameter. According to its definition in (4.2.11), the parameter Φ_2 is the quotient of μR and k_p. Thus, possible values of μ, R, and k_p affect the limits of Φ_2. First, the particle radius R can theoretically be as small or large as possible. However, in reality, the particles have a limited size. Let us suppose that the

particles have a maximum radius R of a millimeter. Second, the particle conductivity k_p for solids ranges from about 0.05 W/m·K for foams to about 1000 W/m·K for silver at normal temperatures and pressures [19]. Third, the contact conductance μ can also be relatively large. For example, μ ranges typically from about 10,000 W/m^2·K to 25,000 W/m^2·K for copper/copper interfaces at moderate pressure and with normal finishes [24]. After taking into account the possible values of μ, R, and k_p, we find that Φ_2 can be small or large relative to one. Therefore, for the present purposes, we let Φ_2 vary between 0 and ∞.

Table 4.1: Relevant Material Constants for Several Material Candidates

Material	Density, ρ, (g/cm^3)	Specific Heat, c, (kJ/kg · K)	Thermal Capacity, ρc, (J/cm^3 · K)
Aluminum	2.72	0.90	2.43
Copper	8.95	0.38	3.40
Glass, window	2.7	0.84	2.27
Lead	11.37	0.13	1.48
Nickel	8.9	0.45	4.00
Platinum	21.4	0.24	5.14
Tin	7.3	0.23	1.68

4.5 Several Limits of General Integro-Differential Equation

We will now find how the general equation (4.2.18) governing matrix temperature limits as Φ_1 and Φ_2 approach their given limits described in the previous section.

As $\Phi_1 \to 0$, which is the lower limit of Φ_1, it can be shown that our general integro-differential equation limits to Fourier's heat equation for the matrix,

$$\partial_t \theta_m = \alpha_m \nabla^2 \theta_m . \tag{4.5.1}$$

This makes sense from a physical standpoint. The particles consume no energy relative to the matrix when Φ_1 is zero, which means that the matrix transfers no energy to the particles relative to the energy it consumes. Without heat transfer to the particles, heat approximately flows

through the matrix according to Fourier's heat equation (4.5.1), just like it does without any particles in the matrix.

Because no definite upper limit was set for Φ_1, we will not take the limit of the general equation (4.2.18) as Φ_1 approaches an upper limit. Nonetheless, we suspect that as Φ_1 increases, the ability of the particles to influence the matrix temperature increases, because the particles are able to consume more energy relative to the matrix as Φ_1 increases.

In the previous section, we set definite lower and upper limits for the non-dimensional parameter Φ_2, which means that we can take the limit of the general equation (4.2.18) as Φ_2 approaches each limit. As $\Phi_2 \to \infty$, which is the upper limit, we obtain the equation for "perfect contact",

$$\partial_t \theta_m - \alpha_m \nabla^2 \theta_m + \frac{6\Phi_1}{\tau_p} \int_0^t \Psi(t-\tau) \partial_t \theta_m d\tau = 0 . \tag{4.5.2}$$

Equation (4.5.2) corresponds to "perfect contact" because μ becomes infinite for perfect contact as $\Phi_2 \to \infty$, according to (4.2.11).

The limit of the general equation (4.2.18) as Φ_2 approaches its lower limit of zero is possible but will not be done in this section. Instead, we will take the limit after we finish non-dimensionalizing (4.2.18) and convert the equation into a purely differential form. In fact, the limit is performed in the next chapter, which is devoted to the special limit of the general equation as $\Phi_2 \to 0$.

4.6 Time Scales

As stated in the previous section, we desire to finish non-dimensionalizing the general equation (4.2.18) that governs the matrix temperature. The general equation contains non-dimensional temperatures, but time and space have not been non-dimensionalized. We will now find time scales that will be used to fully non-dimensionalize the general integro-differential equation (4.2.18) for matrix temperature.

Any time scale can be created to non-dimensionalize (4.2.18), but we want to use time scales associated with physical processes. At this point, we already found one natural time scale

called τ_p, which is the time scale associated with the spherical particles. However, there is another natural time scale for our composite medium. There is a time scale τ_T associated with the transfer of heat between the matrix and the particles through contact layers of conductance μ. The time scale τ_T is the time required to bring the average temperature of a sphere to be roughly the same as a constant matrix temperature. Using non-dimensional temperatures described in (4.2.1), we define the time scale τ_T to be the time after which

$$\frac{1}{\nu_p}\int_{V_p}\theta_p dV = \theta_{p_{AVG}} = \frac{T_{p_{AVG}} - T_p^{\,0}}{T_{ref}} \cong \frac{T_m - T_p^{\,0}}{T_{ref}} = \theta_m - \Delta\theta_0, \tag{4.6.1}$$

where $\theta_{p_{AVG}}$ and $T_{p_{AVG}}$ are the respective average non-dimensional and dimensional particle temperatures, θ_m and T_m are the respective constant non-dimensional and dimensional matrix temperatures, and V_p is the occupied space of the sphere of volume ν_p. We call τ_T a *thermalization time*, because it basically represents the time that it takes for the matrix to heat up a particle for a given value of μ.

Equations from Appendix C can then be used to approximate τ_T, because we find how the Laplace transform $\bar{\theta}_p$ of particle temperature depends on the Laplace transform $\bar{\theta}_m$ of matrix temperature. In order to use our results from Appendix C, we take the Laplace transform of (4.6.1) to obtain

$$\frac{1}{\nu_p}\int_{V_p}\bar{\theta}_p dV \cong \bar{\theta}_m - \overline{\Delta\theta_0}, \tag{4.6.2}$$

where an overbar denotes the Laplace transform of the function. Then, upon substitution of the definition of $\bar{\theta}_p$ from (C.2.8) into (4.6.2), it can be shown that

$$\frac{C(s)}{\nu_p}\int_0^R \frac{\sinh mr}{r} 4\pi r^2 dr \cong \bar{\theta}_m - \overline{\Delta\theta_0}, \tag{4.6.3}$$

where $C(s)$ is defined in (C.2.11), m is defined in (C.2.9), and the integration is now over the dummy radius r for the sphere of outer radius R. Substitution of the definition of sphere volume ν_p into (4.6.3) along with simplification yields

$$\frac{3C(s)}{R^3}\int_0^R r\sinh mr\, dr \cong \bar{\theta}_m - \overline{\Delta\theta_0}. \tag{4.6.4}$$

The integral in (4.6.4) is known according to Equation 2.473(1) of Reference 18. When substituted into (4.6.4), we have

$$\frac{3C(s)}{R^3}\frac{mR\cosh mR-\sinh mR}{m^2}\cong\overline{\theta}_m-\overline{\Delta\theta_0}\,. \tag{4.6.5}$$

Now, substitution of the definition of $C(s)$ from (C.2.11) into (4.6.5) yields

$$\frac{3}{R^3}\frac{\overline{\theta}_m-\overline{\Delta\theta_0}}{\dfrac{k_p}{\mu R}m\cosh mR+\dfrac{1}{R}\left(1-\dfrac{k_p}{\mu R}\right)\sinh mR}\frac{mR\cosh mR-\sinh mR}{m^2}\cong\overline{\theta}_m-\overline{\Delta\theta_0}\,. \tag{4.6.6}$$

Using the definition of Φ_2 from (4.2.11), we can show after much rearrangement that (4.6.6) is

$$\frac{3\Phi_2}{m^2R^2}\frac{mR\cosh mR-\sinh mR}{mR\cosh mR+(\Phi_2-1)\sinh mR}\cong 1\,. \tag{4.6.7}$$

Finally, (4.6.7) becomes

$$\frac{3\Phi_2}{s\tau_p}\frac{\sqrt{s\tau_p}\cosh\sqrt{s\tau_p}-\sinh\sqrt{s\tau_p}}{\sqrt{s\tau_p}\cosh\sqrt{s\tau_p}+(\Phi_2-1)\sinh\sqrt{s\tau_p}}\cong 1\,. \tag{4.6.8}$$

after substitution of the definition of m from (C.2.9) and utilization of the definition of the particle time scale τ_p from (4.2.12).

We now use (4.6.8) to solve for the thermalization time τ_T. Because the thermalization time τ_T is somehow related to the contact conductance μ, the time scale τ_T must be related to the parameter Φ_2, defined in (4.2.11), that contains the parameter μ. It then seems reasonable to attempt to solve for τ_T for different orders of Φ_2. If $\Phi_2 << 1$, then (4.6.8) becomes

$$\frac{3\Phi_2}{s\tau_p}\cong 1\,. \tag{4.6.9}$$

To determine the thermalization time τ_T from (4.6.9), we need to relate the Laplacian variable s to the thermalization time τ_T. To find such a relation, we need to show when the approximation in (4.6.2) is valid. By using the definition (B.1.1) of the Laplace transform, we can show that (4.6.2) holds when

$$s\cong\frac{1}{\tau_T} \tag{4.6.10}$$

for constant non-dimensional matrix temperature θ_m. Substitution of (4.6.10) into (4.6.9) yields

$$\tau_T = \frac{\tau_p}{3\Phi_2} \tag{4.6.11}$$

for $\Phi_2 << 1$. On the other hand, if $\Phi_2 >> 1$, then (4.6.8) becomes

$$\frac{3}{s\tau_p \sinh\sqrt{s\tau_p}} \cong 1. \tag{4.6.12}$$

Using (4.6.10), we find from (4.6.12) that

$$\tau_T \cong \tau_p \tag{4.6.13}$$

for $\Phi_2 >> 1$. In order for (4.6.8) to hold for all Φ_2, we let the thermalization time τ_T be approximately

$$\tau_T = \begin{cases} \dfrac{\tau_p}{3\Phi_2}, & \Phi_2 << 1 \\ \tau_p, & \Phi_2 \text{ otherwise} \end{cases}, \tag{4.6.14}$$

according to (4.6.11) and (4.6.13).

We have just shown how the time τ_T it takes for the matrix to roughly heat up the particles varies with Φ_2. The parameter Φ_2 controls the thermalization time τ_T. When $\Phi_2 << 1$, the piecewise function (4.6.14) reveals that $\tau_p << \tau_T$. This affirms our statement in Section 4.3 that, when $\Phi_2 << 1$, the internal resistance of the particle, such as τ_p, is much *smaller* than the surface resistance, such as τ_T. On the other hand, when Φ_2 of order one or greater, the piecewise function (4.6.14) reveals that τ_T is approximately equal to τ_p. This means that the thermalization time τ_T mainly depends on the particle properties, such as τ_p, and *not* the contact surface properties, such as Φ_2, in such a case. In other words, unlike when $\Phi_2 << 1$, the internal resistance is *not* much smaller than the surface resistance when Φ_2 is around one or greater.

Our original motivation for investigating the thermalization time τ_T was to find a natural time scale, besides the particle time scale τ_p, that we could use to non-dimensionalize our general matrix temperature equation (4.2.18). According to the piecewise function (4.6.14) for the thermalization time τ_T, we can produce another natural time scale by dividing τ_p by the parameter Φ_2. At this point, we define another time scale τ_μ by letting

$$\tau_\mu = \frac{\tau_p}{3\Phi_2}, \tag{4.6.15}$$

which means that (4.6.14) becomes

$$\tau_T = \begin{cases} \tau_\mu, \Phi_2 << 1 \\ \tau_p, \Phi_2 \text{ otherwise} \end{cases}. \tag{4.6.16}$$

We now have two different time scales (τ_p and τ_μ) that are based on physical processes and will be used in the next section to finish our non-dimensionalization of the general matrix temperature equation (4.2.18).

4.7 Creation of Non-Dimensional Integro-Differential Equation

We now non-dimensionalize the general integro-differential equation (4.2.18) for matrix temperature. The two natural time scales (τ_p and τ_μ) will now be used to non-dimensionalize *both* space and time in our general equation. We could use a natural length, like the particle radius *R*, to non-dimensionalize space, but instead, we choose to create length scales by using the thermal conductivity α_m of the matrix and our two time scales. We let our two sets of non-dimensional variables be

$$\hat{t} = \frac{t}{\tau_\mu} \text{ and } \hat{x}_i = \frac{x_i}{\sqrt{\alpha_m \tau_\mu}}, \tag{4.7.1}$$

and

$$\tilde{t} = \frac{t}{\tau_p} \text{ and } \tilde{x}_i = \frac{x_i}{\sqrt{\alpha_m \tau_p}}, \tag{4.7.2}$$

where *i* ranges from 1 to 3, and x_1, x_2, and x_3 are the given independent spatial coordinates. The non-dimensional variables in (4.7.1) that contain τ_μ are convenient to use when $\Phi_2 << 1$, because the thermalization time τ_T is equal to τ_μ for that case, according to the piecewise function (4.6.16). On the other hand, when Φ_2 is not much less than one, the thermalization time τ_T is approximately equal to τ_p, which means that the non-dimensional variables in (4.7.2) that contain τ_p are convenient to use in such a case.

The two sets of non-dimensional variables in (4.7.1) and (4.7.2) can be used to non-dimensionalize the general integro-differential equation (4.2.18) in space and time. First, by

using the definition (4.6.15) of τ_μ and the first set (4.7.1) of non-dimensional variables, the general equation (4.2.18) and the initial condition (4.2.17) become

$$\Phi_2(\partial_{\hat{t}}\theta_m - \hat{\nabla}^2\theta_m) + 2\int_0^{\hat{t}} \mathrm{Y}(\hat{t}-\hat{\tau})\partial_{\hat{t}}(\Phi_1\theta_m + \partial_{\hat{t}}\theta_m - \hat{\nabla}^2\theta_m)d\hat{\tau} = 0 \tag{4.7.3}$$

and

$$\partial_{\hat{t}}\theta_m\big|_{\hat{t}=0} = \Phi_1\Delta\theta_0, \tag{4.7.4}$$

where

$$\mathrm{Y}(\eta) = \sum_{n=1}^{\infty} e^{-n^2\pi^2\eta/3\Phi_2}, \tag{4.7.5}$$

and $\partial_{\hat{t}}$ and $\hat{\nabla}^2$ are the non-dimensional partial differential and spatial Laplacian operators, respectively. Second, after utilization of the second set (4.7.2) of non-dimensional variables, the general equation (4.2.18) and the initial condition (4.2.17) become

$$\Phi_2\left(\partial_{\tilde{t}}\theta_m - \tilde{\nabla}^2\theta_m + 6\Phi_1\int_0^{\tilde{t}} \mathrm{Z}(\tilde{t}-\tilde{\tau})\partial_{\tilde{t}}\theta_m d\tilde{\tau}\right) + 2\int_0^{\tilde{t}} \mathrm{Z}(\tilde{t}-\tilde{\tau})\partial_{\tilde{t}}(\partial_{\tilde{t}}\theta_m - \tilde{\nabla}^2\theta_m)d\tilde{\tau} = 0 \tag{4.7.6}$$

and

$$\partial_{\tilde{t}}\theta_m\big|_{\tilde{t}=0} = 3\,\Phi_1\Phi_2\,\Delta\theta_0, \tag{4.7.7}$$

where

$$\mathrm{Z}(\eta) = \sum_{n=1}^{\infty} e^{-n^2\pi^2\eta}, \tag{4.7.8}$$

and $\partial_{\tilde{t}}$ and $\tilde{\nabla}^2$ are the non-dimensional partial differential and spatial Laplacian operators, respectively. Equations (4.7.3) are (4.7.6) are two non-dimensional forms of the general integro-differential equation (4.2.18) for non-dimensional matrix temperature θ_m. Equation (4.7.3) will be useful for finding the limit of the general heat equation as $\Phi_2 \to 0$, while (4.7.6) is useful for studying the behavior of the general heat equation for $\Phi_2 \to \infty$.

We can also find non-dimensional forms of the limits of the general equation that are seen in Section 4.5. The non-dimensional form of Fourier's heat equation (4.5.1) for the matrix becomes

$$\partial_{\hat{t}}\theta_m = \hat{\nabla}^2\theta_m \text{ and } \partial_{\tilde{t}}\theta_m = \tilde{\nabla}^2\theta_m, \tag{4.7.9}$$

according to (4.7.1) and (4.7.2), respectively. Equations (4.7.9) are convenient forms of Fourier's heat equation for the matrix, which is why the length scales seen in (4.7.1) and (4.7.2) are used. Furthermore, the "perfect contact" equation (4.5.2) for $\Phi_2 \to \infty$ also becomes

$$\partial_{\tilde{t}}\theta_m - \tilde{\nabla}^2\theta_m + 6\Phi_1\int_0^{\tilde{t}} Z(\tilde{t}-\tilde{\tau})\partial_{\tilde{\tau}}\theta_m d\tilde{\tau} = 0\,, \tag{4.7.10}$$

when (4.7.2) is used to non-dimensionalize the equation. The other non-dimensional variables in (4.7.1) are not used to non-dimensionalize the "perfect contact" equation (4.5.2) because those variables were mainly created for use with small, not large, values of Φ_2.

4.8 Derivation of a Non-Dimensional Differential Equation

We have just created two non-dimensional forms, (4.7.3) and (4.7.6), of the general equation (4.2.18) that governs matrix temperature. Furthermore, we have non-dimensionalized the known limits of the general equation as $\Phi_1 \to 0$ and $\Phi_2 \to \infty$. At this point, we still have not created the special limit of the general equation as $\Phi_2 \to 0$. To do so, we desire to create a purely differential non-dimensional equation that governs matrix temperature. Such an equation will be used in the next chapter to find the special limit of the general equation (4.2.18) as Φ_2 approaches zero.

We begin by rearranging the Laplace transform (4.2.7) of the general heat equation. Using the definitions of Φ_1, Φ_2, α_p, and τ_p, we can show after much rearrangement that (4.2.7) is

$$\tau_p(s\overline{\theta}_m - \alpha_m\nabla^2\overline{\theta}_m)(\Phi_2 - 1 + mR\coth mR) + 3\Phi_1\Phi_2(mR\coth mR - 1)(\overline{\theta}_m - \overline{\Delta\theta_0}) = 0\,. \tag{4.8.1}$$

Then, multiplication of (4.8.1) by $(\sinh mR)/mR$ yields

$$\begin{aligned}&\tau_p(s\overline{\theta}_m - \alpha_m\nabla^2\overline{\theta}_m)\left((\Phi_2 - 1)\frac{\sinh mR}{mR} + \cosh mR\right)\\ &+ 3\Phi_1\Phi_2\left(\cosh mR - \frac{\sinh mR}{mR}\right)(\overline{\theta}_m - \overline{\Delta\theta_0}) = 0\end{aligned}\,. \tag{4.8.2}$$

Next, we replace the hyperbolic-related functions in (4.8.2) by series expressions, which can be written as

$$\frac{\sinh mR}{mR} = \sum_{i=1}^{\infty} \frac{(mR)^{2(i-1)}}{(2i-1)!} = \sum_{i=1}^{\infty} \frac{(s\tau_p)^{i-1}}{(2i-1)!} \tag{4.8.3}$$

and

$$\cosh mR = \sum_{i=1}^{\infty} \frac{(2i-1)(mR)^{2(i-1)}}{(2i-1)!} = \sum_{i=1}^{\infty} \frac{(2i-1)(s\tau_p)^{i-1}}{(2i-1)!}, \tag{4.8.4}$$

where the respective definitions of m and τ_p in (4.2.8) and (4.2.12) have been utilized [18]. With some rearrangement, substitution of the series expressions (4.8.3) and (4.8.4) into (4.8.2) yields

$$\sum_{i=1}^{\infty} \frac{(\tau_p)^{i-1}}{(2i-1)!} \{\tau_p(\Phi_2 + 2(i-1))(s^i \overline{\theta}_m - \alpha_m s^{i-1} \nabla^2 \overline{\theta}_m) + 6\Phi_1\Phi_2(i-1)s^{i-1}(\overline{\theta}_m - \overline{\Delta\theta_0})\} = 0. \tag{4.8.5}$$

We can now invert (4.8.5) to obtain a differential equation governing the matrix temperature. By using the formula (B.3.2) for the Laplace transform of differentiated functions, we can show that

$$\begin{aligned} &\sum_{i=1}^{\infty} \frac{(\tau_p)^{i-1}}{(2i-1)!} [\tau_p(\Phi_2 + 2(i-1))(L\{\partial_t{}^i \theta_m\} - \alpha_m L\{\partial_t{}^{i-1} \nabla^2 \theta_m\}) + 6\Phi_1\Phi_2(i-1)L\{\partial_t{}^{i-1}\theta_m\}] \\ &+ O(s^0, s^1, s^2, s^3, ...) = 0 \end{aligned}, \tag{4.8.6}$$

where $L\{F(t)\}$ denotes the Laplace transform of the general function $F(t)$, and $O(X^n)$ denotes a term that is proportional to X^n for a general variable X and parameter n, i.e., $O(X^n)$ denotes a term "of order n in X." The terms in s of order zero or greater in (4.8.6) depend on the initial conditions for the matrix, including all orders of differentiation of the matrix temperature. Now, when we invert (4.8.6), we find that

$$\sum_{i=1}^{\infty} \frac{(\tau_p)^{i-1}}{(2i-1)!} [\tau_p(\Phi_2 + 2(i-1))(\partial_t{}^i \theta_m - \alpha_m \partial_t{}^{i-1} \nabla^2 \theta_m) + 6\Phi_1\Phi_2(i-1)\partial_t{}^{i-1}\theta_m] = 0 \tag{4.8.7}$$

for all positive time. A little rearranging yields the general differential equation governing matrix temperature,

$$\sum_{i=1}^{\infty} \frac{(\tau_p)^{i-1}}{(2i-1)!} \partial_t{}^{i-1} \{\tau_p(\partial_t \theta_m - \alpha_m \nabla^2 \theta_m)(\Phi_2 + 2(i-1)) + 6\Phi_1\Phi_2(i-1)\theta_m\} = 0. \tag{4.8.8}$$

It must be noted that the inverses of the terms of order zero in s are not seen in the differential equation (4.8.8) for *positive* time because the inverses are Dirac delta functions, which only exist at *zero* time [22]. Similarly, the terms in s of order one or greater do not affect the inversion of (4.8.6) to the positive-time equation (4.8.8) because their inverses only affect the

equation at zero time. Consequently, unlike the general integro-differential equation (4.2.18), the general differential equation (4.8.8) does *not* hold for zero time. However, the general differential equation does hold for zero time in a limiting sense.

Finally, we non-dimensionalize (4.8.8) by using the first set (4.7.1) and second set (4.7.2) of non-dimensional variables to obtain

$$\sum_{i=1}^{\infty} \frac{(3\Phi_2)^{i-1}}{(2i-1)!} \partial_{\hat{t}}^{\,i-1} \{(\partial_{\hat{t}} \theta_m - \hat{\nabla}^2 \theta_m)(\tfrac{1}{2}\Phi_2 + i - 1) + \Phi_1 (i-1)\, \theta_m\} = 0 \tag{4.8.9}$$

and

$$\sum_{i=1}^{\infty} \frac{1}{(2i-1)!} \partial_{\tilde{t}}^{\,i-1} \{(\partial_{\tilde{t}} \theta_m - \tilde{\nabla}^2 \theta_m)(\Phi_2 + 2(i-1)) + 6\Phi_1\Phi_2 (i-1)\, \theta_m\} = 0\,, \tag{4.8.10}$$

respectively.

Equations (4.8.9) and (4.8.10) are two forms of the general non-dimensional differential equation that governs matrix temperature θ_m. They are basically equivalent to both (4.7.3) and (4.7.6), two forms of the general non-dimensional integro-differential equation, except for the fact that the differential equations only hold for positive time while the integro-differential equations hold for zero time, as well.

4.9 Conclusions

We have finished generating the general matrix temperature equation begun in Chapter 3. In this chapter, we used the general energy equation (3.3.18) and results from appendices of this thesis to generate the general integro-differential equation (4.2.18) that governs non-dimensional matrix temperature. It was determined that, like Fourier's heat equation, our general equation (4.2.18) only depends on the initial composite temperatures and *not* on any other initial conditions like temperature rates.

Two non-dimensional parameters (Φ_1 and Φ_2) exist in the general matrix temperature equation (4.2.18). We showed that Φ_1 is a ratio of the total thermal capacity of the particles to that of the matrix, while Φ_2 is a ratio of the internal resistance to the surface resistance of heat transfer for a particle. Using physical values, we then set limits on the values of the parameters, letting Φ_1 be of $O(1)$ at most and Φ_2 be any non-negative number. Next, we determined that the

general equation (4.2.18) limits to Fourier's heat equation as Φ_1 approaches its lower limit of zero. Also, as Φ_2 approaches infinity, it was found that (4.2.18) limits to a "perfect contact" equation. The special limit of (4.2.18) as Φ_2 approaches its lower limit of zero will be determined in the next chapter.

We also investigated the concept of a thermalization time τ_T and created another natural time scale τ_μ, which was used along with τ_p to non-dimensionalize (4.2.18). Finally, we derived a general differential equation that governs the matrix temperature. One of the non-dimensional forms of the differential equation will be used in the next chapter to investigate the special limit of $\Phi_2 \to 0$.

Chapter 5

The Damped Telegraph Equation

5.1 Introduction

We already know that the general integro-differential equation (4.2.18) reduces to Fourier's heat equation (4.5.1) when $\Phi_1 \to 0$ and reduces to the "perfect contact" equation (4.5.2) when $\Phi_2 \to \infty$. In this chapter, the general differential equation (4.8.9) is used to show that the general equation limits to a *damped telegraph equation* when $\Phi_2 \to 0$. It will be shown that the damped telegraph equation has the same form as the dual-phase-lag equation seen in Chapter 1 and is identical to the two-step equation (1.4.6) derived by Vick and Scott [17].

5.2 Generation of Damped Telegraph Equation

We desire to find the limit of the general matrix temperature equation as $\Phi_2 \to 0$. To take the limit, we can use any form of the general matrix temperature equation that we desire. We choose to use one of the non-dimensional, purely differential forms that were created in Chapter 4. In other words, we choose to use either (4.8.9) or (4.8.10), which are equivalent to each other but contain different non-dimensional variables. In order to choose between (4.8.9) and (4.8.10), we remember that the thermalization time τ_T is approximately equal to τ_μ when $\Phi_2 << 1$, according to (4.6.16). Because $\Phi_2 << 1$ is true when $\Phi_2 \to 0$, it makes sense to use the differential equation containing τ_μ. Consequently, we decide to limit the differential form (4.8.9) as $\Phi_2 \to 0$.

A damped telegraph equation will now be generated by limiting the general differential equation (4.8.9) for our composite as $\Phi_2 \to 0$. We first recognize that we may rewrite (4.8.9) as

$$(\partial_{\hat{t}}\theta_m - \hat{\nabla}^2\theta_m)\tfrac{1}{2}\Phi_2 + \frac{3\Phi_2}{3!}\partial_{\hat{t}}((\partial_{\hat{t}}\theta_m - \hat{\nabla}^2\theta_m)(\tfrac{1}{2}\Phi_2 + 1) + \Phi_1\theta_m) + O({\Phi_2}^2) = 0 \qquad (5.2.1)$$

for Φ_1 of $O(1)$ at most, according to our limit set in Section 4.4. We then obtain

$$(\partial_{\hat{t}}\theta_m - \hat{\nabla}^2\theta_m) + \partial_{\hat{t}}((\partial_{\hat{t}}\theta_m - \hat{\nabla}^2\theta_m)(\tfrac{1}{2}\Phi_2 + 1) + \Phi_1\theta_m) + O(\Phi_2) = 0\,, \qquad (5.2.2)$$

after division by $\frac{1}{2}\Phi_2$. Next, we found that if we let

$$\partial_{\hat{t}}, \hat{\nabla}^2, \Phi_1 = O(1) \text{ and } \Phi_2 << 1\,, \qquad (5.2.3)$$

then (5.2.2) becomes

$$(\partial_{\hat{t}}\theta_m - \hat{\nabla}^2\theta_m) + \partial_{\hat{t}}((\partial_{\hat{t}}\theta_m - \hat{\nabla}^2\theta_m) + \Phi_1\theta_m) + O(\Phi_2) = 0 \qquad (5.2.4)$$

when we collect all terms of similar order. Neglecting higher order terms in (5.2.4) yields

$$(1 + \Phi_1)\partial_{\hat{t}}\theta_m + \partial_{\hat{t}\hat{t}}\theta_m = \hat{\nabla}^2\theta_m + \partial_{\hat{t}}\hat{\nabla}^2\theta_m\,. \qquad (5.2.5)$$

Equation (5.2.5), known as the *damped telegraph equation* (DTE), becomes exact as $\Phi_2 \to 0$ with Φ_1 and all derivatives being bounded. We refer to (5.2.5) as the damped telegraph equation because it is a form of the telegraph equation (1.2.2) with an additional third-order mixed-derivative term on the right-hand side that eliminates the possibility of sharp wave-fronts.

5.3 Initial Conditions for DTE

The initial conditions of the damped telegraph equation (5.2.5) are the same as those for the general equations used to generate the DTE. Even as $\Phi_2 \to 0$, all initial conditions still hold. Given the initial non-dimensional temperature (4.2.4) and non-dimensional temperature rate (4.7.4), we then have that

$$(1 + \Phi_1)\partial_{\hat{t}}\theta_m + \partial_{\hat{t}\hat{t}}\theta_m = \hat{\nabla}^2\theta_m + \partial_{\hat{t}}\hat{\nabla}^2\theta_m\,, \qquad (5.3.1)$$

where

$$\theta_m = 0 \text{ and } \partial_{\hat{t}}\theta_m = \Phi_1\Delta\theta_0 \text{ at } t = 0\,, \qquad (5.3.2)$$

and $\Delta\theta_0$ is defined in (4.2.3). The damped telegraph equation (5.3.1) with initial conditions in (5.3.2) will henceforth be called the *damped telegraph model*. The damped telegraph model can be solved with any prescribed boundary conditions.

5.4 Physical Interpretation of Limit Used to Create DTE

It can be shown that the two-step equation (1.4.6) derived by Vick and Scott [17] to approximate the matrix temperature for the composite is *exactly* the same as our damped telegraph equation (5.2.5). Despite the fact that our generation of the DTE is different than theirs, the process they used must be similar to ours. Vick and Scott used a two-step model by assuming diffusion for the matrix and using a lumped-capacity approximation for energy transfer between the matrix and particles. The lumped-capacity approximation is an assumption that the temperature in each particle is *uniform*. In contrast, we did not use a two-step model to derive the damped telegraph equation. Like Vick and Scott, we assumed diffusion for the matrix. However, we took into account the details of heat transfer inside each particle by allowing temperature to *vary* in diffusive particles. After generating a general matrix temperature equation, we were only able to derive the DTE by taking the limit of the general equation as Φ_2 approaches zero. Therefore, upon comparison of our limit and Vick and Scott's assumptions, having $\Phi_2 \to 0$ must be equivalent to assuming that each particle has a uniform temperature.

When $\Phi_2 \to 0$, the temperature in a particle does indeed become uniform. The reason lies in the connection between our time scales and the parameter Φ_2. According to the piecewise function (4.6.14), $\tau_p / \tau_T \to 0$ as $\Phi_2 \to 0$. In other words, the time required for (internal) particle equilibration is *zero relative to* the time it takes for the matrix to heat the particle to (external) equilibrium with the matrix. As far as the matrix is concerned, the particles then have a *uniform temperature* because temperature variations within a particle disperse *infinitely faster than* the matrix can change the particle temperature. Thus, Vick and Scott's assumption that the particles have a "lumped", or uniform, temperature is physically realizable only when $\Phi_2 \to 0$. We then conclude that the damped telegraph equation is only valid when the particles have uniform temperatures in the limit of $\Phi_2 \to 0$.

The physical properties of the composite are also constrained in the limit of $\Phi_2 \to 0$, because the thermalization time τ_μ must be general for the DTE to be general. By using the definitions of Φ_2, τ_p, τ_μ, and α_p, we can show that

$$\frac{\mu}{R\rho_p c_p} = O(1) \tag{5.4.1}$$

in Φ_2 for a general thermalization time τ_μ. Therefore, the ratio seen in (5.4.1) must neither vanish nor become unbounded as $\Phi_2 \to 0$ in order for the DTE to be general. For constant particulate material properties, we then have that $\mu = O(R)$ for the DTE to govern matrix temperature, which means that the contact conductance μ of the contact layers between the particles and matrix must vanish with R as the particles decrease in size. On the other hand, for particles with properties that increase in size as the radius decreases, μ may become unbounded. Consequently, μ is constrained according to (5.4.1) in the limit of $\Phi_2 \to 0$, but the scale of μ in the limit is generally unknown.

5.5 Diffusive Nature of Damped Telegraph and Two-Step Models

The damped telegraph model was produced by limiting a general equation as $\Phi_2 \to 0$. Now, because the diffusive Fourier's heat flux law (1.1.1) was assumed for the whole composite, the damped telegraph model is also based on *diffusion*. Consequently, using the "lumped capacity approximation" by taking the limit of the general equation as $\Phi_2 \to 0$ does not change the diffusive nature of our composite and the DTE. The identical two-step equation (1.4.6) for our matrix-particle system that was derived by Vick and Scott [17] is then based on diffusion. First, Vick and Scott explicitly assumed diffusion for the matrix. Second, as stated in Chapter 2, the contact conductance equation (2.6.2) is based on the diffusive Fourier's law (2.6.1) for sufficiently thin films. Finally, diffusion was implicitly used for the particles through use of the lumped capacity approximation.

Because Vick and Scott [17] used the same assumptions for the matrix-particle system as those for the electron-lattice by Tzou et al. [13], the two-step equation (1.4.3) for lattice temperature is *also* based on diffusion. Even still, Tzou et al. write that the "lattice temperature in the two-step model is sensitive to the temperature rate whereas [Fourier's heat equation] is not" [13]. However, according to the initial condition (5.3.2) in the damped telegraph model, only initial *temperatures* are required, just like for Fourier's heat equation. The lattice temperature does *not* truly depend on an initial temperature rate. A more explicit statement is that the "two-step model accounts for initial temperature differences in the electrons and the

metal lattice, whereas Fourier's heat equation does not." Consequently, the double-derivative term in the left-hand side of (5.3.1) is somewhat deceiving, because it may lead one to forget that the initial temperature rate is dependent on only initial temperatures, just like with Fourier's heat equation.

5.6 Comparison of Damped Telegraph and Dual-Phase-Lag Equations

When the DTE (5.2.5) is converted to a dimensional form by using the relations (4.2.1) and (4.7.1), we find that

$$\frac{(1+\Phi_1)}{\alpha_m}\frac{\partial T_m}{\partial t}+\frac{\tau_\mu}{\alpha_m}\frac{\partial^2 T_m}{\partial t^2}=\nabla^2 T_m+\tau_\mu\frac{\partial}{\partial t}\nabla^2 T_m\,. \tag{5.6.1}$$

Like the two-step equations derived by Tzou et al. [13] and Vick and Scott [17], the damped telegraph equation (5.6.1) is a type of dual-phase-lag (DPL) equation (1.3.4),

$$\frac{1}{\alpha}\frac{\partial T}{\partial t}+\frac{\tau_q}{\alpha}\frac{\partial^2 T}{\partial t^2}=\nabla^2 T+\tau_T\frac{\partial}{\partial t}\nabla^2 T\,. \tag{5.6.2}$$

Consequently, we can equate the respective coefficients of the DTE and the DPL equation. Comparison of the general DTE (5.6.1) with the DPL equation (5.6.2) reveals that

$$\alpha=\frac{\alpha_m}{1+\Phi_1}\,, \tag{5.6.3}$$

$$\tau_q=\frac{\tau_\mu}{1+\Phi_1}\,, \tag{5.6.4}$$

and

$$\tau_T=\tau_\mu\,. \tag{5.6.5}$$

We can learn about the physical significances of the quantities α, τ_q, and τ_T in the dual-phase-lag equation because they are related to the physical parameters α_m, Φ_1, and τ_μ in the damped telegraph equation. First, the composite diffusivity α is an *effective* thermal diffusivity of the matrix. If Φ_1 is not zero, then Φ_1 is necessarily positive and the composite diffusivity α is *less than* the matrix diffusivity α_m. In other words, when the particles absorb energy from the matrix, they effectively "slow down" heat transfer in the matrix by "decreasing" its natural

thermal diffusivity. Second, the time scale τ_T in the DPL model is confirmed to be a thermalization time, specifically τ_μ. Third, because τ_q in not an independent time scale but rather depends on the thermalization time τ_μ, the time scale τ_q seems to have more of a mathematical than a physical meaning for our composite. Thus, even though the DTE has the form of a dual-phase-lag equation, it is truly a two-step equation because τ_q in not an independent time scale.

5.7 Thermal Waves

The two-step models result in non-Fourier diffusion-like conduction because the models are based on diffusion, as revealed in Section 5.5. The mixed-derivative term in the models eliminates the wavefronts caused by the hyperbolic heat equation (1.2.2), such that only diffusion-like behavior is observed. Accordingly, because the DTE (5.6.1) is identical to the two-step equation (1.4.6), the DTE smoothes the wavefronts caused by the hyperbolic heat equation (1.2.2).

Even though the DTE smoothes the wavefronts caused by the hyperbolic heat equation, perhaps the degree of smoothing might be minimal, such that the wavefronts are basically visible for a certain time. In other words, we wonder if the DTE allows for visible pseudo-wavefronts instead of the actual wavefronts caused by the hyperbolic heat equation (1.2.2). If the DTE could limit to a hyperbolic heat equation, then the smoothed wavefronts from the DTE would become visible psuedo-wavefronts during this limiting process. Now, as stated in Section 1.3 of this thesis, the DPL equation (5.6.2) reduces to the hyperbolic heat equation (1.2.2) by limiting τ_T to zero while leaving τ_q general. However, as seen in (5.6.4) and (5.6.5), the time scale τ_T cannot limit to zero without the time scale τ_q also limiting to zero. The two time scales are *not* independent for the DTE because it is a two-step equation and not a general dual-phase-lag equation. This means that the DTE cannot limit to a hyperbolic heat equation. In other words, the mixed-derivative term in the DTE (5.2.5) cannot disappear without the wave term on the left-hand side also disappearing, which would leave the DTE as a type of Fourier heat equation. The

mixed-derivative term is of the same order as the wave terms in the DTE, which means that no wavefront-like behavior should be visible.

5.8 Conclusions

In this chapter, we showed that the general matrix temperature equation (4.2.18) limits to a *damped telegraph equation* (DTE) when $\Phi_2 \to 0$. The DTE (5.2.5) has the same form as the dual-phase-lag equation seen in Chapter 1 and is identical to the two-step equation (1.4.6) derived by Vick and Scott [17]. In fact, it was explained in Section 5.4 how Vick and Scott's assumption that the particles have a uniform temperature is physically realizable only when Φ_2 approaches zero, which is why our two models are identical when $\Phi_2 \to 0$. It was also noted how all two-step models are purely diffusive in nature, which means that they depend on only first-order initial information (i.e., initial temperatures) for solvability. This diffusive nature also eliminates the wavefronts created by the hyperbolic heat equation.

Chapter 6

Discussion of Errors in General Matrix Temperature Equation

6.1 Introduction

The general non-dimensional integro-differential equation, (4.7.3) or (4.7.6), and differential equation, (4.8.9) or (4.8.10), have inherent error due to our assumptions used to derive the equations. In this chapter, we find the conditions that make the errors in the general matrix heat equation be negligible. These conditions are necessary to find now, because we need to know how the parameters Φ_1 and Φ_2 are constrained before we use the parameters while solving the general equation in subsequent chapters.

6.2 Errors in General Heat Equation due to Assumptions in Derivation

We made several assumptions in Chapters 2 and 3 that were used to derive the general non-dimensional integro-differential equation, (4.7.3) or (4.7.6), and differential equation, (4.8.9) or (4.8.10), that govern the non-dimensional matrix temperature. Inherent error exists in the equations due to the assumptions. We can use any form of the general equation in this chapter to investigate these intrinsic errors. We choose to use (3.3.16), which is one of the simplest forms of the general matrix energy equation.

One approximation that contributes error to the general heat equation (3.3.16) is that the temperature in the element of Figure 2.2 has a roughly uniform temperature. In other words, we assume that the heat flux q_μ into the particles does not significantly alter the matrix temperature T_m in the element. However, in reality, heat transfer to the particles causes an error ΔT_m in the matrix temperature T_m. Thus, the general equation (3.3.16) is more accurately

$$\partial_t (T_m + \Delta T_m) - \alpha_m \nabla^2 (T_m + \Delta T_m) + \frac{3}{R} \frac{1}{\rho_m c_m} \frac{n_p v_p}{1 - n_p v_p} q_\mu = 0 . \tag{6.2.1}$$

We also assumed implicitly that the particles do not influence each other significantly, such that each particle in the element of Figure 2.2 has the same heat flux q_μ. In reality, the particles do influence each other, since the temperature field around a particle creates a change in the heat flux into a neighboring particle. So, particle-to-particle interaction creates an error Δq_μ for q_μ in (6.2.1). Consequently, a more precise form of the general equation (6.2.1) is

$$\partial_t(T_m + \Delta T_m) - \alpha_m \nabla^2 (T_m + \Delta T_m) + \frac{3}{R} \frac{1}{\rho_m c_m} \frac{n_p v_p}{1 - n_p v_p} (q_\mu + \Delta q_\mu) = 0 . \qquad (6.2.2)$$

Other errors exist in (6.2.2) due to the geometry of the composite. First, even if no heat is transferred to the particles, temperature variations ΔT_m still exist in the matrix due to the fact that heat flows *around* the particles. Second, we assumed in Chapter 2 that the temperature on the surface of the particles is essentially uniform if the particles are sufficiently small. Third, in Chapter 3, we used the concept of the area fraction from Appendix A to approximate the heat transfer through the exposed bounding surface of the matrix volume in Figure 3.1. Being related to the geometry of the composite, which is closely linked to the *small* ratio $n_p v_p$ of the total volume of particles to the composite volume, all these errors are assumed to be of $o(1)$, which means that the errors are of $O((n_p v_p)^\kappa)$ for positive κ. In other words, each geometry-related error is assumed to *decrease to zero as* $n_p v_p$ *decreases to zero* and is then "higher in order" than terms of $O(1)$ that do not vanish as $n_p v_p$ vanishes. Consequently, (6.2.2) is more accurately

$$\partial_t(T_m + \Delta T_m) - \alpha_m \nabla^2 (T_m + \Delta T_m) + \frac{3}{R} \frac{1}{\rho_m c_m} \frac{n_p v_p}{1 - n_p v_p} (q_\mu + \Delta q_\mu) + o(1) = 0 . \qquad (6.2.3)$$

6.3 Neglect of Errors in General Heat Equation

We desire to neglect all errors in the general equation (6.2.3) due to our assumptions. First, if

$$\frac{MAX(|\Delta T_m|)}{T_m} = o(1) \text{ and } \frac{MAX(|\Delta q_\mu|)}{q_\mu} = o(1) , \qquad (6.3.1)$$

where $MAX(f(x))$ is the largest value of the function $f(x)$ over its x domain, then (6.2.3) becomes

$$\partial_t(1+o(1))T_m - \alpha_m\nabla^2(1+o(1))T_m + \frac{3}{R}\frac{1}{\rho_m c_m}\frac{n_p v_p}{1-n_p v_p}(1+o(1))q_\mu = o(1). \tag{6.3.2}$$

With considerable rearrangement, we can show that (6.3.2) is

$$\partial_{\hat{t}}(1+o(1))\theta_m - \hat{\nabla}^2(1+o(1))\theta_m + \Phi_1(1+o(1))\Delta\theta = o(1), \tag{6.3.3}$$

where

$$\Delta\theta = \theta_m - \theta_p(R) - \Delta\theta_0, \tag{6.3.4}$$

by using the definitions of q_μ, $\Delta\theta_0$, Φ_1, Φ_2, τ_p, and τ_μ from the previous chapters in addition to the non-dimensional variables defined in (4.2.1) and (4.7.1). If Φ_1 does not vanish with $n_p v_p$ because it is of $O(1)$, then (6.3.3) becomes

$$\partial_{\hat{t}}\,\theta_m - \hat{\nabla}^2\theta_m + \Phi_1\Delta\theta = 0, \tag{6.3.5}$$

when the higher-order terms of $o(1)$ are neglected. Equation (6.3.5) is a non-dimensional form of (3.3.16), which is one form of the general matrix energy equation.

In summary, if the conditions in (6.3.1) are valid *and* Φ_1 is also of $O(1)$, then we are justified in using our general matrix temperature equations derived in Chapter 4 and hence the damped telegraph equation seen in Chapter 5. Thus, we need to determine when the conditions in (6.3.1) are true.

6.4 Approximation of Error due to Assumption of Uniform Matrix Temperature

We need to find $MAX(|\Delta T_m|)$, which is required to determine when the first condition in (6.3.1) is valid. The value of $MAX(|\Delta T_m|)$ depends on *all* the particles in the matrix. However, in order to approximate $MAX(|\Delta T_m|)$, we begin by imagining that only a *single* particle exists and acts as a "sink" with a maximum heat flux q_μ. The heat flux is set to be a maximum, because the change ΔT_m in matrix temperature should then also be a maximum in magnitude.

We desire to find the greatest change $\Delta T_{\max}$ in matrix temperature at all matrix points caused by the "sink". To do so, we first imagine that heat is transferred to the lone, embedded particle from an infinite matrix of thermal conductivity k_m and temperature T_0. Next, to determine the greatest change $\Delta T_{\max}$ in matrix temperature requires that we solve for the temperature field T_m that surrounds the particle. It can be shown that the matrix temperature T_m is spherically symmetric, being a function $T_m(r)$ of radial distance r from the sphere, and that the greatest change $\Delta T_{\max}(r)$ in matrix temperature at all matrix points occurs at equilibrium. At equilibrium, Fourier's heat equation (1.1.3) for the matrix reduces to

$$\frac{d}{dr}\left(r^2 \frac{dT_m}{dr} \right) = 0 \tag{6.4.1}$$

for the spherically-symmetric matrix temperature $T_m(r)$ [19]. The boundary conditions with which to solve (6.4.1) are then

$$q_\mu = k_m \left. \frac{\partial T_m}{\partial r} \right|_R \quad \text{and} \quad T_m(r \to \infty) = T_0 \tag{6.4.2}$$

for the diffusive particle of radius R embedded in the infinite matrix. The boundary-value problem formed by Fourier's heat equation (6.4.1) and the boundary conditions in (6.4.2) is seen in Figure 6.1.

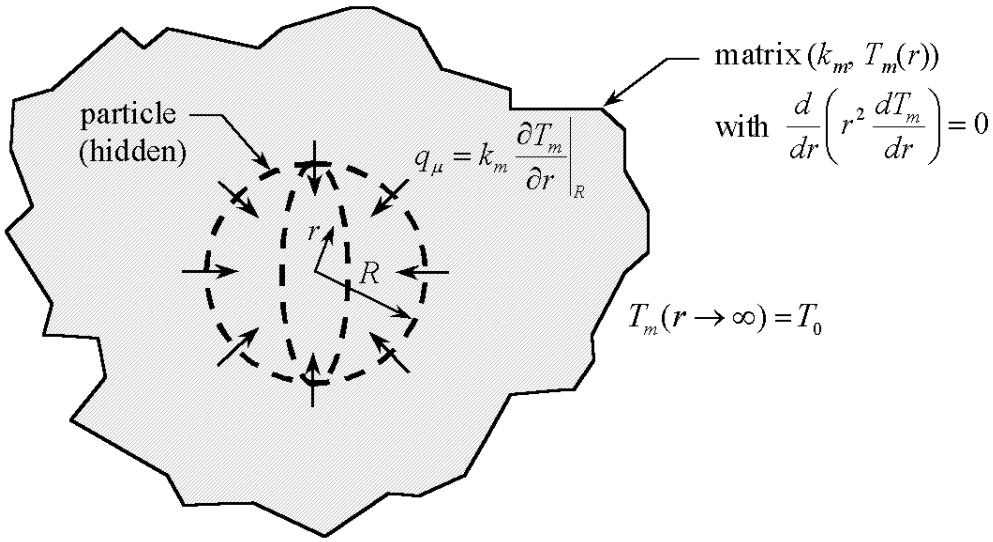

Figure 6.1: Boundary-Value Problem Used to Find Error in General Heat Equation

In order to determine $MAX(|\Delta T_m|)$, we begin by finding the greatest change $\Delta T_{\max}$ in matrix temperature at all matrix points due to the lone "sink". The greatest change $\Delta T_{\max}$ in matrix temperature due to the influence of the particle in Figure 6.1 can be shown to be

$$\Delta T_{\max}(r) = T_m(r) - T_0 = -\frac{q_\mu R^2}{k_m r} \tag{6.4.3}$$

for $r \geq R$ by solving (6.4.1) with boundary conditions (6.4.2). We note that the greatest magnitude change $MAX(|\Delta T_{\max}|)$ in matrix temperature due to the lone particle is at the surface of the sphere ($r = R$).

We can now use the maximum change $\Delta T_{\max}(r)$ in matrix temperature due to a *single* particle to approximate $MAX(|\Delta T_m|)$, which is due to *all* particles. First, we observe that every particle in the matrix has a countable number of nearest neighbors, each roughly a distance d from the given particle, as seen in Figure 6.2.

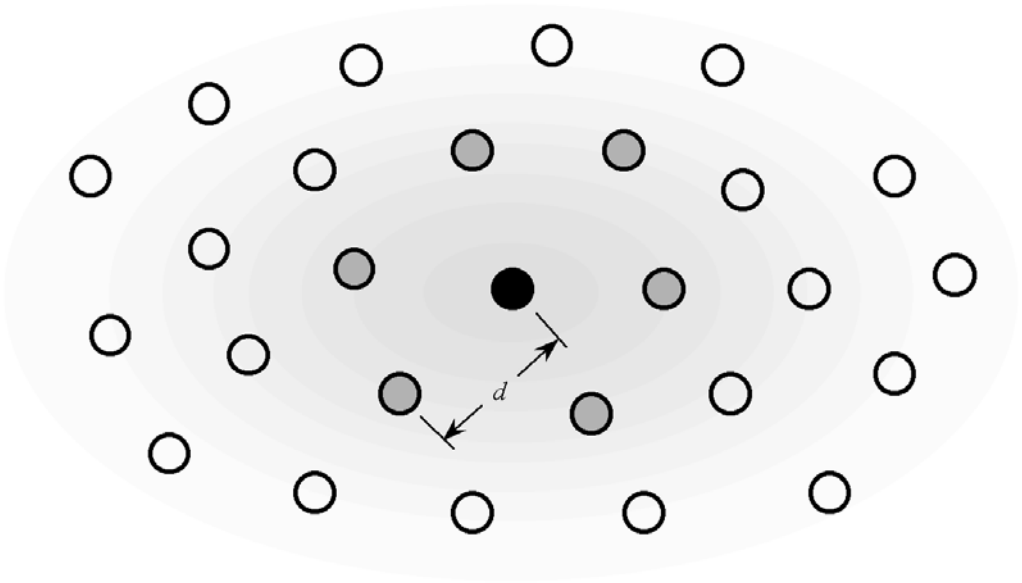

Figure 6.2: (Black) Particle with (Shaded) Nearest Neighbors

In order to get an estimate of $MAX(|\Delta T_m|)$, we let the (black) particle *and* its (shaded) nearest neighbors act as sinks in the matrix, such that each produces the field $\Delta T_{\max}(r)$ in (6.4.3), where r is measured relative to each particle center. Thus, the (shaded) neighboring particles *increase*

the maximum change in matrix temperature that occurs at the surface of the (black) center particle. The maximum deviation $MAX(|\Delta T_m|)$ in matrix temperature near the center particle is then approximately the *sum* of the temperature deviation $\Delta T_{\max}(R)$ due to the particle *and* the deviation $\Delta T_{\max}(d)$ from each of its nearest-neighboring particles. In other words,

$$MAX(|\Delta T_m|) = |\Delta T_{\max}(R)| + O(|\Delta T_{\max}(d)|). \tag{6.4.4}$$

We note that the influence of the nearest-neighboring particles seen in (6.4.4) is not discrete but rather an order-of-magnitude. This is because the number of nearest-neighboring particles is countable, instead of being a fixed number.

We can simplify (6.4.4) by using the definition of $\Delta T_{\max}$. Substitution of (6.4.3) into (6.4.4) yields

$$MAX(|\Delta T_m|) = \frac{q_\mu R}{k_m}(1 + O(R/d)). \tag{6.4.5}$$

We can simplify (6.4.5) even further. Because d represents the distance between neighboring particles, about one particle is embedded in a matrix volume of d^3, i.e.,

$$n_p = O(1/d^3), \tag{6.4.6}$$

where n_p is the number of particles per unit volume. When (6.4.6) is multiplied by the volume v_p of a spherical particle of radius R, we have

$$n_p v_p = O(R^3/d^3). \tag{6.4.7}$$

Substitution of (6.4.7) into (6.4.5) yields

$$MAX(|\Delta T_m|) = \frac{q_\mu R}{k_m}(1 + O((n_p v_p)^{1/3})). \tag{6.4.8}$$

Because $(n_p v_p)^{1/3}$ is higher in order than $(n_p v_p)^0$, which is one, for $n_p v_p << 1$, it is inferred from (6.4.8) that

$$MAX(|\Delta T_m|) = O\left(\frac{q_\mu R}{k_m}\right). \tag{6.4.9}$$

We have just used our approximation of each particle as a "sink" to find the order of $MAX(|\Delta T_m|)$, which is required to determine when the first condition in (6.3.1) is valid. We now need to substitute an expression for the maximum heat flux q_μ into (6.4.9). According to the

definition of q_μ in (2.6.2), the heat flux q_μ will be as large as possible when the temperature difference in (2.6.2) is as large as possible. Thus, we let

$$q_\mu = \mu \; MAX(\left|T_m - T_p(R)\right|), \tag{6.4.10}$$

which means that (6.4.9) is

$$MAX(\left|\Delta T_m\right|) = O\left(\frac{\mu R}{k_m} MAX(\left|T_m - T_p(R)\right|)\right). \tag{6.4.11}$$

When divided by T_m, (6.4.11) becomes

$$\frac{MAX(\left|\Delta T_m\right|)}{T_m} = O\left(\frac{\mu R}{k_m}\right) O\left(\frac{MAX\left|T_m - T_p(R)\right|}{T_m}\right). \tag{6.4.12}$$

Letting the ratio of temperatures be strictly of $O(1)$ at most, we have

$$\frac{MAX(\left|\Delta T_m\right|)}{T_m} = O\left(\frac{\mu R}{k_m}\right). \tag{6.4.13}$$

We rearrange (6.4.13) even further to find that

$$\frac{MAX(\left|\Delta T_m\right|)}{T_m} = O\left(\frac{\mu R}{k_p}\frac{k_p}{k_m}\right), \tag{6.4.14}$$

which is

$$\frac{MAX(\left|\Delta T_m\right|)}{T_m} = O\left(\Phi_2 \frac{k_p}{k_m}\right) \tag{6.4.15}$$

upon substitution of the definition of Φ_2 from (4.2.11).

Finally, substitution of (6.4.15) into the first condition in (6.3.1) yields

$$\Phi_2 \frac{k_p}{k_m} = o(1). \tag{6.4.16}$$

When (6.4.16) is satisfied, our assumption that the matrix temperature is sufficiently uniform in the element of Figure 2.2 is satisfied.

6.5 Approximation of Error due to Assumption of No Particle-to-Particle Interaction

We now approximate $MAX(|\Delta q_\mu|)$, which is required for the second condition in (6.3.1) to ensure negligible particle-to-particle interaction. Again, we imagine that the (black) center particle and the (shaded) nearest neighbors in Figure 6.2 are all sinks that produce the matrix temperature change $\Delta T_{\max}(r)$ given in (6.4.3), where r is measured relative to each particle center. Consequently, the maximum change in matrix temperature at the (black) center particle caused by a (shaded) neighboring particle a distance d away is about $\Delta T_{\max}(d)$. This maximum temperature change causes a maximum change $\Delta q_{\max}$ in the incoming heat flux into the center particle, which is

$$\Delta q_{\max} = \mu \Delta T_{\max}(d) = -\frac{\mu q_\mu R^2}{k_m d}, \tag{6.5.1}$$

according to the definitions of q_μ in (2.6.2) and $\Delta T_{\max}$ in (6.4.3). The maximum total change $MAX(|\Delta q_\mu|)$ in heat flux into the center particle due to *all* its countable nearest neighbors is then on the order of the change $\Delta q_{\max}$ due to *one* neighboring particle, i.e.,

$$MAX(|\Delta q_\mu|) = O(|\Delta q_{\max}|) = O\left(\frac{\mu q_\mu R^2}{k_m d}\right). \tag{6.5.2}$$

We can now determine when the second condition in (6.3.1) is true. By using the definition (4.2.11) of Φ_2, we rearrange (6.5.2) to find that

$$\frac{MAX(|\Delta q_\mu|)}{q_\mu} = O\left(\Phi_2 \frac{k_p}{k_m}\right) O\left(\frac{R}{d}\right). \tag{6.5.3}$$

When we utilize (6.4.7) and the condition (6.4.16) for negligible matrix temperature variations, we obtain

$$\frac{MAX(|\Delta q_\mu|)}{q_\mu} = o(1). \tag{6.5.4}$$

Consequently, the second condition of (6.3.1), which is (6.5.4), is satisfied when the first condition of (6.3.1), which is (6.4.16), is satisfied. This means that particle-to-particle interaction is negligible when the matrix temperature variations due to the particles are

negligible, which is why the assumption of negligible particle-to-particle interaction was never stated explicitly in Chapter 2.

6.6 Physical Significance of Constraints

We have just shown that two constraints must be satisfied for us to use the general matrix temperature equations from Chapter 4 to approximate heat transfer in our composite. First, as discussed in Section 6.3,

$$\Phi_1 = O(1) \tag{6.6.1}$$

for use of the general matrix temperature equation (6.3.5). Second, as shown in Sections 6.4 and 6.5, the errors due to our assumptions in deriving the general heat equation are negligible when

$$\Phi_2 \frac{k_p}{k_m} = o(1)\,. \tag{6.6.2}$$

At this point, we desire to investigate the physical significance of the constraints.

The first constraint (6.6.1) that the parameter Φ_1 must be of $O(1)$ has a definite physical significance. According to the physical meaning of Φ_1 given in Section 4.3, the first constraint means that the ratio of the total thermal capacity of the particles to that of the matrix must be of $O(1)$. In other words, even as $n_p v_p$ approaches zero, the ratio of thermal capacities should be a finite number. Otherwise, if Φ_1 limited to zero with $n_p v_p$, then the non-Fourier term in (6.3.5), which is the third term on the left-hand side of the equation, would disappear. Consequently, the general matrix temperature equation (6.3.5) becomes Fourier's heat equation (4.7.9) if the parameter Φ_1 is of higher order than $O(1)$. Therefore, we must have that the ratio of thermal capacities be of $O(1)$ in order for the particles to influence the matrix, such that the (non-Fourier) general matrix temperature equation must be used instead of Fourier's heat equation.

The second constraint (6.6.2) is also physically meaningful. The constraint can be written as

$$\Phi_2^* = \frac{\mu R}{k_m} = \frac{R/k_m}{1/\mu} = \frac{\text{internal resistance of matrix across length } R}{\text{surface resistance}} = o(1)\,. \tag{6.6.3}$$

The parameter Φ_2^* is analogous to Φ_2. When $\Phi_2 << 1$, the temperatures in a particle become uniform much faster than the average particle temperature can equilibrate with the matrix. Analogously, when $\Phi_2^* << 1$, the temperatures in the *matrix* that surround a particle are able to become uniform much faster than the average matrix temperature can equilibrate with the particles. Consequently, the errors in the general matrix temperature equation caused by the natural temperature variations in the matrix are negligible when $\Phi_2^* = o(1)$, because the variations generally dissipate faster than the particles can affect the average matrix temperature.

6.7 Physical Admissibility and Implementation of Constraints

We just showed that the two constraints (6.6.1) and (6.6.3) are physically significant. However, for the constraints to have any experimental value, they need to be physically admissible.

The first constraint (6.6.1) that the parameter Φ_1 must be of $O(1)$ is physically admissible. According to Section 4.4, the parameter Φ_1 was set to be of $O(1)$ because of physical reasons. Thus, not only is it physically admissible for Φ_1 to be of $O(1)$, but it is also mathematically necessary for our general heat equation to approximate matrix temperatures.

The second constraint (6.6.3) that Φ_2^* must be of $o(1)$ is also physically admissible. According to Section 4.4, we let Φ_2 vary between 0 and ∞. Because Φ_2^* is composed of the same type of dimensional parameters as those for Φ_2, the parameter Φ_2^* can also vary between 0 and ∞. Consequently, having Φ_2^* limit to zero by being of $o(1)$ is physically admissible.

We have just shown that the two constraints (6.6.1) and (6.6.3) that validate our use of the general matrix temperature equations are physically admissible. Now, when we implement the general matrix temperature equation in subsequent chapters, values that we choose for Φ_1 and Φ_2 need to satisfy both constraints. First, when we choose values for Φ_1 in later chapters, they should be of $O(1)$. For all practical purposes, this means that Φ_1 should not be much less than or much greater than one. Second, when we choose a value for Φ_2 while solving the general matrix temperature equation (4.2.18), we can choose *any* value of Φ_2, because only Φ_2^* needs to be of

$o(1)$. Experimentally, any value of Φ_2 is possible if the ratio of thermal conductivities in (6.6.2) is chosen just right.

6.8 Conclusions

We have just shown that if

$$\Phi_1 = O(1) \tag{6.8.1}$$

and

$$\Phi_2^* = \frac{\mu R}{k_m} = o(1), \tag{6.8.2}$$

then we are justified in using the general integro-differential matrix temperature equations from Chapter 4 to approximate heat transfer in our composite. The first constraint (6.8.1) ensures that the general matrix temperature equation is general, i.e., non-Fourier. The second constraint (6.8.2) ensures that the error in the general integro-differential equation (4.2.18) is negligible.

Both constraints are physically admissible and can be easily implemented when solving the general matrix temperature equation. In later chapters, we should choose values of Φ_1 that are not much less than or much greater than one, and we can choose any value of Φ_2 in order to solve the general heat equation.

Chapter 7

IBVP and Numerical Scheme

7.1 Introduction

Now that we know that our general matrix temperature equation (4.7.3) can be used, we desire to learn how it behaves for relatively small and large times and how this behavior depends on the system parameters. In this chapter, we define the general initial-boundary-value problem (IBVP) that is used in later chapters to study the behavior of our general matrix temperature equation. We desire to solve the non-dimensional matrix temperature equation (4.7.3) for the chosen IBVP with general system parameter values. However, a general closed-form solution to the equation cannot be found. Therefore, an approximate solution to the equation will be created. We devise an approximation of the solution of the IBVP such that the difference between the approximate and exact solutions is bounded in magnitude. For computational efficiency, the general approximation is also created to have a minimum number of terms.

7.2 Description of Initial-Boundary-Value Problem

The simplest system with which to investigate the general matrix temperature equation (4.7.3) is an infinite, one-dimensional medium. Thus, we choose to let temperature vary only in the $\hat{x}$-direction. The non-dimensional spatial Laplacian operator $\hat{\nabla}^2$ seen in (4.7.3) then reduces to the second order partial derivative $\partial_{\hat{x}}^2$ with respect to the $\hat{x}$-direction. Equation (4.7.3) governing the non-dimensional matrix temperature θ_m is then

$$\Phi_2(\partial_{\hat{t}}\theta_m - \partial_{\hat{x}}^2\theta_m) + 2\int_0^{\hat{t}} \mathrm{Y}(\hat{t}-\hat{\tau})\partial_{\hat{t}}(\Phi_1\theta_m + \partial_{\hat{t}}\theta_m - \partial_{\hat{x}}^2\theta_m)d\hat{\tau} = 0 \text{ for } \hat{x} > 0 \text{ and } \hat{t} > 0, \quad (7.2.1)$$

where the function Y is defined in (4.7.5) and θ_m is a function $\theta_m(\hat{x},\hat{t})$ of the non-dimensional variables $\hat{x}$ and $\hat{t}$ for any given system parameters.

The one-dimensional equation (7.2.1) can be solved once initial and boundary conditions are prescribed. Now, in our derivation of (7.2.1), we required that the particles and matrix have initially uniform temperatures, but that these temperatures may be different. For simplicity, we let the *entire* composite for our IBVP have an initial temperature of T_0. In other words, we let both the initial particle temperature T_p^0 and the initial matrix temperature T_m^0 be equal to T_0. Without an initial temperature difference between the particles and matrix,

$$\Delta\theta_0 = 0\,, \tag{7.2.2}$$

according to (4.2.3). Our two initial conditions required for (7.2.1) are then

$$\theta_m = 0 \text{ and } \partial_{\hat{t}}\theta_m = 0 \text{ for } \hat{x} \geq 0 \text{ at } \hat{t} = 0\,, \tag{7.2.3}$$

according to (4.2.1) and (4.7.4). The two boundary conditions also need to be established for our IBVP. We let the boundary condition at $\hat{x} = 0$ be mixed, i.e.,

$$\theta_m - \beta\frac{\partial\theta_m}{\partial\hat{x}} = 1 \text{ at } \hat{x} = 0 \text{ for } \hat{t} > 0\,, \tag{7.2.4}$$

where the non-dimensional constant β is non-negative, such that the equilibrium temperature θ_m at $\hat{x} = 0$ is finite and equal to one. We also let the boundary condition at infinity be that

$$\theta_m \text{ is bounded as } \hat{x} \to \infty \text{ for } \hat{t} > 0\,. \tag{7.2.5}$$

The general heat equation (7.2.1), initial conditions in (7.2.3), and boundary conditions (7.2.4) and (7.2.5) constitute the IBVP that we will use in this paper to study our general heat equation. The numerical scheme described in this chapter approximates the solution of (7.2.1) within a certain tolerance for general $\hat{x}, \hat{t}, \Phi_1, \Phi_2,$ and β.

7.3 Exact Solution of IBVP

There is no need to find an approximate solution of the IBVP described in Section 7.2 if an explicit solution can be found. An exact solution of (7.2.1) is known in terms of the Bromwich integral,

$$\theta_m(\hat{x},\hat{t}) = \frac{1}{2\pi i}\int_{\gamma-i\infty}^{\gamma+i\infty} \overline{\theta}_m(\hat{x},\hat{s})\, e^{\hat{s}\hat{t}}\, d\hat{s}\,, \tag{7.3.1}$$

where i is the imaginary number $\sqrt{-1}$, γ is *any* real constant that is greater than the real part of all the singularities of $\overline{\theta}_m$ [18] and, according to (B.1.1),

$$\overline{\theta}_m(\hat{x},\hat{s}) = \int_0^{\infty} e^{-\hat{s}\hat{t}}\, \theta_m(\hat{x},\hat{t})\, d\hat{t}\,, \tag{7.3.2}$$

where the non-dimensional Laplacian variable $\hat{s}$ is generally complex. An explicit, or closed-form, expression of the integral seen in (7.3.1) cannot generally be found. Therefore, we expect that a general explicit solution of our IBVP is not known. However, once $\overline{\theta}_m$ is known, an approximation of the integral seen in (7.3.1) would yield an approximate solution of (7.2.1). We follow this approach in the rest of this chapter.

Now, before we approximate the integral in (7.3.1), we need to determine $\overline{\theta}_m$ for the integral. The Laplace transforms of the equations that constitute our IBVP will be used to find $\overline{\theta}_m$. We start by finding the Laplace transform of the non-dimensional governing equation (7.2.1). One way of doing so is by rearranging the Laplace transform (4.8.1) of the general dimensional equation (4.2.18). By letting

$$\hat{s} = \tau_\mu\, s \tag{7.3.3}$$

and using the definitions of τ_p and τ_μ and the first set (4.7.1) of non-dimensional variables, we can show that (4.8.1) is

$$(\hat{s}\,\overline{\theta}_m - \hat{\nabla}^2\overline{\theta}_m)(\Phi_2 + (\hat{m}\coth\hat{m} - 1)) + \Phi_1(\hat{m}\coth\hat{m} - 1)(\overline{\theta}_m - \overline{\Delta\theta_0}) = 0\,, \tag{7.3.4}$$

where

$$\hat{m} = \sqrt{3\Phi_2\,\hat{s}}\,, \tag{7.3.5}$$

$\overline{\theta}_m$ is defined in (7.3.2), and $\overline{\Delta\theta_0}$ is the Laplace transform of $\Delta\theta_0$ in the $\hat{s}$ domain. Now, because the Laplacian operator $\hat{\nabla}^2$ reduces to the second order partial derivative $\partial^2_{\hat{x}}$ for our one-dimensional problem, the transformed equation (7.3.4) becomes

$$(\hat{s}\,\overline{\theta}_m - \partial^2_{\hat{x}}\,\overline{\theta}_m)(\Phi_2 + (\hat{m}\coth\hat{m} - 1)) + \Phi_1(\hat{m}\coth\hat{m} - 1)(\overline{\theta}_m - \overline{\Delta\theta_0}) = 0\,. \tag{7.3.6}$$

Because $\Delta\theta_0$ is zero, according to (7.2.2), the Laplace transform $\overline{\Delta\theta_0}$ is also zero, which means that (7.3.6) is

$$(\hat{s}\,\overline{\theta}_m - \partial_{\hat{x}}^2\,\overline{\theta}_m)(\Phi_2 + (\hat{m}\coth\hat{m} - 1)) + \Phi_1(\hat{m}\coth\hat{m} - 1)\,\overline{\theta}_m = 0\,. \tag{7.3.7}$$

Equation (7.3.7) is the Laplace transform of the governing equation (7.2.1) for our IBVP.

We can finish determining $\overline{\theta}_m$ by using the boundary conditions of our IBVP with the transformed equation (7.3.7). First, (7.3.7) can be rearranged into the form

$$\partial_{\hat{x}}^2\,\overline{\theta}_m = \left(\hat{s} + \frac{\Phi_1(\hat{m}\coth\hat{m} - 1)}{\Phi_2 + (\hat{m}\coth\hat{m} - 1)}\right)\overline{\theta}_m\,, \tag{7.3.8}$$

the solution of which is

$$\overline{\theta}_m(\hat{x}, \hat{s}) = A_1(\hat{s})\,e^{-\hat{x}\sqrt{\hat{s} + \frac{\Phi_1(\hat{m}\coth\hat{m} - 1)}{\Phi_2 + (\hat{m}\coth\hat{m} - 1)}}} + A_2(\hat{s})\,e^{\hat{x}\sqrt{\hat{s} + \frac{\Phi_1(\hat{m}\coth\hat{m} - 1)}{\Phi_2 + (\hat{m}\coth\hat{m} - 1)}}}\,, \tag{7.3.9}$$

where A_1 and A_2 are functions of $\hat{s}$. The functions $A_1(\hat{s})$ and $A_2(\hat{s})$, and hence $\overline{\theta}_m$, will now be determined by using the Laplace transforms of the boundary conditions (7.2.4) and (7.2.5). First, because θ_m is bounded as $\hat{x} \to \infty$, according to (7.2.5), it is required that $\overline{\theta}_m$ must be bounded as $\hat{x} \to \infty$ for all $\hat{s}$. This is only possible if $A_2(\hat{s})$ is zero in (7.3.9), which leaves us with

$$\overline{\theta}_m(\hat{x}, \hat{s}) = A_1(\hat{s})\,e^{-\hat{x}\sqrt{\hat{s} + \frac{\Phi_1(\hat{m}\coth\hat{m} - 1)}{\Phi_2 + (\hat{m}\coth\hat{m} - 1)}}}\,. \tag{7.3.10}$$

Now, in order to use the boundary condition (7.2.4) at $\hat{x} = 0$ to find $A_1(\hat{s})$, we need to know the Laplace transform of the boundary condition. The Laplace transform of (7.2.4) is

$$\overline{\theta}_m - \beta\frac{\partial\overline{\theta}_m}{\partial\hat{x}} = \frac{1}{\hat{s}} \text{ at } \hat{x} = 0\,, \tag{7.3.11}$$

where several Laplace transform properties from Appendix B and the table of Laplace transforms in Reference 22 have been used. Substitution of (7.3.10) into (7.3.11) yields

$$A_1(\hat{s}) - \beta\left(-A_1(\hat{s})\sqrt{\hat{s} + \frac{\Phi_1(\hat{m}\coth\hat{m} - 1)}{\Phi_2 + (\hat{m}\coth\hat{m} - 1)}}\right) = \frac{1}{\hat{s}}\,. \tag{7.3.12}$$

It can be shown that the function $A_1(\hat{s})$ is then

$$A_1(\hat{s}) = \frac{1}{\hat{s}}\left(1 + \beta\sqrt{\hat{s} + \frac{\Phi_1(\hat{m}\coth\hat{m} - 1)}{\Phi_2 + (\hat{m}\coth\hat{m} - 1)}}\right)^{-1}\,. \tag{7.3.13}$$

Finally, when we substitute (7.3.13) into (7.3.10), we find that

$$\overline{\theta}_m(\hat{x},\hat{s}) = \frac{1}{\hat{s}}\left(1+\beta\sqrt{\hat{s}+\frac{\Phi_1(\hat{m}\coth\hat{m}-1)}{\Phi_2+(\hat{m}\coth\hat{m}-1)}}\right)^{-1} e^{-\hat{x}\sqrt{\hat{s}+\frac{\Phi_1(\hat{m}\coth\hat{m}-1)}{\Phi_2+(\hat{m}\coth\hat{m}-1)}}}, \qquad (7.3.14)$$

which is the Laplace transform of the exact solution of our IBVP.

Upon substitution of $\overline{\theta}_m(\hat{x},\hat{s})$ from (7.3.14) into the Bromwich integral (7.3.1), we have the exact solution $\theta_m(\hat{x},\hat{t})$ of our given IBVP from Section 7.2. However, as expected, we cannot find a general closed-form expression for the Bromwich integral that produces $\theta_m(\hat{x},\hat{t})$. Therefore, a numerical scheme will now be created to approximate the non-dimensional temperature $\theta_m(\hat{x},\hat{t})$.

7.4 Rearrangement of Exact Solution of IBVP

We have to approximate the Bromwich integral of (7.3.1) in order to obtain an approximate solution of $\theta_m(\hat{x},\hat{t})$. Before we begin to approximate the integral, however, we desire to rearrange the integral to a more desirable form suited for a numerical scheme.

The Bromwich integral of (7.3.1) requires a complex integration with respect to $\hat{s}$, but we desire to integrate with respect to a *real* variable. To obtain an integration with respect to a real variable, we define the real variable ω such that

$$\hat{s} = \gamma + i\omega. \qquad (7.4.1)$$

After utilization of the relation in (7.4.1), the Bromwich integral of (7.3.1) becomes

$$\theta_m(\hat{x},\hat{t}) = \frac{e^{\gamma\hat{t}}}{2\pi}\int_{-\infty}^{\infty}\overline{\theta}_m(\hat{x},\gamma+i\omega)\,e^{i\omega\hat{t}}\,d\omega. \qquad (7.4.2)$$

We now have the desired integration with respect to a real variable, namely ω. However, we are not finished rearranging the Bromwich integral before we create our numerical scheme to approximate the integral.

Another simplification can be made to the integral of (7.4.2) before our approximation scheme is devised. The integrand of (7.4.2) is complex, yet the non-dimensional temperature

$\theta_m(\hat{x},\hat{t})$ is a real value for all $\hat{x}$ and $\hat{t}$. This fact suggests that the real(imaginary) part of the integrand of (7.4.2) is even(odd) about $\omega = 0$. In other words,

$$\overline{\theta}_m(\hat{x},\gamma+i\omega)\,e^{i\omega\hat{t}} + \overline{\theta}_m(\hat{x},\gamma-i\omega)\,e^{-i\omega\hat{t}} = 2\,\mathrm{Re}[\overline{\theta}_m(\hat{x},\gamma+i\omega)\,e^{i\omega\hat{t}}], \tag{7.4.3}$$

where Re[Z] is the real part of a generally complex number Z. Indeed, it can be shown that (7.4.3) is true for $\overline{\theta}_m(\hat{x},\hat{s})$ defined in (7.3.14). Combining (7.4.2) and (7.4.3) yields

$$\theta_m(\hat{x},\hat{t}) = \frac{e^{\gamma\hat{t}}}{\pi}\int_0^\infty \mathrm{Re}[\overline{\theta}_m(\hat{x},\gamma+i\omega)\,e^{i\omega\hat{t}}]\,d\omega. \tag{7.4.4}$$

Equation (7.4.4), which involves an integration of a real quantity over a real variable, is the desired form of the exact solution (7.3.1) for our given IBVP. We will now use it to create a numerical scheme in the rest of this chapter that will approximate $\theta_m(\hat{x},\hat{t})$ for general variable and parameter values.

7.5 Approximation of Exact Solution of IBVP

We now begin to numerically approximate (7.4.4). There are numerous ways to approximate the integral of (7.4.4). We choose to truncate the integral and then use the trapezoidal rule to approximate the truncated integral. The trapezoidal rule is used because of its simplicity.

According to (7.4.4), the exact solution $\theta_m(\hat{x},\hat{t})$ is

$$\theta_m(\hat{x},\hat{t}) = \int_0^\infty f(\omega)\,d\omega, \tag{7.5.1}$$

where

$$f(\omega) = \frac{e^{\gamma\hat{t}}}{\pi}\mathrm{Re}[\overline{\theta}_m(\hat{x},\gamma+i\omega)\,e^{i\omega\hat{t}}]. \tag{7.5.2}$$

If $f(\omega)$ vanishes sufficiently fast as $\omega\to\infty$, then we can *truncate* the integral in (7.5.1) to obtain

$$\theta_m(\hat{x},\hat{t}) \approx \int_0^{\omega_{\max}} f(\omega)\,d\omega, \tag{7.5.3}$$

where $\omega_{\max}$ is a sufficiently large number. Then, we can use the *trapezoidal rule* with a uniform step size $\Delta\omega$ to approximate the truncated integral as

$$\theta_m(\hat{x},\hat{t}) \approx \frac{1}{2} f(0)\Delta\omega + \sum_{n=1}^{N} f(\omega_n)\Delta\omega, \tag{7.5.4}$$

where N is approximately the number of terms,

$$\omega_{\max} = N\Delta\omega, \tag{7.5.5}$$

and $\omega_n = n\Delta\omega$. Finally, when we substitute the definition of $f(\omega)$ from (7.5.2) into (7.5.4), we find that the approximate solution $\theta_a(\hat{x},\hat{t})$ of the exact solution $\theta_m(\hat{x},\hat{t})$ for our IBVP is

$$\theta_a(\hat{x},\hat{t}) = e^{\gamma\hat{t}}\frac{\Delta\omega}{\pi}\left(\frac{1}{2}\mathrm{Re}[\overline{\theta}_m(\hat{x},\gamma)] + \sum_{n=1}^{N}\mathrm{Re}[\overline{\theta}_m(\hat{x},\gamma+in\Delta\omega)\,e^{in\Delta\omega\hat{t}}]\right). \tag{7.5.6}$$

7.6 Sources of Error in Approximation and Error Bounds

Error exists between the approximate solution $\theta_a(\hat{x},\hat{t})$, defined in (7.5.6), and the exact solution $\theta_m(\hat{x},\hat{t})$, defined in (7.4.4). We define the error function $E(\hat{x},\hat{t})$ as

$$E(\hat{x},\hat{t}) = \theta_a(\hat{x},\hat{t}) - \theta_m(\hat{x},\hat{t}), \tag{7.6.1}$$

which is

$$E(\hat{x},\hat{t}) = \theta_a(\hat{x},\hat{t}) - \frac{e^{\gamma\hat{t}}}{\pi}\int_0^{\infty}\mathrm{Re}[\overline{\theta}_m(\hat{x},\gamma+i\omega)\,e^{i\omega\hat{t}}]d\omega, \tag{7.6.2}$$

according to (7.4.4).

Specifically, two types of error exist in $E(\hat{x},\hat{t})$, because our approximation $\theta_a(\hat{x},\hat{t})$ was created by applying the *trapezoidal rule* to a *truncated* integral. In order to reveal the errors caused by these two approximations, we divide the integral in (7.6.2) into two parts. We split up the integral of (7.6.2) to obtain

$$\begin{aligned} E(\hat{x},\hat{t}) = &\left(-\frac{e^{\gamma\hat{t}}}{\pi}\int_{\omega_{\max}}^{\infty}\mathrm{Re}[\overline{\theta}_m(\hat{x},\gamma+i\omega)\,e^{i\omega\hat{t}}]d\omega\right) \\ &+\left(\theta_a(\hat{x},\hat{t}) - \frac{e^{\gamma\hat{t}}}{\pi}\int_0^{\omega_{\max}}\mathrm{Re}[\overline{\theta}_m(\hat{x},\gamma+i\omega)\,e^{i\omega\hat{t}}]d\omega\right), \end{aligned} \tag{7.6.3}$$

where $\omega_{\max}$ is defined in (7.5.5). Each parenthesized error in (7.6.3) is caused by one of our approximations. According to the previous equation, the total error $E(\hat{x},\hat{t})$ between the approximate and exact solution is

$$E(\hat{x},\hat{t}) = E_1(\hat{x},\hat{t}) + E_2(\hat{x},\hat{t}), \tag{7.6.4}$$

where the *truncation error* $E_1(\hat{x},\hat{t})$ is

$$E_1(\hat{x},\hat{t}) = -\frac{e^{\gamma\hat{t}}}{\pi}\int_{\omega_{\max}}^{\infty} \mathrm{Re}[\overline{\theta}_m(\hat{x},\gamma+i\omega)\, e^{i\omega\hat{t}}]\, d\omega, \tag{7.6.5}$$

the *trapezoidal error* $E_2(\hat{x},\hat{t})$ is

$$E_2(\hat{x},\hat{t}) = \theta_a(\hat{x},\hat{t}) - \frac{e^{\gamma\hat{t}}}{\pi}\int_{0}^{\omega_{\max}} \mathrm{Re}[\overline{\theta}_m(\hat{x},\gamma+i\omega)\, e^{i\omega\hat{t}}]\, d\omega, \tag{7.6.6}$$

and $\theta_a(\hat{x},\hat{t})$ is given by (7.5.6). In other words, the error $E_1(\hat{x},\hat{t})$ is associated with the truncation seen in (7.5.3), and the other error $E_2(\hat{x},\hat{t})$ is associated with application of the trapezoidal rule seen in (7.5.4).

We need to make sure that the total error $E(\hat{x},\hat{t})$ is bounded for general $\hat{x}$ and $\hat{t}$. Thus, we let

$$\left|E(\hat{x},\hat{t})\right| \le \sigma, \tag{7.6.7}$$

where σ is a given small parameter representing the maximum total possible error. Equation (7.6.7) is satisfied strictly when

$$\left|E_1(\hat{x},\hat{t})\right| + \left|E_2(\hat{x},\hat{t})\right| \le \sigma, \tag{7.6.8}$$

according to (7.6.4). In order to satisfy (7.6.8), we let

$$\left|E_1(\hat{x},\hat{t})\right| \le \lambda\sigma \text{ and } \left|E_2(\hat{x},\hat{t})\right| \le (1-\lambda)\sigma, \tag{7.6.9}$$

where λ represents a positive weighting factor that is less than one. At this point, the weighting factor λ is unknown.

7.7 Goals of Numerical Scheme

We will now devise a process, henceforth called the *numerical scheme*, to determine the approximate temperature $\theta_a(\hat{x},\hat{t})$ for a general error bound σ. However, before we create the numerical scheme, we need to discuss the goals of our numerical scheme. First, the numerical scheme needs to be able to fulfill the error constraints given in (7.6.9). Second, the numerical scheme needs to be computationally efficient, which means that the computational time required for use of our numerical scheme is minimum.

For the most part, the second goal of computational efficiency requires that the number of terms *N* in the approximation $\theta_a(\hat{x},\hat{t})$ is *minimum*, because computational run-time decreases as fewer terms need to be summed in (7.5.6). However, if we minimize the number of terms *N*, we need to make sure that we satisfy our first goal of the numerical scheme that the error constraints in (7.6.9) are fulfilled. In order to ensure that the error constraints in (7.6.9) are satisfied, we let the maximum possible values of $\left|E_1(\hat{x},\hat{t})\right|$ and $\left|E_2(\hat{x},\hat{t})\right|$ be as large as possible. According to the error constraints given in (7.6.9), this means that

$$\left|E_1\right|_{\max} = \lambda\sigma \text{ and } \left|E_2\right|_{\max} = (1-\lambda)\sigma, \tag{7.7.1}$$

where a "max" subscript indicates the largest possible value of the given function over space $\hat{x}$ and time $\hat{t}$. The equations given in (7.7.1) are called *constraint equations* because they constrain the truncation and trapezoidal errors. When the constraint equations in (7.7.1) are satisfied and the number of terms *N* is a minimum, we will essentially satisfy the two goals of our numerical scheme.

However, in order to maintain computational efficiency, we desire that analytical expressions exist for the three parameters (*N*, $\Delta\omega$, and γ) required for the approximate solution $\theta_a(\hat{x},\hat{t})$ given in (7.5.6). Analytical expressions are relatively fast to implement and run in a computer program. Both a minimum number of terms *N* and analytical expressions for *N*, $\Delta\omega$, and γ will minimize the computational time for our numerical scheme, and consequently satisfy the second goal of our numerical scheme. Thus, we desire to create analytical expressions for the two constraint equations in (7.7.1).

In summary, we desire to satisfy the two goals of the numerical scheme, which are the fulfillment of error constraints and computational efficiency. To do so, we need to find analytical expressions for the two constraint equations in (7.7.1) and then minimize N to find analytical expressions for N, $\Delta\omega$, and γ, which are all required for our approximate non-dimensional temperature $\theta_a(\hat{x},\hat{t})$ defined in (7.5.6). Therefore, our *numerical scheme* contains the approximate solution $\theta_a(\hat{x},\hat{t})$ of our IBVP and the analytical expressions of N, $\Delta\omega$, and γ required for the approximation, with the number of terms N being as small as possible while the constraint equations in (7.7.1) are satisfied.

7.8 Constraint Equation for Truncation Error

As required for our numerical scheme, an analytical expression of the constraint equation for truncation error will now be created. Substitution of the definition (7.6.5) of E_1 into the first equation of (7.7.1) yields

$$\left| \frac{e^{\gamma\hat{t}}}{\pi} \int_{\omega_{\max}}^{\infty} \mathrm{Re}[\overline{\theta}_m(\hat{x},\gamma+i\omega)\, e^{i\omega\hat{t}}]\, d\omega \right|_{\max} = \lambda\sigma, \tag{7.8.1}$$

which is our constraint equation for truncation error. We now need to simplify (7.8.1) by approximating the complicated integral. To do so, numerous assumptions need to be made that will be validated later in this thesis.

We begin our approximation of (7.8.1) by approximating its integrand. First, we assume that $\omega_{\max} >> 1$. According to (7.4.1), if $\omega_{\max} >> 1$, then $\|\hat{s}\| >> 1$ when $\omega \geq \omega_{\max}$, where $\|\hat{s}\|$ is the norm of the complex $\hat{s}$. Because $\omega \geq \omega_{\max}$ for the integral of (7.8.1), $\|\hat{s}\| >> 1$ in its integrand. This means that we can simplify the Laplace transform $\overline{\theta}_m(\hat{x},\hat{s})$ for the integrand by letting $\|\hat{s}\| >> 1$. Now, we showed in Chapter 6 that Φ_1 must be of $O(1)$ and that Φ_2 can be any non-negative number for our general equation (7.2.1). Consequently, these restrictions also hold for the solution $\overline{\theta}_m$ of (7.2.1). It can be shown that the Laplace transform $\overline{\theta}_m$ from (7.3.14) can be approximated as

$$\bar{\theta}_m(\hat{x},\hat{s}) \approx \frac{1}{\hat{s}}(1+\beta\sqrt{\hat{s}})^{-1}e^{-\hat{x}\sqrt{\hat{s}}} \tag{7.8.2}$$

when $\|\hat{s}\| >> 1$ for Φ_1 of $O(1)$ with any non-negative Φ_2. Next, substitution of the definition of $\hat{s}$ from (7.4.1) into (7.8.2) yields

$$\bar{\theta}_m(\hat{x},\gamma+i\omega) \approx \frac{1}{\gamma+i\omega}(1+\beta\sqrt{\gamma+i\omega})^{-1}e^{-\hat{x}\sqrt{\gamma+i\omega}}. \tag{7.8.3}$$

Finally, when (7.8.3) is substituted into (7.8.1), we find that the constraint equation (7.8.1) for truncation error can be approximated as

$$\left|\frac{e^{\gamma\hat{t}}}{\pi}\int_{\omega_{\max}}^{\infty}\mathrm{Re}[\frac{1}{\gamma+i\omega}(1+\beta\sqrt{\gamma+i\omega})^{-1}e^{-\hat{x}\sqrt{\gamma+i\omega}}\ e^{i\omega\hat{t}}]d\omega\right|_{\max} = \lambda\sigma. \tag{7.8.4}$$

We can simplify the constraint equation (7.8.4) even further by making several assumptions about when the integral is a maximum. We assume that the integral in (7.8.4) is approximately a maximum for $\beta = 0$. Now, the boundary temperature "jumps" from its initial value of zero, according to (7.2.3), to its permanent value of one, according to (7.2.4), when $\beta = 0$. Consequently, we assume that the integral in (7.8.4) is approximately a maximum for a jump $(\beta = 0)$ in boundary temperature. Equation (7.8.4) becomes

$$\left|\frac{e^{\gamma\hat{t}}}{\pi}\int_{\omega_{\max}}^{\infty}\mathrm{Re}[\frac{1}{\gamma+i\omega}e^{-\hat{x}\sqrt{\gamma+i\omega}}\ e^{i\omega\hat{t}}]d\omega\right|_{\max} = \lambda\sigma \tag{7.8.5}$$

for a jump in boundary temperature. Finally, because the norm of the exponential term in the integrand of (7.8.5) decreases as $\hat{x}$ increases, we also assume that the integral is approximately a maximum when $\hat{x} = 0$, meaning that

$$\left|\frac{e^{\gamma\hat{t}}}{\pi}\int_{\omega_{\max}}^{\infty}\mathrm{Re}[\frac{1}{\gamma+i\omega}e^{i\omega\hat{t}}]d\omega\right|_{\max} = \lambda\sigma. \tag{7.8.6}$$

In summary, by assuming that the integral in (7.8.4) is a maximum when $\beta = 0$ and $\hat{x} = 0$, we obtain the constraint equation (7.8.6) for truncation error.

Our constraint equation (7.8.6) for truncation error will now be rearranged before any more approximations and assumptions are utilized. First, it can be shown that the integral operator and the real operator can be switched in (7.8.6). In other words, (7.8.6) can be written as

$$\left| \frac{e^{\gamma \hat{t}}}{\pi} \mathrm{Re}\left[\int_{\omega_{\max}}^{\infty} \frac{e^{i\omega \hat{t}}}{\gamma + i\omega} \, d\omega \right] \right|_{\max} = \lambda \sigma . \tag{7.8.7}$$

Second, because the right-hand side of (7.8.7) is independent of variables $\hat{x}$ and $\hat{t}$, the left-hand side must also be independent of space and time. In the spirit of variable-independence, we let

$$\gamma = \Gamma / \hat{t} \text{ and } \omega = \Omega / \hat{t} , \tag{7.8.8}$$

where both Γ and Ω are positive and independent of $\hat{x}$ and $\hat{t}$. When the equations in (7.8.8) are substituted into (7.8.7), we find that

$$\left| \frac{e^{\Gamma}}{\pi} \mathrm{Re}\left[\int_{\Omega_0}^{\infty} \frac{e^{i\Omega}}{\Gamma + i\Omega} \, d\Omega \right] \right|_{\max} = \lambda \sigma , \tag{7.8.9}$$

where

$$\Omega_0 = \omega_{\max} \hat{t} , \tag{7.8.10}$$

and Ω_0 is positive and independent of $\hat{x}$ and $\hat{t}$. Because of our rearrangement of the error constraint for truncation error, the error constraint (7.8.9) is now clearly independent of space and time. In other words, the truncation error E_1 is bounded in magnitude by the product $\lambda \sigma$ for *all* allowable $\hat{x}$ and $\hat{t}$, as required by the first constraint in (7.7.1).

We now continue to approximate the constraint equation for truncation error, which is in its rearranged form of (7.8.9). Assuming that $\Omega_0 >> \Gamma$, we approximate (7.8.9) as

$$\left| \frac{e^{\Gamma}}{\pi} \mathrm{Re}\left[-i \int_{\Omega_0}^{\infty} \frac{e^{i\Omega}}{\Omega} \, d\Omega \right] \right|_{\max} = \lambda \sigma . \tag{7.8.11}$$

When the integral in (7.8.11) is integrated by parts, we have

$$\left| \frac{e^{\Gamma}}{\pi} \mathrm{Re}\left[\frac{e^{i\Omega_0}}{\Omega_0} - \int_{\Omega_0}^{\infty} \frac{e^{i\Omega}}{\Omega^2} \, d\Omega \right] \right|_{\max} = \lambda \sigma . \tag{7.8.12}$$

Assuming that $\Omega_0 >> 1$, we neglect the integral in (7.8.12) because it is much smaller than the term preceding it. Equation (7.8.12) can then be approximated as

$$\left| \frac{e^{\Gamma}}{\pi} \mathrm{Re}\left[\frac{e^{i\Omega_0}}{\Omega_0} \right] \right|_{\max} = \lambda \sigma , \tag{7.8.13}$$

which is

$$\left| \frac{e^{\Gamma}}{\pi} \frac{\cos(\Omega_0)}{\Omega_0} \right|_{\max} = \lambda \sigma , \tag{7.8.14}$$

according to Euler's formula for complex numbers. Now, because the largest magnitude of the cosine function is unity, the constraint equation (7.8.14) is

$$\frac{e^{\Gamma}}{\pi \Omega_0} = \lambda \sigma . \tag{7.8.15}$$

When we solve for Ω_0 using (7.8.15), we obtain

$$\Omega_0 = \frac{e^{\Gamma}}{\pi \lambda \sigma} . \tag{7.8.16}$$

Equation (7.8.16) is the final form of the constraint equation for truncation error. We note that the first constraint equation (7.8.16) is analytical, as desired, and involves the parameters Ω_0, Γ, and λ, which are yet to be determined. We now need to derive the second constraint equation, which bounds the error due to use of the trapezoidal rule. Both analytical constraint equations will then be used to solve for all unknown parameters by minimizing the number of terms N in our approximate solution $\theta_a(\hat{x}, \hat{t})$.

7.9 Constraint Equation for Trapezoidal Error

An analytical expression of the constraint equation for trapezoidal error will now be created. The constraint equation for trapezoidal error is the second constraint of (7.7.1). Substitution of the definition (7.6.6) of the trapezoidal error E_2 into the second constraint of (7.7.1) yields

$$\left| \frac{e^{\gamma \hat{t}}}{\pi} \int_0^{\omega_{\max}} \mathrm{Re}[\overline{\theta}_m(\hat{x}, \gamma + i\omega)\, e^{i\omega \hat{t}}]\, d\omega - \theta_a(\hat{x}, \hat{t}) \right|_{\max} = (1 - \lambda)\sigma , \tag{7.9.1}$$

which is our constraint equation for trapezoidal error. We now desire to rearrange (7.9.1) before we approximate the constraint equation. We first substitute the definition of $\theta_a(\hat{x}, \hat{t})$ from (7.5.6) into (7.9.1) to obtain

$$\left| \begin{array}{l} \dfrac{e^{\gamma \hat{t}}}{\pi} \displaystyle\int_0^{\omega_{\max}} \mathrm{Re}[\bar{\theta}_m(\hat{x}, \gamma + i\omega)\, e^{i\omega \hat{t}}]\, d\omega \\ - e^{\gamma \hat{t}}\, \dfrac{\Delta\omega}{\pi} \left(\dfrac{1}{2} \mathrm{Re}[\bar{\theta}_m(\hat{x}, \gamma)] + \displaystyle\sum_{n=1}^{N} \mathrm{Re}[\bar{\theta}_m(\hat{x}, \gamma + i n \Delta\omega)\, e^{i n \Delta\omega \hat{t}}] \right) \end{array} \right|_{\max} = (1-\lambda)\sigma . \qquad (7.9.2)$$

Finally, we solve for N from (7.5.5) and substitute the result into (7.9.2) to find that

$$\left| \begin{array}{l} \dfrac{e^{\gamma \hat{t}}}{\pi} \displaystyle\int_0^{\omega_{\max}} \mathrm{Re}[\bar{\theta}_m(\hat{x}, \gamma + i\omega)\, e^{i\omega \hat{t}}]\, d\omega \\ - e^{\gamma \hat{t}}\, \dfrac{\Delta\omega}{\pi} \left(\dfrac{1}{2} \mathrm{Re}[\bar{\theta}_m(\hat{x}, \gamma)] + \displaystyle\sum_{n=1}^{\omega_{\max}/\Delta\omega} \mathrm{Re}[\bar{\theta}_m(\hat{x}, \gamma + i n \Delta\omega)\, e^{i n \Delta\omega \hat{t}}] \right) \end{array} \right|_{\max} = (1-\lambda)\sigma . \qquad (7.9.3)$$

Our constraint equation (7.9.3) for trapezoidal error will now be approximated.

As with the derivation of the first constraint equation (7.8.16), numerous assumptions will be used to approximate the second constraint equation (7.9.3), all of which will be verified later in this thesis. First, we assume that we can approximate (7.9.3) by letting $\omega_{\max} \to \infty$. In other words, we assume that the maximum trapezoidal error changes minimally if we do not truncate the exact solution $\theta_m(\hat{x},\hat{t})$ while creating the approximate solution $\theta_a(\hat{x},\hat{t})$. When $\omega_{\max}$ approaches infinity, (7.9.3) becomes

$$\left| \begin{array}{l} \dfrac{e^{\gamma \hat{t}}}{\pi} \displaystyle\int_0^{\infty} \mathrm{Re}[\bar{\theta}_m(\hat{x}, \gamma + i\omega)\, e^{i\omega \hat{t}}]\, d\omega \\ - e^{\gamma \hat{t}}\, \dfrac{\Delta\omega}{\pi} \left(\dfrac{1}{2} \mathrm{Re}[\bar{\theta}_m(\hat{x}, \gamma)] + \displaystyle\sum_{n=1}^{\infty} \mathrm{Re}[\bar{\theta}_m(\hat{x}, \gamma + i n \Delta\omega)\, e^{i n \Delta\omega \hat{t}}] \right) \end{array} \right|_{\max} = (1-\lambda)\sigma . \qquad (7.9.4)$$

Then, because of the definition (7.4.4) of the exact solution $\theta_m(\hat{x},\hat{t})$, the second constraint equation (7.9.4) is recognized to be

$$\left| \theta_m(\hat{x},\hat{t}) - e^{\gamma \hat{t}}\, \frac{\Delta\omega}{\pi} \left(\frac{1}{2} \mathrm{Re}[\bar{\theta}_m(\hat{x}, \gamma)] + \sum_{n=1}^{\infty} \mathrm{Re}[\bar{\theta}_m(\hat{x}, \gamma + i n \Delta\omega)\, e^{i n \Delta\omega \hat{t}}] \right) \right|_{\max} = (1-\lambda)\sigma . \qquad (7.9.5)$$

We now approximate the constraint equation (7.9.5) for trapezoidal error by using several approximations used for deriving the constraint equation (7.8.16) for truncation error. Like with $|E_1|$, we assume that $|E_2|$ is a maximum at the boundary $\hat{x} = 0$ for an initial jump $(\beta = 0)$ in boundary temperature. When $\hat{x} = 0$ and $\beta = 0$, the boundary temperature $\theta_m(0,\hat{t})$ is

$$\theta_m(0,\hat{t}) = 1 \qquad (7.9.6)$$

and its Laplace transform is

$$\overline{\theta}_m(0,\hat{s}) = 1/\hat{s}\,, \tag{7.9.7}$$

according to the boundary condition (7.2.4) and the Laplace transform in (7.3.14), respectively. Upon use of (7.9.6) and (7.9.7) for the constraint equation (7.9.5) when $\hat{x} = 0$ and $\beta = 0$, we find that

$$\left| 1 - e^{\gamma \hat{t}} \frac{\Delta\omega}{\pi} \left(\frac{1}{2\gamma} + \sum_{n=1}^{\infty} \mathrm{Re}[\, \frac{e^{i n \Delta\omega \hat{t}}}{\gamma + i n \Delta\omega}] \right) \right|_{\max} = (1-\lambda)\sigma\,. \tag{7.9.8}$$

Like the constraint equation (7.8.16) for truncation error, the constraint equation (7.9.8) for trapezoidal error must be independent of space and time because the right-hand side of (7.9.8) is independent of both $\hat{x}$ and $\hat{t}$. We can rearrange (7.9.8) by using already existing definitions from Section 7.8 to reveal this fact. When the definitions in (7.8.8) are substituted into (7.9.8), we obtain

$$\left| 1 - e^{\Gamma} \frac{\Delta\omega}{\pi} \left(\frac{\hat{t}}{2\Gamma} + \sum_{n=1}^{\infty} \mathrm{Re}[\frac{e^{i n \Delta\omega \hat{t}}}{\Gamma/\hat{t} + i n \Delta\omega}] \right) \right|_{\max} = (1-\lambda)\sigma\,. \tag{7.9.9}$$

Now, even though the left-hand side of (7.9.9) is independent of time $\hat{t}$, the time variable is still seen in the left-hand side of (7.9.9). Thus, in the spirit of variable-independence, we let

$$\Delta\Omega = \Delta\omega\, \hat{t}\,, \tag{7.9.10}$$

where $\Delta\Omega$ is a positive constant that is independent of $\hat{x}$ and $\hat{t}$. It can be shown that the constraint equation (7.9.9) becomes

$$\left| 1 - e^{\Gamma} \frac{\Delta\Omega}{\pi} \left(\frac{1}{2\Gamma} + \sum_{n=1}^{\infty} \mathrm{Re}[\frac{e^{i n \Delta\Omega}}{\Gamma + i n \Delta\Omega}] \right) \right|_{\max} = (1-\lambda)\sigma \tag{7.9.11}$$

upon utilization of (7.9.10). As desired, the constraint equation (7.9.11) for trapezoidal error is clearly independent of space and time, just like the constraint equation (7.8.16) for truncation error. In other words, the trapezoidal error E_2 is bounded in magnitude by the product $(1-\lambda)\sigma$ for *all* allowable $\hat{x}$ and $\hat{t}$, as required by the second constraint in (7.7.1).

We can rearrange the constraint equation (7.9.11) even further before any additional assumptions are made to obtain the final form of the constraint equation. First, switching the summation operator with the real operator in the equation yields

$$\left| 1 - e^{\Gamma} \frac{\Delta\Omega}{\pi} \left(\frac{1}{2\Gamma} + \mathrm{Re}\left[\sum_{n=1}^{\infty} \frac{e^{i n \Delta\Omega}}{\Gamma + i n \Delta\Omega} \right] \right) \right|_{\max} = (1 - \lambda)\sigma \,. \tag{7.9.12}$$

Next, rearrangement of (7.9.12) yields

$$\left| 1 - e^{\Gamma} \frac{\Delta\Omega}{\pi} \left(\frac{1}{2\Gamma} + \mathrm{Re}\left[-\frac{i e^{i \Delta\Omega} \Phi(e^{i \Delta\Omega}, 1, 1 - i\Gamma/\Delta\Omega)}{\Delta\Omega} \right] \right) \right|_{\max} = (1 - \lambda)\sigma \,, \tag{7.9.13}$$

where

$$\Phi(A, B, C) = \sum_{n=0}^{\infty} \frac{A^n}{(C + n)^B} \,. \tag{7.9.14}$$

We then rearrange (7.9.13) to obtain

$$\left| 1 - \frac{e^{\Gamma}}{\pi} \left(\mathrm{Im}\left[e^{i \Delta\Omega} \Phi(e^{i \Delta\Omega}, 1, 1 - i\Gamma/\Delta\Omega) \right] + \frac{\Delta\Omega}{2\Gamma} \right) \right| = (1 - \lambda)\sigma \,. \tag{7.9.15}$$

At this point, we need to approximate the constraint equation (7.9.15). We numerically found that, for $0.3 \le \Delta\Omega \le 2.0$ and $0.75 \le \Gamma \le 1.25$,

$$\left| 1 - \frac{e^{\Gamma}}{\pi} \left(\mathrm{Im}\left[e^{i \Delta\Omega} \Phi(e^{i \Delta\Omega}, 1, 1 - i\Gamma/\Delta\Omega) \right] + \frac{\Delta\Omega}{2\Gamma} \right) \right| \cong e^{-2\pi\Gamma/\Delta\Omega} \,, \tag{7.9.16}$$

where the left-hand side of (7.9.16) is off by about 10% at most from the right-hand side. Now, substitution of (7.9.16) into (7.9.15) yields that

$$e^{-2\pi\Gamma/\Delta\Omega} = (1 - \lambda)\sigma \,. \tag{7.9.17}$$

It is worthwhile to note that when $\Delta\Omega \to 0$, or when $\Delta\omega \to 0$ according to (7.9.10), the left-hand side of (7.9.17) approaches zero. The maximum trapezoidal error limiting to *zero* is expected as $\Delta\omega$ vanishes, since the trapezoidal approximation becomes *exact* as the step size vanishes. Now, solving for $\Delta\Omega$ from (7.9.17) yields

$$\Delta\Omega = -\frac{2\pi\Gamma}{\ln((1 - \lambda)\sigma)} \,. \tag{7.9.18}$$

Equation (7.9.18) is the final form of the constraint equation for E_2, which is the error in our approximate solution $\theta_a(\hat{x}, \hat{t})$ due to use of the trapezoidal rule for approximating the exact solution $\theta_m(\hat{x}, \hat{t})$.

In summary, we currently have two analytical constraint equations, (7.8.16) and (7.9.18), one for each type of error in our approximation $\theta_a(\hat{x}, \hat{t})$, defined in (7.5.6), of the exact solution

$\theta_m(\hat{x},\hat{t})$, defined in (7.4.4), for our IBVP described in Section 7.2. The two constraint equations bound the truncation and trapezoidal errors according to (7.7.1), where σ is the maximum possible error between the approximate and exact solutions of our IBVP.

We are now able to solve for all unknowns ($\Delta\omega$, γ, and N) that are required for our approximate solution $\theta_a(\hat{x},\hat{t})$. The first constraint equation (7.8.16) is analytical, as desired, and involves the given error bound σ in addition to the parameters Ω_0, Γ, and λ, which are yet to be determined. The second constraint equation (7.9.18) is also analytical and involves the given error bound σ in addition to the parameters $\Delta\Omega$, Γ, and λ, which are yet to be determined. In the next section, both constraint equations will be used to minimize the number of terms N in our approximate solution $\theta_a(\hat{x},\hat{t})$, and in the process, we will solve for all unknown parameters. We note that the number of terms N and all parameters must depend on *only* the error bound σ, because it is the only given parameter in the two constraint equations. Then, once the two parameters $\Delta\Omega$ and Γ are known along with the minimum number of terms N, we know the three variables ($\Delta\omega$, γ, and N) that are required for $\theta_a(\hat{x},\hat{t})$.

7.10 Determination of Unknowns Through Minimization of *N*

We will now use our two analytical error constraint equations, (7.8.16) and (7.9.18), to solve for the three unknowns ($\Delta\omega$, γ, N) necessary for $\theta_a(\hat{x},\hat{t})$, which is defined in (7.5.6), in addition to the one weighting factor λ used for (7.7.1), which is the original form of the constraint equations. All unknowns will be determined through the necessary minimization of the number of terms N in the approximate solution $\theta_a(\hat{x},\hat{t})$ of our IBVP.

The two constraint equations will now be used to create a general expression for the number of terms N, which will then be used to find the minimum number of terms. From (7.5.5), the number of terms N is simply

$$N = \frac{\omega_{\max}}{\Delta\omega}. \tag{7.10.1}$$

Using (7.8.10) and (7.9.10), we find that the number of terms can also be expressed as

$$N = \frac{\Omega_0}{\Delta\Omega}. \tag{7.10.2}$$

We note that the numerator and the denomenator in (7.10.2) are defined in (7.8.16) and (7.9.18), respectively, which are the two constraint equations. When they are substituted into (7.10.2), we find that

$$N(\lambda,\Gamma) = -\frac{e^{\Gamma}\ln((1-\lambda)\sigma)}{2\pi^2\Gamma\lambda\sigma}, \tag{7.10.3}$$

where N is now a function of the variables λ and Γ and the given parameter σ.

Now that we have a general expression for N, we now seek the minimum value of N with respect to λ and Γ. Because N is a smooth function, we can set

$$\frac{\partial N}{\partial \lambda} = \frac{\partial N}{\partial \Gamma} = 0 \tag{7.10.4}$$

in order to find the critical points. By substituting (7.10.3) into (7.10.4), we can show that

$$\Gamma = 1 \tag{7.10.5}$$

for Γ being necessarily positive and

$$0.86 \le \lambda \le 0.95 \tag{7.10.6}$$

for $10^{-6} \le \sigma \le 10^{-2}$, which is a reasonable range for non-dimensional error. For simplicity, we fix λ to be

$$\lambda = 9/10 \tag{7.10.7}$$

for any given σ. Notice that the weighting factor λ is close to unity, which means that, according to (7.7.1), "loosening" the truncation error while "tightening" the trapezoidal error minimizes the number of terms N in the approximate solution $\theta_a(\hat{x},\hat{t})$.

Before we find the values of $\Delta\omega$, γ, and N, we need to make sure that (7.10.5) and (7.10.7) truly minimize $N(\lambda,\Gamma)$ over its whole domain. Inspection of (7.10.3) reveals that N approaches infinity when $\lambda \to 0$ or 1 and when $\Gamma \to 0$ or ∞. In other words, N becomes infinite as the boundaries of its domain are approached. In order for N to become positively infinite at its boundaries, the *one* critical point that occurs when (7.10.5) and (7.10.7) are satisfied has to be a *global minimum*. Therefore, when (7.10.5) and (7.10.7) are substituted into (7.10.3), we find that the minimum number of terms N is roughly

$$N = \text{Ceil}\left[\frac{5e\ln(10/\sigma)}{9\pi^2\sigma}\right], \tag{7.10.8}$$

where Ceil[X] gives the smallest integer equal to or greater than X. The function Ceil is sufficient to make the number of terms N be an integer.

Finally, having found the minimum number of terms N, we will now find the unique values of $\Delta\omega$ and γ by using the values of Γ and λ. First, substitution of Γ from (7.10.5) and λ from (7.10.7) into the constraint equation (7.9.18) yields

$$\Delta\Omega = \frac{2\pi}{\ln(10/\sigma)}. \tag{7.10.9}$$

Second, (7.10.9) is substituted into (7.9.10) to reveal that

$$\Delta\omega = \frac{2\pi}{\ln(10/\sigma)\hat{t}}. \tag{7.10.10}$$

Finally, substitution of Γ from (7.10.5) into the first equation of (7.8.8) yields

$$\gamma = \frac{1}{\hat{t}}. \tag{7.10.11}$$

In summary, the values of N, $\Delta\omega$, and γ required for our approximate solution $\theta_a(\hat{x},\hat{t})$ defined in (7.5.6) are given by (7.10.8), (7.10.10), and (7.10.11), respectively. Once the non-dimensional error σ is specified, (7.10.8), (7.10.10), and (7.10.11) can be used in (7.5.6) to numerically approximate the matrix temperature $\theta_m(\hat{x},\hat{t})$ for any admissible values of $\hat{x}$ and $\hat{t}$. All parameters were found by minimizing the number of terms N, which is dependent on only the non-dimensional error σ. However, our equations for N, $\Delta\omega$, and γ are only valid if our assumptions used in the process of deriving the equations are valid.

7.11 Verification of Assumptions Used For Optimization

If our assumptions utilized while deriving (7.10.8), (7.10.10), and (7.10.11) are valid, then our optimization for N is valid and the total error in our matrix temperature approximation is bounded by σ in magnitude, as desired. Therefore, we need to verify our assumptions, if

possible, to validate our numerical scheme. We can use our results from our optimization to verify some of the assumptions.

7.11.1 Assumptions Used for Constraint Equation for Truncation Error

First, we assumed that $\omega_{\max} >> 1$. Substitution of the definition (7.10.8) of N and the definition (7.10.10) of $\Delta\omega$ into the definition (7.5.5) of $\omega_{\max}$ reveals that

$$\omega_{\max} = \frac{10e}{9\pi\sigma\hat{t}}. \tag{7.11.1}$$

Therefore, in order for $\omega_{\max} >> 1$, we have to let

$$\sigma\hat{t} << 1 \tag{7.11.2}$$

for any chosen time $\hat{t}$ and given error bound σ. When (7.11.2) is satisfied, our assumption that $\omega_{\max} >> 1$ is true.

Second, we assumed that $\Omega_0 >> 1$ and that $\Omega_0 >> \Gamma$. According to the definition of Γ in (7.10.5), these two assumptions are equivalent. Now, when we substitute the definition of $\omega_{\max}$ from (7.11.1) into the definition (7.8.10) of Ω_0, we find that

$$\Omega_0 = \frac{10e}{9\pi\sigma} >> \Gamma = 1, \tag{7.11.3}$$

because $\sigma << 1$ in order for the truncation and trapezoidal errors to be negligible. Therefore, our assumptions that $\Omega_0 >> 1$ and that $\Omega_0 >> \Gamma$ are both valid.

Third, we assumed that the greatest possible magnitude of the truncation error E_1 occurs at $\hat{x} = 0$ when $\beta = 0$. Instead of validating these assumptions analytically, we will validate these assumptions numerically in the next chapter.

7.11.2 Assumptions Used for Constraint Equation for Trapezoidal Error

First, we assumed that values used for $\Delta\Omega$ and Γ are within the given ranges for the approximation (7.9.16). However, when we found the minimum value of N, we violated the ranges for (7.9.16) by letting Γ, and consequently $\Delta\Omega$, range from 0 to ∞. Nonetheless, it can be

shown that the optimum values of Γ and $\Delta\Omega$ in (7.10.5) and (7.10.9), respectively, are within the given ranges for the approximation (7.9.16) when $10^{-6} \le \sigma \le 10^{-2}$. Consequently, the values of $\Delta\Omega$ and Γ that are associated with the minimum value of N are within the limits that were used to create the approximation (7.9.16). This means that the number of terms N in (7.10.8) is at least a *local* minimum, because the function $N(\lambda,\Gamma)$ in (7.10.3) is valid around the minimum. However, in order for N to be a *global* minimum, the approximation (7.9.16) must be able to be violated while minimizing the number of terms N. We assume that the approximation (7.9.16) can be violated while minimizing N, such that the number of terms N defined in (7.10.8) is the global minimum. However, even if N is not a global minimum, we can still use the results of our minimization if the error between the approximate and exact solutions of our IBVP is bounded by σ in magnitude.

We also assumed that we could approximate the constraint equation for trapezoidal error by letting $\omega_{\max} \to \infty$. Furthermore, like for the truncation error, we assumed that the largest possible magnitude of trapezoidal error E_2 occurs at $\hat{x} = 0$ when $\beta = 0$. Again, instead of validating these assumptions analytically, we will validate these assumptions numerically in the next chapter.

7.12 Conclusions

We can now define our numerical scheme to approximate the solution of the IBVP described in Section 7.2. First, one should choose a time $\hat{t}$. Second, one should choose an error bound σ that is very small, i.e. $\sigma << 10^{-1}$, and where $\sigma\hat{t} << 1$, according to (7.11.2). Then, any values for the system parameters β, Φ_1, and Φ_2 can be chosen and substituted into the Laplace transform $\overline{\theta}_m(\hat{x},\hat{s})$, which is defined in (7.3.14), provided that Φ_1 is of $O(1)$, according to (6.8.1). The resulting Laplace transform should be substituted into the approximate solution $\theta_a(\hat{x},\hat{t})$ in (7.5.6). Next, the values of N, $\Delta\omega$, and γ can be determined by using (7.10.8), (7.10.10), and (7.10.11), respectively, and then substituted into the approximate solution $\theta_a(\hat{x},\hat{t})$. The result is an approximate solution $\theta_a(\hat{x},\hat{t})$ of the IBVP that holds for $\hat{x} \ge 0$.

Finally, a plot of the approximate solution $\theta_a(\hat{x},\hat{t})$ can be made for any admissible $\hat{x}$-domain. The approximate solution $\theta_a(\hat{x},\hat{t})$ should only differ from the exact solution $\theta_m(\hat{x},\hat{t})$ by σ in magnitude for all values of $\hat{x}$.

We have analytically validated our numerical scheme fairly well. In other words, without actually testing our numerical scheme, we have shown with some reasonableness that the numerical scheme bounds the error between the approximate and exact solutions of our IBVP as desired. It is now time to finish showing that our numerical scheme works by actually testing the numerical scheme. In the next chapter, we will use our numerical scheme to calculate the approximate solution $\theta_a(\hat{x},\hat{t})$ for a wide range of possible values of our parameters (Φ_1, Φ_2, and β) and our variables ($\hat{x}$ and $\hat{t}$). If the error between the approximate and exact solutions is bounded in magnitude by σ when $\sigma\hat{t} << 1$ and Φ_1 is of $O(1)$, then our numerical scheme works.

Chapter 8

Validation of Numerical Scheme

8.1 Introduction

In Chapter 7, we created a numerical scheme to approximate the general solution of the non-dimensional matrix temperature equation (4.7.3) for our chosen IBVP. The numerical scheme was created to constrain the difference between the approximate solution $\theta_a(\hat{x},\hat{t})$, defined in (7.5.6), and the exact solution $\theta_m(\hat{x},\hat{t})$, defined in (7.4.4), to within a magnitude of σ, our general error bound. Through analytical means, we justified certain assumptions used in creating the numerical scheme. However, we did not validate *all* the assumptions. In this chapter, we will test our numerical scheme for a multitude of cases to validate the scheme, i.e., to show that the error *E* between the approximate and exact solutions of our IBVP is indeed bounded by σ for all admissible values of our system parameters (Φ_1, Φ_2, and β) and variables ($\hat{x}$ and $\hat{t}$). Once our numerical scheme is shown to work, we can use it in later chapters to investigate the behavior of the general matrix temperature equation.

8.2 Normalization of Error

We desire to show that our numerical scheme bounds the error $E(\hat{x},\hat{t})$ between the approximate solution $\theta_a(\hat{x},\hat{t})$ and the exact solution $\theta_m(\hat{x},\hat{t})$ to within a magnitude of σ, our general error bound. To do so, it may be desirable to plot multiple curves of $E(\hat{x},\hat{t})$ versus $\hat{x}$ for various values of σ on the same plot. However, because the error *E* is at most σ in magnitude, curves of differing σ may have very different maximum magnitudes, which is undesirable for plotting purposes because some curves may not be visible. Consequently, we

desire to normalize the error, such that all normalized curves of *differing* σ will have roughly the *same* maximum magnitude and will therefore be visible when plotted together.

We normalize the error E by letting

$$\hat{E}(\hat{x},\hat{t}) = \frac{E(\hat{x},\hat{t})}{\sigma} = \frac{\theta_a(\hat{x},\hat{t}) - \theta_m(\hat{x},\hat{t})}{\sigma}, \tag{8.2.1}$$

where $\hat{E}$ is the normalized error between the approximate and exact solutions of our IBVP. Substitution of the definition (7.6.4) of $E(\hat{x},\hat{t})$ into (8.2.1) then yields

$$\hat{E}(\hat{x},\hat{t}) = \hat{E}_1(\hat{x},\hat{t}) + \hat{E}_2(\hat{x},\hat{t}), \tag{8.2.2}$$

where

$$\hat{E}_1(\hat{x},\hat{t}) = \frac{E_1(\hat{x},\hat{t})}{\sigma} \text{ and } \hat{E}_2(\hat{x},\hat{t}) = \frac{E_2(\hat{x},\hat{t})}{\sigma}, \tag{8.2.3}$$

and $\hat{E}_1$ and $\hat{E}_2$ are the normalized truncation and trapezoidal errors, respectively. When we utilize the two error constraints (7.7.1) with the normalized errors in (8.2.3), we find that

$$\left|\hat{E}_1\right|_{\max} = \lambda \text{ and } \left|\hat{E}_2\right|_{\max} = 1 - \lambda, \tag{8.2.4}$$

where $\left|\hat{E}_1\right|_{\max}$ and $\left|\hat{E}_2\right|_{\max}$ are the maximum magnitudes of the normalized errors over space $\hat{x}$ and time $\hat{t}$. According to the definition (7.10.7) of λ, the normalized error constraints in (8.2.4) are

$$\left|\hat{E}_1\right|_{\max} = 9/10 \text{ and } \left|\hat{E}_2\right|_{\max} = 1/10. \tag{8.2.5}$$

The maximum possible normalized error $\left|\hat{E}\right|_{\max}$ is then

$$\left|\hat{E}\right|_{\max} = 1, \tag{8.2.6}$$

upon addition of the values in (8.2.5). Consequently, the normalized error $\hat{E}$ is a mathematically convenient expression, because it enables us to plot multiple curves of $\hat{E}$ versus $\hat{x}$ for *different* orders of σ on the *same* plot with a range of ± 1 for $\hat{E}$ and with all curves being then equally visible.

8.3 Validation of Numerical Scheme for $\Phi_1 = 0$

For all practical purposes, we need to know an *explicit* form of the exact solution $\theta_m(\hat{x},\hat{t})$ in order to calculate $\hat{E}(\hat{x},\hat{t})$ in (8.2.1) *exactly*. However, an explicit form of the exact solution of our IBVP is not known in general. In fact, as previously stated, the numerical scheme was created precisely because an explicit solution of our IBVP is generally unknown. We were generally not able to invert $\overline{\theta}_m$, seen in (7.3.14), which contains the parameters Φ_1, Φ_2, and β. However, when $\Phi_1 = 0$, the general matrix temperature equation (4.7.3) is equivalent to Fourier's heat equation (4.7.9) for the matrix, and $\overline{\theta}_m$ in (7.3.14) is

$$\overline{\theta}_m(\hat{x},\hat{s}) = \frac{1}{\hat{s}}(1+\beta\sqrt{\hat{s}})^{-1}e^{-\hat{x}\sqrt{\hat{s}}}, \tag{8.3.1}$$

which is *explicitly* invertible. The inverse of (8.3.1) is

$$\theta_m(\hat{x},\hat{t}) = \operatorname{erfc}(\hat{x}/2\sqrt{\hat{t}}) - e^{\hat{x}/\beta}e^{\hat{t}/\beta^2}\operatorname{erfc}(\sqrt{\hat{t}}/\beta + \hat{x}/2\sqrt{\hat{t}}), \tag{8.3.2}$$

where

$$\operatorname{erfc}(X) = \frac{2}{\sqrt{\pi}}\int_X^\infty e^{-\eta^2}d\eta \tag{8.3.3}$$

and is known as the complementary error function [20]. By substituting the explicit solution of $\theta_m(\hat{x},\hat{t})$ from (8.3.2) into the definition (8.2.1) of $\hat{E}(\hat{x},\hat{t})$, we can calculate $\hat{E}(\hat{x},\hat{t})$ *exactly* for $\Phi_1 = 0$. Consequently, it is natural for us to first test if our numerical scheme created in Chapter 7 works when $\Phi_1 = 0$.

The procedure for calculating $\hat{E}(\hat{x},\hat{t})$ when $\Phi_1 = 0$ is fairly straightforward. First, after a value is chosen for β, the exact solution $\theta_m(\hat{x},\hat{t})$ required for $\hat{E}(\hat{x},\hat{t})$ in (8.2.1) is given by the explicit solution in (8.3.2). Second, once an error bound σ is chosen, the approximate solution $\theta_a(\hat{x},\hat{t})$ required for $\hat{E}(\hat{x},\hat{t})$ is obtained by using the numerical scheme described in the Conclusions section of Chapter 7. It utilizes the Laplace transform $\overline{\theta}_m(\hat{x},\hat{s})$ from (8.3.1) for $\Phi_1 = 0$, and since Φ_2 is not seen in $\overline{\theta}_m(\hat{x},\hat{s})$, a value for the parameter does not need to be

chosen. Finally, both the approximate solution $\theta_a(\hat{x},\hat{t})$ and the exact solution $\theta_m(\hat{x},\hat{t})$ are substituted into (8.2.1) to yield $\hat{E}(\hat{x},\hat{t})$ for $\Phi_1 = 0$.

We will now calculate $\hat{E}(\hat{x},\hat{t})$ for multiple values of β, which is the only system parameter remaining in both $\theta_m(\hat{x},\hat{t})$ and $\overline{\theta}_m(\hat{x},\hat{s})$, and for numerous small values of our error bound σ required for the numerical scheme. Now, according to (8.2.6), the error $\hat{E}(\hat{x},\hat{t})$ is within one in magnitude. A way to ensure this for all space $\hat{x}$ is to choose a time $\hat{t}$ such that $\sigma\hat{t} << 1$, as required by our numerical scheme. However, it can be shown that while being sufficient, the condition that $\sigma\hat{t} << 1$ is not necessary for $\Phi_1 = 0$, because the condition does not need to be satisfied for (7.8.2) to be true when $\Phi_1 = 0$. Therefore, we will also calculate $\hat{E}$ for $\sigma\hat{t} >> 1$, as well, when $\Phi_1 = 0$.

We computed $\hat{E}(\hat{x},\hat{t})$ for all combinations of $\beta = 0$, 10^{-3}, 1, and 10^3, $\sigma = 5(10^{-3})$, $5(10^{-4})$, and $5(10^{-5})$, and $\hat{t} = 10^{-3}$, 1, 10^3, and 10^9 over suitable $\hat{x}$ domains such that important behaviors were noticed in the plots of $\hat{E}$ versus $\hat{x}$. A total of 48 parameter combinations exist. Figure 8.1 is a plot of $\hat{E}$ versus $\hat{x}$ for several cases.

It was found that the error $\hat{E}(\hat{x},\hat{t})$ is bounded everywhere by one in magnitude for *all* combinations of the values for β, σ, and $\hat{t}$. Because $\hat{E}$ is no greater than one in magnitude, our numerical scheme is valid for the Fourier heat equation $(\Phi_1 = 0)$. In fact, the validity of the numerical scheme is supported by the behavior of the curves in Figure 8.1. For instance, after an initial "damping stage", the value of each curve is approximately equal to 0.1, which is $\left|\hat{E}_2\right|_{\max}$ according to (8.2.5).

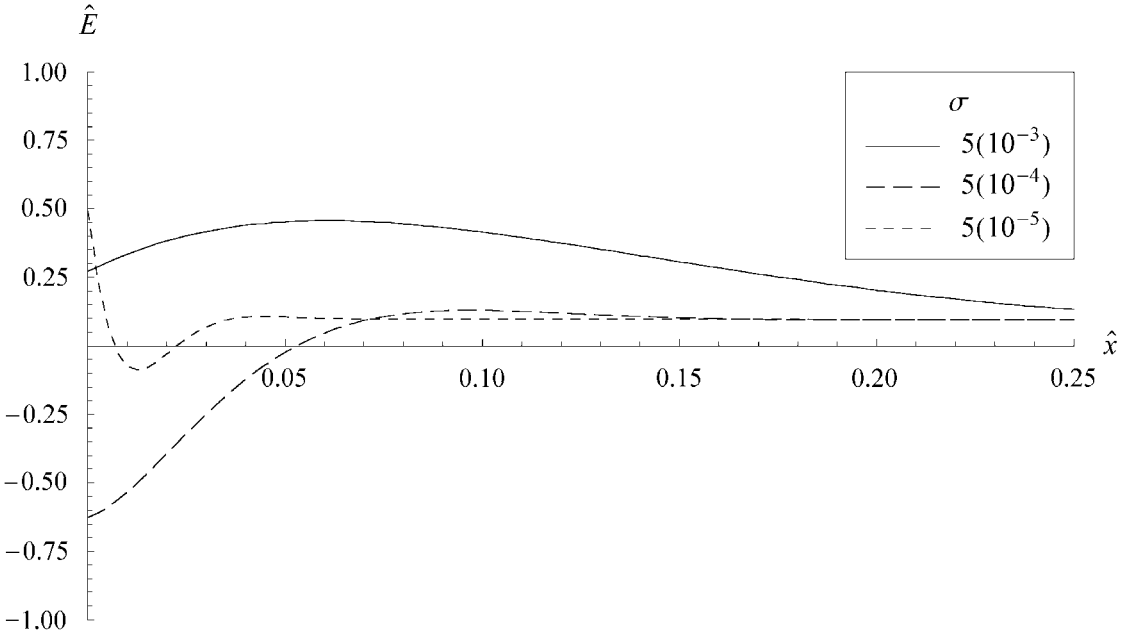

Figure 8.1: $\hat{E}$ vs. $\hat{x}$ for $\hat{t} = 1$, $\Phi_1 = 0$, and $\beta = 0$

8.4 Validation of Numerical Scheme for $\Phi_1 > 0$

We showed in Section 8.3 that our numerical scheme works for $\Phi_1 = 0$ because $\hat{E}(\hat{x},\hat{t})$ is bounded by one in magnitude for all small σ. We now desire to test the validity of our numerical scheme when $\Phi_1 > 0$.

We need to know an explicit form of the exact solution $\theta_m(\hat{x},\hat{t})$ in order to calculate $\hat{E}(\hat{x},\hat{t})$ exactly for $\Phi_1 > 0$. However, it was only when $\Phi_1 = 0$ that an explicit solution was found and we were consequently able to find $\hat{E}$ exactly. For non-zero Φ_1, an explicit form of the exact solution $\theta_m(\hat{x},\hat{t})$ of our IBVP is not known, which means that we need to approximate $\hat{E}$ for this case. We can approximate $\hat{E}$ by using two numerical approximations of different orders of σ. The approximate error $\hat{E}_a$ is defined as

$$\hat{E}_a = \frac{\theta_a(\sigma) - \theta_a(\sigma/10)}{\sigma}, \tag{8.4.1}$$

where $\theta_a(X)$ is the approximate numerical solution (7.5.6) for $\sigma = X$. If the numerical scheme works, then the approximate solution $\theta_a(\sigma/10)$ serves as a fairly exact solution *relative to* $\theta_a(\sigma)$, because $\theta_a(\sigma/10)$ is a much more accurate approximation of the exact solution than $\theta_a(\sigma)$.

We will now calculate $\hat{E}_a$ for multiple values of Φ_1, Φ_2, and β and for numerous small values of our error bound σ, but we can only use parameter values that are admissible. First, as stated in the Conclusions section of Chapter 7, our numerical scheme was devised for Φ_1 being of $O(1)$ without Φ_1 being too large relative to one. Second, no limits are needed for both parameters β and Φ_2. Thus, we should use values for both β and Φ_2 that are very small and large relative to one. Consequently, we calculated $\hat{E}_a$ for all combinations of $\beta = 0$, 10^{-3}, 1, and 10^3, $\sigma = 5(10^{-2})$, $5(10^{-3})$, and $5(10^{-4})$, $\Phi_1 = 0$, 1, and 10, $\Phi_2 = 10^{-3}$, 1, and 10^3, and $\hat{t} = 10^{-3}$, 1, 10^3, 10^6, and 10^9 over suitable $\hat{x}$ domains such that important behaviors are noticed. A total of 540 combinations exist.

When $\Phi_1 = 0$, we find that $\hat{E}_a$ closely resembles $\hat{E}$. For example, when (8.4.1) is applied to two of the values of σ used for Figure 8.1, we get Figure 8.2. As expected, the two curves in Figure 8.2 resemble the analogous curves seen in Figure 8.1. Therefore, our approximate normalized error $\hat{E}_a$ given by (8.4.1) approximates the actual error $\hat{E}$ for $\Phi_1 = 0$.

For $\Phi_1 > 0$, it was found that $\hat{E}_a$ is bounded by one in magnitude for *all* combinations when $\sigma\hat{t} << 1$. For example, Figure 8.3 is a plot of $\hat{E}_a$ for several cases of varying σ for $\sigma\hat{t} << 1$ and non-zero Φ_1, Φ_2, and β. The similarity of the behavior of $\hat{E}_a$ in Figure 8.3 with the behavior of $\hat{E}$ in Figure 8.1 supports our assertion that $\hat{E}_a$ is a sufficient approximation of the exact error $\hat{E}$.

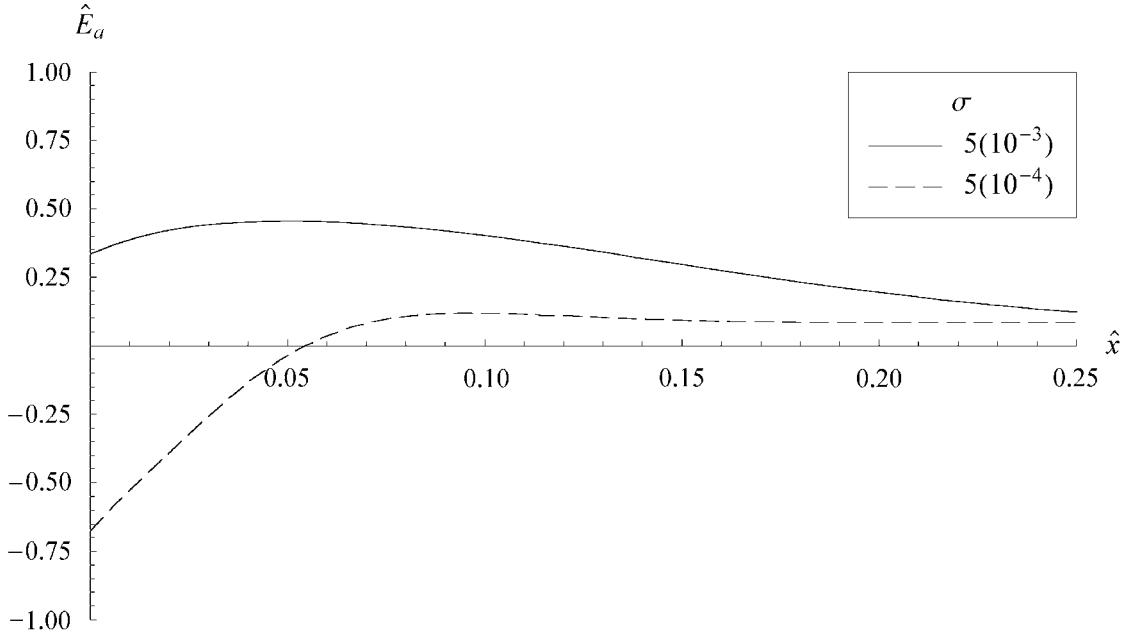

Figure 8.2: $\hat{E}_a$ vs. $\hat{x}$ for $\hat{t} = 1$, $\Phi_1 = 0$, and $\beta = 0$

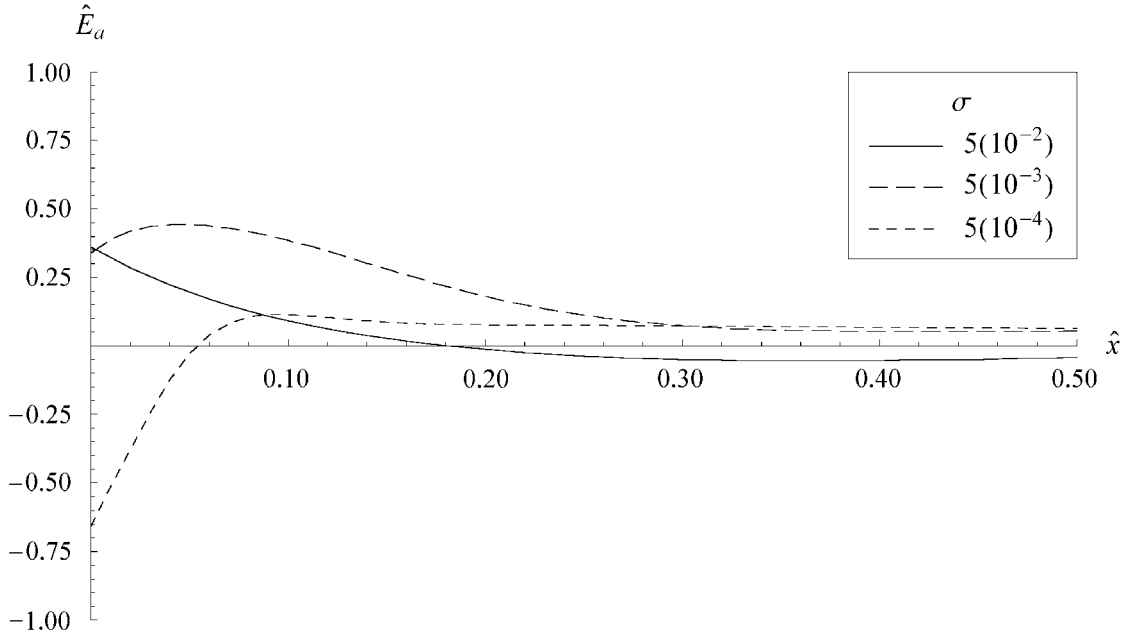

Figure 8.3: $\hat{E}_a$ vs. $\hat{x}$ for $\hat{t} = 1$, $\Phi_1 = 10$, $\Phi_2 = 1$, and $\beta = 10^{-3}$

On the other hand, $\hat{E}_a$ was not bounded by one in magnitude for some of the combinations when $\sigma\hat{t} >> 1$. A case where $\hat{E}_a$ can be large relative to one is depicted in Figure 8.4. When $\sigma\hat{t} >> 1$, the numerical scheme may not be reliable because $\hat{E}_a$ can be much greater than one in magnitude, as seen in Figure 8.4. In summary, because $\hat{E}_a$ is no greater than one in magnitude when $\sigma\hat{t} << 1$, our numerical scheme works as desired.

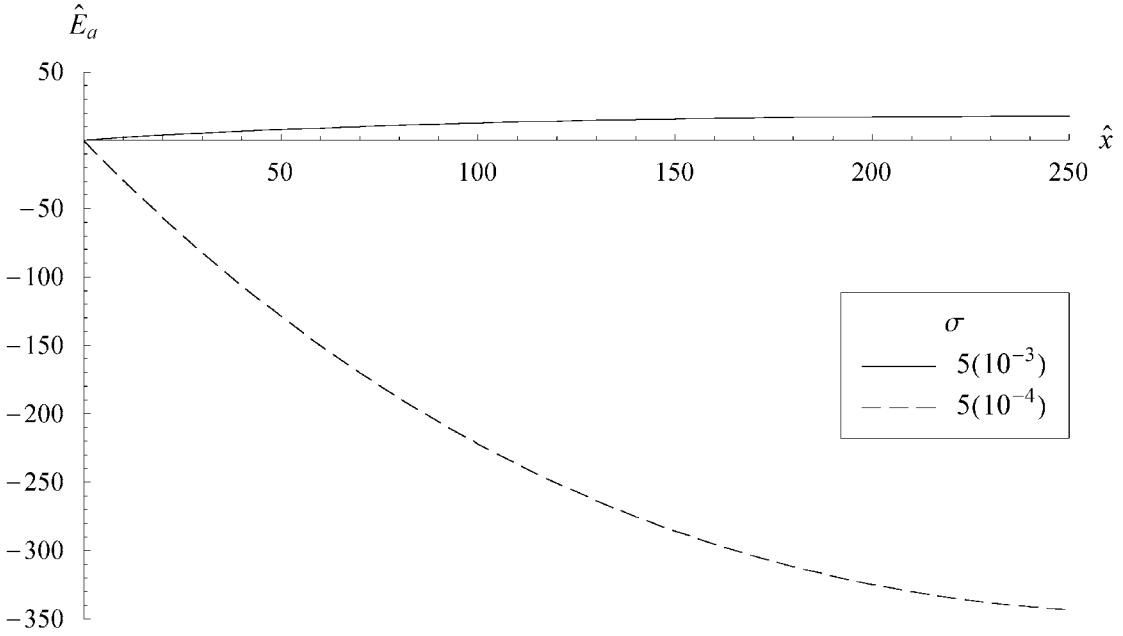

Figure 8.4: $\hat{E}_a$ vs. $\hat{x}$ for $\hat{t} = 10^6$, $\Phi_1 = 1$, and $\Phi_2 = \beta = 10^{-3}$

8.5 Conclusions

By testing the numerical scheme developed in Chapter 7, we showed that the numerical scheme works, i.e., that the error $\hat{E}(\hat{x},\hat{t})$ between the approximate solution $\theta_a(\hat{x},\hat{t})$ from (7.5.6) and the exact solution $\theta_m(\hat{x},\hat{t})$ from (7.4.4) is bounded by σ in magnitude when $\sigma\hat{t} << 1$ and Φ_1 is of $O(1)$. In other words, if $\sigma\hat{t} << 1$ and Φ_1 is of $O(1)$, then we are guaranteed that the approximate solution of our IBVP from Chapter 7 is within $\pm\sigma$ of the generally unknown exact

solution. Consequently, we can now use our numerical scheme with confidence to determine how the behavior of the general matrix temperature equation (4.7.3) depends on the system variables and parameters.

Chapter 9

Approximate Analytical Solution of Unit Step Response

9.1 Introduction

In Chapter 7, we created a general numerical scheme to approximate the solution of the general matrix temperature equation (4.7.3) for the given IBVP described in the same chapter. We tested the numerical scheme in Chapter 8 and showed that, as hypothesized in Chapter 7, our numerical scheme bounds the error $E(\hat{x},\hat{t})$ between the numerical approximation $\theta_a(\hat{x},\hat{t})$, defined in (7.5.6), and the exact solution $\theta_m(\hat{x},\hat{t})$, defined in (7.4.4), to be at most σ in magnitude.

The general numerical scheme was invented because a general closed-form solution of our IBVP cannot be found. However, an analytically approximate solution of our IBVP can be found for small parameter values by using perturbation methods. In this chapter, such an approximation will be created for the unit step response of our general heat equation. An analytically approximate unit step response for small Φ_1 and Φ_2 may provide us with a greater understanding of the physics of heat transfer through the composite.

9.2 Approximation of Unit Step Response

When the non-dimensional parameter Φ_1 is zero, an explicit solution of the IBVP exists. To be precise, according to (8.3.2),

$$\theta_m(\hat{x},\hat{t}) = \operatorname{erfc}(\hat{x}/2\sqrt{\hat{t}}) - e^{\hat{x}/\beta}e^{\hat{t}/\beta^2}\operatorname{erfc}(\sqrt{\hat{t}}/\beta + \hat{x}/2\sqrt{\hat{t}}) \tag{9.2.1}$$

when $\Phi_1 = 0$. Because (9.2.1) is an explicit solution of $\theta_m(\hat{x},\hat{t})$ for $\Phi_1 = 0$, we may be able to find an analytical approximation of $\theta_m(\hat{x},\hat{t})$ for *small* Φ_1 that is a *perturbation* away from (9.2.1). However, when Φ_1 is non-zero, the non-dimensional parameter Φ_2 also appears in the

Laplace transform $\overline{\theta}_m$, according to (7.3.14). Thus, we hypothesize that we are able to find an analytical approximation of $\theta_m(\hat{x},\hat{t})$ for small Φ_1 and Φ_2 and general β that is a perturbation away from (9.2.1).

Despite our assertion that an analytical approximation of $\theta_m(\hat{x},\hat{t})$ can be found for general β for small Φ_1 and Φ_2, we will only find a small-parameter analytical approximation of the *unit step response* ($\beta = 0$). This means that we limit ourselves to finding the approximate unit step response for small Φ_1 and Φ_2 that is a perturbation away from the unit step response for $\Phi_1 = 0$, which is

$$\theta_m(\hat{x},\hat{t}) = \operatorname{erfc}(\hat{x}/2\sqrt{\hat{t}}) \tag{9.2.2}$$

according to (9.2.1). Perhaps an analytically approximate unit step response for small Φ_1 and Φ_2 may be used to gain a greater understanding of the physics of the general matrix temperature equation (4.7.3).

We can use Laplace transforms to create the approximate unit step response for small parameters. The Laplace transform of the unit step response ($\beta = 0$) is

$$\overline{\theta}_m = \frac{1}{\hat{s}} e^{-\hat{x}\sqrt{\hat{s}+\frac{\Phi_1(\hat{m}\coth\hat{m}-1)}{\Phi_2+(\hat{m}\coth\hat{m}-1)}}}, \tag{9.2.3}$$

according to (7.3.14). Thus, the general unit step response is

$$\theta_m = L^{-1}\left\{\frac{1}{\hat{s}} e^{-\hat{x}\sqrt{\hat{s}+\frac{\Phi_1(\hat{m}\coth\hat{m}-1)}{\Phi_2+(\hat{m}\coth\hat{m}-1)}}}\right\}, \tag{9.2.4}$$

where $L^{-1}\{\overline{X}\}$ is the inverse Laplace transform of a general transformed function $\overline{X}$. It can be shown that when the argument of the inverse Laplace transform function is expanded about the zero values of Φ_1 and Φ_2, the unit step response ($\beta = 0$) is

$$\begin{aligned}\theta_m = L^{-1}\Bigg\{&\frac{e^{-\hat{x}\sqrt{s}}}{\hat{s}} - \frac{\hat{x}e^{-\hat{x}\sqrt{\hat{s}}}}{2(1+\hat{s})\sqrt{\hat{s}}}\Phi_1 + \frac{\hat{x}}{8(1+\hat{s})^2}\left(\frac{e^{-\hat{x}\sqrt{\hat{s}}}}{\sqrt{\hat{s}}} + \hat{x}e^{-\hat{x}\sqrt{\hat{s}}}\right)\Phi_1{}^2 \\ &+ \frac{\hat{x}\hat{s}e^{-\hat{x}\sqrt{\hat{s}}}}{10(1+\hat{s})^2\sqrt{\hat{s}}}\Phi_1\Phi_2 + O(\Phi_1{}^3, \Phi_2{}^3, \Phi_1{}^2\Phi_2, \Phi_1\Phi_2{}^2)\Bigg\}\end{aligned} \tag{9.2.5}$$

for small Φ_1 and Φ_2.

We can invert each term of (9.2.5) to create an expression for the approximate unit step response. However, while being mathematically correct, such an expression would not reveal much about the physics of the step response. Instead, we want an analytical approximation that we can use to learn about the physics of heat transfer through the composite. As previously stated, such an approximation for small Φ_1 and Φ_2 should be a *perturbation* away from the unit step response for zero Φ_1, which is given in (9.2.2). Mathematically, such a perturbation of (9.2.2) would really be a perturbation in space, time, or both space and time. Thus, we perturb the argument of the error function in (9.2.2) with an undetermined function $u(\hat{x},\hat{t})$ to find that the unit step response ($\beta = 0$) for general Φ_1 and Φ_2 is

$$\theta_m = \operatorname{erfc}(\hat{x}(1+u(\hat{x},\hat{t}))/2\sqrt{\hat{t}}\,). \tag{9.2.6}$$

Once the perturbation function $u(\hat{x},\hat{t})$ is determined, the unit step response for non-zero Φ_1 and Φ_2 is known.

We expect that $u(\hat{x},\hat{t})$ is small relative to one for small Φ_1 and Φ_2. Consequently, it can be shown that expansion of (9.2.6) about $u(\hat{x},\hat{t}) = 0$ yields

$$\theta_m = \operatorname{erfc}(\hat{x}/2\sqrt{\hat{t}}\,) - \frac{\hat{x}\,e^{-\hat{x}^2/4\hat{t}}}{\sqrt{\pi\hat{t}}}u + \frac{\hat{x}^3\,e^{-\hat{x}^2/4\hat{t}}}{4\sqrt{\pi\hat{t}^3}}u^2 + O(u^3). \tag{9.2.7}$$

Equation (9.2.7) is equivalent to (9.2.5), since they are both expressions for the unit step response for small Φ_1 and Φ_2. Thus, we can equate the two expressions to determine $u(\hat{x},\hat{t})$. However, before equating (9.2.5) and (9.2.7), we should have the perturbation function $u(\hat{x},\hat{t})$ as a function of the small parameters Φ_1 and Φ_2. Thus, we perform a pedestrian expansion of $u(\hat{x},\hat{t})$ in terms of the parameters Φ_1 and Φ_2. Because Φ_1 and Φ_2 are independent, we account for cross products when we expand $u(\hat{x},\hat{t})$ in a straightforward manner to obtain

$$u(\hat{x},\hat{t}) = \Phi_1 u_1 + \Phi_2 v_1 + {\Phi_1}^2 u_2 + {\Phi_2}^2 v_2 + \Phi_1\Phi_2 w + O({\Phi_1}^3, {\Phi_2}^3, {\Phi_1}^2\Phi_2, \Phi_1{\Phi_2}^2), \tag{9.2.8}$$

where u_1, u_2, v_1, v_2, and w are functions of $\hat{x}$ and $\hat{t}$ but independent of the parameters Φ_1 and Φ_2. With some rearrangement, we find that the unit step response for small Φ_1 and Φ_2 is

$$\theta_m = \operatorname{erfc}(\hat{x}/2\sqrt{\hat{t}}) + \left(-\frac{\hat{x}\, e^{-\hat{x}^2/4\hat{t}}}{\sqrt{\pi \hat{t}}} u_1 \right) \Phi_1 + \left(-\frac{\hat{x}\, e^{-\hat{x}^2/4\hat{t}}}{\sqrt{\pi \hat{t}}} v_1 \right) \Phi_2$$
$$+ \left(\frac{\hat{x}^3\, e^{-\hat{x}^2/4\hat{t}}}{4\sqrt{\pi \hat{t}^3}} u_1^{\,2} - \frac{\hat{x}\, e^{-\hat{x}^2/4\hat{t}}}{\sqrt{\pi \hat{t}}} u_2 \right) \Phi_1^{\,2} + \left(\frac{\hat{x}^3\, e^{-\hat{x}^2/4\hat{t}}}{4\sqrt{\pi \hat{t}^3}} v_1^{\,2} - \frac{\hat{x}\, e^{-\hat{x}^2/4\hat{t}}}{\sqrt{\pi \hat{t}}} v_2 \right) \Phi_2^{\,2} \tag{9.2.9}$$
$$+ \left(-\frac{\hat{x}\, e^{-\hat{x}^2/4\hat{t}}}{\sqrt{\pi \hat{t}}} w + \frac{\hat{x}^3\, e^{-\hat{x}^2/4\hat{t}}}{4\sqrt{\pi \hat{t}^3}} u_1 v_1 \right) \Phi_1 \Phi_2 + O(\Phi_1^{\,3}, \Phi_2^{\,3}, \Phi_1^{\,2}\Phi_2, \Phi_1 \Phi_2^{\,2})$$

upon substitution of (9.2.8) into (9.2.7).

We can now equate our two expressions in (9.2.5) and (9.2.9) for the unit step response to solve for $u(\hat{x}, \hat{t})$. Equating the two expressions is a simple matter of equating the respective coefficients of the parameter combinations for Φ_1 and Φ_2. When we equate coefficients, we obtain

$$L^{-1}\left\{ -\frac{\hat{x}\, e^{-\hat{x}\sqrt{\hat{s}}}}{2(1+\hat{s})\sqrt{\hat{s}}} \right\} = -\frac{\hat{x}\, e^{-\hat{x}^2/4\hat{t}}}{\sqrt{\pi \hat{t}}} u_1 , \tag{9.2.10}$$

$$L^{-1}\left\{ \frac{\hat{x}}{8(1+\hat{s})^2} \left(\frac{e^{-\hat{x}\sqrt{\hat{s}}}}{\sqrt{\hat{s}}} + \hat{x}\, e^{-\hat{x}\sqrt{\hat{s}}} \right) \right\} = -\frac{\hat{x}\, e^{-\hat{x}^2/4\hat{t}}}{\sqrt{\pi \hat{t}}} u_2 + \frac{\hat{x}^3\, e^{-\hat{x}^2/4\hat{t}}}{4\sqrt{\pi \hat{t}^3}} u_1^{\,2} , \tag{9.2.11}$$

$$L^{-1}\left\{ \frac{\hat{x}\, \hat{s}\, e^{-\hat{x}\sqrt{\hat{s}}}}{10(1+\hat{s})^2\sqrt{\hat{s}}} \right\} = -\frac{\hat{x}\, e^{-\hat{x}^2/4\hat{t}}}{\sqrt{\pi \hat{t}}} w , \tag{9.2.12}$$

and

$$v_1 = v_2 = 0 . \tag{9.2.13}$$

The inversions required for the left-hand sides of (9.2.10) through (9.2.12) are determined using the convolution rule (B.3.5) along with the table of Laplace transforms in Reference 19. Without showing any details, we solve (9.2.10) for u_1, substitute u_1 into (9.2.11) to solve for u_2, and then solve for w with (9.2.12) to find that

$$u_1 = \frac{1}{2} \int_0^{\hat{t}} e^{\frac{\hat{x}^2}{4}\left(\frac{1}{\hat{t}} - \frac{1}{\hat{\tau}}\right)} e^{-(\hat{t}-\hat{\tau})} \sqrt{\hat{t}/\hat{\tau}}\; d\hat{\tau} , \tag{9.2.14}$$

$$u_2 = \frac{\hat{x}^2}{4\hat{t}} u_1^{\,2} - \frac{1}{8} \int_0^{\hat{t}} \left(1 + \frac{\hat{x}^2}{2\hat{\tau}} \right) e^{\frac{\hat{x}^2}{4}\left(\frac{1}{\hat{t}} - \frac{1}{\hat{\tau}}\right)} e^{-(\hat{t}-\hat{\tau})} \sqrt{\hat{t}/\hat{\tau}}\, (\hat{t} - \hat{\tau})\, d\hat{\tau} , \tag{9.2.15}$$

and

$$w = -\frac{1}{10}\int_0^{\hat{t}} e^{\frac{\hat{x}^2}{4}\left(\frac{1}{\hat{t}}-\frac{1}{\hat{\tau}}\right)} e^{-(\hat{t}-\hat{\tau})}(1-(\hat{t}-\hat{\tau}))\sqrt{\hat{t}/\hat{\tau}}\, d\hat{\tau}\,. \tag{9.2.16}$$

Equations (9.2.13) through (9.2.16) then indicate that the perturbation function $u(\hat{x},\hat{t})$, defined in (9.2.8), can be approximated as

$$\begin{aligned} u(\hat{x},\hat{t}) = {} & \frac{\Phi_1{}^2}{16}\frac{\hat{x}^2}{\hat{t}}\left(\int_0^{\hat{t}} e^{\frac{\hat{x}^2}{4}\left(\frac{1}{\hat{t}}-\frac{1}{\hat{\tau}}\right)} e^{-(\hat{t}-\hat{\tau})}\sqrt{\hat{t}/\hat{\tau}}\, d\hat{\tau}\right)^2 \\ & + \frac{\Phi_1}{2}\int_0^{\hat{t}}\left(1-\frac{\Phi_2}{5}+(\hat{t}-\hat{\tau})\left(\frac{\Phi_2}{5}-\frac{\Phi_1}{4}\left(1+\frac{x^2}{2\hat{\tau}}\right)\right)\right) e^{\frac{\hat{x}^2}{4}\left(\frac{1}{\hat{t}}-\frac{1}{\hat{\tau}}\right)} e^{-(\hat{t}-\hat{\tau})}\sqrt{\hat{t}/\hat{\tau}}\, d\hat{\tau} \end{aligned} \tag{9.2.17}$$

when the parameters Φ_1 and Φ_2 are of the same small order. If Φ_2 is sufficiently small, then the terms containing Φ_2 in (9.2.17) can be neglected, meaning that

$$\begin{aligned} u(\hat{x},\hat{t}) = {} & \frac{\Phi_1{}^2}{16}\frac{\hat{x}^2}{\hat{t}}\left(\int_0^{\hat{t}} e^{\frac{\hat{x}^2}{4}\left(\frac{1}{\hat{t}}-\frac{1}{\hat{\tau}}\right)} e^{-(\hat{t}-\hat{\tau})}\sqrt{\hat{t}/\hat{\tau}}\, d\hat{\tau}\right)^2 \\ & + \frac{\Phi_1}{2}\int_0^{\hat{t}}\left(1-\frac{\Phi_1}{4}(\hat{t}-\hat{\tau})\left(1+\frac{\hat{x}^2}{2\hat{\tau}}\right)\right) e^{\frac{\hat{x}^2}{4}\left(\frac{1}{\hat{t}}-\frac{1}{\hat{\tau}}\right)} e^{-(\hat{t}-\hat{\tau})}\sqrt{\hat{t}/\hat{\tau}}\, d\hat{\tau} \end{aligned} \tag{9.2.18}$$

when Φ_2 is of higher order than Φ_1. Because Φ_2 can be thought of as being zero for (9.2.18), the expression for $u(\hat{x},\hat{t})$ in (9.2.18) is the approximate perturbation function for the unit step response of the damped telegraph equation ($\Phi_2 = 0$), which is defined in (5.2.5), for small Φ_1.

Now that $u(\hat{x},\hat{t})$ is determined, the unit step response ($\beta = 0$) for small parameters is known. The unit step response is defined in (9.2.6), where $u(\hat{x},\hat{t})$ is defined by (9.2.17) or (9.2.18) if Φ_2 has the same or higher order than Φ_1, respectively.

9.3 Conclusions

We approximated the unit step response ($\beta = 0$) of our IBVP for small Φ_1 and Φ_2 by perturbing the exact solution for zero Φ_1 with an arbitrary function $u(\hat{x},\hat{t})$, according to (9.2.6). The perturbation function $u(\hat{x},\hat{t})$ was then found to be (9.2.17) or (9.2.18) if Φ_2 has the same or higher order than Φ_1, respectively.

We ignored cubic terms and terms of higher order in all our expansions in order to create our approximate unit step response. This means that the error σ in our approximation of the unit step response is of $O(\Phi_1^3)$. Consequently, the only way to increase the order of σ is to include at least cubic terms in our expansions used to create the perturbation function $u(\hat{x}, \hat{t})$.

Chapter 10

Overall Behavior of General Matrix Temperature Equation

10.1 Introduction

In Chapter 7, we created an IBVP in order to study the behavior of our general equation for matrix temperature. We chose to study the heat transfer in an infinite, one-dimensional composite governed by the general equation

$$\Phi_2(\partial_{\hat{t}}\theta_m - \partial_{\hat{x}}^2\theta_m) + 2\int_0^{\hat{t}} \mathrm{Y}(\hat{t}-\hat{\tau})\partial_{\hat{\tau}}(\Phi_1\theta_m + \partial_{\hat{\tau}}\theta_m - \partial_{\hat{x}}^2\theta_m)d\hat{\tau} = 0, \qquad (10.1.1)$$

where the entire composite (matrix and particles) for our IBVP has an initially uniform temperature. The Laplace transform of the governing equation (10.1.1) for our IBVP was found to be

$$(\hat{s}\overline{\theta}_m - \partial_{\hat{x}}^2\overline{\theta}_m)(\Phi_2 + (\hat{m}\coth\hat{m} - 1)) + \Phi_1(\hat{m}\coth\hat{m} - 1)\overline{\theta}_m = 0. \qquad (10.1.2)$$

Even though a general explicit solution of the IBVP described in Chapter 7 cannot be found, the general equation (10.1.1) may behave in a describable way when time is infinitesimally small or infinitely large. Accordingly, in this chapter, we desire to learn how the general equation (10.1.1) for our IBVP behaves for infinitesimally small time (or *small time*, for short) and infinitely large time (or *large time*, for short). By learning how the general equation behaves over time, we will learn more about the physics of heat transfer in our composite.

10.2 Small and Large-Time Limits of General Matrix Temperature Equation

We can use the Laplace transform (10.1.2) of the general matrix temperature equation for our IBVP to find how the general equation (10.1.1) behaves when time is infinitesimally small or infinitely large. The small-time and large-time limits are found by taking the limit of (10.1.2) as $\hat{s}$ goes to infinity and zero, respectively [20]. It can be shown that

$$\hat{s}\,\overline{\theta}_m = \partial_{\hat{x}}^2 \overline{\theta}_m \text{ as } \hat{s} \to \infty \tag{10.2.1}$$

and that

$$\hat{s}\,\overline{\theta}_m = \hat{\alpha}\,\partial_{\hat{x}}^2 \overline{\theta}_m \text{ as } \hat{s} \to 0\,, \tag{10.2.2}$$

where

$$\hat{\alpha} = \frac{1}{1+\Phi_1}\,. \tag{10.2.3}$$

When (10.2.1) and (10.2.2) are inverted as usual, we find that

$$\partial_{\hat{t}}\theta_m = \partial_{\hat{x}}^2 \theta_m \text{ as } \hat{t} \to 0 \tag{10.2.4}$$

and that

$$\partial_{\hat{t}}\theta_m = \hat{\alpha}\,\partial_{\hat{x}}^2 \theta_m \text{ as } \hat{t} \to \infty\,, \tag{10.2.5}$$

respectively, where the matrix temperature steadies to equilibrium with time [23]. When (10.2.4) and (10.2.5) are converted to dimensional forms by using (4.2.1) and (4.7.1), we find that

$$\partial_t T_m = \alpha_m \partial_x^2 T_m \text{ as } t \to 0 \tag{10.2.6}$$

and that

$$\partial_t T_m = \alpha_{eff}\,\partial_x^2 T_m \text{ as } t \to \infty\,, \tag{10.2.7}$$

where the effective thermal diffusivity α_{eff} is

$$\alpha_{eff} = \frac{\alpha_m}{1+\Phi_1}\,. \tag{10.2.8}$$

The small-time limit of the non-dimensional general heat equation (10.1.1) is in (10.2.4) and the large-time limit of the general equation is in (10.2.5). Comparison of both (10.2.4) and (10.2.6) with (4.7.9) reveals that the general heat equation (10.1.1) for the composite behaves as the Fourier heat equation for the matrix, which we call *the* Fourier heat equation (FHE) for simplicity, when time is infinitesimally small. On the other hand, as seen in (10.2.5) and (10.2.7), the general heat equation behaves as the *modified* Fourier heat equation (MFHE) when time is infinitely large.

10.3 Physical Interpretation of Progression from FHE to MFHE

Thus far, we have revealed that the general matrix temperature equation (10.1.1) for our IBVP diverges from the Fourier heat equation (FHE) in (10.2.4) and converges to the *modified* Fourier heat equation (MFHE) in (10.2.5) as the matrix temperature equilibrates over time. At this point, we would like to explain the physics of this evolution of the general equation.

The transition from the FHE to the MFHE can be explained from an energy standpoint. Because our general heat equation accounts for the energy transfer between the matrix and particles, we expect that the parameter Φ_1, which is particularly related to this energy transfer, is crucial to understanding the temporal evolution of the general heat equation. As stated in Chapter 4, the parameter Φ_1 represents the amount of energy that the particles are able to consume relative to the matrix. Thus, when Φ_1 is zero, the particles consume *no energy* relative to the matrix. In fact, we learned in Chapter 4 that the general heat equation (4.7.3) for the composite is identical to Fourier's heat equation (4.7.9) for the matrix for *all* time when Φ_1 is zero. In other words, when *no heat* transfers to the particles, the matrix temperature for our IBVP is determined by the FHE in (10.2.4), just as it is when no particles are embedded in the matrix. Consequently, there is no evolution of the general matrix temperature equation when Φ_1 is zero. As far as the matrix is concerned, the particles act as "holes", i.e., as vacuums, for all time when Φ_1 is zero, because no energy is transferred to the particles.

On the other hand, if Φ_1 is positive, energy is able to transfer to the particles, meaning that the particles are not "holes". However, the general heat equation (10.1.1) does behave as the FHE (10.2.4) for *small time*, even if Φ_1 is positive. Therefore, as far as the matrix is concerned, the particles act as "holes" *initially*, which means that no energy is transferred initially to the particles. Indeed, because there is no initial temperature difference between the matrix and particles for our IBVP, there is initially *no heat transfer* from the matrix to the particles, no matter what the value of Φ_1. Without any initial heat transfer to the particles, the matrix temperature in our composite is governed initially by the Fourier heat equation for the matrix.

Then, as time increases, heat transfers through the matrix, causing the matrix temperature to increase and energy to transfer to the particles when Φ_1 is positive. The particles are no longer permanent "holes", because the particles consume energy from the matrix for positive

Φ_1. Consequently, the particles still act as "holes" initially, but then the general matrix temperature equation (10.1.1) begins to *diverge* from the FHE for the matrix. In fact, according to (10.2.5), the general equation *converges* with time to the MFHE that contains the modified non-dimensional thermal diffusivity $\hat{\alpha}$, which is *less than* the non-dimensional matrix thermal diffusivity of unity in the FHE. Thus, as the matrix equilibrates, the heat transfer to the particles causes a "decrease" in the non-dimensional thermal diffusivity of the matrix from unity (in the FHE) to a lesser value of $\hat{\alpha}$ (in the MFHE). In other words, the particles effectively "slow down" heat transfer in the matrix by consuming energy from the matrix. In fact, as Φ_1 increases, the modified diffusivity $\hat{\alpha}$ decreases, which means that the particles "slow down" heat transfer in the matrix more and more as their ability to consume energy from the matrix increases.

We can explain why the large-time limit of the general heat equation, which is the MFHE, is a type of Fourier heat equation. Our reasoning lies in the fact that the particles equilibrate with the matrix as the matrix equilibrates. Consequently, the particles have essentially the *same* temperature as its surrounding matrix for large time. This means that the details of heat transfer between the particles and matrix can be ignored for large time, such that *bulk properties* of the composite, like the effective thermal diffusivity α_{eff}, can be used instead.

In summary, the general matrix heat equation (10.1.1) diverges from the Fourier heat equation (FHE) in (10.2.4) and converges over time to the modified Fourier heat equation (MFHE) in (10.2.5) as the composite temperatures equilibrate. Because no energy is initially transferred to the particles, the particles act as "holes" initially, such that the FHE holds for small time. On the other hand, the MFHE governs the matrix temperature for large time when the particles are essentially in *equilibrium* with the matrix.

10.4 Application of Numerical Scheme

We now want to visualize the evolution of the general matrix temperature equation (10.1.1) from the FHE to the MFHE. In order to do so, we will use the numerical scheme devised in Chapter 7 to approximate the matrix temperature $\theta_m(\hat{x},\hat{t})$. When Φ_1 is of $O(1)$ and

$\sigma\hat{t} << 1$, the error between the approximate and the exact solutions of our IBVP is bounded in magnitude by the error bound σ. Thus, to make sure that our application of the numerical scheme is justified in this chapter, we will make sure that Φ_1 is of $O(1)$ and $\sigma\hat{t} << 1$ when applying the numerical scheme.

First, we need to choose a value for the error bound σ that is required in our numerical scheme. As stated in Chapter 7, once σ is specified, values for N, $\Delta\omega$, and γ are determined using (7.10.8), (7.10.10), and (7.10.11), respectively, which are subsequently used in (7.5.6) to determine our approximate solution $\theta_a(\hat{x}, \hat{t})$ of the IBVP. We let σ be equal to $5(10^{-4})$, which is very small compared to one, ensuring that our approximate solution is relatively close to the exact solution. When our value for σ is substituted into (7.10.8), (7.10.10), and (7.10.11), we find that $N = 3031$, $\Delta\omega = 0.634/\hat{t}$, and $\gamma = 1/\hat{t}$, respectively. When these expressions for N, $\Delta\omega$, and γ are substituted into (7.5.6) and the parameters (β, Φ_1, and Φ_2) are chosen, the approximate solution $\theta_a(\hat{x}, \hat{t})$ is known.

Once values for β, Φ_1, Φ_2, and $\hat{t}$ are chosen, we can plot $\theta_a(\hat{x}, \hat{t})$ for a suitable $\hat{x}$ domain, such that important behaviors are seen in the resulting temperature curve or *temperature profile*. Table 10.1 contains the limits of the values for β, Φ_1, Φ_2, and $\hat{t}$ for application of the numerical scheme in this chapter.

Table 10.1: Limits of Parameter and Variable Values for Numerical Scheme

Parameter or Variable	Lower Limit	Upper Limit
Φ_1	0	10
Φ_2	0	∞
β	0	∞
$\hat{t}$	0	$5(10^3)$

As required, the limits in Table 10.1 meet the constraints for our numerical scheme. The upper limit of $\hat{t}$ ensures that $\sigma\hat{t} << 1$ for all possible values of $\hat{t}$, and the upper limit of Φ_1 ensures that all possible values of Φ_1 are of $O(1)$ with Φ_1 not being very large compared to one.

Furthermore, no constraints exist for the non-negative parameters β and Φ_2, meaning that both β and Φ_2 can be any non-negative number, as seen in Table 10.1.

We can now visualize the temporal evolution of the general matrix temperature equation from the FHE in (10.2.4) to the MFHE in (10.2.5) by using the numerical scheme just described.

10.5 Visualization of Progression of General Heat Equation from FHE to MFHE

The progression of the general heat equation from the FHE to the MFHE is most easily seen in the temporal evolution of the general unit step response ($\beta = 0$) for our IBVP. Accordingly, it would be instructive to know the small and large-time limits of the general unit step response. Simply put, the limits of the general unit step response are the unit step responses of the limits of the general heat equation. In other words, the general unit step response must limit to the unit step response of both the FHE as $\hat{t} \to 0$ and the MFHE as $\hat{t} \to \infty$. This means that

$$\theta_m = \operatorname{erfc}(\hat{x}/2\sqrt{\hat{t}}) \text{ as } \hat{t} \to 0 \tag{10.5.1}$$

and

$$\theta_m = \operatorname{erfc}(\hat{x}/2\sqrt{\hat{\alpha}\hat{t}}) \text{ as } \hat{t} \to \infty, \tag{10.5.2}$$

according to (10.2.4) and (10.2.5), respectively [19]. Therefore, the unit step response ($\beta = 0$) for our IBVP must diverge from the small-time error function in (10.5.1) for the FHE and converge to the large-time error function in (10.5.2) for the MFHE as time increases.

Using our numerical scheme described in Section 10.4, we now visualize the progression of the general unit step response from the small-time error function in (10.5.1) to the large-time error function in (10.5.2). As a first attempt, Figure 10.1 contains a plot of the general unit step response ($\beta = 0$) for certain values of Φ_1 and Φ_2 and multiple values of time $\hat{t}$. While it is obvious from Figure 10.1 that the matrix temperature generally increases with time $\hat{t}$ as the matrix equilibrates toward the boundary value of unity, it may not be so obvious how the unit step response transitions from the small-time error function in (10.5.1) to the large-time error function in (10.5.2). To see such a transition, we need to scale our domain. We need to replace

$\hat{x}$ as the independent variable of Figure 10.1 by some quantity that depends on at least both $\hat{x}$ and $\hat{t}$. In the spirit of the error functions in (10.5.1) and (10.5.2), we decide to scale $\hat{x}$ by $\hat{t}^{-1/2}$.

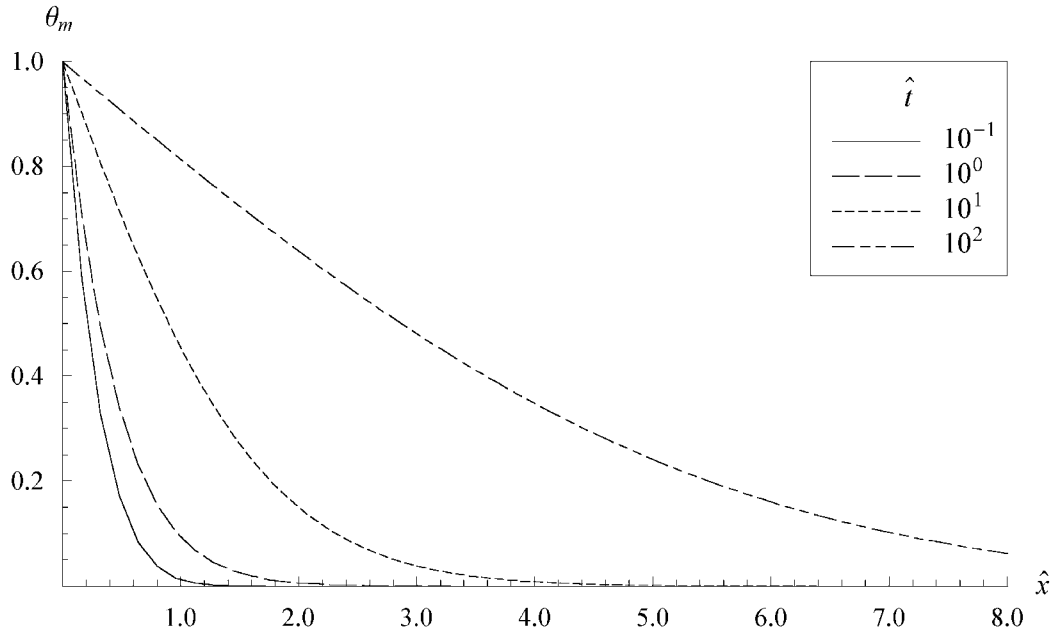

Figure 10.1: θ_m vs. $\hat{x}$ for $\Phi_1 = 10$, $\Phi_2 = 0.1$, and $\beta = 0$

Figure 10.2 contains the general unit step response ($\beta = 0$) for our IBVP as time $\hat{t}$ varies with the new scaling of the abscissa. As seen in Figure 10.2, the general unit step response diverges from the initial unit step response for the FHE and converges over time to the unit step response for the MFHE. We also note that temperature generally *decreases* as time increases for fixed $\hat{x}/\sqrt{\hat{t}}$ in Figure 10.2, even though temperature *increases* with time for fixed $\hat{x}$ in Figure 10.1. The matrix temperature generally decreases in Figure 10.2 because the general matrix temperature equation (10.1.1) is evolving from the FHE to the MFHE, while temperature increases in Figure 10.1 because the matrix is simply reaching equilibrium.

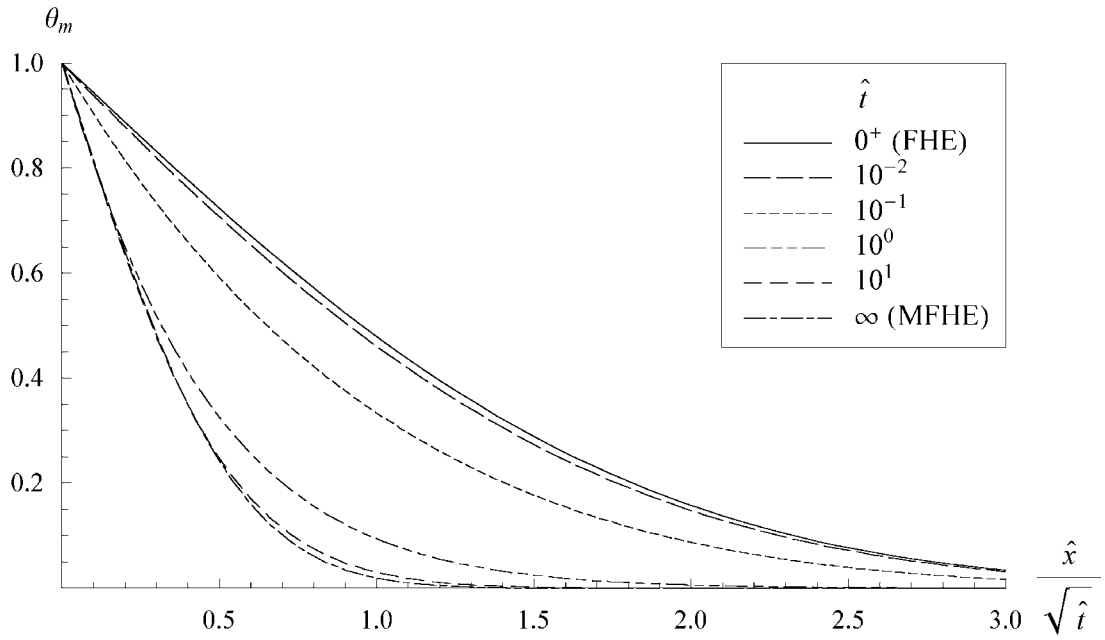

Figure 10.2: θ_m vs. $\hat{x}/\sqrt{\hat{t}}$ for $\Phi_1 = 10$, $\Phi_2 = 0.1$, and $\beta = 0$

We can also use analytical means to show how the unit step response evolves from the small-time error function in (10.5.1) to the large-time error function in (10.5.2). In Chapter 9, we approximated the general unit step response for small Φ_1 and Φ_2. According to (9.2.6), we determined that the unit step response of the general heat equation (10.1.1) is

$$\theta_m = \operatorname{erfc}(\hat{x}(1+u(\hat{x},\hat{t}))/2\sqrt{\hat{t}}\,), \tag{10.5.3}$$

where the perturbation function $u(\hat{x},\hat{t})$ is approximately that given in (9.2.17) for small Φ_1 and Φ_2. Now, comparison of the small and large-time unit step responses in (10.5.1) and (10.5.2) with the general unit step response in (10.5.3) reveals that

$$u(\hat{x},\hat{t}) \to 0 \text{ as } \hat{t} \to 0 \tag{10.5.4}$$

and

$$u(\hat{x},\hat{t}) \to \hat{\alpha}^{-1/2} - 1 \text{ as } \hat{t} \to \infty\,. \tag{10.5.5}$$

Therefore, the approximation of $u(\hat{x},\hat{t})$ in (9.2.17) must satisfy the limits in (10.5.4) and (10.5.5) in at least an approximate sense for small parameters. Once we show that the approximation of $u(\hat{x},\hat{t})$ in (9.2.17) satisfies the limits in (10.5.4) and (10.5.5), we will use our

analytical approximation of $u(\hat{x},\hat{t})$ to visualize the evolution of the general heat equation from the FHE to the MFHE.

We can show that the small and large-time limits in (10.5.4) and (10.5.5), respectively, are approximated by our perturbation function $u(\hat{x},\hat{t})$ in (9.2.17). First, it can be shown that $u(\hat{x},\hat{t}) \to 0$ as $\hat{t} \to 0$ in (9.2.17), which is in accordance with (10.5.4). Second, it can be shown that

$$u(\hat{x},\hat{t}) \to \frac{\Phi_1}{2} - \frac{\Phi_1^{\,2}}{8} \text{ as } \hat{t} \to \infty \tag{10.5.6}$$

in an approximate sense for small Φ_1. Now, the limit in (10.5.6) must be an approximation of the exact limit in (10.5.5) for small Φ_1. To prove this, we first substitute the definition (10.2.3) of $\hat{\alpha}$ into (10.5.5) to find that

$$u(\hat{x},\hat{t}) \to \sqrt{1+\Phi_1} - 1 \text{ as } \hat{t} \to \infty. \tag{10.5.7}$$

Next, by expanding the limit in (10.5.7), we can show that

$$u(\hat{x},\hat{t}) \to \frac{\Phi_1}{2} - \frac{\Phi_1^{\,2}}{8} + O(\Phi_1^{\,3}) \text{ as } \hat{t} \to \infty \tag{10.5.8}$$

for $\Phi_1 << 1$. Indeed, the large-time limit in (10.5.6) is an approximation of the exact limit seen in (10.5.8) for small Φ_1. To be more precise, the limit in (10.5.6) is the first two terms of the expansion of the exact limit seen in (10.5.8).

If we plot the approximation of $u(\hat{x},\hat{t})$ versus time $\hat{t}$, we can visualize $u(\hat{x},\hat{t})$ diverge from its zero value (for the FHE) and converge to its approximate non-zero value (for the MFHE) given in (10.5.6). Consequently, we can use our analytical approximation of $u(\hat{x},\hat{t})$ in (9.2.17) to visualize the progression of the general unit step response. Figure 10.3 is such a plot of the evolution of $u(\hat{x},\hat{t})$ over time. The figure includes a plot of the approximation (9.2.17) of u versus $\hat{t}$ for certain parameter and variable values. As known, u starts at zero (for the FHE) and limits to its non-zero value (for the MFHE) as time increases. The evolution of u from its initially zero value to its limiting non-zero value is coincident with the evolution of the general unit step response from the small-time error function for the FHE in (10.5.1) to the large-time error function for the MFHE in (10.5.2).

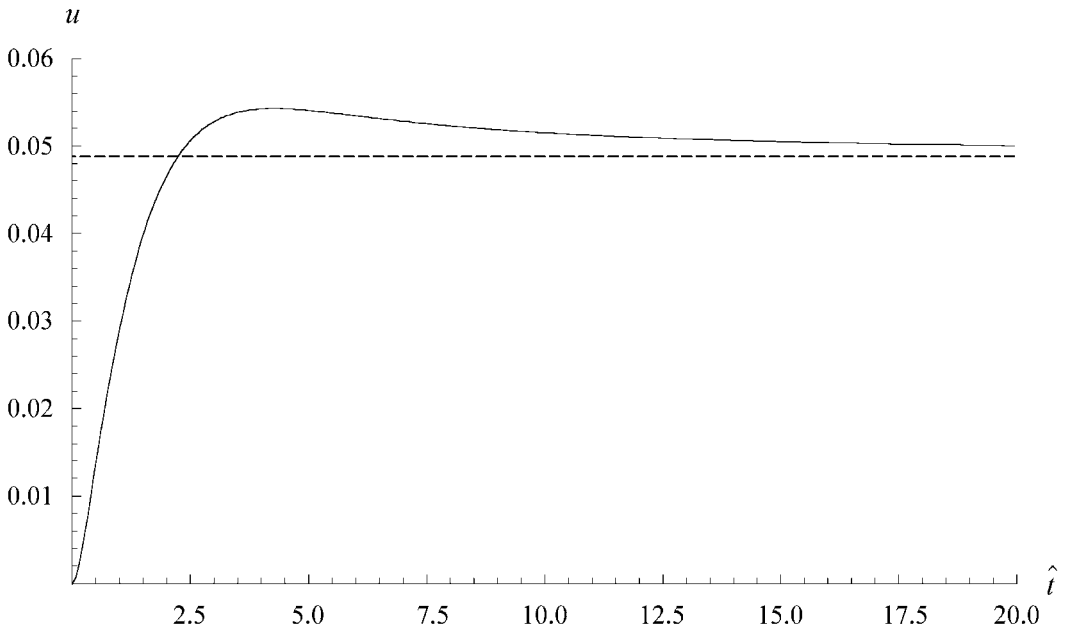

Figure 10.3: u vs. $\hat{t}$ for $\hat{x} = 1$, $\Phi_1 = 0.1$, and $\Phi_2 = 0.2$

10.6 Difference Between Damped Telegraph Equation and General Equation

We now desire to know how the matrix temperature depends on Φ_2. Specifically, we want to know how the matrix temperature for the DTE ($\Phi_2 = 0$) differs from that for general Φ_2. We begin by noting that the general equation (10.1.1) for our IBVP limits to the Fourier heat equation for the matrix as time becomes infinitesimally small and, on the other hand, limits to the *modified* Fourier heat equation as time become infinitely large. Those limits are true for all fixed Φ_2, including Φ_2 being zero. Consequently, the limit of $\Phi_2 \to 0$ does *not* affect the small and large-time limits of the general heat equation for our IBVP. In other words, the parameter Φ_2 does not affect the small and large-time matrix temperatures. The error functions in (10.5.1) and (10.5.2) for the unit step response of the general heat equation are then independent of Φ_2, which is why the parameter Φ_2 is not seen in both (10.5.1) and (10.5.2).

Even though Φ_2 is not associated with the temporal *limits* of the general matrix heat equation, the parameter Φ_2 is related to the *limiting* of the general equation, i.e., the parameter Φ_2 affects the matrix temperature for moderate times. The parameter Φ_2 affects the transient nature

of the general heat equation and we desire to find how Φ_2 affects these transient matrix temperatures. It is then wise to know the limits of the general heat equation (10.1.1) as Φ_2 approaches its limits seen in Table 10.1. First, when $\Phi_2 \to 0$, we know that the general equation (10.1.1) limits to the one-dimensional damped telegraph equation,

$$(1+\Phi_1)\partial_{\hat{t}}\theta_m + \partial_{\hat{t}}^2\theta_m = \partial_{\hat{x}}^2\theta_m + \partial_{\hat{t}}\partial_{\hat{x}}^2\theta_m . \tag{10.6.1}$$

On the other hand, when $\Phi_2 \to \infty$, it can be shown that the general heat equation (10.1.1) reduces to the Fourier heat equation for the matrix. The limits may help us to physically interpret how the matrix temperature depends on the parameter Φ_2.

By plotting the unit step response for various values of Φ_2, we can determine how the matrix temperature varies generally with Φ_2. Figure 10.4 shows a plot of the general unit step response ($\beta = 0$) for various values of Φ_2 when $\hat{t} = 1$ and $\Phi_1 = 10$ over a suitable $\hat{x}$ range. We see in Figure 10.4 that the temperatures are the lowest for $\Phi_2 = 0$ (damped telegraph equation) and highest for $\Phi_2 \to \infty$ (Fourier heat equation) when $\hat{t} = 1$. In other words, the matrix temperature generally *increases* as Φ_2 increases.

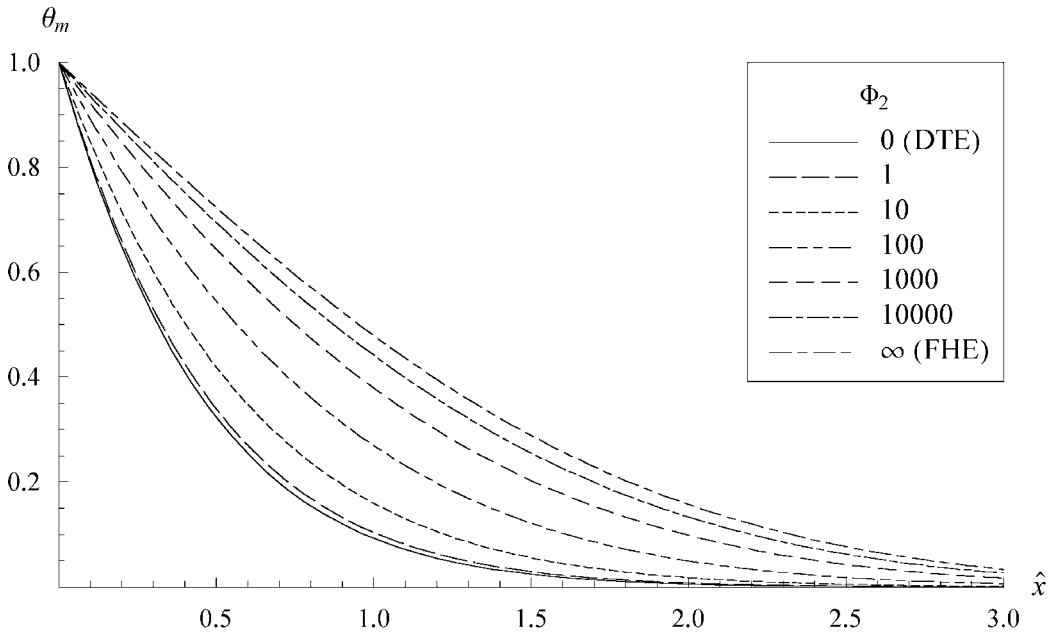

Figure 10.4: θ_m vs. $\hat{x}$ for $\hat{t} = 1$, $\Phi_1 = 10$, and $\beta = 0$

The fact that temperature generally increases as Φ_2 increases is explainable from a physical point of view. First, by substituting the definitions of τ_p and Φ_2 from Chapter 4 into the definition (4.6.15) of τ_μ, we find that

$$\tau_\mu = \frac{R\rho_p c_p}{3\mu}, \tag{10.6.2}$$

where

$$\Phi_2 = \mu R / k_p \,. \tag{10.6.3}$$

Now, in Figure 10.4, the parameter Φ_2 is increased from its zero value while $\hat{x}$ and $\hat{t}$ are held fixed. According to the non-dimensional variables in (4.7.1), we can fix $\hat{x}$ and $\hat{t}$ by fixing x, t, α_m, and, most importantly, τ_μ. As seen in (10.6.2) and (10.6.3), we can keep τ_μ fixed while increasing Φ_2 by *decreasing* the particle thermal conductivity k_p. Consequently, as Φ_2 increases from zero in Figure 10.4, the particle thermal conductivity k_p decreases from its infinite value (for $\Phi_2 = 0$) to a non-zero value (for non-zero Φ_2).

Finally, we can use the fact that k_p decreases as Φ_2 increases to explain why the matrix temperature increases with Φ_2. As the particle conductivity k_p decreases, less heat is generally conducted to the particles, which means that the matrix temperature will generally increase because it retains more energy. As $\Phi_2 \to \infty$, $k_p \to 0$ according to (10.6.3), which means that no heat is transferred to the particles from the matrix. Then, without any heat transfer between the matrix and the particles, the matrix temperature is not affected by the particles, which means that the matrix is governed by Fourier's heat equation for $\Phi_2 \to \infty$. Thus, as Φ_2 increases, the matrix temperature generally increases from that for the DTE to that for the FHE for fixed space $\hat{x}$ and time $\hat{t}$.

Of course, the non-dimensional variables $\hat{x}$ and $\hat{t}$, which are seen in the general equation (10.1.1), were created to use when Φ_2 is small and definitely *not* infinite in value. Consequently, if one truly desires to let $\Phi_2 \to \infty$, it is more appropriate to limit a form of the general heat equation (10.1.1) that contains $\tilde{x}$ and $\tilde{t}$, which were created to use when Φ_2 is large relative to one. If this limit is performed, then a one-dimensional form of the "perfect contact" equation (4.7.10) is obtained, instead of the Fourier heat equation (10.2.4) for the matrix.

10.7 Discussion of Thermal Waves

If thermal waves are observable, we expect that they would be observed in the unit step response of the general matrix temperature equation (10.1.1) because an initially sharp jump in boundary temperature should cause a wavefront if possible. However, only diffusion-like behavior is observed in the unit step responses of Figure 10.2.

The diffusion-like behavior of the general heat equation (10.1.1) is expected, because the general equation was created after assuming diffusion for the composite materials. In fact, the small-time limit (the *Fourier* heat equation) and large-time limit (the modified *Fourier* heat equation) of the general heat equation are both explicitly diffusive in nature and in name. As stated in Section 5.7, the mixed-derivative term in the damped telegraph equation (10.6.1) eliminates wavefronts, and this is illustrated in Figure 10.4.

10.8 Conclusions

In this chapter, we revealed that the general matrix temperature equation (10.1.1) is initially the Fourier heat equation (FHE) in (10.2.4) and limits to the modified Fourier heat equation (MFHE) in (10.2.5) as the matrix equilibrates. This temporal evolution is visualized in Figure 10.2 for the unit step response of the general heat equation.

We then explained why the general heat equation (10.1.1) evolves from the FHE to the MFHE. Because no energy is transferred initially to the particles, the particles act initially as "holes", such that the Fourier heat equation for the matrix governs the matrix temperature for small time. Then, as the particles and matrix equilibrate over time, the non-dimensional thermal diffusivity of the matrix "decreases" from unity (in the FHE) to a lesser value of $\hat{\alpha}$ (in the MFHE). The MFHE, which includes the bulk thermal diffusivity of $\hat{\alpha}$, exists when the particles are essentially in *equilibrium* with the matrix for large time.

While Φ_2 does not affect the small and large-time matrix temperatures associated with the FHE and MFHE, respectively, the parameter does affect the transient matrix temperatures. It was shown how the matrix temperature for the unit step response generally *increases* as Φ_2 increases for fixed space $\hat{x}$ and time $\hat{t}$. As seen in Figure 10.4, the unit step response of the

damped telegraph equation ($\Phi_2 = 0$) generally has the smallest temperatures relative to the unit step responses for positive Φ_2.

Finally, we could not find any wavefronts associated with thermal waves, which was expected because our general heat equation (10.1.1) is based on *diffusion*.

Chapter 11

Large-Time Behavior of General Matrix Temperature Equation

11.1 Introduction

In Chapter 10, we discovered that the general matrix heat equation,

$$\Phi_2(\partial_{\hat{t}}\theta_m - \partial_{\hat{x}}^2\theta_m) + 2\int_0^{\hat{t}} \mathrm{Y}(\hat{t}-\hat{\tau})\partial_{\hat{t}}(\Phi_1\theta_m + \partial_{\hat{t}}\theta_m - \partial_{\hat{x}}^2\theta_m)d\hat{\tau} = 0, \tag{11.1.1}$$

for our IBVP is initially the Fourier heat equation (FHE) for the matrix,

$$\partial_{\hat{t}}\theta_m = \partial_{\hat{x}}^2\theta_m, \tag{11.1.2}$$

and limits to the modified Fourier heat equation (MFHE),

$$\partial_{\hat{t}}\theta_m = \hat{\alpha}\,\partial_{\hat{x}}^2\theta_m, \tag{11.1.3}$$

as the particles and matrix equilibrate, where

$$\hat{\alpha} = \frac{1}{1+\Phi_1}. \tag{11.1.4}$$

Consequently, it was found that the general unit step response of (11.1.1) limits from the small-time error function,

$$\theta_m = \mathrm{erfc}(\hat{x}/2\sqrt{\hat{t}}), \tag{11.1.5}$$

to the large-time error function,

$$\theta_m = \mathrm{erfc}(\hat{x}/2\sqrt{\hat{\alpha}\hat{t}}), \tag{11.1.6}$$

as time increases.

The small-time limit (11.1.5) and large-time limit (11.1.6) of the general unit step response are independent of the parameter Φ_2, as noted in Chapter 10. However, the way the general unit step response limits to the large-time error function (11.1.6) with time depends on Φ_2, because the heat transfer from the matrix to the particles depends on Φ_2. In fact, we remarked about how the matrix temperature generally depends on Φ_2 in Section 10.6. In this chapter, we will learn more about the dependence of temperature of Φ_2 by creating conditions

that, when satisfied, render the general unit step response to be sufficiently close to its large-time limit (11.1.6). By learning more about how the general heat equation (11.1.1) limits in time to the modified Fourier heat equation (11.1.3), we hope to discover more about the physics of heat transfer in the composite.

11.2 Large-Time Behavior of General Heat Equation for Zero Φ_2

We desire to create conditions for all Φ_2 that render the general unit step response to be sufficiently close to its large-time limit (11.1.6). We first choose to find the conditions for zero Φ_2, which are associated with the damped telegraph equation ($\Phi_2 = 0$). First, after utilization of (11.1.4), it can be shown that the one-dimensional damped telegraph equation (DTE) (10.6.1) is

$$\partial_{\hat{t}}\theta_m + \hat{\alpha}\partial_{\hat{t}\hat{t}}\theta_m = \hat{\alpha}\hat{\nabla}^2\theta_m + \hat{\alpha}\partial_{\hat{t}}\hat{\nabla}^2\theta_m, \tag{11.2.1}$$

which was created in Chapter 5 by taking the limit of the general heat equation as $\Phi_2 \to 0$. Upon comparison of the DTE (11.2.1) with the MFHE (11.1.3), it is seen that the first terms on each side of the DTE constitute the MFHE. Accordingly, if the second terms are sufficiently small relative to the respective first terms on each side of the DTE (11.2.1), then the DTE is approximately the MFHE. Therefore, when

$$\frac{\hat{\alpha}\partial_{\hat{t}\hat{t}}\theta_m}{\partial_{\hat{t}}\theta_m} << 1 \text{ and } \frac{\partial_{\hat{t}}\hat{\nabla}^2\theta_m}{\hat{\nabla}^2\theta_m} << 1, \tag{11.2.2}$$

the damped telegraph equation, i.e., the general heat equation for zero Φ_2, is approximately the modified Fourier heat equation.

The conditions in (11.2.2) are important because if the DTE is approximately the MFHE, then the unit step response of the DTE should approximate the unit step response of the MFHE. In other words, if the conditions in (11.2.2) are satisfied, then the approximate unit step response of the DTE is the large-time error function (11.1.6). Consequently, we can substitute (11.1.6) into (11.2.2) to find the conditions that make the general unit step response for zero Φ_2 be approximately the large-time error function. Substitution of (11.1.6) into (11.2.2) yields

$$\frac{\hat{x}^2 - 6\hat{t}\hat{\alpha}}{4\hat{t}^2} << 1 \text{ and } \frac{\hat{x}^2 - 6\hat{t}\hat{\alpha}}{4\hat{t}^2\hat{\alpha}} << 1. \tag{11.2.3}$$

Because $\hat{\alpha}$ is at most unity, it can be shown that

$$\left(\frac{\hat{x}}{2\sqrt{\hat{\alpha}\hat{t}}} \right)^2 << \hat{t} \text{ and } \hat{t} >> 1 \tag{11.2.4}$$

satisfy the conditions in (11.2.3) roughly. When the conditions in (11.2.4) are satisfied, the general unit step response for the DTE is approximately its large-time limit in (11.1.6).

The physical significance of the conditions in (11.2.4) can be understood by using the definition of the thermalization time τ_T in (4.6.16). According to (4.7.1), the second condition in (11.2.4) is simply a statement that time *t* must be *large* compared to the time scale τ_μ, which is why the conditions in (11.2.4) are for *large* time. Now, when $\Phi_2 = 0$, the time scale τ_μ is equivalent to the thermalization time τ_T, according to (4.6.16). The second condition in (11.2.4) then means that time *t* much be large compared to the thermalization time τ_T. Therefore, the latter condition in (11.2.4) is interpreted to mean that time *t* must be much greater than the time required to roughly heat up a particle to be in equilibrium with the matrix. For the particles in the matrix domain that satisfy the first condition of (11.2.4), the second condition of (11.2.4) means that those particles have a roughly uniform temperature that approximately matches and changes with the matrix temperature. In other words, when the conditions in (11.2.4) are satisfied, the MFHE approximates the DTE because certain particles are fairly equilibrated with the matrix. Because the DTE (11.2.1) limits to the MFHE (11.1.3) as particles become fully equilibrated with the matrix for infinite time, the connection of the conditions in (11.2.4) to the thermalization time of the particles makes sense.

11.3 Hypothesis About Large-Time Behavior for All Φ_2

We showed in the previous section that time *t* must be much larger than the thermalization time τ_T for the general heat equation to be approximately its large-time limit (the MFHE) for zero Φ_2. By extrapolation, we now hypothesize that time *t* must be relatively large compared to the thermalization time τ_T for *all* Φ_2, and not just when Φ_2 is zero, in order for the general heat equation to sufficiently converge to the modified Fourier heat equation. Thus, according to the definition (4.6.16) of τ_T, we hypothesize that time *t* much be large compared to

τ_μ for $\Phi_2 << 1$ and τ_p otherwise, respectively, for the general heat equation to be approximately its large-time limit (the MFHE). In other words, we hypothesize that when $\hat{t} >> 1$ for $\Phi_2 << 1$ and when $\tilde{t} >> 1$ for all other Φ_2, the general heat equation (11.1.1) is approximately its large-time limit (11.1.3) within a certain domain.

Because we hypothesize that the size of $\tilde{t}$ governs how the general matrix temperature equation limits to the modified Fourier heat equation for moderate-to-large Φ_2, it may be wise to investigate this hypothesis by using equations that directly contain $\tilde{t}$. The non-dimensional variable $\tilde{t}$, which is the ratio of t to τ_p, was used to non-dimensionalize the general heat equation (4.2.18) to form (4.7.6). Therefore, it will be convenient to use (4.7.6) to analyze the large-time behavior of the general unit step response for moderate-to-large Φ_2. Perhaps our hypothesis that the order of $\tilde{t}$ governs how the general heat equation converges to its large-time limit is correct.

If we use the form of the general matrix temperature equation that contains $\tilde{t}$, we should also use forms of the MFHE (11.1.3) and its unit step response (11.1.6) that contain $\tilde{t}$. Both equations can be rearranged to be

$$\partial_{\tilde{t}}\theta_m = \hat{\alpha}\partial^2_{\tilde{x}}\theta_m \tag{11.3.1}$$

and

$$\theta_m = \operatorname{erfc}(\tilde{x}/2\sqrt{\hat{\alpha}\tilde{t}}), \tag{11.3.2}$$

respectively, for our one-dimensional medium by using (4.7.1) and (4.7.2). Equations (11.3.1) and (11.3.2) will be used to analyze the validity of our hypothesis about the time it take for the general heat equation to limit to its large-time limit (the modified Fourier heat equation).

11.4 Large-Time Behavior of General Heat Equation For Infinite Φ_2

Let us begin to test our hypotheses set forth in the previous section by determining if our hypotheses are at least true for infinite Φ_2. In the limit of $\Phi_2 \to \infty$ for our IBVP, the general matrix temperature equation (4.7.6) becomes the one-dimensional "perfect contact" equation (4.7.10),

$$\partial_{\tilde{t}}\theta_m - \partial_{\tilde{x}}^2\theta_m + 6\Phi_1\int_0^{\tilde{t}} \mathrm{Z}(\tilde{t}-\tilde{\tau})\partial_{\tilde{t}}\theta_m(\tilde{\tau})d\tilde{\tau} = 0\,. \tag{11.4.1}$$

For sufficiently large $\tilde{t}$, the general heat equation for infinite Φ_2 must be approximately its large-time limit (11.3.1), which is rearranged to be

$$\partial_{\tilde{t}}\theta_m - \partial_{\tilde{x}}^2\theta_m + \Phi_1\partial_{\tilde{t}}\theta_m = 0 \tag{11.4.2}$$

by using (11.1.4). We must then have that

$$6\Phi_1\int_0^{\tilde{t}}\sum_{n=1}^{\infty} e^{-n^2\pi^2(\tilde{t}-\tilde{\tau})}\partial_{\tilde{t}}\theta_m(\tilde{\tau})d\tilde{\tau} = \Phi_1\partial_{\tilde{t}}\theta_m \tag{11.4.3}$$

in an approximate sense for large time, upon equating (11.4.1) and (11.4.2) and using (4.7.8) to rearrange the result. By comparison of the left-hand and right-hand sides of (11.4.3), the integral in (11.4.3) must only depend on the local temporal derivative $\partial_{\tilde{t}}\theta_m(\tilde{t})$ of matrix temperature in some approximate sense. We need to find the conditions that make this possible.

We need to show how (11.4.3) can be true, which will either confirm of refute our hypothesis that $\tilde{t}$ must be large relative to one for the general heat equation to be approximately its large-time limit (11.1.3) for $\Phi_2 \to \infty$. The key to determining how (11.4.3) is true is revealed in the behavior of the exponentials in (11.4.3). Figure 11.1 contains a plot of the first two exponentials ($n = 1$ and $n = 2$) in the summation seen in (11.4.3) along with a general curve of the temporal derivative of matrix temperature. All the exponentials in (11.4.3), like those seen in Figure 11.1, are greatest in value for $\tilde{\tau} = \tilde{t}$ and decrease as $\tilde{\tau}$ decreases below $\tilde{t}$. When $\tilde{\tau} = \tilde{t} - 1$, the exponentials are much smaller in magnitude compared to their values near $\tilde{\tau} = \tilde{t}$. Because of the damping nature of the exponentials, if $\partial_{\tilde{t}}\theta_m(\tilde{\tau})$ is approximately constant between $\tilde{\tau} = \tilde{t} - 1$ and $\tilde{\tau} = \tilde{t}$, then we might be able to regard the derivative as being constant for integration purposes. According to Figure 11.1, if

$$\frac{\partial_{\tilde{t}\tilde{t}}\theta_m}{\partial_{\tilde{t}}\theta_m} << 1\,, \tag{11.4.4}$$

then we might be able to approximate $\partial_{\tilde{t}}\theta_m(\tilde{\tau})$ as $\partial_{\tilde{t}}\theta_m(\tilde{t})$ and consequently move it from inside the integral of (11.4.3) to outside the integral.

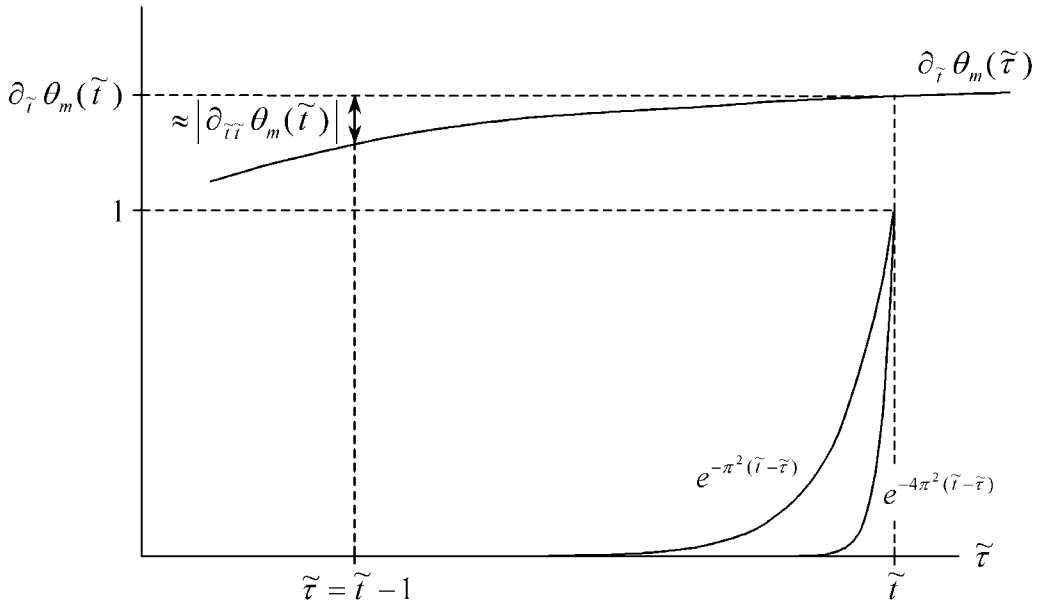

Figure 11.1: Several Exponentials Seen in (11.4.3)

Assuming that (11.4.4) is sufficient, we find that the left-hand side of (11.4.3) becomes approximately

$$6\Phi_1\int_0^{\tilde{t}}\sum_{n=1}^{\infty}e^{-n^2\pi^2(\tilde{t}-\tilde{\tau})}\partial_{\tilde{t}}\theta_m(\tilde{\tau})d\tilde{\tau}=6\Phi_1\partial_{\tilde{t}}\theta_m\int_0^{\tilde{t}}\sum_{n=1}^{\infty}e^{-n^2\pi^2(\tilde{t}-\tilde{\tau})}d\tilde{\tau}\,, \tag{11.4.5}$$

which, upon integration, can be shown to be

$$6\Phi_1\int_0^{\tilde{t}}\sum_{n=1}^{\infty}e^{-n^2\pi^2(\tilde{t}-\tilde{\tau})}\partial_{\tilde{t}}\theta_m(\tilde{\tau})d\tilde{\tau}=6\Phi_1\partial_{\tilde{t}}\theta_m\sum_{n=1}^{\infty}\frac{1}{n^2\pi^2}(1-e^{-n^2\pi^2\tilde{t}})\,. \tag{11.4.6}$$

If $\tilde{t}\ >> 1$, then (11.4.6) is approximately

$$6\Phi_1\int_0^{\tilde{t}}\sum_{n=1}^{\infty}e^{-n^2\pi^2(\tilde{t}-\tilde{\tau})}\partial_{\tilde{t}}\theta_m(\tilde{\tau})d\tilde{\tau}=6\Phi_1\partial_{\tilde{t}}\theta_m\sum_{n=1}^{\infty}\frac{1}{n^2\pi^2}\,. \tag{11.4.7}$$

Finally, because

$$\sum_{n=1}^{\infty}\frac{1}{n^2\pi^2}=\frac{1}{6} \tag{11.4.8}$$

according to Reference 18, (11.4.7) becomes

$$6\Phi_1 \int_0^{\tilde{t}} \sum_{n=1}^{\infty} e^{-n^2\pi^2(\tilde{t}-\tilde{\tau})} \partial_{\tilde{t}} \theta_m(\tilde{\tau}) d\tilde{\tau} = \Phi_1 \partial_{\tilde{t}} \theta_m \,. \tag{11.4.9}$$

Equation (11.4.9) is the same as (11.4.3). Consequently, if $\tilde{t} >> 1$ and (11.4.4) is satisfied, then the general heat equation may be approximately its large-time limit (11.3.1) for infinite Φ_2. This means that when (11.4.4) is satisfied and $\tilde{t} >> 1$, the large-time error function (11.3.2) might approximate the unit step response of the general matrix temperature equation for infinite Φ_2.

In order to find the conditions that satisfy (11.4.4), we can then substitute the approximate unit step response, which is the large-time unit step response (11.3.2), into our necessary condition (11.4.4). Doing so, we find that

$$\left(\frac{\tilde{x}}{2\sqrt{\hat{\alpha}\tilde{t}}} \right)^2 << \tilde{t} \quad \text{and} \quad \tilde{t} >> 1 \tag{11.4.10}$$

satisfy (11.4.4) roughly. We note that the hypothesis that $\tilde{t} >> 1$ is correct according to the second condition of (11.4.10). Therefore, if time t is *large* relative to the thermalization time τ_T, then the unit step response of the general heat equation for infinite Φ_2 might be sufficiently close to its large-time limit (11.3.2) in the domain defined by the first condition in (11.4.10). The sufficiency of (11.4.10) will be verified later numerically.

Notice the similarity between (11.2.4) for the damped telegraph equation (the limit of the general heat equation as $\Phi_2 \to 0$ for fixed $\hat{t}$) and (11.4.10) for the "perfect contact" equation (the limit of the general heat equation as $\Phi_2 \to \infty$ for fixed $\tilde{t}$). The two sets of conditions are identical except for the difference in notation between $\hat{t}$ and $\tilde{t}$. The ratios $\hat{t}$ and $\tilde{t}$ must be large for the general matrix temperature equation to limit sufficiently to the modified Fourier heat equation for $\Phi_2 \to 0$ and $\Phi_2 \to \infty$ within the domains defined in (11.2.4) and (11.4.10), respectively.

We can even amalgamate these conditions into one general statement. When the non-dimensional conditions in (11.2.4) and (11.4.10) are converted to dimensional conditions using (4.7.1) and (4.7.2), respectively, we find that

$$\left(\frac{x}{2\sqrt{\alpha_{eff}\, t}} \right)^2 << \frac{t}{\tau_T} \quad \text{and} \quad \frac{t}{\tau_T} >> 1, \tag{11.4.11}$$

where the effective large-time thermal diffusivity α_{eff} and the thermalization time τ_T are defined in (10.2.8) and (4.6.16), respectively. Furthermore, when we convert (11.1.3) and (11.1.6) to dimensional forms by using (4.7.1), we find that

$$\partial_t \theta_m = \alpha_{eff} \partial_x^2 \theta_m \tag{11.4.12}$$

and

$$\theta_m = \operatorname{erfc}(x / 2\sqrt{\alpha_{eff}\, t}) . \tag{11.4.13}$$

Consequently, the modified Fourier heat equation (11.4.12) and the unit step response (11.4.13) approximate the general heat equation and general unit step response, respectively, for both zero and infinite Φ_2 when the conditions in (11.4.11) are satisfied. Therefore, our hypothesis that the thermalization time τ_T dominates the limiting of the general matrix temperature equation to the modified Fourier heat equation seems to be correct for both zero and infinite Φ_2.

11.5 Large-time Behavior of General Heat Equation for General Φ_2

Because the conditions in (11.4.11) govern how the general heat equation limits to the modified Fourier heat equation for zero and infinite Φ_2, it seems reasonable to hypothesize that the conditions in (11.4.11) hold for *all* Φ_2. In other words, when time t is large relative to the thermalization time τ_T, which depends on Φ_2 according to (4.6.16), we suppose that the general unit step response is approximately its large-time limit (11.4.13) within the spatial domain satisfying (11.4.11). Consequently, we hypothesize that the conditions in (11.2.4) work for small Φ_2 and that those in (11.4.10) work for moderate-to-large Φ_2.

Instead of using analytical means to test our hypothesis that the unit step response for all Φ_2 is approximately the error function (11.4.13) when the conditions in (11.4.11) are satisfied, we will test our hypothesis numerically. We will use the numerical scheme devised in Chapter 7 to approximate the unit step response ($\beta = 0$) of our general matrix temperature equation (11.1.1) for general Φ_2 and determine if the approximation is close enough to the large-time error function (11.1.6). We let r be the ratio of the large-time unit step response (11.1.6) to the general unit step response, i.e.,

$$r = \frac{\theta_m \text{ from (11.1.6)}}{\theta_a \text{ from (7.5.6) with } \beta = 0}. \tag{11.5.1}$$

If the conditions in (11.4.11) are true for all Φ_2, then r should be close to unity within the domain satisfying (11.4.11).

First, we test to see if the conditions in (11.2.4) are sufficient to render r close to unity for $\Phi_2 << 1$. The ratio r is shown in Figure 11.2 for large Φ_1 and multiple small values of Φ_2. A non-dimensional time of $\hat{t} = 10$ was chosen because it is much greater than unity, as required by (11.2.4). The $\hat{x}$ domain in the figure is also as large as possible while still being constrained by (11.2.4). Furthermore, a non-dimensional error of $\sigma = 10^{-4}$ was used for our numerical scheme, being sufficient to approximate the necessary step responses within the constrained $\hat{x}$ domain.

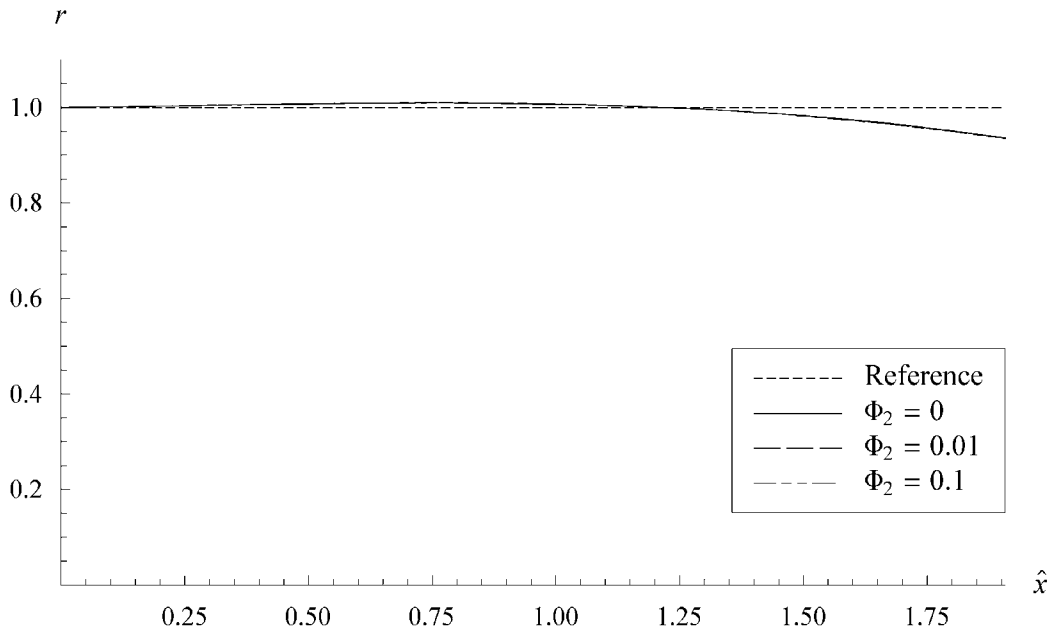

Figure 11.2: r vs. $\hat{x}$ for $\hat{t} = 10$ and $\Phi_1 = 10$

Several deductions can be made from inspection of Figure 11.2. First, the differences between the curves of differing Φ_2 are so small that all the curves appear as one curve compared to the reference line of unity in Figure 11.2. This means that, for the conditions in (11.2.4), the unit step responses for small Φ_2 are sufficiently close to that for the damped telegraph equation ($\Phi_2 = 0$). Now, because r does not deviate by more than 10% from unity in the figure, the conditions in (11.2.4) are sufficient to approximate the general heat equation as the MFHE for

$\hat{t} = 10$ with $\Phi_2 << 1$ and $\Phi_1 = 10$. Furthermore, it was determined through numerical analysis with varying orders of Φ_1 that the deviation of r from the reference curve is greatest for large Φ_1. Thus, the conditions in (11.2.4) are also valid for $\hat{t} = 10$ with $\Phi_2 << 1$ and Φ_1 of $O(1)$. We can also see in Figure 11.2 that the ratio r begins to deviate more from unity as $\hat{x}$ approaches the constraint for $\hat{x}$ set by (11.2.4), which indicates that our constraint on $\hat{x}$ in (11.2.4) is the *least* stringent as possible for $\hat{t} = 10$.

One may then wonder if our conditions in (11.2.4) for $\Phi_2 << 1$ are valid for a larger time $\hat{t}$. Figure 11.3 shows r for $\Phi_2 = 0.1$ when $\hat{t} = 50$. In Figure 11.3, the curves for other Φ_2 are not shown because, like for Figure 11.2, all the curves would unnecessarily appear as a single curve if this were done.

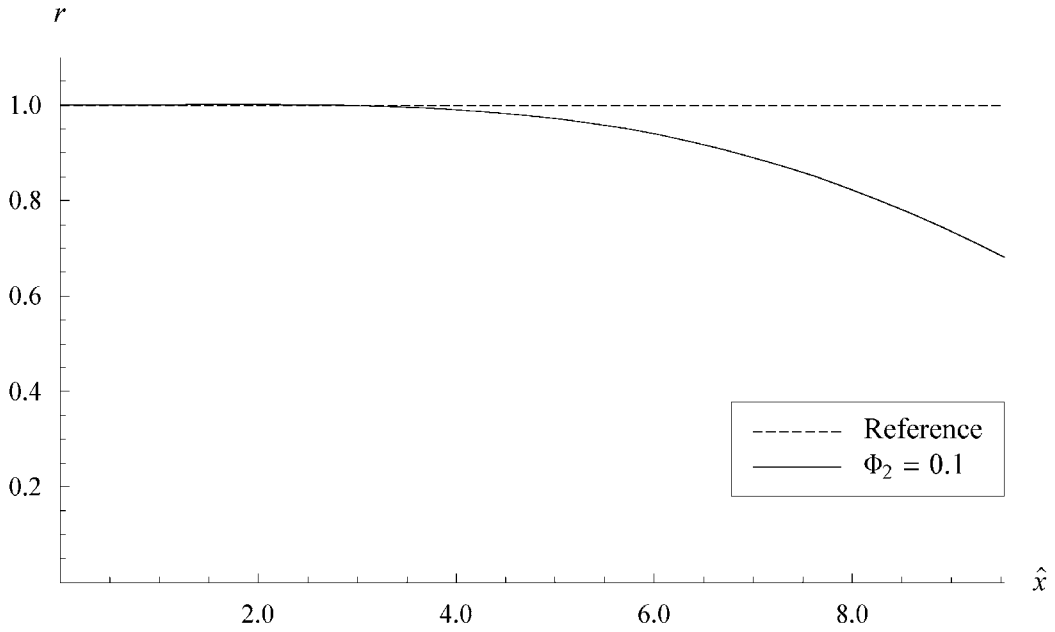

Figure 11.3: r vs. $\hat{x}$ for $\hat{t} = 50$ and $\Phi_1 = 10$

Again, like in Figure 11.2, the ratio r in Figure 11.3 begins to deviate more from unity as $\hat{x}$ approaches the constraint set by (11.2.4). However, the deviation is not insignificant, with the curve for $\Phi_2 = 0.1$ being as much as about 30% off from the reference line. Thus, the conditions in (11.2.4) for $\Phi_2 << 1$ are not as stringent as desired for $\hat{t} = 50$. We would have liked for there to be no more than a 10% deviation between the curve and the reference line in Figure 11.3, such

the general unit step response is sufficiently close to the large-time error function (11.1.6). Now, it was found that the actual temperature values near the maximum $\hat{x}$ values in Figure 11.3 are around 10^{-3}. Because these temperatures are much smaller than the maximum temperature of unity at $\hat{x} = 0$, we will excuse the undesired deviation of 30% for these small temperature values and assume that the conditions in (11.2.4) are satisfied for $\Phi_2 << 1$ for $\hat{t} = 50$.

For even larger $\hat{t}$ in order, values for *r* could not be produced as easily for very large $\hat{x}$ and for $\Phi_2 << 1$ because the temperatures needed to be approximated for *r* were so low that they were even below the default machine precision of 10^{-16} in *Mathematica*. However, because *r* is close enough to unity for testable values of $\hat{x}$ and $\hat{t}$, we can safely say at this point that the conditions in (11.2.4), and hence (11.4.11), are valid for $\Phi_2 << 1$. In other words, the general unit step response for $\Phi_2 << 1$ is sufficiently close to its large-time limit (11.4.13), as hypothesized, when the conditions in (11.4.11) are satisfied.

We now need to test whether or not the general unit step response is sufficiently close to its large-time limit when Φ_2 is not much less than one. Like for small Φ_2, we need to test the conditions in (11.4.11) for moderate-to-large Φ_2 by plotting the ratio *r* and determining if *r* is sufficiently close to unity for all $\tilde{x}$ and $\tilde{t}$. In other words, the ratio *r* should be close to one for moderate-to-large Φ_2 when the conditions in (11.4.11), or (11.4.10), are satisfied. Figure 11.4 is a plot of *r* for $\Phi_1 = 10$ and for values of moderate-to-large Φ_2. A large non-dimensional time of $\tilde{t} = 50$ and a large Φ_1 were also chosen for the plot, in order to produce the greatest deviations in *r* from the reference value of unity. The $\tilde{x}$ domain is also as large as possible while still being constrained by (11.4.10). Furthermore, a non-dimensional error of $\sigma = 10^{-4}$ was used, just like for the previous plots with $\Phi_2 << 1$.

The maximum difference from the reference value of unity is for the curve of $\Phi_2 = 0.5$ and is about 30% at most in Figure 11.4. We would have liked for there to be no more than a 10% deviation between all the curves and the reference line in Figure 11.4. However, it can be shown that the temperature values near the maximum $\tilde{x}$ value for the curve of $\Phi_2 = 0.5$ are around 10^{-3}, which is significantly smaller than the largest temperature of unity. If we ignore the relatively large deviations in *r* for those small temperatures, then we can state that the conditions in (11.4.10), and hence (11.4.11), are satisfied for moderate-to-large Φ_2 when $\tilde{t} = 50$.

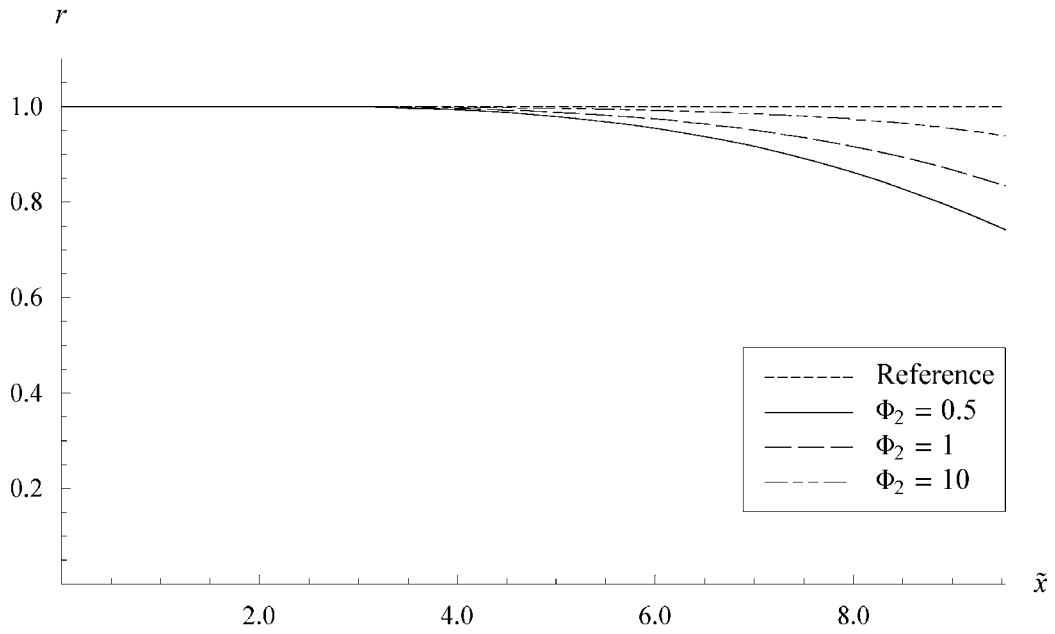

Figure 11.4: r vs. $\tilde{x}$ for $\tilde{t}$ = 50 and $\Phi_1 = 10$

For even larger $\tilde{t}$ in order, we cannot create reliable values of r for $\Phi_2 >> 1$, because of our constraint that $\sigma\hat{t} << 1$ for our numerical scheme with our chosen value of σ. However, by inspection of Figure 11.3, it seems that r becomes closer to unity as Φ_2 increases, which means that r is probably bounded to be sufficiently close to unity for very large Φ_2.

Having shown that r is sufficiently close to unity for all possible testing, we stop the numerical testing of our hypothesis and now state with as much confidence as possible that (11.4.11) is valid for moderate-to-large Φ_2. Because the conditions in (11.4.11) are also valid for $\Phi_2 << 1$, the general unit step response for *all* Φ_2 is sufficiently close to its large-time limit (11.4.13), as hypothesized, when the conditions in (11.4.11) are satisfied.

11.6 Conclusions

We determined with reasonable certainty that the general matrix heat equation (11.1.1) is approximately its large-time limit, which is the modified Fourier heat equation (11.4.12), when the conditions in (11.4.11) are satisfied. Thus, the unit step response for all Φ_2 is approximately

the large-time error function (11.4.13) in the domain satisfying the first constraint of (11.4.11) when time t is large compared to the thermalization time τ_T that is defined in (4.6.16).

As hypothesized from physical arguments, the thermalization time τ_T does indeed govern the limiting of the general matrix heat equation (11.1.1) to the modified Fourier heat equation (11.4.12). Furthermore, because the thermalization time τ_T is a function of the parameter Φ_2, the time it takes for the unit step response to limit to the modified error function depends on Φ_2. Thus, as alluded to in Chapter 10, Φ_2 is mainly thought of as being related to the transient nature of the general matrix heat equation.

Chapter 12

Crossing of Paths Phenomenon

12.1 Introduction

As stated in Chapter 10, the matrix temperature for the unit step response of our IBVP *generally* increases as Φ_2 increases for fixed space $\hat{x}$ and time $\hat{t}$. However, it does *not always* increase with Φ_2. Temperature profiles can cross each other, meaning that temperature does not always increase or decrease monotonically with the system parameters. For example, as seen in Figure 12.1, the unit step response for $\Phi_2 = 10$ crosses the unit step response for the damped telegraph equation ($\Phi_2 = 0$) for certain parameters.

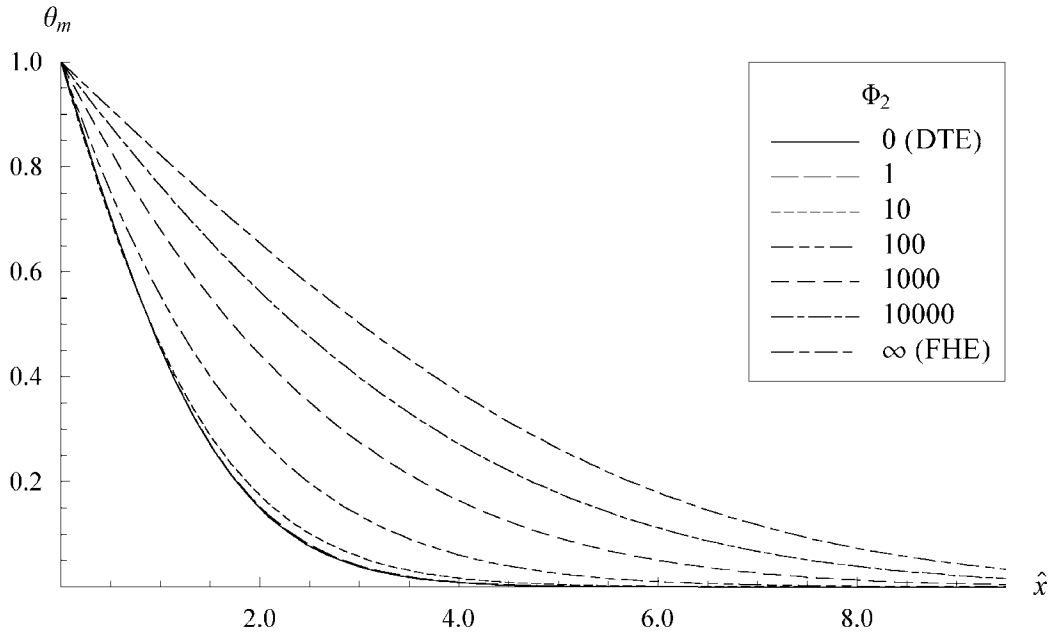

Figure 12.1: θ_m vs. $\hat{x}$ for $\hat{t}$ = 10, Φ_1 = 10, and β = 0

Even though it may be difficult to see in Figure 12.1, the curve for $\Phi_2 = 10$ intersects the curve for the damped telegraph equation ($\Phi_2 = 0$) at about $\hat{x} = 0.8$. The curve for $\Phi_2 = 10$ is slightly

lower than the curve for $\Phi_2 = 0$ when $\hat{x}$ is less than about 0.8 and, on the other hand, higher than the curve for $\Phi_2 = 0$ when $\hat{x}$ is greater than about 0.8.

The intersection of temperature profiles, which we also call the *crossing of paths*, was a surprising phenomenon. In Chapter 10, we found that the matrix temperature for the unit step response ($\beta = 0$) generally increases as Φ_2 increases for constant $\hat{x}$ and $\hat{t}$. We then explained why this pattern makes sense to us. In summary, as the particle thermal conductivity k_p decreases with increasing Φ_2, less heat generally conducts to the particles, which means that the matrix temperature generally increases as Φ_2 increases. However, as seen in Figure 12.1, temperature profiles of differing Φ_2 are able to cross each other, which is a non-monotonic behavior. The slight crossing of paths, being a non-monotonic behavior, was surprising because it did not align with how we believed Φ_2 affects temperature.

In fact, we found that unit step responses for differing Φ_2 still intersect each other even as $\hat{t}$ increases to infinity. Because this phenomenon is not fleeting with time, we will investigate the crossing of paths in this chapter. We desire to determine where certain temperature profiles intersect, in the hopes of learning more about the physics of heat transfer in our composite.

12.2 Definition of a Crossing Point

At this point, we will define a crossing point $\hat{x}_{cp}$, which is where certain temperature profiles intersect. Because we are interested in the relation of the damped telegraph equation ($\Phi_2 = 0$) to the general heat equation, we choose to investigate where the temperature profiles for zero Φ_2 and non-zero Φ_2 intersect. Consequently, we define a crossing point $\hat{x}_{cp}$ as a non-zero value of $\hat{x}$ where the temperature profile for the damped telegraph equation ($\Phi_2 = 0$) intersects the temperature profile for non-zero Φ_2, with all other parameters and variables being identical between the two temperature profiles. In other words, for general β, Φ_1, and $\hat{t}$, a crossing point $\hat{x}_{cp}$ satisfies

$$\theta_m(\hat{x} = \hat{x}_{cp}, \hat{t}, \beta, \Phi_1, \Phi_2 \neq 0) = \theta_m(\hat{x} = \hat{x}_{cp}, \hat{t}, \beta, \Phi_1, \Phi_2 = 0). \tag{12.2.1}$$

Thus, when we speak of $\hat{x}_{cp}$, we are speaking of a non-zero $\hat{x}$ value where the temperature profile for non-zero Φ_2 intersects the temperature profile for the damped telegraph equation $(\Phi_2 = 0)$.

12.3 Proof of Existence of Crossing of Paths Phenomenon

Because the difference between intersecting unit step responses in Figure 12.1 is relatively small, we wonder if the crossing of paths is due to numerical error from the numerical scheme used to create the approximate unit step responses in the figure. In order to investigate if the crossing of paths is a real phenomenon associated with our general matrix temperature equation, we let

$$\Delta\theta_m(\hat{x},\hat{t}) = \theta_m(\hat{x},\hat{t},\beta,\Phi_1,\Phi_2 \neq 0) - \theta_m(\hat{x},\hat{t},\beta,\Phi_1,\Phi_2 = 0), \tag{12.3.1}$$

where $\Delta\theta_m$ is the difference between the solutions of our IBVP for non-zero Φ_2 and zero Φ_2. The temperature difference $\Delta\theta_m$ is zero at $\hat{x}_{cp}$, according to (12.2.1). Therefore, if $\Delta\theta_m$ is zero at a non-zero value for $\hat{x}$, then the temperature profiles for zero Φ_2 and non-zero Φ_2 intersect. As an example, Figure 12.2 is a plot of $\Delta\theta_m$ for two values of Φ_2 used in Figure 12.1, where (12.3.1) was solved by using our numerical scheme from Chapter 7 with $\sigma = 10^{-4}$ for both curves in Figure 12.2. Both curves of Figure 12.2 cross the abscissa at their respective $\hat{x}_{cp}$. Thus, the crossing point for the unit step response for $\Phi_2 = 10$ is about $\hat{x}_{cp} = 0.8$, which was also seen in Figure 12.1, while the crossing point for the unit step response for $\Phi_2 = 1$ is about $\hat{x}_{cp} = 1.1$.

We can use Figure 12.2 to prove that the crossing of temperature profiles is a real phenomenon. Our reasoning lies in the fact that the magnitudes of the extrema for each curve in Figure 12.2 are *much greater* than the value of σ that was used to create the curves. This means that, instead of being due to numerical error, the exact temperature difference $\Delta\theta_m$ is truly negative at one extremum and positive at another extremum. Consequently, a crossing point $\hat{x}_{cp}$ exists, in order for the sign of $\Delta\theta_m$ to change. Thus, the crossing of temperature profiles is a *real phenomenon*.

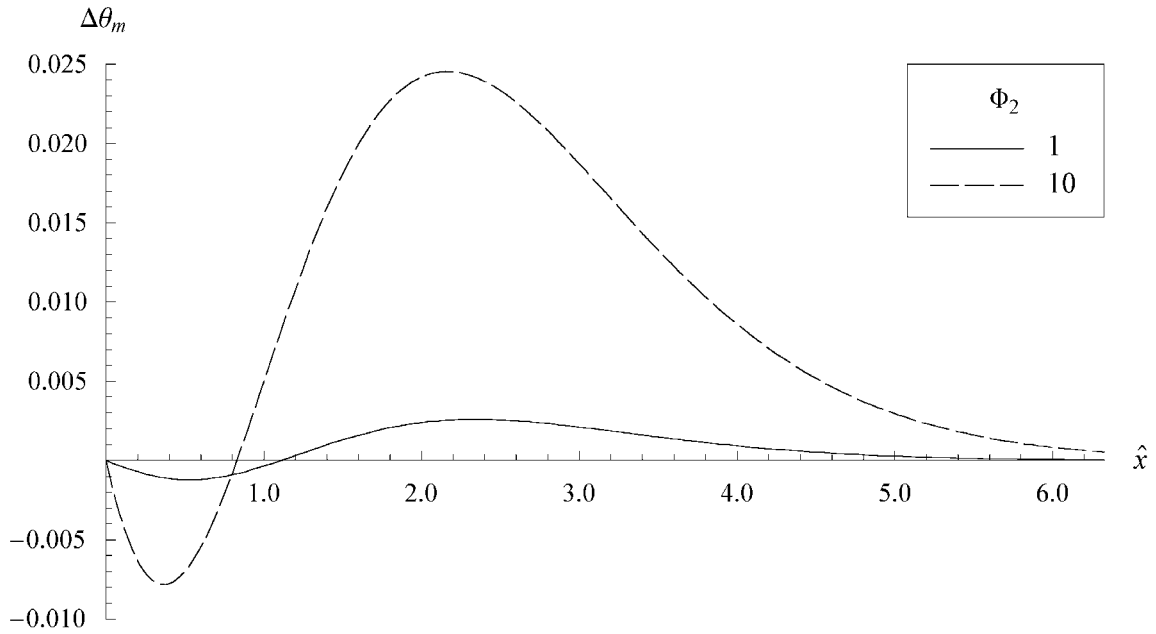

Figure 12.2: $\Delta\theta_m$ vs. $\hat{x}$ for $\hat{t}$ = 10, Φ_1 = 10, and β = 0

We can also prove that the crossing of temperature profiles is a real phenomenon through analytical means. By using the procedure set forth in Appendix E, we can show that the unit step response ($\beta = 0$) for infinitesimally small Φ_2 must cross the unit step response of the damped telegraph equation when time $\hat{t}$ is sufficiently large. We begin by stating that when Φ_2 is infinitesimally small, the difference $\Delta\theta_m$ for the unit step response ($\beta = 0$) can be shown to be

$$\Delta\theta_m(\hat{x},\hat{t}) = \left(\left. \frac{\partial\theta_m}{\partial\Phi_2} \right|_{\beta=0,\Phi_2=0} \right) \Phi_2 . \tag{12.3.1}$$

Then, by utilizing the Laplace transform (7.3.14) of the exact solution of our IBVP for our procedure in Appendix E, we can find the large-time expansion of the partial derivative in (12.3.1). Following this approach, we obtain

$$\left. \frac{\partial\theta_m}{\partial\Phi_2} \right|_{\beta=0,\Phi_2=0} = -\frac{\Phi_1}{\hat{t}\sqrt{\pi(1+\Phi_1)}} \left(\frac{\hat{x}}{20\hat{t}^{1/2}} + \frac{3\hat{x}(4+3\Phi_1-\hat{x}^2(1+\Phi_1)^2)}{80\hat{t}^{3/2}(1+\Phi_1)} + O\left(\frac{1}{\hat{t}^{5/2}}\right) \right). \tag{12.3.2}$$

When (12.3.2) is substituted into (12.3.1), we find that

$$\Delta\theta_m(\hat{x},\hat{t}) = -\frac{\Phi_1\Phi_2}{\hat{t}\sqrt{\pi(1+\Phi_1)}} \left(\frac{\hat{x}}{20\hat{t}^{1/2}} + \frac{3\hat{x}(4+3\Phi_1-\hat{x}^2(1+\Phi_1)^2)}{80\hat{t}^{3/2}(1+\Phi_1)} + \ldots \right) \tag{12.3.3}$$

for large time $\hat{t}$ and infinitesimally small Φ_2.

The exact difference $\Delta\theta_m$ in (12.3.3) for the unit step response ($\beta = 0$) can be used to show that the crossing of paths is a real phenomenon. For example, when Φ_1 is infinitesimally small, the difference $\Delta\theta_m$ in (12.3.3) can be shown to be

$$\Delta\theta_m(\hat{x},\hat{t}) = -\frac{\Phi_1\Phi_2}{\hat{t}\sqrt{\pi}}\left(\frac{\hat{x}}{20\hat{t}^{1/2}} + \frac{3\hat{x}(4-\hat{x}^2)}{80\hat{t}^{3/2}} + \ldots\right) \tag{12.3.4}$$

for infinitesimally small Φ_1 and Φ_2. We can now use our exact difference $\Delta\theta_m$ in (12.3.4) for infinitesimal Φ_1 and Φ_2 to approximate $\Delta\theta_m$ for small Φ_1 and Φ_2 by truncating the exact solution of (12.3.4) to a finite number of terms.

Figure 12.3 contains such an analytical approximation, along with the standard approximation from our numerical scheme. Because our analytical approximation crosses the abscissa in Figure 12.3, the unit step response for small Φ_2 crosses the unit step response for zero Φ_2 when time $\hat{t}$ is sufficiently large. Consequently, we have just used analytical means to prove that temperature profiles can intersect for sufficiently large time $\hat{t}$.

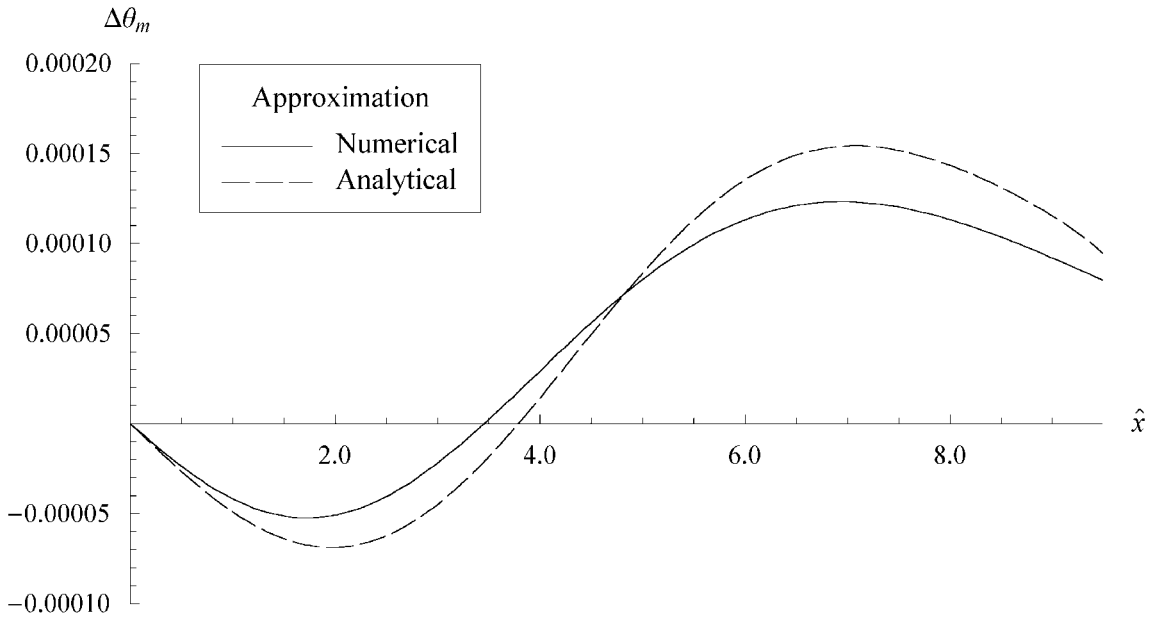

Figure 12.3: $\Delta\theta_m$ vs. $\hat{x}$ for $\hat{t}$ = 10, Φ_1 = 0.2, Φ_2 = 0.2, and β = 0

12.4 Approximate Equation Governing Crossing Point for Unit Step Response

For general system parameters (β, Φ_1, and Φ_2) and time $\hat{t}$, a formula for the crossing point $\hat{x}_{cp}$ may be complicated to formulate. Accordingly, we restrict ourselves by seeking a formula that describes $\hat{x}_{cp}$ for only the unit step response ($\beta = 0$) with small Φ_1 and Φ_2. The advantage to restricting our system parameters this way is that we can now use our analytical approximation of the general unit step response from Chapter 9 to approximate $\hat{x}_{cp}$. For Φ_1 and Φ_2 being the same small order, the unit step response is approximated as

$$\theta_m(\hat{x},\hat{t}) = \operatorname{erfc}\left(\frac{\hat{x}}{2\sqrt{\hat{t}}}(1+\Phi_1 u_1+\Phi_1{}^2 u_2+\Phi_1\Phi_2 w)\right), \tag{12.4.1}$$

according to (9.2.6), (9.2.8), and (9.2.13), where u_1, u_2, and w are defined in (9.2.14), (9.2.15), and (9.2.16), respectively. Then, according to (12.2.1), the crossing point $\hat{x}_{cp}$ for this special case occurs approximately where

$$\operatorname{erfc}\left(\frac{\hat{x}_{cp}}{2\sqrt{\hat{t}}}(1+\Phi_1 u_1+\Phi_1{}^2 u_2+\Phi_1\Phi_2 w)\right) = \operatorname{erfc}\left(\frac{\hat{x}_{cp}}{2\sqrt{\hat{t}}}(1+\Phi_1 u_1+\Phi_1{}^2 u_2)\right), \tag{12.4.2}$$

and all values of u_1, u_2, and w are evaluated at $\hat{x}_{cp}$ and $\hat{t}$. For non-zero Φ_1 and Φ_2, (12.4.2) is satisfied when w is zero at non-zero $\hat{x}_{cp}$, i.e.,

$$w(\hat{x}_{cp},\hat{t}) = -\frac{1}{10}\int_0^{\hat{t}} e^{\frac{\hat{x}_{cp}{}^2}{4}\left(\frac{1}{\hat{t}}-\frac{1}{\hat{\tau}}\right)} e^{-(\hat{t}-\hat{\tau})}(1-(\hat{t}-\hat{\tau}))\sqrt{\hat{t}/\hat{\tau}}\, d\hat{\tau} = 0 \tag{12.4.3}$$

according to the definition (9.2.16) of w. Because (12.4.3) is independent of both Φ_1 and Φ_2, (12.4.3) applies as long as Φ_1 and Φ_2 are small, as assumed. Therefore, *all* unit step responses for small Φ_1 and Φ_2 cross each other at approximately $\hat{x}_{cp}$ that satisfies (12.4.3).

12.5 Large-Time Approximation of Crossing Point for Unit Step Response

As shown analytically in Section 12.3, temperature profiles are able to cross when time $\hat{t}$ is sufficiently large. In fact, as seen in Figure 12.1, temperature profiles are able to cross when $\hat{t} = 10$, which is large relative to one. Thus, we are motivated to find a large-time approximation of $\hat{x}_{cp}$. An equation relating the crossing point $\hat{x}_{cp}$ for the unit step response to the non-dimensional time $\hat{t}$ will now be derived for sufficiently large $\hat{t}$ by using (12.4.3).

Before we create our approximation of $\hat{x}_{cp}$ for large time, we will rearrange (12.4.3). By letting

$$\xi = \frac{\hat{\tau}}{\hat{t}}, \tag{12.5.1}$$

we find that (12.4.3) is

$$\int_0^1 e^{\frac{\hat{x}_{cp}^{\,2}}{4\hat{t}}\left(1-\frac{1}{\xi}\right)} e^{-\hat{t}(1-\xi)} (1-\hat{t}(1-\xi)) \sqrt{1/\xi}\, d\xi = 0\,. \tag{12.5.2}$$

Then, when we let

$$\Theta = \frac{\hat{x}_{cp}^{\,2}}{4\hat{t}}, \tag{12.5.3}$$

(12.5.2) becomes

$$\int_0^1 B(\xi)\, d\xi = 0, \tag{12.5.4}$$

where

$$B(\xi) = e^{\Theta\left(1-\frac{1}{\xi}\right)} e^{-\hat{t}(1-\xi)} (1-\hat{t}(1-\xi)) \sqrt{1/\xi}\,. \tag{12.5.5}$$

The integral in (12.5.4) is difficult to evaluate explicitly and is not even necessary for our needs. We desire to only approximate the integral for large time $\hat{t}$, in order to produce a large-time approximation of the crossing point $\hat{x}_{cp}$ for the unit step response.

We now desire to approximate (12.5.4) for $\hat{t} >> 1$, which will yield our large-time approximation of $\hat{x}_{cp}$. Figure 12.4 shows a typical plot of $B(\xi)$ for the required range of ξ in the integral of (12.5.4) when $\hat{t} >> 1$.

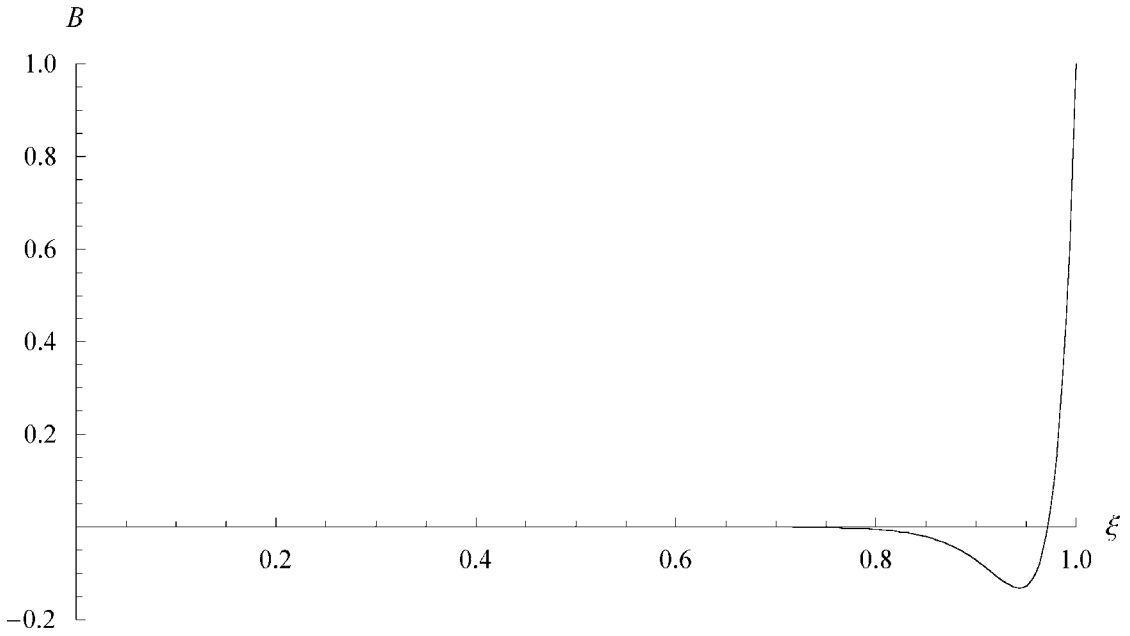

Figure 12.4: B vs. ξ for $\Theta = 1$ and $\hat{t} = 35$

It is apparent from Figure 12.4 that the integrand in (12.5.4) damps out quickly near $\xi = 1$ for large $\hat{t}$. Therefore, in order to approximate the integral in (12.5.4) for large $\hat{t}$, we can approximate the integrand $B(\xi)$, which is described in (12.5.5), by linearizing some of its terms around $\xi = 1$. By linearizing both the exponent of the first exponential and the radical in $B(\xi)$ around $\xi = 1$, we approximate (12.5.4) as

$$\int_0^1 e^{\Theta(\xi-1)} e^{-\hat{t}(1-\xi)} (1-\hat{t}(1-\xi))\,(3-\xi) d\xi = 0 \qquad (12.5.6)$$

for large $\hat{t}$. Unlike the integral in (12.5.4), its approximation in (12.5.6) can be easily integrated, which is why the approximation was created.

We will now finish approximating $\hat{x}_{cp}$ for large time. It can be shown upon integration that the integral in (12.5.6) is

$$2\Theta^2 - \hat{t} + \Theta(1+2\hat{t}) + e^{-(\Theta+\hat{t})}(3\Theta^2(\hat{t}-1) + \hat{t}(1+\hat{t}+3\hat{t}^2) + \Theta(6\hat{t}^2 - 2\hat{t} - 1)) = 0\,. \qquad (12.5.7)$$

For sufficiently large time, the terms in (12.5.7) that include the exponential are small compared to all other terms, which means that we can approximate (12.5.7) as

$$2\Theta^2 - \hat{t} + \Theta(1 + 2\hat{t}) = 0 \tag{12.5.8}$$

for large $\hat{t}$. Furthermore, if we assume that $\hat{t}$ is much larger than Θ, then the terms in (12.5.8) that contain $\hat{t}$ are dominating, which means that (12.5.8) reduces to

$$\hat{t}(2\Theta - 1) = 0\,. \tag{12.5.9}$$

We then have that

$$\Theta = \frac{1}{2} \tag{12.5.10}$$

for sufficiently large time $\hat{t}$. Because large time $\hat{t}$ is indeed much greater than Θ, as assumed, our approximation of Θ in (12.5.10) is valid. Finally, substitution of (12.5.10) into (12.5.3) yields that the crossing point for the unit step response is approximately

$$\hat{x}_{cp} = \sqrt{2\hat{t}} \tag{12.5.11}$$

for large time $\hat{t}$.

Figure 12.5 shows the numerical solution of (12.4.3) for $\hat{x}_{cp}$ with the large-time analytical approximation (12.5.11), both of which are approximations of $\hat{x}_{cp}$ for small Φ_1 and Φ_2 with $\beta = 0$. One can see in Figure 12.5 that the analytical approximation (12.5.11) for $\hat{x}_{cp}$ does indeed approximate the numerical approximation fairly well for $\hat{t} >> 1$. Furthermore, we learn from the numerical approximation in Figure 12.5 that $\hat{x}_{cp}$ does *not* exist when $\hat{t}$ is below about 2.2 for small Φ_1 and Φ_2. As $\hat{t}$ increases above about 2.2, then the crossing point $\hat{x}_{cp}$ increases monotonically from its initial value of zero. Thus, it seems to "take some time" for the unit step response for small Φ_1 and Φ_2 to intersect the unit step response of the damped telegraph equation ($\Phi_2 = 0$). Because time $\hat{t}$ is less than 2.2 in Figure 10.4, it is now understood why we did not observe the crossing of unit step responses in the figure.

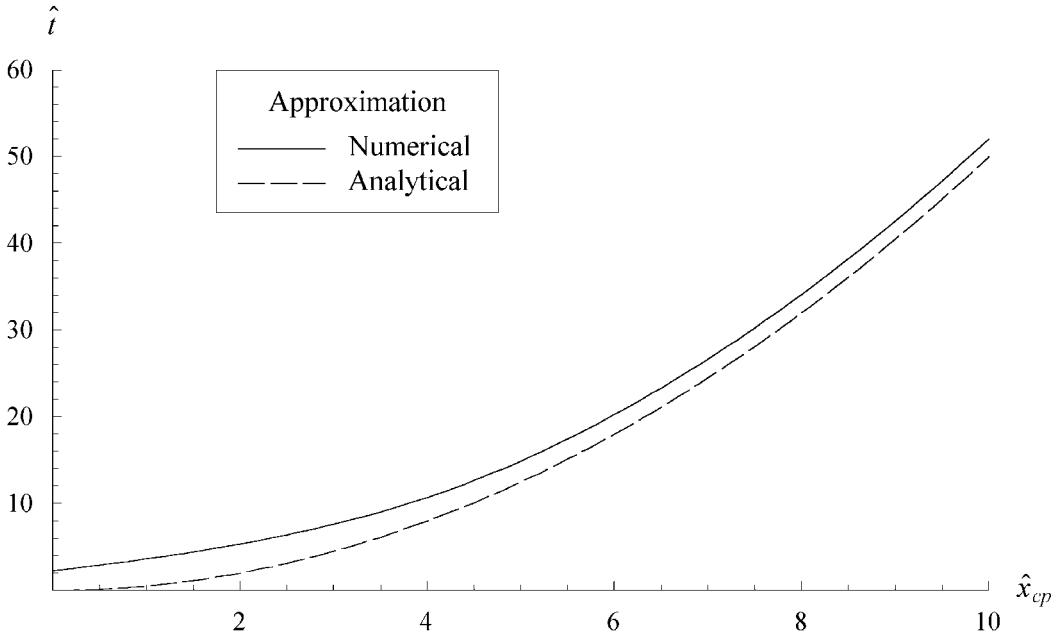

Figure 12.5: $\hat{t}$ vs. $\hat{x}_{cp}$

12.6 Physical Interpretation of Crossing of Paths Phenomenon

A definite physical reason for the crossing of unit step responses could not be found. There might be a physical interpretation of the crossing of paths, or perhaps its nature is mainly mathematical. Either way, the crossing of temperature profiles is a slight aberration from the general behavior observed in Chapter 10, and as such, it is difficult to determine the physical reason for the crossing of temperature profiles.

12.7 Conclusions

We proved that temperature profiles of varying Φ_2 are able to intersect and that the unit step response for small Φ_1 and Φ_2 crosses the unit step response for the damped telegraph equation ($\Phi_2 = 0$) at approximately the crossing point $\hat{x}_{cp}$ in (12.5.11) for large time $\hat{t}$.

However, a definitive reason for the crossing of unit step responses was not stated here in this thesis.

Chapter 13

Comparison to Experimental Data

13.1 Introduction

In this thesis, we derived a general equation that governs the matrix temperature in a composite composed of a matrix with embedded particles. Throughout other chapters, we investigated the general matrix temperature equation using numerical and analytical means in order to understand the behavior of heat transfer in our heterogeneous composite. However, in order for our general heat equation to be useful, it needs to be able to predict experimental values. In this chapter, we attempt to determine if our general matrix temperature equation can be used to adequately predict experimental values collected from an experiment with sand.

13.2 Description of Experiment

An experiment with sand was performed by Yun-Sheng Xu, Ying-Kui Guo, and Zeng-Yuan Guo at the Thermophysics Division of the Department of Engineering Mechanics at Tsinghua University in Beijing, China [14]. The following details of the experiment were obtained from Reference 14.

A container was filled with casting sand having a mean particle size of 0.2 mm and ranging in size from dust to a particle size of 0.8 mm. Air fills the gaps in the sand, such that a sand-air composite exists in the container. The effective thermal diffusivity α_{eff} of the sand-air composite was measured experimentally to be

$$\alpha_{eff} = 0.3(10^{-6})\ \mathrm{m}^2/\mathrm{s}. \tag{13.2.1}$$

A thin-film heater is also buried in the midplane of the sandbox and is connected to a power supply. Half of the sand-filled container with the buried heater is seen in the diagram of Figure 13.1. The median cross section of the filled container is seen in the front face in the figure.

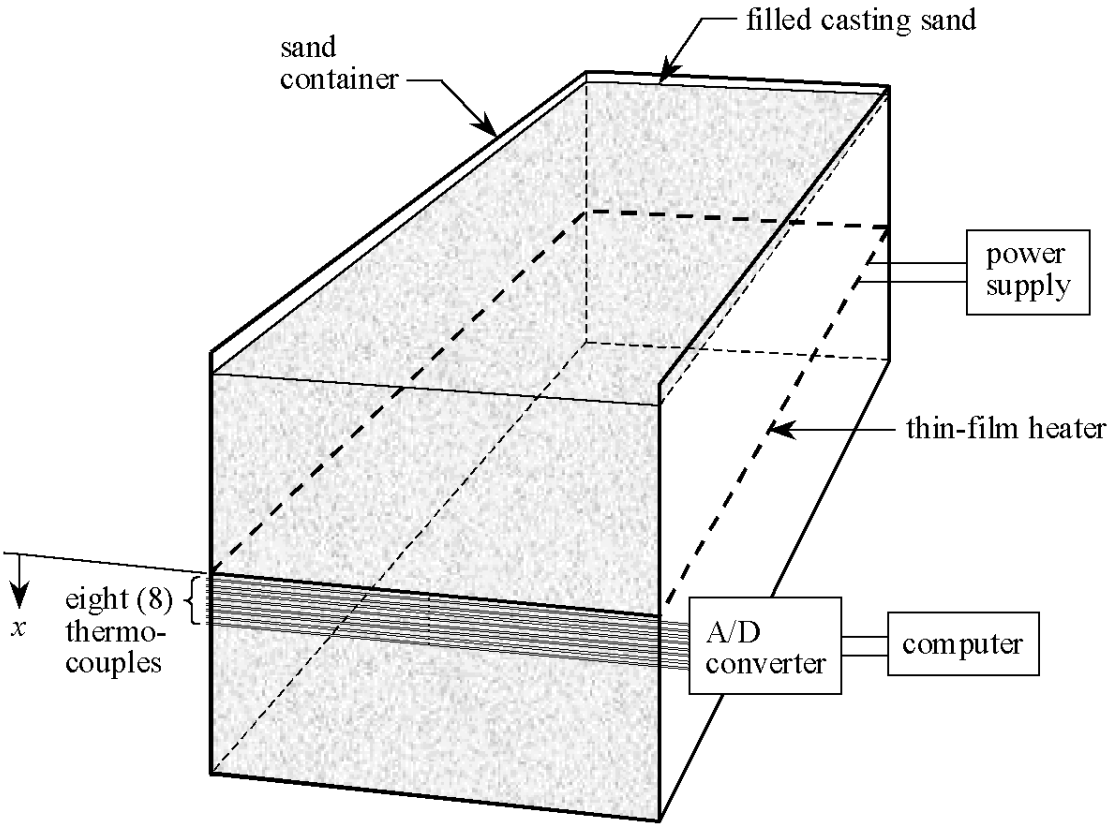

Figure 13.1: Experimental Setup for Measuring the Response in Casting Sand

When energy is supplied to the thin-film heater, heat flows through the sand-air composite above and below the heater. The temperatures in the composite consequently change. As seen in Figure 13.1, eight copper/constantan thermocouples were buried in the median cross section of the container, below the thin-film heater, in order to measure the local temperature change at $x = 0.4$, 1.5, 2.1, 3.6, 4.5, 5.7, 8.3, and 10.2 mm. The bottom of the container is at about $x = 70$ mm. Furthermore, the measured temperatures are accurate to within ±0.15 °C of the actual temperatures.

The sand was stabilized for several days before each run of the experiment. After the sand had stabilized, energy was supplied at a constant rate to the thin-film heater for either 0.14 s or 0.56 s. This energy from the pulse width of either 0.14 s or 0.56 s conducted to the sand-air composite, which caused temperatures to change. Temperature changes were measured at the eight x locations at a frequency of 100 Hz during and after the pulse duration. Figures 13.2 and

13.3 contain plots of the temperature change ΔT at x = 0.4, 1.5, and 2.1 mm versus time t for a pulse width of 0.14 s and 0.56 s, respectively. The experimental data in the plots were obtained from Reference 14.

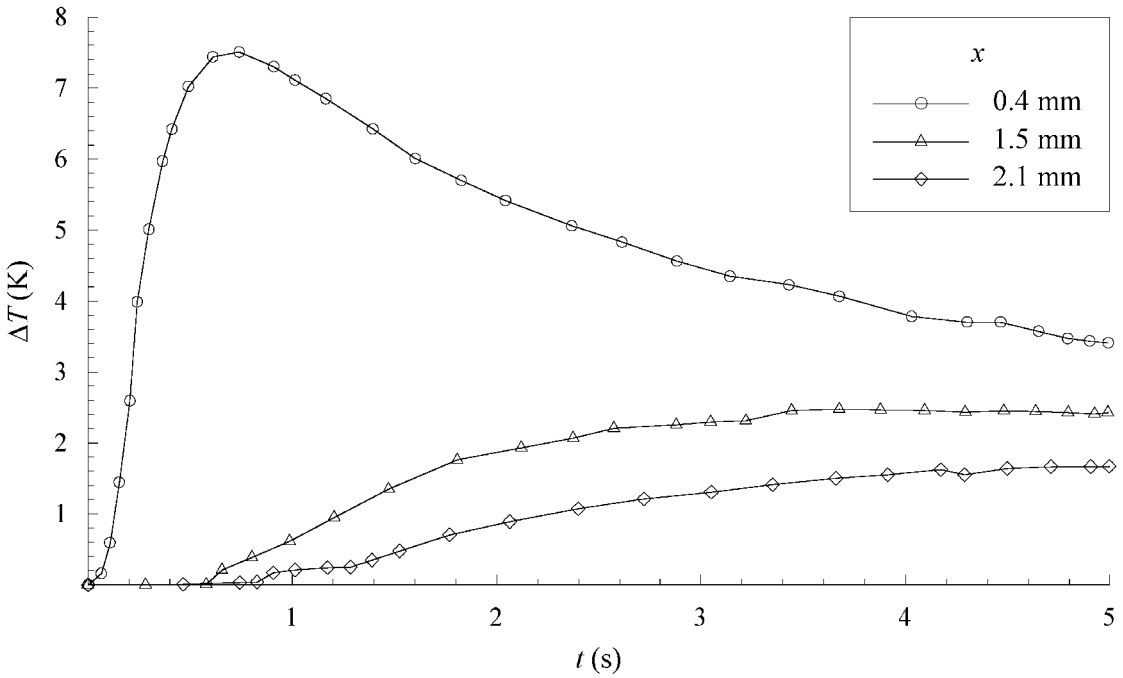

Figure 13.2: ΔT vs. t for a Pulse Width of 0.14 s

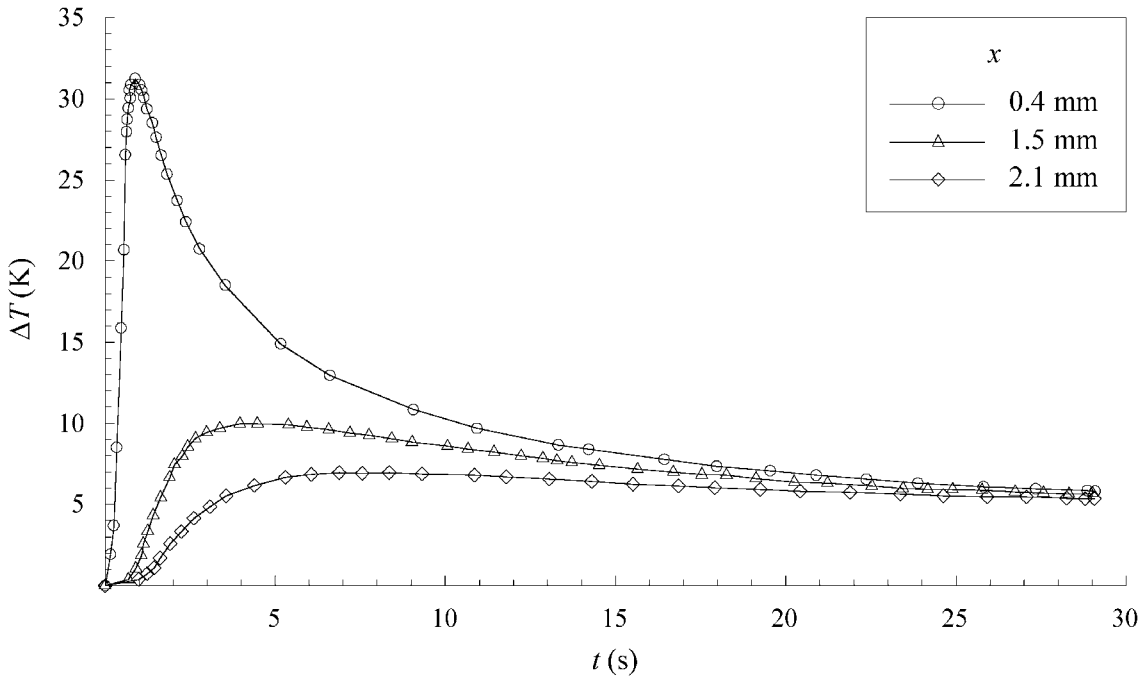

Figure 13.3: ΔT vs. t for a Pulse Width of 0.56 s

13.3 Prediction of Temperature Changes

We now want to determine if our general matrix temperature equation can predict the experimental values in Figures 13.2 and 13.3. In order to do so, we first need to relate the sand-air composite with the composite described in Chapter 2 of this thesis. First, because heat flows mainly through the sand, the sand is like the matrix and the air that fills the gaps is like the particles. Second, we approximate that the measured temperatures are those of the sand, i.e., the matrix. Consequently, if we want to predict the measured temperature changes seen in the previous figures, then we need to solve our general heat equation (4.2.18) that describes the change in matrix temperature. We will now use it to predict the temperature changes collected from the experiment by fitting our general model to the experimental data.

We now begin to apply the general equation (4.2.18) to the experiment described in Section 13.2. First, heat flows generally along the x-direction, which means that we can use the one-dimensional form,

$$\Phi_2\left(\partial_t\theta_m-\alpha_m\partial_x^2\theta_m+\frac{6\Phi_1}{\tau_p}\int_0^t\Psi(t-\tau)\partial_\tau\theta_m\,d\tau\right)+2\int_0^t\Psi(t-\tau)\partial_\tau(\partial_\tau\theta_m-\alpha_m\partial_x^2\theta_m)\,d\tau=0\,,\quad(13.3.1)$$

of the general heat equation (4.2.18) to describe heat transfer in the sand-air composite, where θ_m is the non-dimensional sand "matrix" temperature change, the function Ψ is defined in (4.2.14), Φ_1 and Φ_2 are the non-dimensional parameters in our general model, α_m is the thermal diffusivity of the sand "matrix", and τ_p is a measure of the time scale of the air "particles" that fill the gaps in the sand. The dimensional form (13.3.1) of the one-dimensional general heat equation is used, instead of the non-dimensional form (7.2.1), because all of our data is given in dimensional quantities.

We will now attempt to find values for Φ_1, Φ_2, and τ_p that describe the sand-air system by fitting (13.3.1) to the experimental data. We begin by solving for the temperature change in the sand. First, the Laplace transform of (13.3.1) is

$$\tau_p(s\overline{\theta}_m-\alpha_m\partial_x^2\overline{\theta}_m)(\Phi_2-1+mR\coth mR)+3\Phi_1\Phi_2(mR\coth mR-1)(\overline{\theta}_m-\overline{\Delta\theta_0})=0\,,\quad(13.3.2)$$

according to (4.8.1), where an overbar denotes the Laplace transform of the function in the *s*-domain,

$$m=\sqrt{s/\alpha_p}\,,\quad(13.3.3)$$

and R and α_m are measures of the respective "radius" and thermal diffusivity of the air "particles" that fill the gaps in the sand. Second, because the sand-air composite is at equilibrium before each trial, the composite has an initially uniform temperature, which means that $\Delta\theta_0=0$ and

$$\tau_p(s\overline{\theta}_m-\alpha_m\partial_x^2\overline{\theta}_m)(\Phi_2-1+mR\coth mR)+3\Phi_1\Phi_2(mR\coth mR-1)\overline{\theta}_m=0\,.\quad(13.3.4)$$

Then, because θ_m is proportional to the change ΔT is matrix temperature, according to (4.2.1), we find that

$$\tau_p(s\overline{\Delta T}-\alpha_m\partial_x^2\overline{\Delta T})(\Phi_2-1+mR\coth mR)+3\Phi_1\Phi_2(mR\coth mR-1)\overline{\Delta T}=0\,.\quad(13.3.5)$$

Finally, the solution of (13.3.5) can be shown to be

$$\overline{\Delta T}(x,s)=B_1(s)\,e^{-\frac{x}{\sqrt{\alpha_m}}\sqrt{s+\frac{3\Phi_1\Phi_2(mR\coth mR-1)}{\tau_p(\Phi_2+mR\coth mR-1)}}}+B_2(s)\,e^{\frac{x}{\sqrt{\alpha_m}}\sqrt{s+\frac{3\Phi_1\Phi_2(mR\coth mR-1)}{\tau_p(\Phi_2+mR\coth mR-1)}}}\,,\quad(13.3.6)$$

where B_1 and B_2 are functions of s that are yet to be determined. The solution (13.3.6) is the dimensional version of (7.3.9), which is the solution of the general non-dimensional heat equation. After determining B_1 and B_2, we can invert (13.3.6) to obtain the predicted temperature change $\Delta T(x, t)$ from our general model.

To determine B_2, we can use the observation that temperature decreases with increasing x in Figures 13.2 and 13.3. Because temperature decreases as x increases, we imagine that the temperatures at the bottom of the container ($x = 70$ mm) are sufficiently negligible compared to those seen in the figures. Thus, for our purposes, we assume that heat cannot reach the bottom of the container, which means that we assume that the experimental temperatures are like those when the container is infinitely deep ($x \to \infty$). This means that, like $A_2(\hat{s})$ being zero in (7.3.9) for our infinite-domain from Chapter 7, we let $B_2(s)$ be zero for our "infinite" sand-filled container. We then have that

$$\overline{\Delta T}(x, s) = B_1(s)\, e^{-\frac{x}{\sqrt{\alpha_m}}\sqrt{s+\frac{3\Phi_1\Phi_2\,(mR\coth mR-1)}{\tau_p\,(\Phi_2+mR\coth mR-1)}}}, \tag{13.3.7}$$

which is rearranged to be

$$\overline{\Delta T}(x, s) = B_1(s)\, e^{-\frac{x}{\sqrt{\alpha_m}}\sqrt{s+\frac{3\Phi_1\Phi_2\,(\sqrt{s\,\tau_p}\coth\sqrt{s\,\tau_p}-1)}{\tau_p\,(\Phi_2+\sqrt{s\,\tau_p}\coth\sqrt{s\,\tau_p}-1)}}} \tag{13.3.8}$$

by using the definition (13.3.3) of m and the definition (4.2.12) of τ_p. Furthermore, according to the definition (10.2.8) of the effective thermal diffusivity α_{eff} of the composite, the Laplace transform $\overline{\Delta T}$ is

$$\overline{\Delta T}(x, s) = B_1(s)\, e^{-\frac{x}{\sqrt{\alpha_{eff}\,(1+\Phi_1)}}\sqrt{s+\frac{3\Phi_1\Phi_2\,(\sqrt{s\,\tau_p}\coth\sqrt{s\,\tau_p}-1)}{\tau_p\,(\Phi_2+\sqrt{s\,\tau_p}\coth\sqrt{s\,\tau_p}-1)}}}, \tag{13.3.9}$$

where α_{eff} is given in (13.2.1).

Now, we need to determine the function B_1 to obtain our complete expression of $\overline{\Delta T}(x, s)$. If we knew the temperatures at the thin-film heater ($x = 0$), we could solve for $B_1(s)$ by using that boundary data. Even though we do not know the boundary temperatures at $x = 0$, we have data for the closest thermocouple (at $x = x_1 = 0.4$ mm) to the thin-film heater. Accordingly, we decide to use the data collected at the first thermocouple to solve for the

function B_1, because it represents the closest data we have to a boundary condition. Equation (13.3.9) can be used to show that

$$B_1(s) = \overline{\Delta T}(x_1, s)\, e^{\frac{x_1}{\sqrt{\alpha_{eff}(1+\Phi_1)}}\sqrt{s+\frac{3\Phi_1\Phi_2(\sqrt{s\tau_p}\coth\sqrt{s\tau_p}-1)}{\tau_p(\Phi_2+\sqrt{s\tau_p}\coth\sqrt{s\tau_p}-1)}}}, \tag{13.3.10}$$

where the Laplace transform $\overline{\Delta T}(x_1, s)$ will be determined by using the data at the first thermocouple. Finally, substitution of (13.3.10) into (13.3.9) yields

$$\overline{\Delta T}(x, s) = \overline{\Delta T}(x_1, s)\, e^{\frac{x_1 - x}{\sqrt{\alpha_{eff}(1+\Phi_1)}}\sqrt{s+\frac{3\Phi_1\Phi_2(\sqrt{s\tau_p}\coth\sqrt{s\tau_p}-1)}{\tau_p(\Phi_2+\sqrt{s\tau_p}\coth\sqrt{s\tau_p}-1)}}}, \tag{13.3.11}$$

which is the Laplace transform of the predicted temperature function $\Delta T(x, t)$.

Before we can invert (13.3.11) to solve for $\Delta T(x, t)$, we need to use our data at $x = x_1$ from Figure 13.2 or 13.3 to determine $\overline{\Delta T}(x_1, s)$. We choose to approximate $\overline{\Delta T}(x_1, s)$ by approximating the temperature function at the first thermocouple. Perhaps the simplest way to approximate the temperature function is to connect consecutive data points at $x = 0.4$ mm with straight lines, as seen in Figures 13.2 and 13.3. For simplicity, we catalog the data at $x = 0.4$ mm in either Figure 13.2 or Figure 13.3 according to the scheme seen in Figure 13.4. It can then be shown that the approximate temperature at the first thermocouple is

$$\Delta T(x_1, t) = \sum_{i=1}^{N-1} (\Delta T_i + b_i t)(H(t - t_i) - H(t - t_{i+1})), \tag{13.3.12}$$

where the slope b_i of the line segment joining the data points at t_i and t_{i+1} in Figure 13.4 is

$$b_i = \frac{\Delta T_{i+1} - \Delta T_i}{t_{i+1} - t_i}, \tag{13.3.13}$$

for $i = 1, 2, \ldots, N-1$, and the Heaviside function H [22] is defined as

$$H(\eta) = \begin{cases} 0, & \eta < 0 \\ 1, & \eta \geq 0 \end{cases}. \tag{13.3.14}$$

Then, by using the table of Laplace transforms in Reference 22, we can show that the Laplace transform of the approximation (13.3.12) is

$$\overline{\Delta T}(x_1, s) = e^{-t_1 s}\left(\frac{\Delta T_1}{s} + \frac{b_1}{s^2}\right) - e^{-t_N s}\left(\frac{\Delta T_N}{s} + \frac{b_{N-1}}{s^2}\right) + \sum_{i=2}^{N-1} \frac{e^{-t_i s}}{s^2}(b_i - b_{i-1}). \tag{13.3.15}$$

Finally, substitution of (13.3.15) into (13.3.11) yields

$$\overline{\Delta T}(x,s)=\left(\begin{array}{l} e^{-t_1 s}\left(\dfrac{\Delta T_1}{s}+\dfrac{b_1}{s^2}\right)-e^{-t_N s}\left(\dfrac{\Delta T_N}{s}+\dfrac{b_{N-1}}{s^2}\right) \\ +\displaystyle\sum_{i=2}^{N-1}\frac{e^{-t_i s}}{s^2}(b_i-b_{i-1}) \end{array}\right) e^{\frac{x_1-x}{\sqrt{\alpha_{eff}(1+\Phi_1)}}\sqrt{s+\frac{3\Phi_1\Phi_2(\sqrt{s\tau_p}\coth\sqrt{s\tau_p}-1)}{\tau_p(\Phi_2+\sqrt{s\tau_p}\coth\sqrt{s\tau_p}-1)}}} \quad (13.3.16)$$

Once values for Φ_1, Φ_2, and τ_p are chosen, the predicted temperature function $\Delta T(x,t)$ can be calculated by inverting (13.3.16) through use of the numerical scheme from Chapter 7. By using (7.5.6), we can show that the predicted temperature change ΔT is

$$\Delta T(x,t)=\frac{e^{\Gamma}}{\pi}\frac{\Delta\Omega}{t}\left(\frac{1}{2}\mathrm{Re}[\overline{\Delta T}(x,s=\Gamma/t)]+\sum_{n=1}^{N}\mathrm{Re}[\overline{\Delta T}(x,s=(\Gamma+in\Delta\Omega)/t)\,e^{in\Delta\Omega}]\right), \quad (13.3.17)$$

where Γ, N, and $\Delta\Omega$ are given in (7.10.5), (7.10.8), and (7.10.9), respectively, and the error bound σ is sufficiently small according to (7.11.2).

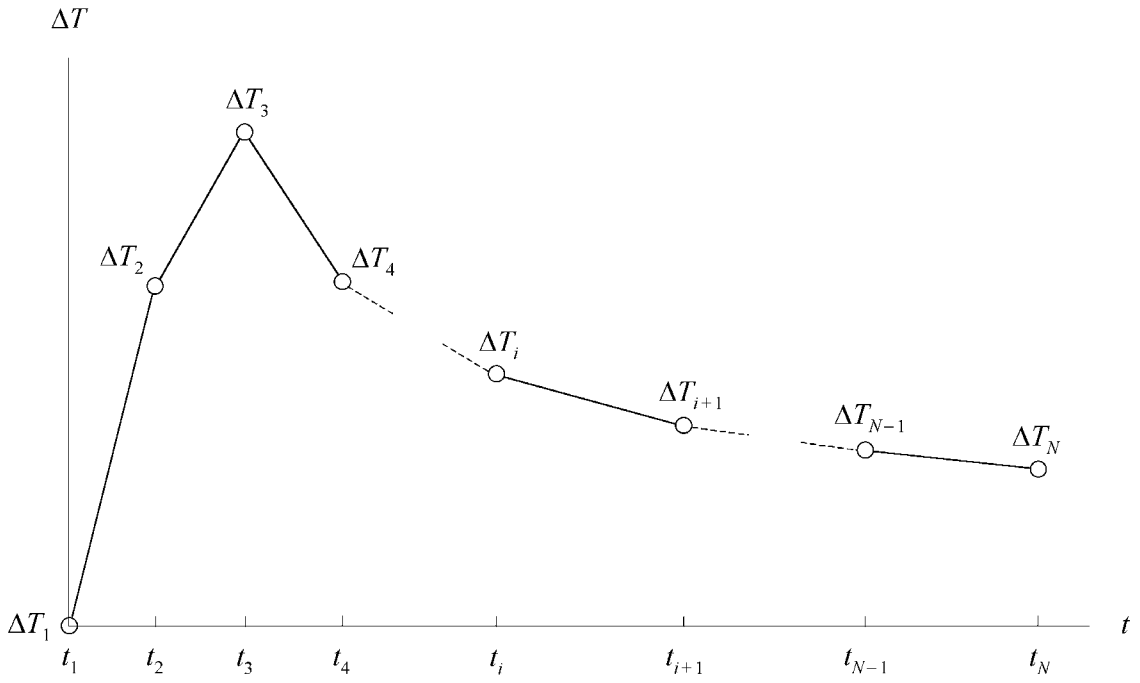

Figure 13.4: Catalog of Data Collected at First Thermocouple

We can now predict temperatures by using (13.3.17) and compare the predicted temperatures to the measured data. Specifically, by using the experimental data at the first

thermocouple to create (13.3.16), we can predict the temperature changes at the other thermocouples through use of (13.3.17).

13.4 Fitting of General Model to Experimental Data

We wish to fit our general model in (13.3.17) to the experimental data collected from the experiment with sand described in Section 13.2. This means that we desire to find unique values of Φ_1, Φ_2, and τ_p that best characterize the sand-air composite used for the experiment. We choose to use the data in Figure 13.3 for a pulse width of 0.56 s to determine the values of Φ_1, Φ_2, and τ_p that characterize the composite, leaving the data in Figure 13.2 for testing the model containing the optimum values of the system parameters. In other words, once we obtain values for the parameters of our general model, we will predict the temperature changes for a pulse width of 0.14 s, which can then be compared to the measured data in Figure 13.2.

If the system parameters (Φ_1, Φ_2, and τ_p) are chosen wisely, then the *predicted* temperature changes ΔT at the second and third thermocouples might be the *actual* temperature changes. This occurs when the difference between the predicted and measured temperatures could be due to *only* measurement error, i.e., the difference is bounded by ±0.15 K. Thus, the goal of this section is to find values of the system parameters that render the predicted temperatures from our general model to be as close as possible to, while being within ±0.15 K of, the measured temperatures at the second and third thermocouples for a pulse width of 0.56 s. In other words, we desire to find the best fit of our general model to the experimental data, with the hope that the best fit is physically possible.

We will now attempt to find the *optimum* values of the system parameters (Φ_1, Φ_2, and τ_p), which yield the best fit of our general model to the experimental data in Figure 13.3. While optimizing, we also allow the experimentally measured locations x_2 and x_3 of the second and third thermocouples, respectively, and the effective thermal diffusivity α_{eff} to vary slightly from their respective measured values of 1.5 mm, 2.1 mm, and $0.3(10^{-6})$ m^2/s. The experimentally

measured parameters are allowed to vary from their measured values because, by definition, their values are measured and are not perfect.

We will find the optimum values of two thermocouple locations (x_2 and x_3) and the system parameters (α_{eff} , Φ_1, Φ_2, and τ_p) by minimizing an objective function. The objective function F_{obj} is defined as

$$F_{obj}(x_2, x_3, \alpha_{eff}, \Phi_1, \Phi_2, \tau_p) = \sum_{i=1}^{M} (\Delta T(\hat{t}_i; x_2, \alpha_{eff}, \Phi_1, \Phi_2, \tau_p) - \Delta\hat{T}_i)^2 + \sum_{i=1}^{M} (\Delta T(\breve{t}_i; x_3, \alpha_{eff}, \Phi_1, \Phi_2, \tau_p) - \Delta\breve{T}_i)^2 , \quad (13.4.1)$$

where $(\hat{t}_1, \Delta\hat{T}_1)$, $(\hat{t}_2, \Delta\hat{T}_2)$, …, and $(\hat{t}_M, \Delta\hat{T}_M)$ are an M number of chosen data points at the second thermocouple in Figure 13.3, and $(\breve{t}_1, \Delta\breve{T}_1)$, $(\breve{t}_2, \Delta\breve{T}_2)$, …, and $(\breve{t}_M, \Delta\breve{T}_M)$ are an M number of chosen data points at the third thermocouple in Figure 13.3. Furthermore, the function ΔT is determined by substituting (13.3.16) into (13.3.17), where the values for $t_1, t_2, \ldots, t_N$ and $\Delta T_1, \Delta T_2, \ldots, \Delta T_N$ in (13.3.16) are determined by using the cataloging scheme in Figure 13.4 to label the data at the first thermocouple ($x = 0.4$ mm) in Figure 13.3.

As seen in the definition (13.4.1), the objective function F_{obj} is the sum of squares of the difference between an M number of predicted and measured temperature changes at both the second and third thermocouples for a pulse width of 0.56 s. A relative minimum of F_{obj} was found with $\sigma = 10^{-3}$ by using a numerical gradient-search algorithm to minimize F_{obj} with respect to all variables (x_2 , x_3 , α_{eff} , Φ_1, Φ_2, and τ_p). The optimum values are seen in Table 13.1, and Figure 13.5 contains a plot of the optimum fits, i.e., the temperature changes predicted by using the values in Table 13.1, with the measured data for a pulse width of 0.56 s.

A close examination of Figure 13.5 reveals that the predicted temperatures differ by more than ±0.15 K from the experimental values at several points. However, the optimum fits seem to match the measurements fairly well at all other points, which means that the values of α_{eff} , Φ_1, Φ_2, and τ_p in Table 13.1 characterize the sand-air composite rather well. Furthermore, the locations x_2 and x_3 of the second and third thermocouple, respectively, in Table 13.1 might be closer than the measured values to the actual locations of the thermocouples.

Table 13.1: Optimum Values for General Model from Minimization of F_{obj}

Parameter	Optimum Value
x_2 (mm)	1.542
x_3 (mm)	2.118
α_{eff} (m^2/s)	$0.285(10^{-6})$
Φ_1	0.1452
Φ_2	$0.8(10^{-4})$
τ_p (s)	$7.7(10^{-4})$

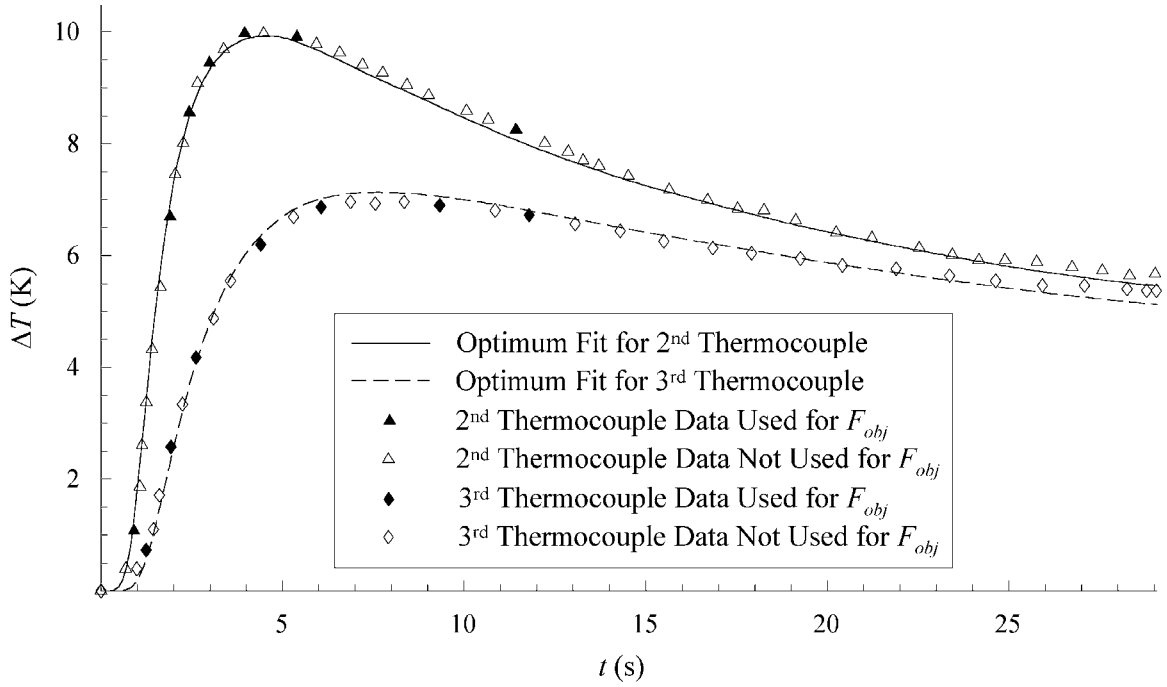

Figure 13.5: ΔT vs. t for a Pulse Width of 0.56 s

13.5 Prediction of Temperature Changes

We can now use our model with the values in Table 13.1, which were produced by using the data for a pulse width of 0.56 s, to predict the temperature changes at the second and third thermocouples for a pulse width of 0.14 s. A comparison of predicted and measured

temperatures will give us a measure of how well our model from Table 13.1 characterizes the sand-air composite.

The procedure for predicting temperature changes for a pulse width of 0.14 s is straightforward. First, the values for $t_1, t_2, \ldots, t_N$ and $\Delta T_1, \Delta T_2, \ldots, \Delta T_N$ in (13.3.16) are determined by using the cataloging scheme in Figure 13.4 to label the data at the first thermocouple (x = 0.4 mm) in Figure 13.2. The values for α_{eff}, Φ_1, Φ_2, and τ_p required for the Laplace transform $\overline{\Delta T}$ in (13.3.16) are then given in Table 13.1. When (13.3.16) is substituted into (13.3.17), the predicted temperature change $\Delta T(x, t)$ is known at the second thermocouple ($x = x_2$) and the third thermocouple ($x = x_3$) for a pulse width of 0.14 s.

Figure 13.6 contains a plot of the predicted temperature changes at the second and third thermocouples for a pulse width of 0.14 s. The predicted curve at the second thermocouple seems to be within about ±0.15 K from the experimental values for all times below about 3.4 s, where the experimental data deviates from the predicted trend. In fact, the measured data at the second thermocouple seem to be systematically above the predicted curve after 3.4 s in time, which suggests that there might be systematic error in the data collection. The measured data at the third thermocouple are also systematically greater than the predicted temperature changes for most time. Even still, the predicted curve at the third thermocouple is within about ±0.15 K from the experimental values for all times. Consequently, our optimized model for the sand-air composite seems to be able to predict temperatures fairly well within the given temperature error tolerance, even if systematic errors exist in the measured data.

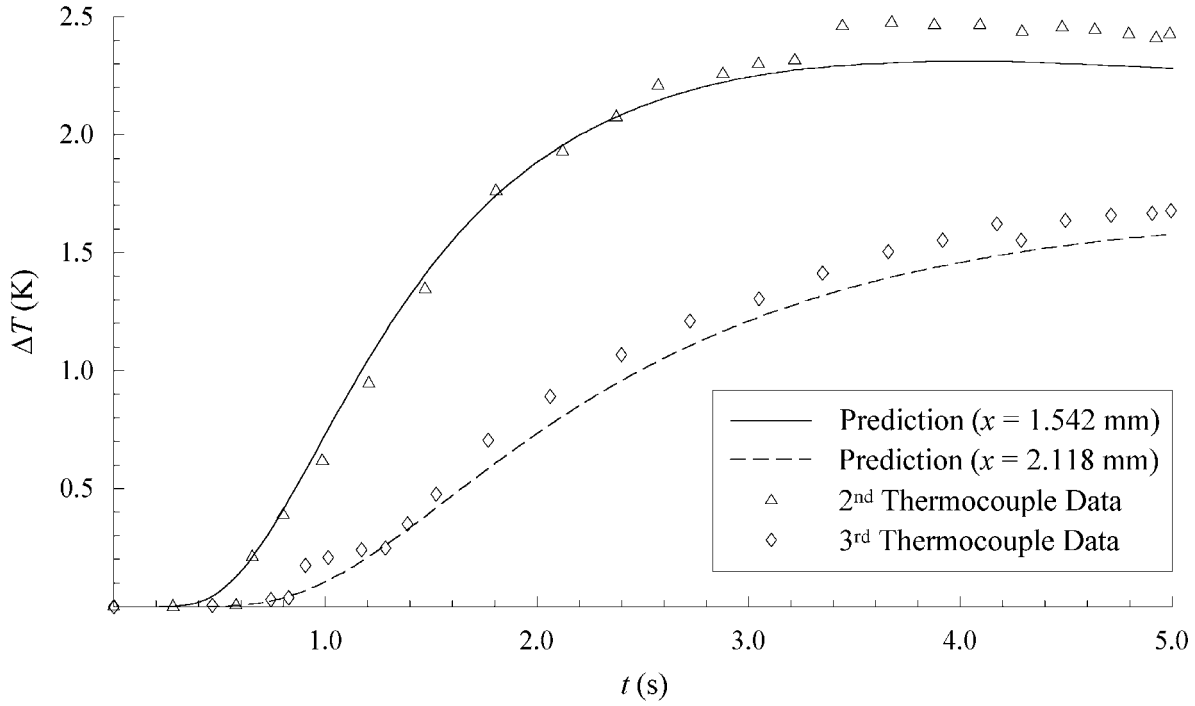

Figure 13.6: ΔT vs. t for a Pulse Width of 0.14 s

13.6 Physical Interpretation of Results

If our general model is able to truly characterize the heat transfer in the sand-air composite, then the optimum values in Table 13.1 for the non-dimensional parameters (Φ_1 and Φ_2) and the air "particle" time scale τ_p should be physically reasonable. At this point, we will use the definitions of Φ_1, Φ_2, and τ_p to interpret the results found in Table 13.1.

We will first determine if the optimum value of Φ_1 is reasonable from a physical point of view. In Chapter 2, we introduced the properties of a general composite composed of a solid matrix with embedded particles. For a *solid* matrix made of the sand material with embedded particles of air, the value of the parameter Φ_1 is given in (4.2.10). According to the definition (4.2.10) of Φ_1 for a sand-air composite,

$$\Phi_1 = \frac{(\rho c)_{air}}{(\rho c)_{sand}} \frac{n_p v_p}{1 - n_p v_p}, \tag{13.6.1}$$

where $(\rho c)_{air}$ and $(\rho c)_{sand}$ are the respective thermal capacities of the air (the particle material) and sand (the matrix material), and $n_p v_p$ is the ratio of total air volume to composite volume. By using the physical properties of air at standard temperature and pressure and dry quartz sand from Reference 21, we can show that

$$\frac{(\rho c)_{air}}{(\rho c)_{sand}} = \frac{(1.24 \text{ kg}/\text{m}^3)(1007 \text{ J}/\text{kg} \cdot \text{K})}{(1657 \text{ kg}/\text{m}^3)(7960 \text{ J}/\text{kg} \cdot \text{K})} = 10^{-4}. \tag{13.6.2}$$

The ratio of thermal capacities in (13.6.2) is very small relative to one, which means that the value of Φ_1 in (13.6.1) for a solid matrix is also very small relative to one. Consequently, our definition of Φ_1 predicts that Φ_1 is *very* small relative to one for a *solid* matrix made of the sand material with embedded particles of air. However, as shown in Table 13.1, the optimum value of Φ_1 is *not* very small relative to one. The optimum value of Φ_1 in Table 13.1 is much larger than the predicted value from (13.6.1).

Perhaps there is a simple explanation for why the optimum value of Φ_1 is very different from the predicted value. As stated in Chapter 4, the parameter Φ_1 for our general model is the ratio of the energies required to heat up the particles and the matrix the same degree. In the general heat equation (6.3.5), the parameter Φ_1 is the coefficient in the third term, meaning that Φ_1 represents the general ability of the embedded particles to influence the temperature in the *solid* matrix of our general model. Because we used our general equation to model heat transfer through the experimental composite, the parameter Φ_1 still represents the general ability of the surrounding air "particles" to influence the *grainy* sand "matrix" in our experimental composite. Since the optimum value of Φ_1 in Table 13.1 (for the experimental composite) is much greater than the predicted value from (13.6.1) (for the general composite set up in Chapter 2), we then conclude that air is generally able to influence grains of sand much more than a solid matrix.

We suspect that the optimum value of Φ_1 (for the experimental composite with sand grains) is very different from the predicted value (for the general model with a solid matrix) because of the difference in how heat transfers in the two composites. For either a solid or grainy matrix, heat transfers in the sand material. However, heat must transfer *between* sand grains in the experimental sand-air composite, while it can flow relatively easily *through* the solid matrix of our general model. An additional contact conductance exists between sand grains due to imperfect contact, which means that the air between sand grains impedes the flow of heat

transfer relative to that through a solid matrix. Consequently, air has a greater impact on heat transfer in the experimental sand-air composite (with sand grains) than in the composite described in Chapter 2 (with a solid matrix). This may explain why the optimum value of Φ_1 for the experimental composite is much greater than the predicted value for the general model. Even though the optimum value of Φ_1 is very different than the predicted value, the larger optimum value may still be physically reasonable because it represents the increased ability of the air to influence the experimental sand "matrix" temperatures due to extra contact conductance between sand grains.

We suspect that the optimum values for Φ_2 and τ_p are more physically acceptable than that for Φ_1. Whether the sand material is solid (for our composite described in Chapter 2) or in grains (for the composite used in the experiment), heat still transfers between the sand and the air particles. The contact conductance μ between the air and sand is the same, independent of whether the sand is solid or in grains. If the air "particles" between the sand grains are about the same size as those embedded in a solid matrix, then the particle time scale τ_p and the parameter Φ_2 should both be fairly independent of whether the sand is solid or in grains.

We will now determine if our hypothesis about the value of τ_p is valid. For the composite described in Chapter 2, the particle time scale τ_p is defined in (4.2.12). For "particles" made of air, we then have that

$$\tau_p = \frac{R^2}{\alpha_p}. \tag{13.6.3}$$

By using the time scale τ_p from Table 13.1 and the thermal diffusivity of air at standard temperature and pressure from Reference 21, we find that

$$7.7(10^{-4})\ \text{s} = \frac{R^2}{0.23(10^{-4})\ \text{m}^2/\text{s}}. \tag{13.6.4}$$

Therefore, we find that

$$R = 0.13\ \text{mm}, \tag{13.6.5}$$

which means that the air "particles" have a size around 0.26 mm. Because the grains of sand have a mean size of 0.2 mm, it seems reasonable that the air "particles" have around the same size. Accordingly, our optimum value for τ_p is physically reasonable, as hypothesized.

Because the optimum value for τ_p is physically reasonable, we expect that the optimum value for the parameter Φ_2 is also physically realistic. For the composite described in Chapter 2, the parameter Φ_2 is defined in (4.2.11) and is associated with the thermalization time τ_T. Because Φ_2 is much less than one, the thermalization time is

$$\tau_T = \frac{\tau_p}{3\Phi_2}, \tag{13.6.6}$$

according to (4.6.15) and (4.6.16). Substitution of the optimum values from Table 13.1 into (13.6.6) then yields that

$$\tau_T = 3.2 \text{ s}, \tag{13.6.7}$$

which is a measure of the time is takes for the sand to heat up its surrounding air "particles". If the value in (13.6.7) is sensible, then our value of Φ_2 in Table 13.1 is also physically realistic. However, it is difficult to know whether the value for τ_T is realistic without knowing the details of heat transfer between the sand and air.

13.7 Comparison of General Model to Other Models

In Section 13.5, we attempted to use our general model that was created in this thesis to characterize the sand-air composite that was used in a heat transfer experiment. We found values of the system parameters (α_{eff}, Φ_1, Φ_2, and τ_p) for the general model that characterize the sand-air composite such that the model was able to predict the experimental values fairly well. However, perhaps we can predict the experimental values almost equally well with a less general model. In fact, we can create two simple models by *limiting* certain parameters in the general model.

The first model is the damped telegraph equation. In Chapter 5, we showed how the non-dimensional general heat equation (4.7.3) reduces to the damped telegraph equation (5.2.5) when the parameter Φ_2 limits to zero for general space $\hat{x}$ and time $\hat{t}$. According to the non-dimensional variables in (4.7.1), this means that the damped telegraph equation (DTE) was created by taking the limit of general heat equation as Φ_2 approaches zero for general τ_μ. Then,

according to the definition (4.6.15) of τ_μ, this means that the DTE was created by letting both the parameter Φ_2 and the particle time scale τ_p approach zero with the thermalization time τ_μ being general. It can be shown that when both Φ_2 and τ_p approach zero for general τ_μ, the Laplace transform $\overline{\Delta T}(x, s)$ in (13.3.11) approaches

$$\overline{\Delta T}(x, s) = \overline{\Delta T}(x_1, s)\, e^{\frac{x_1 - x}{\sqrt{\alpha_{eff}(1+\Phi_1)}}\sqrt{s + \frac{s\Phi_1}{1+s\tau_\mu}}}, \tag{13.7.1}$$

which means that this transform is for the DTE. We note that the number of parameters in (13.7.1) for the damped telegraph equation is one less than that for the general model (13.3.11), because the one parameter τ_μ exists in (13.7.1) instead of two parameters (Φ_2 and τ_p) in (13.3.11). Consequently, the DTE is a simpler model that the general model.

The second model is the modified Fourier heat equation. In Chapter 10, we showed that the general heat equation limits to the modified Fourier heat equation (MFHE) in (10.2.7) as time increases and the particles equilibrate with the matrix. In Chapter 11, we showed that the particle thermalization time τ_T is crucial in determining when the general heat equation can be approximated by the MFHE. As seen in the conditions in (11.4.11), it was found that time *t* must be large compared to τ_T for the MFHE to sufficiently approximate the general heat equation for the general unit step response. Accordingly, when the thermalization time τ_T is zero and time is always much greater than τ_T, we expect that the general equation should reduce to the MFHE for all time. For general Φ_2, we can let the thermalization time τ_T be zero by letting the particle time scale τ_p be zero, according to the definition (4.6.16) of τ_T. When τ_p approaches zero, the Laplace transform $\overline{\Delta T}(x, s)$ in (13.3.11) approaches

$$\overline{\Delta T}(x, s) = \overline{\Delta T}(x_1, s)\, e^{(x_1 - x)\sqrt{s/\alpha_{eff}}}, \tag{13.7.2}$$

which is the transform for the MFHE. We note that the number of parameters in (13.7.2) for the modified Fourier heat equation is three less than that for the general model (13.3.11), because the three parameters (Φ_1, Φ_2 and τ_p) in (13.3.11) for the general model are not seen in (13.7.2) for the MFHE. Consequently, like the DTE, the MFHE is simpler than the general model.

By using the same procedure as that seen in Section 13.4, we can fit the DTE and the MFHE to the experimental data by using the transforms in (13.7.1) and (13.7.2), respectively, to

solve for the optimum values of the parameters in each model. The optimum values for the DTE and MFHE are seen in Table 13.2, and Figure 13.7 contains a plot of the optimum fits, i.e., the temperature changes predicted by using the values in Table 13.2, with the measured data for a pulse width of 0.56 s.

Table 13.2: Optimum Values for DTE and MFHE from Minimization of F_{obj}

Parameter	Optimum Value for DTE	Optimum Value for MFHE
x_2 (mm)	1.544	1.512
x_3 (mm)	2.120	2.082
α_{eff} (m^2/s)	$0.285(10^{-6})$	$0.289(10^{-6})$
Φ_1	0.145	N/A
τ_μ (s)	3.20	N/A

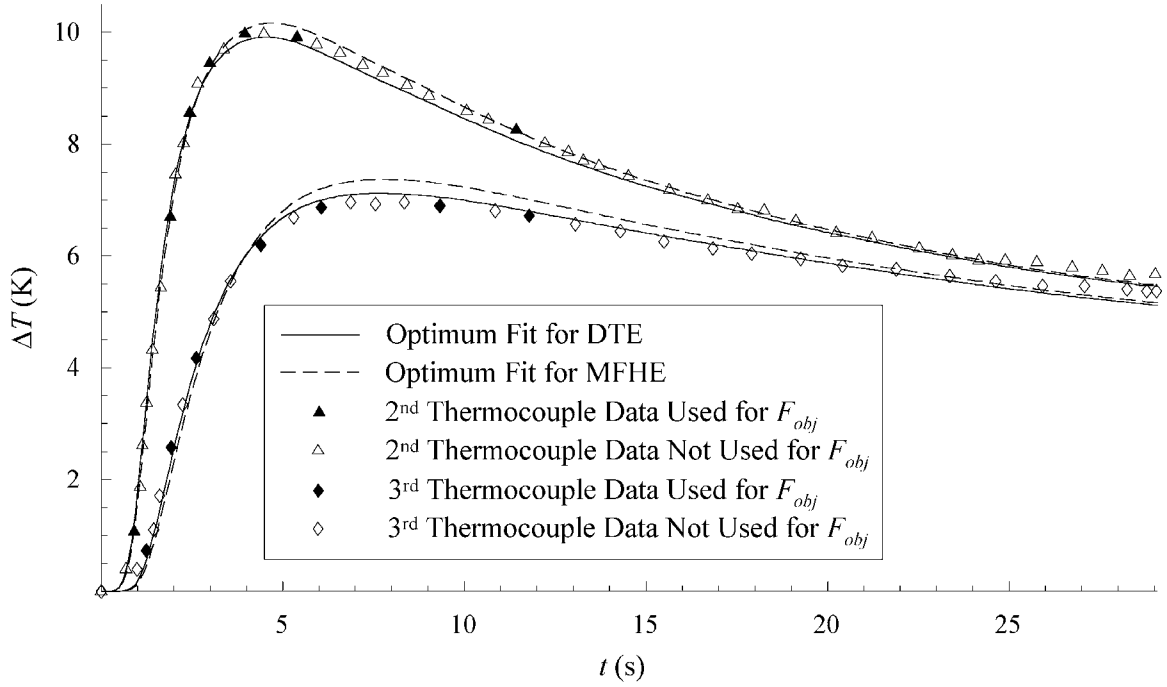

Figure 13.7: ΔT vs. t for a Pulse Width of 0.56 s

The predicted temperatures in Figure 13.7 differ by more than ±0.15 K from the experimental values at several points. Because this lack of accuracy was also seen in Figure

13.5, none of our three models is able to predict the experimental values within the given error tolerance. However, perhaps one model fits the experimental data better than the remaining models. Indeed, it is noticeable in Figure 13.7 that the optimum fit for the MFHE is generally not as accurate as that for the damped telegraph equation. On the other hand, the difference between the respective optimum fits for the general equation and the DTE in Figures 13.5 and 13.7 is hardly noticeable. This is because the optimum Φ_2 in Table 13.1 for the general heat equation is so small that the optimum general model is basically the damped telegraph equation ($\Phi_2 = 0$).

Based on these observations, we conclude that both the general heat equation (4.7.3) and the damped telegraph equation (5.2.5) are better than the modified Fourier heat equation in (10.2.5) at predicting the experimental values for the given sand experiment. This is mainly because the optimum thermalization time τ_μ is *not* much smaller than time *t* in most of Figure 13.7. However, the optimum fits for the general and damped telegraph models are too close for us to draw any general conclusions about which model is truly better at approximating the experimental temperature changes.

13.8 Conclusions

We attempted to use our general composite model that was created in this thesis in order to characterize the sand-air composite that was used in a heat transfer experiment. By using some experimental data, we found values of the system parameters α_{eff}, Φ_1, Φ_2, and τ_p that best characterize the sand-air composite used for the experiment. The optimum model was then used to predict other experimental data.

Even though our general model with the optimum system parameters was able to predict the experimental values fairly well, it seems that our general model cannot be used to model the experimental sand-air composite. First, the differences between the predicted and experimental temperatures were not always within the measurement error. Second, while the optimum value of τ_p seems physically realistic, the values of Φ_1 and Φ_2 may not be reasonable.

Because the heat transfer in a solid matrix (for the composite described in Chapter 2) is different than the heat transfer between grains of sand (for the composite used in the experiment), it is understandable that our general model does not perfectly model the experimental sand-air composite. The contact conductance between sand grains was not accounted for in our general model because the general composite has a solid matrix instead of sand grains. Consequently, we found that the optimum value of Φ_1 for the grains of sand is very different from the value of Φ_1 for a solid matrix. In order to model the sand-air composite more adequately, a model should be created that details at least the heat transfer between the sand grains. Furthermore, our general model assumes only solid materials, whereas air is a non-solid material; convection also occurs in air. While the effect of convection may be minimal, it could still be included in a more general model.

Because our general model is for a solid matrix but was applied to model a grainy matrix, we cannot determine the accuracy of our general model (for a solid matrix) by using the results from this chapter (for a grainy matrix). Even still, the results from this chapter reveal that the general and the damped telegraph equations are better than the modified Fourier heat equation at predicting the given experimental values. This means that the general model is better than the modified Fourier heat equation because it has more parameters for fitting purposes. On the other hand, we cannot state with confidence the general ability of the parameters Φ_1 and Φ_2 to model the physics of heat transfer in a composite with a solid matrix by using the results from this chapter for a "matrix" made of sand grains. This is especially true since the parameter Φ_2 was unnecessary for modeling temperatures in the experimental sand-air composite because the optimum general model (for non-zero Φ_2) and damped telegraph model (for zero Φ_2) were virtually indistinguishable. Consequently, we conclude that the general heat equation is generally better than the MFHE equation, but the accuracy of the general model is still suspect.

Chapter 14

Summary of Results and Recommendations for Future Work

14.1 General Matrix Temperature Equation

Many researchers use a Fourier heat equation,

$$\partial_t T = \alpha \nabla^2 T \,, \tag{14.1.1}$$

a non-Fourier model like the hyperbolic heat equation,

$$\partial_t T + \tau \partial_t{}^2 T = \alpha \nabla^2 T \,, \tag{14.1.2}$$

or a dual-phase-lag equation,

$$\frac{1}{\alpha}\partial_t T + \frac{\tau_q}{\alpha}\partial_t{}^2 T = \nabla^2 T + \tau_T \, \partial_t \nabla^2 T \,, \tag{14.1.3}$$

to model heat transfer through engineering materials. For a matrix with embedded particles, Vick and Scott [17] derived a type of dual-phase-lag equation called a two-step equation,

$$\frac{1}{\alpha_{eff}}\partial_t T_m + \frac{\tau_{eff}}{\alpha_{eff}}\partial_t{}^2 T_m = \nabla^2 T_m + \tau_{eff}\frac{\alpha_m}{\alpha_{eff}}\partial_t \nabla^2 T_m \,, \tag{14.1.4}$$

by ignoring the details of heat transfer within the particles.

In this thesis, we also studied how the matrix temperature behaves in a composite with embedded particles. We let both the matrix and particles be diffusive, i.e., both are governed by a Fourier heat equation (14.1.1), and we let heat conduct between the matrix and particles through contact conductance layers. Unlike the two-step equation (14.1.4), our general equation approximates the matrix temperature while accounting for the detailed transfer of heat *within* the particles. After making certain assumptions about heat transfer in the composite, we created our general non-dimensional integro-differential equation,

$$\Phi_2(\partial_{\hat{t}}\theta_m - \hat{\nabla}^2\theta_m) + 2\int_0^{\hat{t}} \mathrm{Y}(\hat{t}-\hat{\tau})\partial_{\hat{t}}(\Phi_1\theta_m + \partial_{\hat{t}}\theta_m - \hat{\nabla}^2\theta_m)\,d\hat{\tau} = 0 \,, \tag{14.1.5}$$

where Φ_1 and Φ_2 are non-dimensional parameters defined in (4.2.10) and (4.2.11), respectively, and the function Y is defined in (4.7.5). It was shown in Chapter 5 that as Φ_2 approaches zero, our general equation (14.1.5) becomes the non-dimensional form,

$$(1+\Phi_1)\partial_{\hat{t}}\theta_m + \partial_{\hat{t}\hat{t}}\theta_m = \hat{\nabla}^2\theta_m + \partial_{\hat{t}}\hat{\nabla}^2\theta_m, \tag{14.1.6}$$

of the two-step equation used by Vick and Scott. Consequently, our general model is better than the two-step model because it holds for *all* Φ_2, and not just when Φ_2 is zero, by accounting for the details of heat transfer within the particle.

Two non-dimensional parameters (Φ_1 and Φ_2) exist in the general matrix temperature equation (14.1.5). We showed in Chapter 4 that Φ_1 is a ratio of the total thermal capacity of the particles to that of the matrix, while Φ_2 is a ratio of the internal resistance to the surface resistance of heat transfer for a particle. In Chapter 6, we determined that if

$$\Phi_1 = O(1) \tag{14.1.7}$$

and

$$\Phi_2^* = \frac{\mu R}{k_m} = o(1), \tag{14.1.8}$$

then we are justified in using the general integro-differential matrix temperature equation to approximate heat transfer in our composite. The first constraint (14.1.7) ensures that the general matrix temperature equation is general, i.e., "non-Fourier", in the sense that it differs in form from the Fourier heat equation (14.1.1). The second constraint (14.1.8) ensures that the error in the general integro-differential equation (14.1.5) is negligible.

Because the general matrix temperature equation is based on diffusion, the solution depends on only the initial uniform temperatures assumed for the matrix and particles. Like the Fourier heat equation (14.1.1), our general equation (14.1.5) depends on the initial composite temperatures and *not* on any other initial conditions like temperature rates. The diffusive nature of the general heat equation also eliminates the wavefronts created by the hyperbolic heat equation (14.1.2).

14.2 Behavior of General Matrix Temperature Equation

In Chapter 10, we revealed that the one-dimensional form of the general matrix temperature equation is initially the Fourier heat equation (FHE) for the matrix, i.e.,

$$\partial_t T_m = \alpha_m \partial_x^2 T_m \text{ as } t \to 0 \tag{14.2.1}$$

and that the general equation limits to the modified Fourier heat equation (MFHE) as the matrix equilibrates, i.e.,

$$\partial_t T_m = \alpha_{eff} \partial_x^2 T_m \text{ as } t \to \infty, \tag{14.2.2}$$

where the effective thermal diffusivity α_{eff} is

$$\alpha_{eff} = \frac{\alpha_m}{1+\Phi_1}. \tag{14.2.3}$$

We were able to explain why the general heat equation evolves from the FHE to the MFHE. Because no energy is initially transferred to the particles, the particles initially act as "holes", such that the Fourier heat equation for the matrix governs the matrix temperature initially. Then, as the particles and matrix equilibrate over time, the thermal diffusivity of the matrix "decreases" from the matrix thermal diffusivity α_m (in the FHE) to a lesser value of α_{eff} (in the MFHE). In other words, the particles effectively "slow down" heat transfer in the matrix by receiving energy from the matrix. The MFHE, which includes the bulk thermal diffusivity of α_{eff}, exists when the particles are essentially in *equilibrium* with the matrix for large time. In fact, as Φ_1 increases, the effective diffusivity α_{eff} in (14.2.3) decreases, which means that the particles "slow down" heat transfer in the matrix more and more as their ability to store energy increases. This is why Φ_1 is thought of as a gross measure of how much the particles are able to affect the matrix temperature.

On the other hand, the small-time limit in (14.2.1) and the large-time limit in (14.2.2) of the one-dimensional general heat equation are independent of the parameter Φ_2. However, the way the general equation limits to the large-time limit in (14.2.2) depends on Φ_2, because the heat transfer from the matrix to the particles depends on Φ_2. In Chapter 11, we determined that the general matrix temperature equation (14.1.5) is approximately its large-time limit in (14.2.2) for the one-dimensional unit step response when

$$\left(\frac{x}{2\sqrt{\alpha_{eff}\, t}}\right)^2 << \frac{t}{\tau_T} \text{ and } \frac{t}{\tau_T} >> 1, \tag{14.2.4}$$

where the thermalization time τ_T is

$$\tau_T = \begin{cases} \tau_\mu, \Phi_2 << 1 \\ \tau_p, \Phi_2 \text{ otherwise} \end{cases} \tag{14.2.5}$$

and τ_μ and τ_p are two natural time scales. Thus, the general heat equation for all Φ_2 is approximately the MFHE in (14.2.2) in the domain satisfying the first constraint of (14.2.4) when time *t* is large compared to the thermalization time τ_T that is defined in (14.2.5). The thermalization time τ_T governs the large-time limiting of the general matrix temperature equation because equilibration of the particles with the matrix depends on the thermalization time. Consequently, the parameter Φ_2 is thought of as mainly being related to the transient nature of the general matrix temperature equation.

14.3 Recommendations for Future Work

It would be appropriate if the general theory developed in this thesis were expanded upon. First, if the theory were able to account for temperature differences across the particle surfaces, then the resulting general heat equation would be more accurate than the general equation in (14.1.5). Second, if the theory were able to account for non-diffusive heat transfer within the matrix and the particles, then the resulting general heat equation would be more realistic because heat would travel at finite speeds. For instance, one could let the matrix and particles be governed each by a hyperbolic heat equation (14.1.2).

Before the general matrix temperature equation (14.1.5) is improved, it may be wise to test the equation experimentally. This means that a composite should be created that is composed of a matrix with small, embedded particles of random distribution. Just like in the sand-experiment of Chapter 13, matrix temperatures should be collected at various locations throughout the composite and then the general equation should be fitted to the experimental data.

We recommend using a particulate material with a much greater thermal capacity than the matrix material, so that Φ_1 is as large as possible. As stated in this thesis, the parameter Φ_1 is

a measure of the general influence of the particles on the matrix temperature. Consequently, Φ_1 should be as large as possible, so that the particles have the most influence on the measured matrix temperatures and give analysts the greatest possibility of verifying or denouncing the theory presented in this thesis.

We also recommend choosing the material properties such that the thermalization time τ_T is not on a microscale range. The larger the thermalization time, the longer the time it takes for the general heat equation to transition from the Fourier heat equation in (14.2.1) to the modified Fourier heat equation in (14.2.2), giving researchers a greater chance of measuring how the particles influence the matrix behavior.

References

[1] Yang, H. Q., 1991, "Non-Fourier Effect on Heat Conduction During Welding," Int. J. Heat Mass Transfer, 34(11), pp. 2921-2924.

[2] Herwig, H., and Beckert, K., 2000, "Fourier Versus Non-Fourier Heat Conduction in Materials With a Nonhomogeneous Inner Structure," J. Heat Transfer, **122**, pp. 363-365.

[3] Glass, D. E., Özişik, M. N., and McRae, D. S., 1985, "On the Numerical Solution of Hyperbolic Heat Conduction," Numerical Heat Transfer, **8**, pp. 497-504.

[4] Antaki, P. J., 1998, "Solution for Non-Fourier Dual Phase Lag Heat Conduction in a Semi-Infinite Slab With Surface Heat Flux," Int. J. Heat Mass Transfer, **41**(14), pp. 2253-2258.

[5] Vedavarz, A., Kumar, S., and Moallemi, M. K., 1994, "Significance of Non-Fourier Heat Waves in Conduction," J. Heat Transfer, **116**, pp. 116-224.

[6] Tang, D. W., and Araki, N., 1996, "Non-Fourier Heat Conduction in a Finite Medium Under Periodic Surface Thermal Disturbance," Int. J. Heat Mass Transfer, **39**(8), pp. 1585-1590.

[7] Qiu, T. Q., and Tien, C. L., 1993, "Heat Transfer Mechanisms During Short-Pulse Laser Heating of Metals," J. Heat Transfer, **115**, pp. 835-841.

[8] Tzou, D. Y., 1993, "An Engineering Assessment to the Relaxation Time in Thermal Wave Propagation," Int. J. Heat Mass Transfer, **36**(7), pp. 1845-1851.

[9] Cattaneo, C., 1958, "A Form of Heat Conduction Equation Which Eliminates the Paradox of Instantaneous Propagation," C. R. Acad. Sci. Paris, **247**, pp. 431-433.

[10] Vernotte, P., 1958, "Les Paradoxes de la Theorie Continue de l'Equation de la Chaleur," C. R. Acad. Sci. Paris, **246**, pp. 3154-3155.

[11] Özişik, M. N., and Tzou, D. Y., 1994, "On the Wave Theory in Heat Conduction," J. Heat Transfer, **116**, pp. 526-535.

[12] Qiu, T. Q., and Tien, C. L., 1992, "Short-Pulse Laser Heating on Metals," Int. J. Heat Mass Transfer, **35**, pp. 719-726.

[13] Tzou, D. Y., Özişik, M. N., and Chiffelle, R. J., 1994, "The Lattice Temperature in the Microscopic Two-Step Model," J. Heat Transfer, **116**, pp. 1034-1038.

[14] Tzou, D. Y., 1997, *Macro- to Microscale Heat Transfer: The Lagging Behavior*, Taylor & Francis, Washington, DC, pp. 32.

[15] Mitra, K., Kumar, S., Vedavarz, A., and Moallemi, M. K., 1995, "Experimental Evidence of Hyperbolic Heat Conduction in Processed Meat," J. Heat Transfer, **117**, pp. 568-573.

[16] Kaminski, W., 1990, "Hyperbolic Heat Conduction Equation for Materials With a Nonhomogeneous Inner Structure," J. Heat Transfer, **112**, pp. 555-560.

[17] Vick, B., and Scott, E. P., 1998, "Heat Transfer in a Matrix With Embedded Particles," *Proceeding of the Int. Mech. Eng. Congress and Exposition*, Anaheim, CA.

[18] Gradshteyn, I. S., and Ryzhik, I. M., 1980, *Table of Integrals, Series, and Products*, Academic Press, New York, pp. 7, 24, 34, 36, 120, 310, 921, 933, 938, 1079, 1142.

[19] Kakaç, S., and Yener, Y., 1993, *Heat Conduction*, Taylor & Francis, Washington, DC, pp. 18, 53, 265, 266, 274, 278, 279, 343-345.

[20] Özişik, M. N., 1980, *Heat Conduction*, John Wiley & Sons, New York, pp. 16, 259, 261, 262, 275, 284, 657.

[21] Özişik, M. N., 1977, *Basic Heat Transfer*, McGraw-Hill, New York, pp. 60, 498, 505.

[22] O'Neil, P. V., 1995, *Advanced Engineering Mathematics*, Brooks/Cole Publishing Co., Pacific Grove, CA, pp. 115, 119, 121, 124, 129, 141, 145.

[23] Franklin, G. F., Powell, J. D., Emami-Naeini, A., 1994, *Feedback Control of Dynamic Systems*, Addison-Wesley Publishing Co., Reading, MA, pp. 103.

[24] Lienhard, J. H., 1987, *A Heat Transfer Textbook*, Prentice-Hall, Inc., Englewood Cliffs, NJ, pp. 68.

Appendix A

Area Fraction for Plane that Intersects Composite

A.1 Introduction

If a plane intersects our composite, then the plane intersects both particles and matrix. A fraction f of the total area of intersection between the plane and composite intersects the matrix and the complementary fraction $(1-f)$ of the total area of intersection bounds the particles of volume fraction $n_p v_p$. We desire to find f, which we call the *area fraction*, for our composite.

A.2 Derivation of Area Fraction

Figure A.1 depicts a composite piece of cross-sectional area A_T and volume V_T bound between two parallel planes labeled P_1 and P_2 and separated by a distance of δ. The area of intersection between plane P_1 and the matrix is A_m, while the matrix volume bound between the planes is of size V_m. The area of intersection A_m between plane P_1 and the matrix is a fraction f of the composite area A_T. In other words, the area fraction f is

$$f = A_m / A_T \ . \tag{A.2.1}$$

The area fraction f is not generally a constant but rather a function of the orientation of plane P_1 relative to the composite. Furthermore, inspection of Figure A.1 reveals that A_T is related to the total composite volume V_T by

$$V_T = A_T \delta \ . \tag{A.2.2}$$

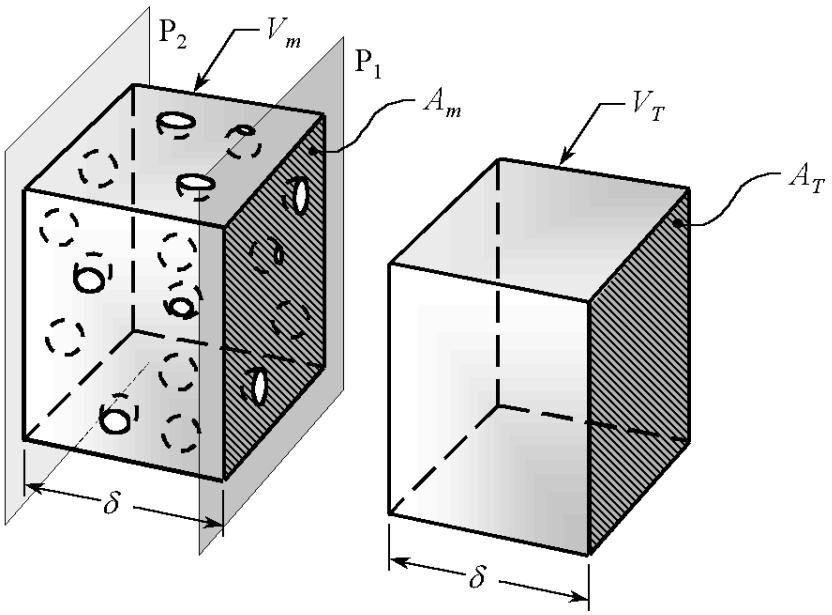

Figure A.1: Planes Bounding Composite Piece

Even though f varies with the orientation of plane P_1, we can approximate f as a constant by using our approximations from Chapter 2. Assuming that the slab contains a sufficiently large number of particles, we find that (2.5.2) holds, which means that the matrix volume V_m between the planes is

$$V_m = (1 - n_p v_p) A_T \delta , \tag{A.2.3}$$

upon substitution of (A.2.2) into (2.5.2). Now, as δ goes to zero, planes P_1 and P_2 approach each other. When the planes are sufficiently close to each other, which is when δ is much smaller than the radius R of the particles, the slab basically becomes a thin plate with holes in it. Thus, when $\delta << R$, the volume V_m is approximately

$$V_m \approx A_m \delta , \tag{A.2.4}$$

because the volume of a thin plate with holes in it is the area of the plate multiplied by its thickness. When we substitute (A.2.4) into (A.2.3) and then divide by δ, we obtain

$$A_m \approx (1 - n_p v_p) A_T , \tag{A.2.5}$$

which holds when plane P_1 intersects a sufficiently large number of random particles. Finally, upon comparison of (A.2.5) and (A.2.1), we find that the area fraction is

$$f = (1 - n_p v_p). \tag{A.2.6}$$

In summary, when a plane intersects our composite, the area of intersection with the matrix is a fraction *f* of the area of intersection with the composite (matrix and particles), where *f* is given approximately by (A.2.6). This statement is true when the plane passes through a sufficiently large number of random particles.

Appendix B

The Laplace Transform

B.1 Definition of Laplace Transform

We define the Laplace transform $\overline{F}(s)$ or $L\{F(t)\}$ of any function $F(t)$, which only exists for non-negative time *t*, as

$$\overline{F}(s) = L\{F(t)\} = \int_{0^-}^{\infty} e^{-st} F(t)\, dt\,, \tag{B.1.1}$$

where the Laplacian variable *s* is generally complex and 0^- means that the lower limit approaches zero from the left. Equation (B.1.1) is a valid definition for a given *s* if the integral exists, i.e., the improper integral converges [22].

In principal, if the Laplace transform $\overline{F}(s)$ is known, the function $F(t)$ can be deduced from it. The inverse Laplace transform $L^{-1}\{\overline{F}(s)\}$ returns the original function $F(t)$, i.e.,

$$L^{-1}\{\overline{F}(s)\} = L^{-1}\{L\{F(t)\}\} = F(t)\,. \tag{B.1.2}$$

The inverse Laplace transform operator returns a unique continuous function $F(t)$ [22].

B.2 Linear Nature of Laplace Transform

The linear nature of the Laplace transform can be found by inspection of the Laplace transform (B.1.1). First, if $F(t)$ is a sum of *n* functions $F_i(t)$, we find that

$$\overline{F}(s) = \sum_{i=1}^{n} \overline{F}_i(s)\,, \tag{B.2.1}$$

where

$$F(t) = \sum_{i=1}^{n} F_i(t)\,. \tag{B.2.2}$$

Equation (B.2.1) is true because the integral of a sum is the sum of the individual integrals, provided that all integrals are convergent, as assumed. Furthermore, we know that scaling $F(t)$ by a factor α scales the Laplace transform of the function by the same factor, i.e.,

$$\alpha \overline{F}(t) = L\{\alpha F(t)\}. \tag{B.2.3}$$

Equation (B.2.3) exists because scaling an integrand scales the integral by the same factor. Because of (B.2.1) and (B.2.3), we know that the Laplace transform, and hence the inverse Laplace transform, are linear operators.

B.3 Various Formulas About Laplace Transforms

Laplace transforms of various functions can be found by inputting different functions into the defintion (B.1.1). Let a function *F* depend on variables *x* and *t*. Through integration by parts, it can be shown that

$$L\{\partial_t F(x,t)\} = s\overline{F}(x,s) - F(x,0), \tag{B.3.1}$$

where $\overline{F}(x,s)$ is the Laplace transform of $F(x,t)$ according to (B.1.1), and ∂_t is the partial differential operator with respect to time *t*. Equation (B.3.1) is valid if the functions $\partial_t F(x,t)$ and $F(x,t)$ are piecewise continuous and continuous, respectively [22]. It can also be shown that, in general,

$$L\{\partial_t^{\,n} F(x,t)\} = s^n \overline{F}(x,s) - s^{n-1}F(x,0) - s^{n-2}\partial_t F(x,0) - \ldots - s\,\partial_t^{\,n-2} F(x,0) - \partial_t^{\,n-1} F(x,0), \tag{B.3.2}$$

where *n* is an integer greater than one. Equation (B.3.2) is valid if the functions $\partial_t^{\,n} F(x,t)$ and $\partial_t^{\,m} F(x,t)$ are piecewise continuous and continuous, respectively, where *m* is an integer between and inclusive of 0 and $(n-1)$ [22]. When *n* = 2, we have the condition that

$$L\{\partial_t^{\,2} F(x,t)\} = s^2 \overline{F}(x,s) - sF(x,0) - \partial_t F(x,0), \tag{B.3.3}$$

where $\partial_t^{\,2} F(x,t)$ is piecewise continuous and both $\partial_t F(x,t)$ and $F(x,t)$ are continuous. The condition for *n* = 2 is stated explicitly in (B.3.3) for ease of reference. On the other hand, for differentiation with respect to space, it can be shown that

$$L\{\partial_x^{\,n} F(x,t)\} = \partial_x^{\,n} \overline{F}(x,s), \tag{B.3.4}$$

where ∂_x is the partial differential operator with respect to space *x*, and *n* is a non-negative integer.

Other formulas related to the Laplace transformation (B.1.1) can also be derived. It can be shown that

$$\overline{F}\,\overline{G} = L\left\{\int_{0^-}^{t} F(t-\tau)G(\tau)d\tau\right\}, \tag{B.3.5}$$

where $\overline{F}$ and $\overline{G}$ are the Laplace transforms of *F* and *G*, respectively [22]. Equation (B.3.5) is the *convolution rule* for Laplace transforms. Furthermore, through differentiation of (B.1.1) with respect to *s*, it is known that

$$\overline{F}^m(s) = \frac{d^m\overline{F}(s)}{ds^m} = (-1)^m\int_{0^-}^{\infty} e^{-st}t^m F(t)\,dt\,, \tag{B.3.6}$$

where *m* is the order of differentiation and is consequently a non-negative integer.

Appendix C

Solution of Initial-Boundary-Value Problem for the Sphere

C.1 Introduction

Equation (4.2.6) is the Laplace transform of the general equation that governs the non-dimensional matrix temperature θ_m in our composite. We desire to invert the equation to form a general equation that contains only θ_m. However, because (4.2.6) contains both $\bar{\theta}_m$ and $\bar{\theta}_p(R)$, we cannot invert it to produce an equation that contains only the matrix temperature θ_m. If we can find how $\bar{\theta}_p(R)$ depends on $\bar{\theta}_m$, we could substitute the relation into (4.2.6) and then invert the result to derive a general equation that contains only θ_m. This appendix finds how $\bar{\theta}_p(R)$ depends on $\bar{\theta}_m$ and the result is used in Chapter 4 to finish deriving the general equation that governs the non-dimensional matrix temperature θ_m.

C.2 Solution of IBVP for the Sphere

The non-dimensional transformed temperature $\bar{\theta}_p(R)$ is determined by solving the initial-boundary-value problem (IBVP) for a typical spherical particle with uniform surface heat flux q_μ. Each sphere of temperature T_p has an initial uniform temperature of T_p^0 as heat begins to transfer between the particle and the surrounding matrix of temperature T_m. The uniform heat flux q_μ into the sphere is governed by contact conductance μ, according to (2.6.2), through the contact surface between the sphere and matrix. The heat flux in the particle is also governed by Fourier's law (2.6.1), and Fourier's heat equation,

$$\partial_t T_p = \alpha_p \nabla^2 T_p, \tag{C.2.1}$$

holds within the particle. Figure C.1 depicts the IBVP for a typical sphere. Only the radial coordinate is included in the figure because the initial and boundary conditions produce a spherically symmetric temperature distribution $T_p(r)$ for all time within the sphere [19].

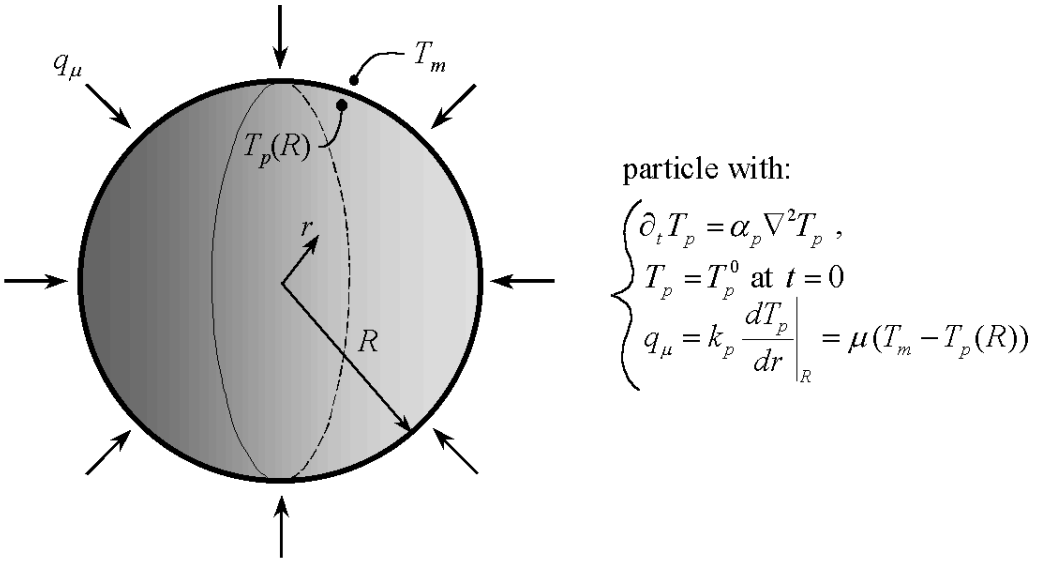

Figure C.1: Initial-Boundary-Value Problem for the Sphere

When we apply Fourier's law (2.6.1) for the sphere of Figure C.1, we find that

$$q_\mu = k_p \left. \frac{dT_p}{dr} \right|_R , \tag{C.2.2}$$

as seen in the figure. Now, the contact conductance expression in (2.6.2) for q_μ must be equivalent to the Fourier form of q_μ in (C.2.2). Equating the two expressions for q_μ yields

$$k_p \left. \frac{dT_p}{dr} \right|_R = \mu(T_m - T_p(R)) , \tag{C.2.3}$$

which is also seen in Figure C.1.

Let us non-dimensionalize the temperatures in our IBVP of Figure C.1. We non-dimensionalize (C.2.1) and (C.2.3) according to (4.2.1) to find that

$$\partial_t \theta_p = \alpha_p \nabla^2 \theta_p \tag{C.2.4}$$

and

$$k_p \left. \frac{d\theta_p}{dr} \right|_R = \mu(\theta_m - \theta_p(R) - \Delta\theta_0), \tag{C.2.5}$$

where

$$\Delta\theta_0 = \frac{T_p^0 - T_m^0}{T_{ref}} \tag{C.2.6}$$

and the initial value of θ_p is zero. Now, by using both (B.2.3) and (B.3.4) for the left-hand side of (C.2.5) and both (B.2.1) and (B.2.3) for the right-hand side of (C.2.5), we can show that the Laplace transform of (C.2.5) is

$$k_p \left. \frac{d\overline{\theta}_p}{dr} \right|_R = \mu(\overline{\theta}_m - \overline{\theta}_p(R) - \overline{\Delta\theta_0}), \tag{C.2.7}$$

where an overbar denotes the Laplace transform of the function.

We now solve for $\overline{\theta}_p(R)$ as a function of $\overline{\theta}_m$. When the result is substituted into (4.2.6), $\overline{\theta}_m$ will be the only transformed variable in the result, as desired. In order to solve for $\overline{\theta}_p(R)$ as a function of $\overline{\theta}_m$, we need a general expression for $\overline{\theta}_p$. It can be shown that for a sphere governed by (C.2.4) with zero initial non-dimensional temperature and spherically symmetric temperature $\theta_p(r)$,

$$\overline{\theta}_p = \frac{C(s)}{r} \sinh mr, \tag{C.2.8}$$

where

$$m = \sqrt{s/\alpha_p}, \tag{C.2.9}$$

s is the independent variable for the Laplace domain, $C(s)$ is a function yet to be determined [19], and sinh(X) gives the hyperbolic sine of a general complex number X [18]. Substitution of (C.2.8) into the boundary condition (C.2.7) yields

$$k_p C(s)\left(-\frac{\sinh mR}{R^2} + \frac{m\cosh mR}{R}\right) = \mu(\overline{\theta}_m - \frac{C(s)}{R}\sinh mR - \overline{\Delta\theta_0}), \tag{C.2.10}$$

where cosh(X) gives the hyperbolic cosine of a general complex number X [18]. Equation (C.2.10) can now be solved for $C(s)$ to yield:

$$C(s) = \frac{\overline{\theta}_m - \overline{\Delta\theta_0}}{\frac{k_p}{R\mu} m \cosh mR + \frac{1}{R}\left(-\frac{k_p}{R\mu} + 1\right)\sinh mR}. \tag{C.2.11}$$

Finally, substituting (C.2.11) into (C.2.8) yields

$$\overline{\theta}_p(R) = \frac{\overline{\theta}_m - \overline{\Delta\theta_0}}{1 + \frac{k_p}{\mu R}\left(mR\coth mR - 1\right)}, \tag{C.2.12}$$

where coth(X) gives the hyperbolic cotangent of a general complex number X [18].

Equation (C.2.12) yields the relationship between $\overline{\theta}_p(R)$ and an arbitrary $\overline{\theta}_m$. In principle, one can invert (C.2.12) to find $\theta_p(R)$ as a function of time t. However, for the purposes of this thesis, we only need the expression for $\overline{\theta}_p(R)$, which will be substituted into (4.2.6) to form an equation with $\overline{\theta}_m$ as the only transformed variable. The equation is then inverted in Chapter 4 to create the general equation (4.2.9) that governs the non-dimensional matrix temperature θ_m.

Appendix D

Laplace Inverses Required for Inversion of General Equation

D.1 Introduction

Equation (4.2.7) is the Laplace transform of the general equation that governs the non-dimensional matrix temperature θ_m in our composite. The equation needs to be inverted, but to do so requires the inverses of particular expressions seen in (4.2.7). To fully invert (4.2.7), the inverses for $(m\coth mR - 1/R)(s\overline{\theta}_m - \alpha_m \nabla^2 \overline{\theta}_m)$ and $(m\coth mR - 1/R)(\overline{\theta}_m - \overline{\Delta\theta_0})$ must be known. In this appendix, the needed inverses are created.

D.2 General Laplace Inverse Required for Inversion of General Equation

At this point, we do not know the inverses of $(m\coth mR - 1/R)(s\overline{\theta}_m - \alpha_m \nabla^2 \overline{\theta}_m)$ and $(m\coth mR - 1/R)(\overline{\theta}_m - \overline{\Delta\theta_0})$. To find the inverses, we will first show that for a general function θ,

$$L^{-1}\{(\sqrt{s/\alpha_p}\coth R\sqrt{s/\alpha_p} - 1/R)\overline{\theta}\} = \frac{2}{R}\int_0^t \sum_{n=1}^{\infty} e^{-\alpha_p n^2\pi^2(t-\tau)/R^2} L^{-1}\{s\overline{\theta}\}d\tau, \qquad \text{(D.2.1)}$$

where L^{-1} is the inverse Laplace transform operator defined in (B.1.2). In reality, θ may depend on both variables *x* and *t*, but since the Laplace transform (B.1.1) only deals with integration in the time domain, the unseen variable *x* can be regarded as a parameter in (D.2.1). Once (D.2.1) is derived, $\overline{\theta}$ in (D.2.1) will be replaced by both $(\overline{\theta}_m - \overline{\Delta\theta_0})$ and $(s\overline{\theta}_m - \alpha_m \nabla^2 \overline{\theta}_m)$ to produce the two inverses needed for inversion of (4.2.7).

In order to prove (D.2.1), we begin by using Equation 1.421(4) in [18]. The latter equation can be used to show that

$$\frac{R\sqrt{s/\alpha_p}\coth R\sqrt{s/\alpha_p}-1}{2s}=\sum_{n=1}^{\infty}\frac{1}{s+\alpha_p n^2\pi^2/R^2}. \tag{D.2.2}$$

Then, multiplication of (D.2.2) by $2s\bar{\theta}/R$ yields

$$(\sqrt{s/\alpha_p}\coth R\sqrt{s/\alpha_p}-1/R)\bar{\theta}=\frac{2s\bar{\theta}}{R}\sum_{n=1}^{\infty}\frac{1}{s+\alpha_p n^2\pi^2/R^2}. \tag{D.2.3}$$

Utilizing the scaling law (B.2.3) for the right-hand side of (D.2.3), we invert both sides of the latter equation to obtain

$$L^{-1}\{(m\coth mR-1/R)\bar{\theta}\}=\frac{2}{R}L^{-1}\left\{s\bar{\theta}\sum_{n=1}^{\infty}\frac{1}{s+\alpha_p n^2\pi^2/R^2}\right\}, \tag{D.2.4}$$

where

$$m=\sqrt{s/\alpha_p}. \tag{D.2.5}$$

The right-hand side of (D.2.4) needs to be inverted by using the convolution theorem (B.3.5). Using (B.3.5), we can show that (D.2.4) can be written as

$$L^{-1}\{(m\coth mR-1/R)\bar{\theta}\}=\frac{2}{R}\int_0^t L^{-1}\left\{\sum_{n=1}^{\infty}\frac{1}{s+\alpha_p n^2\pi^2/R^2}\right\}\Big|_{t-\tau}L^{-1}\{s\bar{\theta}\}\big|_{\tau}d\tau, \tag{D.2.6}$$

where it is understood that the lower limit of the integral approaches zero from the left. Now, according to the table of Laplace transforms in Reference 22,

$$L^{-1}\left\{\frac{1}{s+a}\right\}=e^{-at} \tag{D.2.7}$$

for $s > -a$. When the transform (D.2.7) is used along with the summation rule (B.2.1) for Laplace transforms, we find that (D.2.6) is

$$L^{-1}\{(m\coth mR-1/R)\bar{\theta}\}=\frac{2}{R}\int_0^t\sum_{n=1}^{\infty}e^{-\alpha_p n^2\pi^2(t-\tau)/R^2}L^{-1}\{s\bar{\theta}\}d\tau. \tag{D.2.8}$$

We have just derived the general Laplace transform (D.2.1).

D.3 First Laplace Inverse Required for Inversion of General Equation

We can now substitute different expressions for $\overline{\theta}$ into the general inverse (D.2.8) to obtain the specific inverses needed for inversion of (4.2.7). Letting $\overline{\theta}$ be $(\overline{\theta}_m - \overline{\Delta\theta_0})$ in (D.2.8), we have

$$L^{-1}\{(m\coth mR - 1/R)(\overline{\theta}_m - \overline{\Delta\theta_0})\} = \frac{2}{R}\int_0^t \sum_{n=1}^{\infty} e^{-\alpha_p n^2\pi^2(t-\tau)/R^2} L^{-1}\{s\overline{\theta}_m - s\overline{\Delta\theta_0}\}d\tau . \quad \text{(D.3.1)}$$

Now, according to the Laplace transform (B.3.1),

$$L\{\partial_t\theta_m\} = s\overline{\theta}_m - \theta_m\big|_{t=0}, \quad \text{(D.3.2)}$$

where $\theta_m\big|_{t=0}$ is the initial value of the matrix temperature θ_m. After rearrangement and inversion of (D.3.2), we find that

$$L^{-1}\{s\overline{\theta}_m\} = \partial_t\theta_m + L^{-1}\{\theta_m\big|_{t=0}\} . \quad \text{(D.3.3)}$$

Because the initial value of θ_m is zero for our composite, according to the initial condition (4.2.4), (D.3.3) becomes

$$L^{-1}\{s\overline{\theta}_m\} = \partial_t\theta_m . \quad \text{(D.3.4)}$$

Now, using a standard table of Laplace transforms in Reference 22, we know that

$$\overline{\Delta\theta_0} = \Delta\theta_0/s . \quad \text{(D.3.5)}$$

Therefore,

$$s\overline{\Delta\theta_0} = \Delta\theta_0 . \quad \text{(D.3.6)}$$

Then, we know that

$$L^{-1}\{s\overline{\Delta\theta_0}\} = L^{-1}\{\Delta\theta_0\} = \Delta\theta_0\,\delta(t), \quad \text{(D.3.7)}$$

where $\delta(t)$ is the Dirac delta "function" [22], having the properties that

$$\delta(t) = 0 \text{ when } t \neq 0 \text{, and } \int_{-\infty}^{\infty}\delta(t)dt = 1 . \quad \text{(D.3.8)}$$

Subtraction of the inverse in (D.3.7) from that in (D.3.4) yields

$$L^{-1}\{s\overline{\theta}_m - s\overline{\Delta\theta_0}\} = \partial_t\theta_m - \Delta\theta_0\,\delta(t) . \quad \text{(D.3.9)}$$

Next, with some rearrangement, substitution of (D.3.9) into the Laplace inverse (D.3.1) yields

$$L^{-1}\{(m\coth mR-1/R)(\overline{\theta}_m-\overline{\Delta\theta_0})\}=\frac{2}{R}\int_0^t\sum_{n=1}^{\infty}e^{-\alpha_p n^2\pi^2(t-\tau)/R^2}\partial_t\theta_m d\tau \\ -\Delta\theta_0\frac{2}{R}\int_0^t\sum_{n=1}^{\infty}e^{-\alpha_p n^2\pi^2(t-\tau)/R^2}\delta(\tau)d\tau \quad . \tag{D.3.10}$$

Now, according to the integral property in (D.3.8),

$$\int_0^{\infty}f(t)\delta(t)dt=f(0)\,, \tag{D.3.11}$$

where f is integrable on [0, ∞) and continuous at zero [22]. Using the integral property (D.3.11), we can show that the inverse (D.3.10) is

$$L^{-1}\{(m\coth mR-1/R)(\overline{\theta}_m-\overline{\Delta\theta_0})\}=\frac{2}{R}\int_0^t\sum_{n=1}^{\infty}e^{-\alpha_p n^2\pi^2(t-\tau)/R^2}\partial_t\theta_m d\tau-\Delta\theta_0\frac{2}{R}\sum_{n=1}^{\infty}e^{-\alpha_p n^2\pi^2 t/R^2}\,, \tag{D.3.12}$$

which is one of the inverses required for inversion of (4.2.7).

D.4 Second Laplace Inverse Required for Inversion of General Equation

To find the other inverse required for inversion of (4.2.7), we let $\overline{\theta}$ in (D.2.8) be equal to $(s\overline{\theta}_m-\alpha_m\nabla^2\overline{\theta}_m)$, such that (D.2.8) becomes

$$L^{-1}\{(m\coth mR-1/R)(s\overline{\theta}_m-\alpha_m\nabla^2\overline{\theta}_m)\}=\frac{2}{R}\int_0^t\sum_{n=1}^{\infty}e^{-\alpha_p n^2\pi^2(t-\tau)/R^2}L^{-1}\{s^2\overline{\theta}_m-\alpha_m s\nabla^2\overline{\theta}_m\}d\tau\,. \tag{D.4.1}$$

We now need to find the Laplace inverse required for the integral in (D.4.1). First, using the Laplace transform (B.3.1), we can show that

$$L^{-1}\{s\nabla^2\overline{\theta}_m\}=\partial_t\nabla^2\theta_m \tag{D.4.2}$$

for our matrix that has an initially uniform temperature. Second, using the Laplace transform (B.3.3), we can show that

$$L^{-1}\{s^2\overline{\theta}_m\}=\partial_t{}^2\theta_m+L^{-1}\{\partial_t\theta_m\big|_{t=0}\} \tag{D.4.3}$$

for our composite with the zero initial condition (4.2.4), and where $\partial_t \theta_m\big|_{t=0}$ is the initial rate of increase in the matrix temperature θ_m. Then, using a standard table of Laplace transforms [22], we know that (D.4.3) is

$$L^{-1}\{s^2\overline{\theta}_m\} = \partial_t{}^2\theta_m + \partial_t\theta_m\big|_{t=0}\delta(t). \tag{D.4.4}$$

Using the inverses (D.4.2) and (D.4.4), we find that

$$L^{-1}\{s^2\overline{\theta}_m - \alpha_m s\nabla^2\overline{\theta}_m\} = \partial_t{}^2\theta_m + \partial_t\theta_m\big|_{t=0}\delta(t) - \alpha_m\partial_t\nabla^2\theta_m, \tag{D.4.5}$$

which can be shown to be

$$L^{-1}\{s^2\overline{\theta}_m - \alpha_m s\nabla^2\overline{\theta}_m\} = \partial_t(\partial_t\theta_m - \alpha_m\nabla^2\theta_m) + \partial_t\theta_m\big|_{t=0}\delta(t). \tag{D.4.6}$$

Now, with some rearrangement, substitution of the inverse (D.4.6) into the integral of (D.4.1) yields

$$\begin{aligned} L^{-1}\{(m\coth mR - 1/R)(s\overline{\theta}_m - \alpha_m\nabla^2\overline{\theta}_m)\} = {} & \frac{2}{R}\int_0^t \sum_{n=1}^{\infty} e^{-\alpha_p n^2\pi^2(t-\tau)/R^2}\partial_t(\partial_t\theta_m - \alpha_m\nabla^2\theta_m)d\tau \\ & + \frac{2}{R}\partial_t\theta_m\big|_{t=0}\int_0^t \sum_{n=1}^{\infty} e^{-\alpha_p n^2\pi^2(t-\tau)/R^2}\delta(\tau)d\tau \end{aligned}. \tag{D.4.7}$$

Finally, by using the integral property in (D.3.11), we find that (D.4.7) is

$$\begin{aligned} L^{-1}\{(m\coth mR - 1/R)(s\overline{\theta}_m - \alpha_m\nabla^2\overline{\theta}_m)\} = {} & \frac{2}{R}\int_0^t \sum_{n=1}^{\infty} e^{-\alpha_p n^2\pi^2(t-\tau)/R^2}\partial_t(\partial_t\theta_m - \alpha_m\nabla^2\theta_m)d\tau \\ & + \frac{2}{R}\partial_t\theta_m\big|_{t=0}\sum_{n=1}^{\infty} e^{-\alpha_p n^2\pi^2 t/R^2} \end{aligned}. \tag{D.4.8}$$

Like (D.3.12), (D.4.8) is another Laplace inverse required for inversion of (4.2.7). The Laplace inverses will be used to invert (4.2.7) from the *s*-domain to the time domain to produce the general equation that governs matrix temperature. There is a difference, however, between the two inverses that needs to be pointed out to the reader. Unlike (D.3.12), the inverse (D.4.8) contains the initial value $\partial_t\theta_m\big|_{t=0}$ of the function $\partial_t\theta_m$, which is currently unknown. The value of $\partial_t\theta_m\big|_{t=0}$ will be determined after inversion of (4.2.7).

Appendix E

Large-Time Approximation of Temporal Functions

E.1 Creation of Large-Time Approximation of Temporal Functions

In this appendix, we use a known Laplace transform $\overline{F}(s)$ to create a large-time approximation of the generally unknown real temporal function $F(t)$, which we assume to have a limiting value of f_0 as time t approaches infinity. Because the unknown function steadies out to a final value of f_0, we assume that we can let the large-time approximation $F_\infty(t)$ of $F(t)$ be

$$F_\infty(t) = \sum_{i=0}^{n} f_i t^{-i\nu} = f_0 + f_1 t^{-\nu} + f_2 t^{-2\nu} + \ldots + f_{n-1} t^{-(n-1)\nu} + f_n t^{-n\nu}, \tag{E.1.1}$$

where ν is a positive, real number and the coefficients f_i are real constants, all of which are yet to be determined. In other words, we assume that we can approximate $F_\infty(t)$ as a power series in time. Furthermore, we have implicitly assumed in (E.1.1) that the finite series has sufficiently converged for the large-time approximation to be valid.

We can use (B.3.6) and (E.1.1) to solve for ν and f_i, where $i = 0, 1, \ldots n$. First, because $F_\infty(t)$ approximates $F(t)$ for sufficiently large time, (B.3.6) can be approximated as

$$\overline{F}^m(s) \approx (-1)^m \int_{0^-}^{\infty} e^{-st} t^m F_\infty(t)\, dt\,. \tag{E.1.2}$$

Next, substitution of (E.1.1) into (E.1.2) yields

$$\overline{F}^m(s) \approx (-1)^m \sum_{i=0}^{n} f_i \int_{0}^{\infty} e^{-st} t^{m-i\nu}\, dt\,. \tag{E.1.3}$$

The integrals in (E.1.3) can be simplified by using the fact that

$$\int_{0}^{\infty} e^{-st} t^{\mu}\, dt = \Gamma(1+\mu) s^{-\mu-1}, \tag{E.1.4}$$

where $\mathrm{Re}[\mu] > -1$, $\mathrm{Re}[s] > 0$, and $\Gamma(z)$ is the Euler gamma function defined as

$$\Gamma(z) = \int_0^\infty e^{-t} t^{z-1} dt \tag{E.1.5}$$

for Re[z] > 0 [18]. When we apply (E.1.4) to the sum of integrals in (E.1.3), we obtain

$$\overline{F}^m(s) \approx (-1)^m \sum_{i=0}^{n} f_i \, \Gamma(1+m-i\nu) s^{i\nu-m-1}, \tag{E.1.6}$$

where $m - n\nu > -1$ and Re[s] > 0. Rearrangement of (E.1.6) yields

$$\overline{F}^m(s) s^{m+1} \approx (-1)^m \sum_{i=0}^{n} f_i \, \Gamma(1+m-i\nu) s^{i\nu}, \tag{E.1.7}$$

where $m - n\nu > -1$ and Re[s] > 0.

We assumed that (E.1.7) holds, but in order for the series to be valid, it must be convergent in s, just like $F_\infty(t)$ must be convergent in t. If the right-hand side of (E.1.7) is convergent in s, then we should be able to expand the left-hand side of (E.1.7) about s = 0 to create an equally convergent series. We now expand the left-hand side of (E.1.7) about s being zero, keeping the same number of terms as that for right-hand side, to find that

$$\sum_{i=0}^{n} C_i \, s^{i\nu} = (-1)^m \sum_{i=0}^{n} f_i \, \Gamma(1+m-i\nu) s^{i\nu}, \tag{E.1.8}$$

where $m - n\nu > -1$, Re[s] > 0, and C_i is the coefficient of $s^{i\nu}$ in the expansion of $\overline{F}^m(s) s^{m+1}$ about s = 0.

Because $\overline{F}(s)$ is known, we know all the coefficients C_i and we also know the value of ν by inspection of the expansion of $\overline{F}^m(s) s^{m+1}$. Finally, we must equate coefficients of the varied powers of s in (E.1.8) for the equation to hold for general s, meaning that

$$f_i = \frac{C_i (-1)^m}{\Gamma(1+m-i\nu)}, \tag{E.1.9}$$

for i = 0, 1, … n. The coefficients f_i are then substituted along with the known value of ν into (E.1.1) to yield the desired large-time approximation $F_\infty(t)$ of the unknown function $F(t)$. Lastly, one needs to determine what conditions ensure that a particular $F_\infty(t)$ is convergent, so that the approximation is valid.

E.2 First Example of Creation of Large-Time Approximation

Let the known Laplace transform be

$$\overline{F}(s) = \frac{1}{s} e^{-x\sqrt{s}} . \tag{E.2.1}$$

We desire to use the process created in the previous section of this appendix to create a large-time approximation $F_\infty(t)$ of $F(t)$.

First, our process assumes that a steady-state value exists for $F(t)$. If the poles of $\overline{F}(s)$ are in the left-half side of the complex plane for *s*, with only one pole possibly existing at the origin of the complex plane, then $F(t)$ must reach a steady-state value [23]. The only pole of (E.2.1) is at $s = 0$, which is at the origin of the complex plane. Consequently, $F(t)$ has to reach a steady-state value. Therefore, we can proceed with the creation of the large-time approximation. Second, we need to choose a value for *n*, which is required for the definition (E.1.1) of the large-time approximation. We let $n = 5$, meaning that our large-time approximation $F_\infty(t)$ of $F(t)$ is

$$F_\infty(t) = f_0 + f_1 t^{-\nu} + f_2 t^{-2\nu} + f_3 t^{-3\nu} + f_4 t^{-4\nu} + f_5 t^{-5\nu} . \tag{E.2.2}$$

Next, we need to determine the value of ν, which is the order of the power series of $F_\infty(t)$. The value of ν can be determined by noting the order of the power series of the expansion of $\overline{F}(s)$ about $s = 0$. Expansion of $\overline{F}(s)$ in (E.2.1) about $s = 0$ yields

$$\overline{F}(s) = \frac{1}{s} - \frac{x}{\sqrt{s}} + \frac{x^2}{2} - \frac{x^3\sqrt{s}}{6} + \frac{x^4 s}{24} + O(s^{3/2}) . \tag{E.2.3}$$

By inspection of (E.2.3), we find that the given series is a power series with $\nu = 1/2$. This means that (E.2.2) is

$$F_\infty(t) = f_0 + f_1 t^{-1/2} + f_2 t^{-1} + f_3 t^{-3/2} + f_4 t^{-2} + f_5 t^{-5/2} . \tag{E.2.4}$$

We now need to choose a value for *m* such that $m - n\nu > -1$. With $n = 5$ and $\nu = 1/2$, we choose to let $m = 3$, which satisfies the restriction on *m* since 1/2 is greater than –1.

Finally, our method requires us to expand $\overline{F}^m(s)s^{m+1}$ about $s = 0$ and then collect all coefficients C_i that are required to solve for the f_i in (E.2.4). With $m = 3$, it can be shown that expansion of $\overline{F}^m(s)s^{m+1}$ about $s = 0$ yields

$$\overline{F}^3(s)s^4 = -6 + \frac{15x\sqrt{s}}{8} - \frac{x^3 s^{3/2}}{16} + \frac{x^5 s^{5/2}}{320} + O(s^3). \tag{E.2.5}$$

Next, by definition, the coefficient C_i is the coefficient of $s^{i\nu}$ in the expansion of $\overline{F}^m(s)s^{m+1}$, where $i = 0, 1, \ldots n$. Because $n = 5$, $\nu = 1/2$, and $m = 3$, it is revealed through (E.2.5) that

$$C_0 = -6,\ C_1 = \frac{15x}{8},\ C_2 = 0,\ C_3 = -\frac{x^3}{16},\ C_4 = 0,\ \text{and}\ C_5 = \frac{x^5}{320}. \tag{E.2.6}$$

When we substitute (E.2.6) into (E.1.9), while recognizing that $m = 3$ and $\nu = 1/2$, we find that

$$f_0 = \frac{6}{\Gamma(4)},\ f_1 = -\frac{15x/8}{\Gamma(7/2)},\ f_2 = 0,\ f_3 = \frac{x^3/16}{\Gamma(5/2)},\ f_4 = 0,\ \text{and}\ f_5 = -\frac{x^5/320}{\Gamma(3/2)}. \tag{E.2.7}$$

Next, by using known values of the Euler gamma function [18], we can show that

$$f_0 = 1,\ f_1 = -\frac{x}{\sqrt{\pi}},\ f_2 = 0,\ f_3 = \frac{x^3}{12\sqrt{\pi}},\ f_4 = 0,\ \text{and}\ f_5 = -\frac{x^5}{160\sqrt{\pi}}. \tag{E.2.8}$$

We then substitute all f_i into (E.2.4) to find that the large-time approximation $F_\infty(t)$ of $F(t)$ is

$$F_\infty(t) = 1 - \frac{x}{\sqrt{\pi}\,t^{1/2}} + \frac{x^3}{12\sqrt{\pi}\,t^{3/2}} - \frac{x^5}{160\sqrt{\pi}\,t^{5/2}}. \tag{E.2.9}$$

We now have a large-time approximation, but in order for that approximation to be valid, it needs to converge sufficiently as t increases towards infinity. We see that our approximation converges fast when $x^2 << t$. Thus, our large-time approximation (E.2.9) is valid at least when $x^2 << t$. $F_\infty(t)$ is called a large-time approximation because, even though t may be small, the approximation is valid when time t is *large relative to* x^2.

In general, the temporal function $F(t)$ is unknown, which is why an approximation of the function for large time had to be created by using the known Laplace transform $\overline{F}(s)$. However, our example Laplace transform $\overline{F}(s)$ in (E.2.1) was chosen because $F(t)$ is known exactly for that case. The inverse of (E.2.1) is

$$F(t) = \text{erfc}(x/\sqrt{2}\,t), \tag{E.2.10}$$

where erfc(X) is the complementary error function of X [20]. The function (E.2.10) can be expanded exactly for large time to show that

$$F(t) = 1 - \frac{x}{\sqrt{\pi}\,t^{1/2}} + \frac{x^3}{12\sqrt{\pi}\,t^{3/2}} - \frac{x^5}{160\sqrt{\pi}\,t^{5/2}} + O(t^{-7/2}). \tag{E.2.11}$$

Thus, for this example application of the method devised in Section E.1, we see that our large-time approximation (E.2.9) is the first four terms of the exact large-time expansion (E.2.11). If we want more terms in the large-time approximation, we can increase *n* and repeat the method created in Section E.1.

E.3 Second Example of Large-Time Approximation

Let the known Laplace transform be

$$\overline{F}(s) = \frac{1}{1+s}. \tag{E.3.1}$$

We desire to use the process created in Section E.1 of this appendix to create a large-time approximation $F_\infty(t)$ of $F(t)$. Without going through the process as we did in Section E.2, it can be shown that

$$F_\infty(t) = 0 \tag{E.3.2}$$

for *any* admissible values of *n* and *m*. In other words, even if *n* is equal to 100, only *one* term exists in the large-time approximation. The only term seen in (E.3.2) is the limit of $F(t)$ as time approaches infinity. Because only one term exists in (E.3.2), it seems as if our method from Section E.1 fails for this case.

The apparent failure of the method created in Section E.1 can be explained. Like (E.2.1), the Laplace transform (E.3.1) also has a known inverse. According to [22], the inverse of (E.3.1) is

$$F(t) = e^{-t}. \tag{E.3.3}$$

Indeed, the limit of $F(t)$ in (E.3.3) is zero as time approaches infinity, as seen in (E.3.2). However, because the exact $F(t)$ approaches zero much faster than *any* power of time, a series expansion about infinite time for (E.3.3) cannot be carried out. In other words, a power series expansion of (E.3.3) does not exist for large time. Our method from Section E.1 relies on the assumption that a large-time power series expansion exists for $F(t)$. Because a large-time power series expansion does not exist for (E.3.3), our method from Section E.1 *cannot* produce a power series expansion for large time for this case. As evidenced, it does not matter how large

we make *n* because the exponential function in (E.3.3) limits to zero much faster than any power of time.

The lesson learned from the Laplace transform (E.3.1) is that the method from Section E.1 will not work if a large-time power series expansion does not exist. This fact explains why we *assume* that a power series approximation exists for the method described in Section E.1. If a power series does not exist in actuality, then the large-time approximation is just the limit of the function as time approaches infinity.

VITA

I have lived in Reston, Virginia most of my life, so attending Virginia Tech as an undergraduate was only natural for this Virginian that was considering becoming an engineer. However, I wanted to learn and apply physics, mathematics, and engineering. No department felt like home until I discovered the Engineering Science and Mechanics Department and then the light bulb went off above my head. I have been here since 1996 and am finding it hard to leave. My graduate work so far has been a blessing and I hope that my new graduate work will be even more rewarding. After I receive my Ph.D., I might teach or actually apply what I have learned in the "real world". Either way, I hope to still have that same awe of science that drew me here six years ago.